UNIVERSITAT DE BARCELONA

Experiments i models relativistes per a l'astrometria òptica des de l'espai. Aplicació a la missió Gaia

Guillem Anglada Escudé

Experiments i models relativistes per a l'astrometria òptica des de l'espai. Aplicació a la missió Gaia.

Guillem Anglada Escudé

Department d'Astronomia i Meteorologia
Universitat de Barcelona

Treball de tesis supervisat pels doctors

Jordi Torra Roca, Universitat de Barcelona
Sergei A. Klioner, Lohrmann Observatory

Aquesta es la memòria de tesis dipositada en compliment parcial dels requisits per obtenir el títol de Doctor per la

Universitat de Barcelona · Juny 2007 ·

... pel Josep i la Cèlia
el pare i la mare.

Contents

Agraïments

Agraeixo a en Jordi Torra la oportunitat màgica de poder fer un doctorat. Perquè desde que vaig entrar al grup, sempre has vetllat pels teus, per totes les oportunitats i portes que m'has obert, per la confiança, pel suport rebut en el desenvolupament de les meves iniciatives i per la guia tranquila i serena que m'has ofert. Per que en ciència, algú s'ha d'arramangar i invertir temps en moure els fils invisibles que ens aguanten. Per què, al cap i a la fi, he arribat i seré doctor gràcies a la teva empenta.

Ara és el torn d'en Sergei Klioner, per ser el referent e instigador del que n'hagi sortit de bò d'aquesta tesi. La seva ajuda, els seus consells, els seus textos, les seves lliçons, els reptes que em plantejava, les llargues converses i també les discusions acalorades, són les pinzellades de color que de ben segur podreu endevinar quan llegiu aquest text. L'hospitalitat, el tracte humà, i les hores de dedicació que he rebut per part seva han estat un regal agradable d'abraçar i un deute que no se si seré capaç de retornar.

A la Cesca i l'Ignasi, al Xavi, al Claus i a la Carme. Gràcies per animar-me i motivar-me i per moltes d'altres coses, detalls, que no sempre s'expliquen ni se saben. Gràcies a tots vosaltres i a tots els membres del Departament d'Astronomia.

Tots els companys de camí són importants, però com tot a la vida, ja sigui per circumstàncies o per atzar, n'hi ha uns quants amb els que l'experiència d'aquests

darrers anys ha estat més íntima :

Un brindis pel Pau, pel Jan, pel Toni, pel Jordi, pel Fèlix, pel Marc i per l'Otger. Per que l'amistat no es pot descriure amb paraules sense un café calent prenent el sol davant l'entrada de la facultat. I per que segurament teniu raó. La clau és sentir-se insatisfet continuament.

Els companys de departament, de batalles i suades a galeres. Pel J.M. Carrasco i la seva visió pràctica de la vida, de la que tantes vegades he abusat aprofitant que el tenia al despatx. Al Salvador, al Francesc, el Dani, l'Eduard i la Lola, companys de batalles, espatlles sobre les que recolzar-se, per que he après moltes coses de tots vosaltres i sempre hi heu estat quan ha fet falta fer pinya, gràcies!. I a tota la resta del grup HIPPARCOS, també gràcies, per fer-me sentir part d'alguna cosa, d'un lloc.

Com que he tingut molta sort, també tinc una colla d'amics als que agrair que, sense saber-ho, han estat escribint les pàgines d'aquest llibrot. Moltes gràcies a tots!(és que no hi cabeu tots!)

No hi hauria justícia al món sinó dediqués unes paraules de més als meus pares. Per què soc fet de la seva pasta, per que si m'he estat quatre anys per escriure aquesta tesi, ells n'hi han invertit, almenys, vint-i-quatre. Per què en els bons moments sempre hi han estat per celebrar–los i per que els dolents els hem patit tots plegats. Per que el Pare em va ensenyar a estimar la terra i la Mare em va portar de la mà fins a les estrelles. Per que no tenien cap necessitat de fer tot el que els dec, soc com ells m'han fet. Aquesta tesi, també l'heu escrit vosaltres.

Una abraçada a la meva germana xina, que s'estalviarà venir a la lectura. Per que algú havia de fer quelcom de profit a la família, tenim totes les nostres esperances dipositades en tu. Una estrella per la nena que sempre riu! Gràcies Mariona!

I per que sé que s'enfada, la deixo pel final. El meu regal, la meva companya, la saca dels cops, i el centre de les meves mirades. Per que cada pas l'hem fet junts, i

no has dubtat en parar-me els peus quan m'equivocava amb el risc de sortir-ne mal parada. Una abraçada i una promesa : encara hem de compartir moltes coses plegats. Per tu, per la Núria.

Guillem Anglada Escudé.

Juliol 2007

La realització d'aquesta tesi ha estat possible gràcies a la beca FPI ESP-2003-04352 del Ministerio d'Educaciò i Ciència i al suport dels projectes finançats PNE-2003-04352 i PNE-2006-13855-C02-01.

Resum en català

Astrometria des de l'espai i la missió HIPPARCOS

L'astrometria és la branca de l'astronomia que es dedica a mesurar posicions d'estels i altres objectes celests, les seves distàncies i moviment. L'astrometria qunatitativa es remunta, almenys, al astronom grec Hipparcos. En el segle II A.C. va compilar el primer cataleg d'estels i, fent aixo, va inventar l'escala de brillantor (magnitud estelar) que encara s'utilitza en l'actualitat. Es considera que l'astrometria moderna va començar amb Friedrich Bessel i els seus *Fundamenta astronomiae*, que proporcionen la posició mitjana de 3222 estels observats entre 1750 i 17662 per James Bradley.

La historia de l'astrometria està estretament relacionada amb els avenços en els instruments de mesura astronòmica. La invenció del telescopi data del segle XVI i va ser a principis del segle XVII quan Galileu va utilitzar-lo per primera vegada per obtenir medicions astronmiques. Abans d'això, l'astrometria es limitava a les observacions a ull nu ajudades per instruments com l'astrolabi i el sextant, ambdues tècniques utilitzades habitualment per a la navegació i la mesura del temps.

Degut a la precisió i la quantitat de temps requerits per a les observacions astromètriques, les primeres paralaxis trigonomètriques (mesures de distancies a altres estrelles) no van ser obtingudes fins al 1838 per F. Bessel. Va mesurar que la par-

alaxi anual del sistema binari 61 Cygni era de 0.3 segons d'arc. Les paralaxis d'estels brillants com Vega i α Cen van obtenir-se poc després per Wilhelm Struve i Thomas Henderson respectivament.

Les primeres decades del segle XX, van veure millores tant tècniques com instrumentals, incloent grans telescopis refractors i l'ús de plaques fotogràfiques. Això es va traduir en un increment de la precisió tal que durant els any 20 podien mesurar-se ja paralaxis de l'ordre de 0.01 segons d'arc.

Durant el segle 20, els catalegs estelars han anat creixent tant en quantitat d'estels com en precisió de les mesures utilitzant noves observacions i recuperant antigues mesures que són extremadament tils per a obtenir els moviments propis.

També durant el segle 20, es van crear els primers catalegs fonamentals. Un cataleg fonamental consisteix en una llista d'estels *ben comportats* distribuits homogèniament damunt l'esfera celest definint el que s'anomena un marc de referència astronòmic (Astronomical Reference Frame). Un marc de referència astronomic és una realització s'un Sistema de Referència Astronómic, que és un conjunt de regles, convencions i models necessaris per definir a qualsevol instant una triada d'eixos espaials.

La gran revolució en astrometria, però, va arribar amb l'era especial i la missió HIPPARCOS de l'Agencia Espacial Europea(ESA). A l'espai, les observacions astrométriques poden realitzar-se entre estels separats grans angles (¿ 1 grau) gràcies a l'absència de l'atmosfera. Aquest és un requisit indispensable per tal d'obtenir paralaxis lliures d'efectes sistematics locals (els estels al voltant d'una direccio donada tenen moviment paralàctic similar). La mesura d'estels separats grans angles va ser el principi de mesura d'HIPPARCOS i és també un element essencial de les missions d'astrométria des de l'espai com GAIA Perryman *et al.* (2001) o SIM (NASA, Shao (1998)).

En particular, els 110 000 estels observats per HIPPARCOS (Perryman *et al.*

1997b) son la realització en l'optic del Sistema de referencia astronòmic anomenat *International Celestial Reference System* (Sistema Internacional de Refencia Celest), substituint el cataleg FK5 (Fricke *et al.* 1994) utilitzat fins a la dècada dels 90.

L'astrometria no està només restringida al domini òptic. Una de les técniques astromètriques més potents que actualment s'utilitza es l'us de la xarxa de radiotelescopis del VLBI (Very Long Baseline Interferometry) per obtenir mesures astrometriques molt precises de fonts radio. En la xarxa VLBI, el retard del mateix senyal mesurat entre les diferents estacions s'obté amb una precisió molt alta ($\sim 20-30$ picosegons). Ja que les antenes estant separades uns quants milers de kilometres, la orientació de la línia de base (linia ficticia que uneix ambdues estacions) pot mesurarse de forma molt acurada, obtenint mesures astromètriques millors que $\sim 50\,\mu$as quant les condicions ambientals son les apropiades. Un μas (microsegon d'arc) es un milionesima part d'un segon d'arc i equival al gruix aparent d'una moneda a la superficie de la Lluna vista des de la terra.

La xarxa VLBI s'utilitza per produir i mantenir l'ICRF en el domini radio. El sistema ajusta les posicions d'una llista de quasars llunyans a partir dels retards mesurats entre antenes. Un gran esforç teòric i experimental ha estat necessari per definir l'ICRS (McCarthy & Petit 2004) ja que, a més, te aplicacions geodètiques directes (rotació i forma de la terra, d'imporància vital per als satèlits geocèntrics). L'ICRS pot enllaçar-se amb l'ITRS (International Terrestrial Reference System, McCarthy & Petit (2004,Chap. 4)) utilitzant els EOP (Earth Orientation Parameters, Seidelmann (1982)).

L'enllaç entre l'ICRF optic(HIPPARCOS) i la seva contrapartida radio (VLBI), ha estat discutida i elaborada per diversos autors (veure Stone (1998) o bé Hemenway *et al.* (1997) per mencionar-ne alguns d'ells). L'enllaç entre l'ICRF òptic i el ràdio es realitza per mitjà de mesures astromètriques de camp petit dels quasars juntament

amb els estels HIPPARCOS veins.

La xarxa VLBI terrestre està aprop d'assolir la seva maxima precisió teòrica degut a que les linies de base no poden fer-se mes grans que el diametre de la Terra i que certs retards que ocorren a la troposfera escapen a una modelització acurada. Amb l'objectiu d'augmentar les línies de base de la xarxa VLBI, una antena a l'espai està essent utilitzada desde 1996 (veure project VSOP, Levy *et al.* (1989), Linfield *et al.* (1989)). Degut però a les incerteses en la posició orbital de l'antena ($\sim$ 10 metres), no és possible utilitzar-la per fer astrometria global (de grans angles). Tot i això, astrometria de camp petit pot realitzar-se a gran precisió ($\sim$ 40μas) tal i com va demostrar-se per Guirado *et al.* (2001). Està planejat que es llenci una antena de nova generació cap al 2010 (Hirabayashi *et al.* 2007).

A diferència de la contrapartida ràdio, l'ICRF òptic es degrada amb el temps ja que no pot obtenir-se astrometria global de precisió comparable a HIPPARCOS i en una quantitat suficient d'objectes des de terra. Hi han alguns esforços per mantenir l'ICRF optic (Hummel *et al.* 1999), però la precisió és limitada i el nombre d'objectes força baix.

En el domini ràdio, la precisió és molt millor però el nombre de fons radio estables es molt limitat ($\sim$ 200) i moltes regions del cel (especialment a l'hemispheri sud) estant pobrement poblades de fons de calibració. Dues extensions del catàleg inicial de fons han estat incorporades durant els darrers 10 anys per intentar homogenitzar la densitat d'objectes al cel però el nombre de fonts continua sent molt limitat ($<$ 300). A més, ecenment s'ha detectat que alguns d'aquest quasars mostren moviment del fotocentre força elevat degut (probablement) a periòdes d'activitat i jets relativistes movent-se a velocitats superluminiques (aparents).

Diversos projectes per produir versions millorades d'HIPPARCOS han estat cancelats degut a restriccions financeres de les respectives agències : DIVA–

Alemanya(Graue *et al.* 2003) i FAME–USA(Horner *et al.* 1998). Recenment, el USNO ha proposat una missió astrometrica per a ser llençada cap al 2015(Johnston *et al.* 2004). La mission SIM (Space Interferometry Mission) està tecnològicament demostrada però les recents reestructuracions de les prioritats de NASA, n'han rellegat el llençament fins després de 2015. Actualment, la missió GAIA(ESA, Perryman *et al.* (2001)) és l'únic projecte aprovat i amb el finançament garantit que es capaç d'obtenir astrometria d'altra precisió des de l'espai. El seu llençament està previst per finals de 2011.

La missió Gaia. Cap a l'astrometria del microsegon d'arc

Gaia és una missió de l'Agència Espacial Europea (ESA) que preten obtenir astrometria global de tots els objectes celests fins a magnitud ~ 20, al mateix temps que s'obté informació espectrofotomètrica i velocitats radials dels objectes observats amb l'objectiu de crear un mapa tridimensional de la Galàxia. Està previst que es llenci cap a finals del 2011 en una òrbita de Lissajous al punt lagrangia L_2 del sistema Sol-Terra.

L'instrument consistèix en dos telescopis apuntant en dues direccions separades per un angle constant, i que convergeixen en un sol pla focal que conté l'instrument astromètric, l'espectrofotòmetre i l'instrument de velocitats radials. A mida que gira lentament (1 minut d'arc per segon), escaneja continuament el cel. L'eix instantani de rotació precessiona lentament al voltant de la direcció instantania del Sol amb un periode de 2 mesos. El pla focal astromètric cobreix una àrea del cel de 0.7×0.7 graus quadrats. Això garanteix que cada direccio del cel serà observada entre 50 i 200

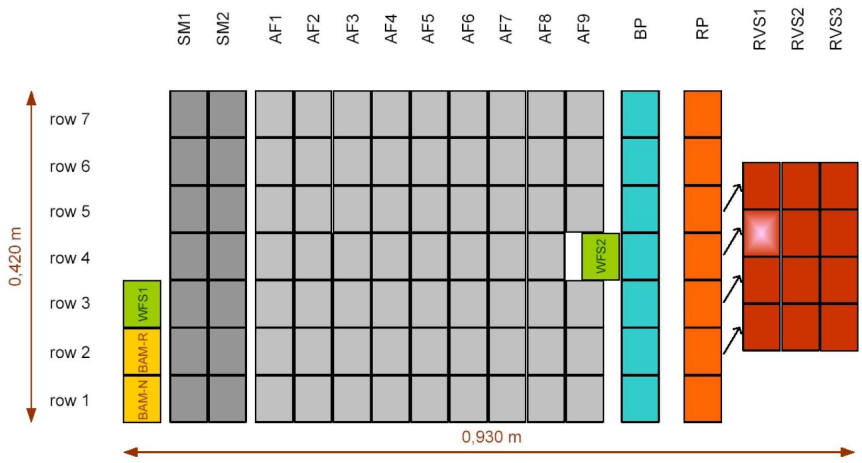

Figure 1: El pla focal de Gaia. Els camps de visió d'ambdós telescopis es sobreimposen en aquest pla focal comú que conté 106 de CCDs distribuits en 7 files i 17 columnes. Cada CCD te 4500 columnes per 1966 files de pixels TDI(línies per on s'arrossega la càrrega). Cada pixel te un tamany de $10\,\mu$m en la direcció d'escaneig(horitzonal) i $30\,\mu$m en la direcció perpendicular que, traduit a mides angulars, són 59×177 milisegons d'arc al quadrat. Les imatges de les estrelles creuen el pla focal de dreta a esquerra. Els CCDs astrometrics són els pintants en gris clar. Figura cortesia de EADS Astrium.

vegades durant els 5 anys de missió nominal.

Al pla focal astromètric, hi ha una matriu de 7 files per 9 columnes de CCDs (veure Fig. 1). A mida que la imatges d'un objecte transita el pla focal, la càrrega es transportada píxel a píxel sincronitzadament amb la el ritme d'escaneig. Aquest mode de lectura s'anomena TDI (Time delayed integration) i maximitza el temps útil d'integració ja que la lectura del xip CCD és fa de forma continuada a la darrera columna de pixels de cada CCD. Si es promitja l'imatge de l'estrella en la direcció perpendicular a l'escaneig, s'obté una mesura astromètrica molt precisa fent l'ajust per centroide del que s'anomena Line Spread Function (versió unidimensional de la PSF o imatge de difracció d'una font monocromàtica, veure Busonero (2006)). El

centroide en la direcció d'escaneig és la mesura astromètrica més precisa i elemental que pot fer Gaia i consisteix essencialment en l'instant de transit del objecte a través del pixel de la darrera columna de cada CCD. Un objecte transitant pel pla focal consisteix en 9 d'aquests instants de trànsit.

La posició de les CCDs en el pla focal (calibració geomètrica) i la direcció d'apuntat com a funció del temps (calibració d'actitud) són *a priori* desconegudes, i s'han d'ajustar utilitzant les mesures mateixes. Per aquesta raó, es diu que el procés de reducció de dades és auto–calibrat, i ha estat desenvolupat curosament durant els darrers anys. Degut a la gran quantitat de dades en brut generades ($\sim$ Terabyte) i els diferents modes que es necessiten per accedir a les dades, ESA va crear un contracte anomenat *Gaia Data Access and Analysis Study* (GDAAS), que va ser encarregat al consorci format per GMV (*Grupo de Mecànica del Vuelo*, Madrid), la Universitat de Barcelona i el CESCA(CEntre de Supercomputació de Catalunya). El contracte es va extendre a una segona fase (GDASS2) que va finalitzar amb èxit al Juny del 2006 (Portell *et al.* 2006). Actualment, l'arquitectura del software i el desenvolupament de la base de dades es realitza al centre de ESA a Madrid (ESAC, Hobbs *et al.* (2007)), essent Barcelona un dels principals centres de computació dedicats al desenvolupament de la Missió. Les instalacions del Barcelona Supercomputing Center (Mare Nostrum) i el CESCA son utilitzats intensivament per a la simulació de dades (Altamirano *et al.* 2005) i al desenvolupament del procés anomenat *Initial Data Treatment* (tractament inicial de les dates, Serraller *et al.* (2007).

Gaia és essencialment una missió astromètrica, per tant la definició estricta dels observables i algoritmes astrométrics hi juguen un paper central. El nucli del procés de reducció de dades s'anomena AGIS(*Astrometric Global Iterative Solution*) i s'encarrega d'ajustar els paràmetres de calibració geométrica, calibració d'actitud i astrometria dels estels de forma iterativa fins que certs llindars de convergència són

assolits. També hi ha un petit nombre de paràmetres anomenats *globals* que afecten a tots els objectes i totes les observacions i que s'ajusten a part en cada iteració (per exemple, el parametre post-Newtonià γ, l'acceleració del baricentre del Sistema Solar,etc.). Un subconjunt d'observacions (entre 10 i 100 milions d'estels ben comportats) seran utilitzats per a construir la solució iterativa global i seran els que defineixin el nou ICRF en óptic. Per tal de processar tal quantitat de dades, els algorismes que contenen el model astromètric dins de AGIS han de ser acurats i computacionalment eficients.

Relativitat i astrometria fonamental

A la precisió d'un μ as, l'astrometria fonamental necessita d'una formulació relativista estricta de lel procés d'observació. Durant la década dels 90, van dedicar-se grans esforços per crear el BCRS (Barycentric Celestrial Reference System), que és essencialment la rerafons físic en termes relativistes utilitzats per descriure l'ICRS (que pot veure's com un cas particular on s'especifica quin és el conveni utilitzat per orientar els eixos espacials en astronomia). El BCRS inclou les propietats de les coordenades utilitzades, la forma del tensor mètric per experiments en el Sistema Solar i les relacions entre altres sistemes coordenats i escales de temps (per exemple, amb el Sistema coordenat Geocentric on s'acostuma a donar les òrbites dels satèl.lits al voltant de la Terra).

La contrucció dels BCRS i les quantitats observables ve donada en l'aproximació post-Newtoniana parametritzada (parameterized post-Newtonian approximation, o ppN), tal i com es descriu a McCarthy & Petit (2004).

El model relativista per a les observacions conté diversos elements que estan desglosats en la Figura 2. Això inclou, la descripció física de les fonts a observar, el

tractament rigurós de la propagació del senyal (fotons en aquest cas), i la correcta interpretació de les quantitats coordenades observades. Tot plegat ha de quedar inclòs i descrit dins el context del BCRS.

El model relativista per a les observacions de Gaia

Els diversos aspectes de la modelització relativista de les observacions astrométriques han estat desenvolupats per diversos autors al llarg del segle XX. Això inclou un dels test classics de la teoria com la deflexió de la llum per un cos am simetria esfèrica (Einstein 1915), estudis detallats de la descripció dels Sistemes de Referencia Relativistes i els observadors (Misner *et al.* 1973,Chap. 6), la descripció dels marcs de referencia astronomics en termes relativistes (Kovalevsky 1971), comprensió del contingut físic dels sistemes de coordenades i la llibertat de *gauge* de les equacions d'Einstein (Will 1980); on només hem mencionat els treballs pioners i algunes referències clàssiques.

El model detallat prou precís al microsegons d'arc incloent tots els elements requerits per a les observacions astrométriques (Sistemes de referencia, propagacio de la llum, i observables) fou donat per primer cop per Klioner & Kopeikin (1992). El treball va ser estimulat pel projecte POINTS(Reasenberg *et al.* 1988) que suggeria l'utilització s'un interferometre en órbita per a obtenir astrometria global amb una precisió de 1 μas.

Diferents models relativistes s'han suggerit per a ser utilitzats per a la missió Gaia (veure de Felice *et al.* (2006) o bé Kopeikin & Schäfer (1999)), però el que millor s'ajusta als requisits de la missió i està formulat de forma més compatible amb la definició del BCRS fou donat per Klioner (2003), que es completa amb la definició del observador i el seu sistema de referència en Klioner (2004). Aquest darrers treballs es basen en una formulació estrictament post-Newtoniana de la gravitació en

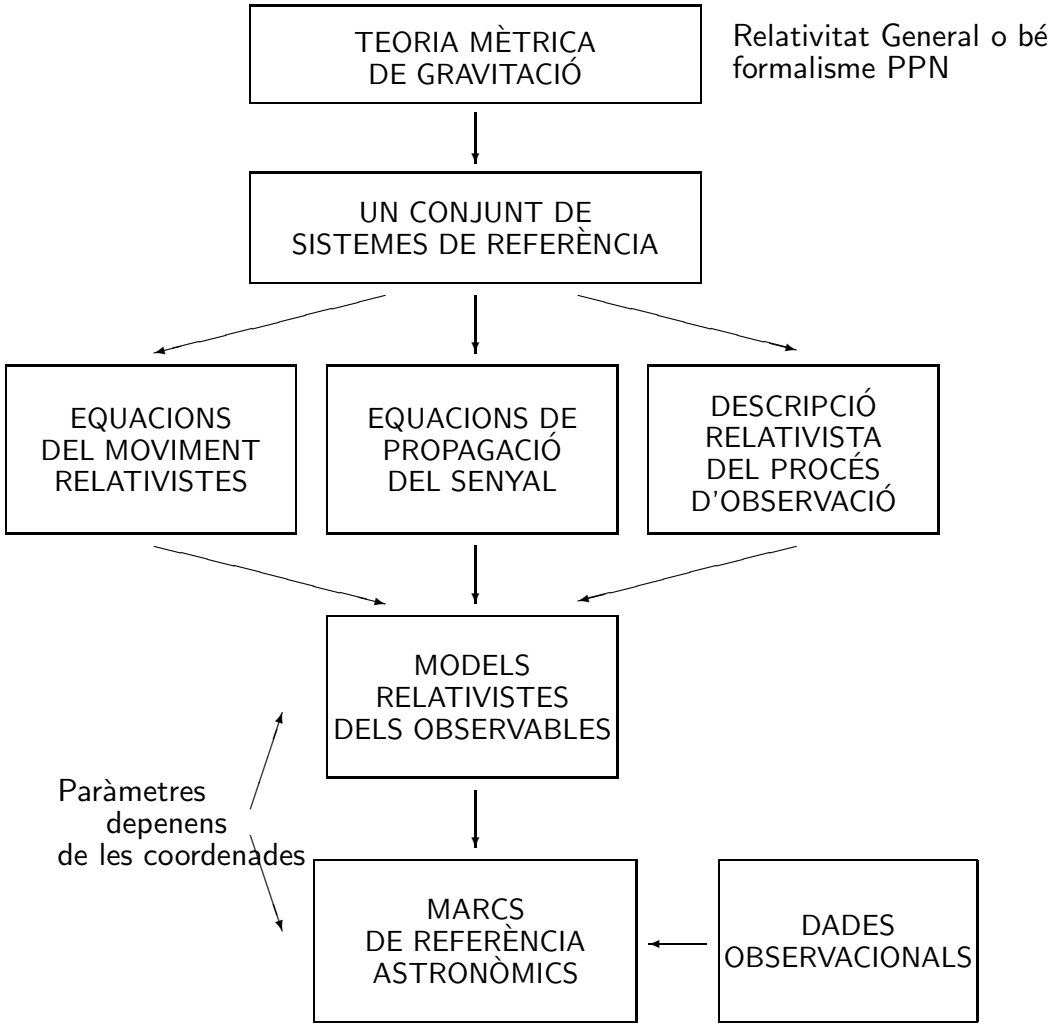

Figure 2: Principis generals per a la descripció relativista d'observacions astronòmiques. Extret de Klioner (2003).

el Sistema Solar. La propagació de les senyals electromagnètiques també ha estat formulada de forma prou precisa en el que s'anomena formulació post-Minkowskiana que parteix d'unes equacions d'Einstein linealitzades que conserven l'invariancia sota transformacion Lorentz i proporcionen prediccions exactes per a qualsevol potencia de $\frac{v}{c}$. En l'aproximació post-Minkowskiana, els termes on s'aplica un desenvolupament pertorbatiu son només aquells proporcionals a G. Pot demostrar-se que ambdues aproximacions proporcionen resultats equivalents a la precisió de Gaia.

Resum del treball desenvolupat en aquesta tesi

Si bé és cert que el models són força complerts en un sentit general, contenen molts detalls i una pila de petits efectes previament indetectables que requereixen un anàlisi detallat per tal d'entendre què és important, i la informació rellevant que se'n pot extreure.

Aquesta tesi s'ha concentrat en tres temes específics amb l'intenció de aconseguir, a través del treball pràctic, una comprensió complerta del model.

Efectes relativistes en l'obtenció d'imatges per un sistema òptic en rotació

Els instruments de gran precisió com Gaia no poden considerar-se com a observadors puntuals en el marc d'una formulació relativista de les quantitats observades. Després d'un anàlisi preliminar dels termes rellevants, s'ha trobat que cal almenys una descripció especial relativista acurada de les diferents parts de l'instrument (miralls, pla focal) degut a que estan en continua rotació.

Per fer-ho hem derivat la forma de la llei de reflexió relativista per a superfícies amb formes i moviment arbitrari en el límit de l'òptica geomètrica (fotons). S'ha

creat un codi de traçat de rajos que permet obtenir els patrons d'aberració (imatges de feixos de rajos paralels incidents) per a un sistema òptic amb qualsevol nombre de superfícies, de forma i en moviment arbitraris. El codi és completament dinàmic, és a dir, no només es te en compte la llei de la reflexió relativista sino també els retards de propagació entre superficies i questions de simultaneitat en les observables: al pla focal, la imatge espaial es correspon als punts d'intersecció dels fotons incidents en una superficie de de temps coordenat constant. Aquest darrer aspecte requereix que el traçat s'hagi de fer de forma iterativa ja que, en general, el temps de propagació de cada fotó dins el sistema òptic serà diferent.

Aquest codi s'ha aplicat a sistemes optics senzills amb les característiques bàsiques de Gaia per tal d'analitzar l'impacte de cadascun dels efectes. S'ha trobat, que l'efecte més notori en les imatges, tant la part provinent dels retards llum com la llei de la reflexió relativista, és un desplaçament constant de tota la imatge respecte al que un esperaria en una aproximació més clàssica (reflexió newtoniana, velocitat de la llum infinita). Això no te consequencies astrometriques greus ja que equival simplement a una direcció d'apuntat efectiva diferent. Per als models òptics simulats, aquest deplaçament total pot superar els $10\,\mu$ as. A part d'aquest despaçament, s'observen distorsions en les imatges al nivell d'$1\,\mu$as, que es preveu que no siguin significants pel cas de Gaia.

Tot i això s'observa que superfícies reflectants molt inclinades respecte l'eix òptic, són les responsables de l'aparició d'aquestes aberracions. Aquesta mena de superfícies són habituals en molts instruments astronòmics (combinadors de feix, focus nasmith, etc.). A més, els efectes dels retards de propagació són proporcionals al tamany dels instruments i s'espera que grans telescopis o instruments extensos (interferometres de sintesi d'apertura, hypertelescopis) siguin especialment sensibles a aquestes *aberracions de retard*.

És, per tant, una conclusió d'aquest treball que és necessari fer un estudi amb cert detall d'aquesta mena d'instruments de nova generació per tal de tenir controlades les aberracions òptiques abans esmentats.

Models astrometrics per a fonts en moviment no lineal

Tant els projectes d'astrometria des de l'espai com els recents desenvolupaments en síntesi d'imatges d'alta resolució requereixen d'una revisió dels efectes a tenir en compte per parametritzar correctament el moviment de les font que segueixen trajectories no lineals. En aquest estudi mostrarem que cal que es tingui en el retard llum per a aquestes fonts, fins hi tot a distàncies estelars.

Una expresió tancada per incloure el retard llum per a fonts en moviment no lineal es donada en aquest càpitol i la signatura astromètrica de l'efecte s'obtindrà per mitjà d'un desenvolupament pertorvatiu dels termes més rellevants. Les expresions que es propocionen poden esser utilitzades de forma pràctica per a la correcta parametrització i reducció de les trajectories observades per a aquestes fonts.

Mostrem també com els efectes del retard temporal són rellevants per a l'astrometria al microsegon d'arc o fins i tot al milisegon d'arc depenén del temps que ens dediquem a observar les fonts. S'obté també, que l'efecte del retard llum pot utilitzar-se per obtenir informació sobre el moviment radial de les fonts aplicant-ho a sistemes binaris propers coneguts. Els resultats no són només aplicables Gaia sinó a qualsevol tècnica que treballi a alta resolució angular (< 1 mas), tal com imatge directe d'exoplanetes o estels observats al voltant de forats negres supermassius (centre galàctic o en cúmuls globulars).

Deflexió de la llum pels planetes del Sistema Solar

Els efectes de la deflexió gravitatoria de la llum en observacions astromètriques de gran precisió al voltant dels planetes del Sistema Solar seran analitzats i discutits des d'una perspectiva pràctica. Després d'una breu introducció del model de propagació de la llum utilitzat, es simularan observacions com les que obtindrà Gaia a fi efecte d'estimar la precisió amb la que els parametres rellevants del model poden ser obtinguts.

Des d'un punt de vista fenomenològic podem parlar de tres efectes rellevants: la deflexió monopolar (provinent de la part del potencial gravitatori amb simetria esfèrica), la deflexió quadrupolar (deguda a la component quadrupolar del camp gravitatori d'un planeta) i els efectes derivats del moviment de translació del planeta durant el temps de propagació del fotó a través del Sistema Solar. Per a cadascun d'aquests efectes, hem introduit un parametre númeric en el model que val 1 si la predicció de la Relativitat General és correcte. Els parametres son γ per al monopol, ϵ per al moment quadrupolar i α_r per a l'efecte de la translació.

Per que les simulacions siguin el màxim de realistes possible, s'han utilitzat catalegs estelars reals (GSC2.3.1 i/o 2MASS), i un model simplificat de la sonda que te en compte els aspectes fonamentals de la missió (òrbita, llei d'escaneig del cel, model geomètric dels 2 plans focals, model d'error en funció de la magnitud,etc). Amb aquesta finalitat hem creat el Simulador de Butxaca de Gaia, per tal de poder simular i reduir aquestes dades sintètiques sense necessitat de fer us d'un centre de supercomputació.

Els resultats d'aquesta secció demostren l'avanç important que hi haurà en aquesta àrea. El parametre γ per Jupiter podrà obtenir-se amb un error relatiu de l'ordre de 10^{-3}, que és millor que la precisió que es va obtenir amb HIPPARCOS per al Sol. Els efectes del moviment dels planetes també podran mesurar-se de forma que el

paràmetre α_r quedarà determinat amb un error relatiu de l'ordre de $2\,10^{-3}$, millorant en dos ordres de magnitud els resultats presentats per Fomalont & Kopeikin (2003) i que van causar la polèmica de la *velocitat de propagació* del camp gravitatori. Les previsions per a la detecció de la deflexió quadrupolar de Jupiter són bones (detecció per sobre de 3σ sense masses dificultats) però els resultats finals dependran críticament d'uns pocs esdeveniments favorables (estels brillant prop del planeta al moment de l'observació). Volem destacar també l'estudi que s'ha fet sobre errors posicionals de les efemerides del sistema solar (models numérics utilitzats per predir el moviment dels planetes). En particular, s'ha trovat que, per permetre una correcta estimació del paràmetre dinàmic α_r i del paràmetre de quadrupol ϵ, cal que la precisió en la posició proporcionada del planeta sigui millor que 100 km, que està en el límit del que avui es te per Jupiter.

S'ha considerat també la possiblitat d'utilitzar les observacions de les llunes de Jupiter. S'ha trobat que, si bé l'experiment és potencialment molt prometeder des d'un punt de vista ideal, els errors posicionals en les orbites de les llunes, les velocitats no menyspreables i el fet de que són fons exteses i amb estructura pot dificultar o fins hi tot, impedir que es puguin processar les mesures per obtenir resultats concluents.

El simulador de butxaca i altre programari

El treball realitzat en els darrers anys ha consistit, en gran part, en el desenvolupament de programari. Tota la comunitat científica de Gaia ha contribuit en el desenvolupament del Simulador *oficial* de missió, que conté models molt detallats per a la població d'estels de la galàxia, dels instruments i l'adquisició de dades. Aquest esforç permet a la comunitat obtenir dades en brut amb un aspecte similar al que tindran les dades reals. Essent tant complet, el simulador oficial de missió requereix

força potencia de càlcul (ara mateix s'acostuma a fer corre sobre uns centenars de nodes del BSC/Marenostrum) i no està pensat per fer petits estudis en ordinadors de sobretaula.

Ja que l'autor de la tesi va estar molt implicat en el desenvolupament inicial del simulador de Gaia, li ha estat possible d'extreure i reutilitzar el conjunt mínim de models per a implementar una versió a escala del sistema que conté tots els detalls del model astrometric relativista. Aquesta és la idea darrera del Simulador de butxaca de Gaia (Gaia Pocket Simulator). Adicionalment, està disenyat per utilitzar directament catalegs estelars reals com el GSC2.3.1(Guide Star Catalog) o el 2MASS (cataleg en l'infraroig). En perspectiva de l'elaboració d'aquesta tesis, l'autor s'ha encarregat també d'incorporar i comprobar la implementació final del elements rellevants per al model relativista dins el Simulador oficial, que després han estat reciclats dins el Simulador de butxaca.

També s'ha desenvolupat el programari necessari per a la reducció de les dades generades pel Simulador de Butxaca, maximitzant la reutilització del codi ja existent. El conjunt de programes de reducció de dades inclouen unes interficies molt generals que permeten *endollar* qualsevol model físic que depengui d'uns pocs paràmetres dins els algorisme propiament dits. En particular hem implementat diferents versions d'algorismes de Mínims quadrats per a models no lineals, i la integració Montecarlo de la funció de versemblança (Estadística Bayesiana).

Conclusions

En aquesta tèsi s'han fet contribucions en els tres àmbits importants del model astromètric relativista : la descripció relativista de l'observador i les mesures (Capítol 2), modelització del moviment de les fonts (Capítol 3) i l'obtenció d'informació sobre

model de propagació de la llum utilitzant les dades de Gaia (Capítol 4). Aquest no ha estat un treball exhaustiu, però ha solventat, o almenys ha posat llum sobre diversos aspectes foscos que havien estat identificats com a crítics per a la explotació satisfactoria de la missió.

A més, la major part del treball desenvolupat durant aquests anys, ha estat desplegat dins les eines de programari per a Gaia, que estant sent desenvolupades per al procés de reducció real de les dades per molts investigadors a pertanyents a paisos membres de l'agència espacial. Una prova d'això n'és el Simulador de Butxaca de Gaia (Appendix A), que no és més que una compilació de les eines desenvolupades o integrades per l'autor en el Simulador de missió i el prototip del model de reducció de dades (dins el contracte GDAAS).

Pel que fa a la modelització de la propagació de la llum en un sistema òptic en rotació, els efectes rellevants (relativitat especial, velocitat de propagació finita) han estat identificats i quantificats. S'ha mostrat com les imatges poden patir d'aberracions d'origen relativista al nivell del μas (deplaçament de la imatge més petites distorsions), però s'ha trovat que són força petits i que, de qualsevol manera, és fàcil de tenir-los calibrats.

També s'ha demostrat que la descripció detallada de la cinemàtica de les fonts es necessaria per entendre correctament el moviment aparent dels estels. En particular aquí s'ha estudiat l'efecte dels retards llum i de canvis de sistema de referencia (sota transformacions de Lorentz). Tenir en compte els retards llum afegeix certa complexitat als models però, per contra, permet obtenir certa informació addicional a partir d'observacions purament astromètriques.

Finalment, hem analitzat el potencial dels experiments de deflexió de la llum utilitzant mesures astromètriques d'astres al voltant dels planetes del Sistema Solar. S'ha vist com experiments molt interessants poden realitzar-se en el cas de Jupiter per

mitjà de l'ajust d'alguns paràmetres lliures que apareixen en el model post-Newtonià de les observacions. Les expectatives per a la mesura de la deflexió quadrupolar de Jupiter són molt altes, i en circumstàncies favorables podem arribar a obtenir una mesura prou significativa. S'ha trobat que la deflexió de la llum podrà mesurar-se en tota la resta de planetes visibles per Gaia, amb l'excepció de Mart que és massa poc massiu per produir una deflexió significativa. S'ha provat també que l'esquema de reducció de dades (mínims quadrats + integració Montecarlo de la funció de versemblança proposat és l'adequat tenint en compte la gran quantitat d'observacions a processar. L'esquema presentat en aquesta tesi assumeix que es disposen de totes les dades de la missió i que la calibració de les mesures està feta. En aquest sentit, els valors obtinguts en els paràmetres no tindran la màxima qualitat fins que la solució astromètrica global per a Gaia no estigui enllestida.

Tal i com hem avançat, en aquesta tesi no hem estudiat tots i cadascun dels aspectes *potencialment* interessants per a la missió Gaia des del punt de vista de la ciencia relativista. Un grup d'experts dins el Consorci de reducció de dades de Gaia s'encarrega de la tasca de coordinar aquest esforç i s'anomena: Relativistic Experiments and Models for Astrometry(REMAT). El grup no només es cuida de l'explotació científica de la missió, sinó que proporciona suport expert en temes com els algoritmes per a reducció astromètrica (dins AGIS) i altres consideracions de caire relativista (sincronització de rellotges, escales de temps, òrbites, precisió de les efemerides pel sistema solar, etc.). A continuació us posem una llista de tasques amb contingut estrictament científic que estant essent estudiades dins del grup REMAT :

- Tests globals
  - Experiments de deflexió de la llum (**)
  - Local Positional Invariance

- Local Lorentz Invariance
- Soroll aleatori provocat per microlens gravitatories(*)
- Ones gravitatòries primordials
- Acceleració del Sistema Solar (*)

- Tests locals
  - Deflexió monopolar en els planetes(**+)
  - Deflexió quadrupolar en els planetes(**+)
  - Deflexió de la llum per masses en moviment(**+)
  - Precessió del periheli, Asteroides (**)
  - Effectes dinamics no-Schwarzschild, Asteroides
  - Principi d'equivalencia, versió forta, Troians(*)
  - J_2 del Sol, Asteroides (**)
  - Variació de la constant gravitatòria (**)

- Objectes relativistes
  - Binaries relativistes(*+)
  - Events de microlents
  - Macrolents de Quasars(*)
  - Forats negres supermassius

Una estrella indica que hi han treballs preliminars sobre el tema. Dues estrelles indiquen que ja s'ha dedicat força esforç en aquest assumpte i que existeixen publicacions revisades o bé notes tècniques amb estimacions precises del efectes detectables. Les creus són parts on l'autor d'aquesta tesi ha participat directament

Tenim l'esperança que de que els resultats presentats en aquesta tesi serveixin com un exemple més de l'excelència i singularitat de la missió Gaia, que ha de ser la bandera insignia del lideratge europeu en el camp de l'astrometria, l'astrofísica i les ciències de l'espai en general.

Traveling through hyperspace ain't like dusting crops, boy. Without precise calculations, we'd fly right through a star, or bounce to close to a supernova, and that would end your trip real quick, wouldn't it.

–Han Solo

Star wars. A new hope

Chapter 1

Introduction

1.1 Space astrometry and the HIPPARCOS mission

Astrometry is a branch of astronomy that deals with the positions of stars and other celestial bodies, their distances and motion. Quantitative astrometry goes back to, at least, the Greek astronomer Hipparcos (or Hipparchus). In the 2nd century B.C. he compiled the first catalogue of stars and, in doing so, invented the brightness scale (stellar magnitude) basically still in use today. Modern astrometry was founded by Friedrich Bessel with his *Fundamenta astronomiae*, which gave the mean position of 3222 stars observed between 1750 and 1762 by James Bradley.

The history of astrometry is tightly bound to the advances in the observing devices. The invention of the telescope dates from the 16th century and it was at the beginning of the 17th century that Galileo used a telescope for the first time to perform astronomical observations. Before that, astrometric observations were limited to naked-eye observations aided by instruments such as the astrolabe and the sextant, both mainly used for maritime navigation.

Due to the accuracy and amount of time required for astrometric observations of stars, the first stellar parallax was not actually detected until 1838 by Friedrich Bessel. He measured the parallax of the 5th magnitude binary star 61 Cygni to be 0.3 arcsec. The parallaxes for the bright stars Vega and α Cen were soon measured

by Wilhelm Struve and Thomas Henderson respectively.

The early decades of the 20th Century saw improved instruments and techniques including large, long refracting telescopes, and photographic plates started being used. This added up to improved precision so that by the 1920s parallaxes as small as 0.01 arcsec could be measured.

During the 20th century a number of catalogs with increasing astrometric accuracy have been created using recent as well as historical observations.

Also during the 20th century, the first fundamental catalogs. A fundamental catalog consists of a list of *well-behaved* stars homogenously distributed on the celestial sphere that define an Astronomical Reference Frame. An Astronomical Reference Frame is a realization of an Astronomical Reference System, which constitutes the set of prescriptions and conventions together with the modeling required to define at any time a triad of axes.

Catalog	Wavelength domain	Number of Objects	Completeness	Accuracy in proper motions	Positional accuracy	Epoch	Reference
Hipparcos	Optical	118 218	7.3	$1-2$ mas/year	$1-3$ mas	1991.25	Perryman *et al.* (1997)
Tycho-2	Optical B,V	2.5 milions	11.0	$1-3$ mas/year[a]	$10-100$ mas	1991.25	Perryman & ESA (1997)
UCAC2	Optical R	48 milions[b]	16.0	$1-7$ mas/year	$20-70$ mas	2000.0	Zacharias *et al.* (2004b)
USNO B1	Optical	1 bilion	20.0 in V	$10-20$ mas/year	~ 200 mas	2000.0	Monet *et al.* (2003)
2MASS	Infrared J,H,K	500 milions	~ 16.0 in K	no proper motions[c]	$> 70mas$	2000.0	Cutri *et al.* (2003)
VLBI ICRF	Radio	212	-	no proper motion[d]	< 0.1 mas	2000.0	Ma *et al.* (1998)
Ext.1		+59	-	no proper motion[d]	< 0.1 mas	2000.0	Gambis (1999)
Ext2		+50	-	no proper motion[d]	< 0.1 mas	2000.0	Fey *et al.* (2004)

Table 1: There are currently a number of recommended catalogs in use. Each one gives several advantadges over the others. In this list, only Hipparcos and the VLBI sources are fundamental catalogs. The information on this table is extracted from the USNO web page at : `http://ad.usno.navy.mil/star/star_cats_rec.html`. [a] *Proper motions derived using old catalog data.* [b] *Only 86% sky coverage* [c] *Proper motions not provided. The NOMAD (Zacharias* et al. *2004a) catalog compilation contains cross references to the optical counterparts.* [d] *Distant quasars should not move.*

The great revolution on astrometry since the invention of the telescope came with the space era and the HIPPARCOS mission. In the space, astrometric measurements can be performed on stars separated large angles ($> 1\,\mathrm{deg}$) thanks to the absence of athmosphere. In order to avoid local systematics in the estimation of parallaxes it is crucial to measure angles between stars separated large angles ($> 90\,\mathrm{deg}$). This was the measurement principle of HIPPARCOS and, this is also an essential element of the planned astrometric space missions like Gaia(ESA, Perryman *et al.* (2001)) or SIM (NASA, Shao (1998)).

In particular, the 110 000 stars observed by the HIPPARCOS mission (Perryman *et al.* 1997b) are the optical realization of the ICRS (International Celestial Reference System), superseding the FK5 catalog Fricke *et al.* (1994).

Astrometry is not only restricted to the optical domain. One of the most successful astrometric techniques that is currently fully functional is the usage of the VLBI network of radiotelescopes to produce extremely precise astrometric measurements. In the VLBI network, the delay measured for the same signal between different antenas is obtained with very high accuracy ($\sim 20 - 30$ picoseconds). Since the antennas are separated some thousands of kilometers, the orientation of the baseline (virtual straight line that connects both stations), can be determined with high accuracy, obtaining astrometric measurements better than $\sim 50\mu$as with favorable weather conditions.

The VLBI network is used to produce and update the ICRF in the radio domain. The System is released by VLBI estimates of equatorial coordinates of a set of extragalactic compact radio sources. A lot of effort was devoted to the definition of the ICRS(McCarthy & Petit 2004) since it has direct application to geodetic sciences (earth rotation and shape). The ICRS can be connected to the International Terrestrial Reference System (ITRS)(McCarthy & Petit 2004,Chap.4) by use of the IERS Earth Orientation Parameters (EOP), Seidelmann (1982).

The link between the optical ICRF and the radio counterpart has been worked out by many authors (see Stone (1998) or Hemenway *et al.* (1997) just to mention some of them). This link is obtained by local astrometric measurements (relatively small fields) of the quasars in the optical range compared to surrounding HIPPARCOS stars.

The earth bound VLBI network is close to its theoretical accuracy due to unmodeled delays in the troposphere and because the baselines cannot be longer than

the earth diameter. In order to increase the VLBI network baselines, a space antenna is being used in orbit around earth since 1996 (see VSOP project Levy *et al.* (1989), Linfield *et al.* (1989)). Due to the uncertainties in the orbital motion of the antenna ($\sim 10m$), it is not possible to perform global astrometry with the current Space VLBI. However small field astrometry can be performed with VSOP at very high accuracy ($< 40\mu$as) as was shown by Guirado *et al.* (2001). A new generation antenna is planned to be launched by 2010 (Hirabayashi *et al.* 2007).

The optical ICRF is degrading with time since no global astrometry with comparable accuracy in the same amount of objects can be obtained from the ground. There are some efforts to upkeep the optical ICRF (Hummel *et al.* 1999) but the accuracy is still very limited and the number of observed objects quite low. In the radio domain the accuracy is much better, but the number of quasars is very limited (~ 200), and many regions of the sky (specially in the southern hemisphere) are poorly populated with calibrating sources (see Table 1.1). Two extensions of the defining QSO have been realized in the last ten years to solve this problem but the number is still very limited. In addition, some active quasars are showing large photocentric motion due to (probably) relativistic jets with superluminal motion(apparent) and unresolved structure.

Several projects to produce an improved versions of HIPPARCOS have been cancelled due to financial restrictions of the funding agencies: DIVA(Graue *et al.* 2003) and FAME(Horner *et al.* 1998). Recently, there are some plans at the USNO to propose a global astrometry mission to be launched by 2015 (Johnston *et al.* 2004). The Space Interferometer Mission (NASA,Shao (1998)) is technologically proven but is also in troubles due to restructuration of the NASA priorities and will not be launched before 2015. Currently, the Gaia(ESA,Perryman *et al.* (2001)) mission is the only fully funded project which is able to perform precise astrometry from space and the current schedule predicts a launch by the end of 2011.

1.2 The Gaia mission. Towards 1μas accuracy

Gaia is a mission of the European Space Agency (ESA) that aims to obtain global astrometry of all the objects up to $V \sim 20$ at the same time of obtaining spectrophotometry and radial velocities. The Gaia probe is planned to be launched at the end of 2011 in a Lissajous orbit at the Earth-Sun L_2 lagrange point.

It consists on two telescopes pointing at two separate direction with a constant basic angle, converging to a single focal plane which contains the astrometric instrument, the spectrophotometer and the radial velocity instrument. As it slowly spins ($60''s^{-1}$), it continuous scans the sky. The instantaneous rotation axis slowly precess around the sun direction with a period of 2 months. The field of view of the astrometric instrument is $0.7 \times 0.7\,\mathrm{deg}^2$. This guarantees that every position of the sky will be observed between 50 and 250 times during the 5 years nominal mission.

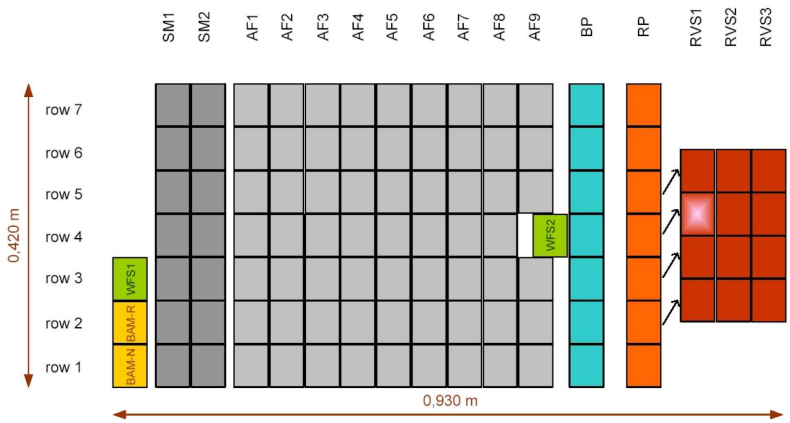

Figure 1.1: The Gaia focal plane. The viewing directions of both telescopes are superimposed on this common focal plane which features 7 CCD rows, 17 CCD strips, and 106 large-format CCDs, each with 4500 TDI lines, 1966 pixel columns, and pixels of size 10μm along scan $\times$30μm across scan (59 mas $\times$ 177 mas). Star images cross the focal plane from the left to the right. The astrometric CCDs are those depicted in light gray. Figure courtesy of EADS Astrium.

At the astrometric focal plane, there is an array of 9 columns and 7 CCD rows(see Fig. 1.1. As the image of an object transits the focal plane, the charge is transported pixel to pixel synchronized with the constant spin rate. This reading mode is called TDI (Time Delayed Integration) and maximizes the useful integration time since the read-out of the pixels is done sequentially as the image of the star reaches the last pixel column of each CCD. If binned in the direction perpendicular to the scan, a very precise astrometric measurement is obtained in the scanning direction by centroiding of the so-called Line Spread Function (1-D version of the PSF, see Busonero (2006)). This is the Gaia most precise measurement which ideally measures the instant of

transit of each star through an ideal line on the last pixel column of each CCDs. A full focal plane transit consists of 9 such transit times.

The position of the CCDs in the focal plane (Geometric calibration) and the pointing direction as a function of time (Attitude calibration) are a priori unknown, and must be obtained using the observations. For this reason, a self calibration data reduction scheme has been carefully developed during the last years. Due to the large amounts of raw data involved ($\sim$ 1 Tbyte) and the different modes required to access to the data, ESA released a contract called GDAAS (Gaia Data Access and Analysis System), which was awarded to the consortia formed by GMV, UB and CESCA. This contract was extended with a second phase (GDAAS2), which finished during 2006, (Portell *et al.* 2006). Currently, the system architecture is organized from ESAC(Madrid)(Hobbs *et al.* 2007), Barcelona being one of the main computation centers devoted to the development of the mission. BSC/Mare Nostrum and CESCA facilities are being intensively used for data simulation(Altamirano *et al.* 2005) and Initial Data Treatment (Serraller *et al.* 2007) studies.

Gaia is essentially an astrometric mission, thus the fundamental definition of the observables and the astrometric algorithms play a very central role. The core of the Gaia data reduction is called AGIS (Astrometric Global Iterative Solution), which performs the attitude calibration, the geometric calibration and solves for the astrometric parameters of the stars in an iterative approach. There is also a small set of Global parameters that affect the whole set of observations. They are also obtained in an additional step (i.e. relativistic γ pPN parameter, acceleration of the Solar System Barycenter, etc.). A subset of the observations ($\sim 10 - -100$ million sources) will be used to build the astrometric solution and will define an Astronomical Reference Frame. To process efficiently such amount of data, the algorithms on the core of AGIS must be accurate and computationally efficient as well.

1.3 Relativity and fundamental astrometry

At the μas accuracy, Fundamental astrometry is no longer independent of the precise fully relativistic description of the observations. A lot of effort was spend during the nineties to create the Barycentric Celestrial Reference System, which represents the relativistic definition of the Astronomical Reference Systems. This includes the properties of the coordinates used, the form of the metric tensor and the relations

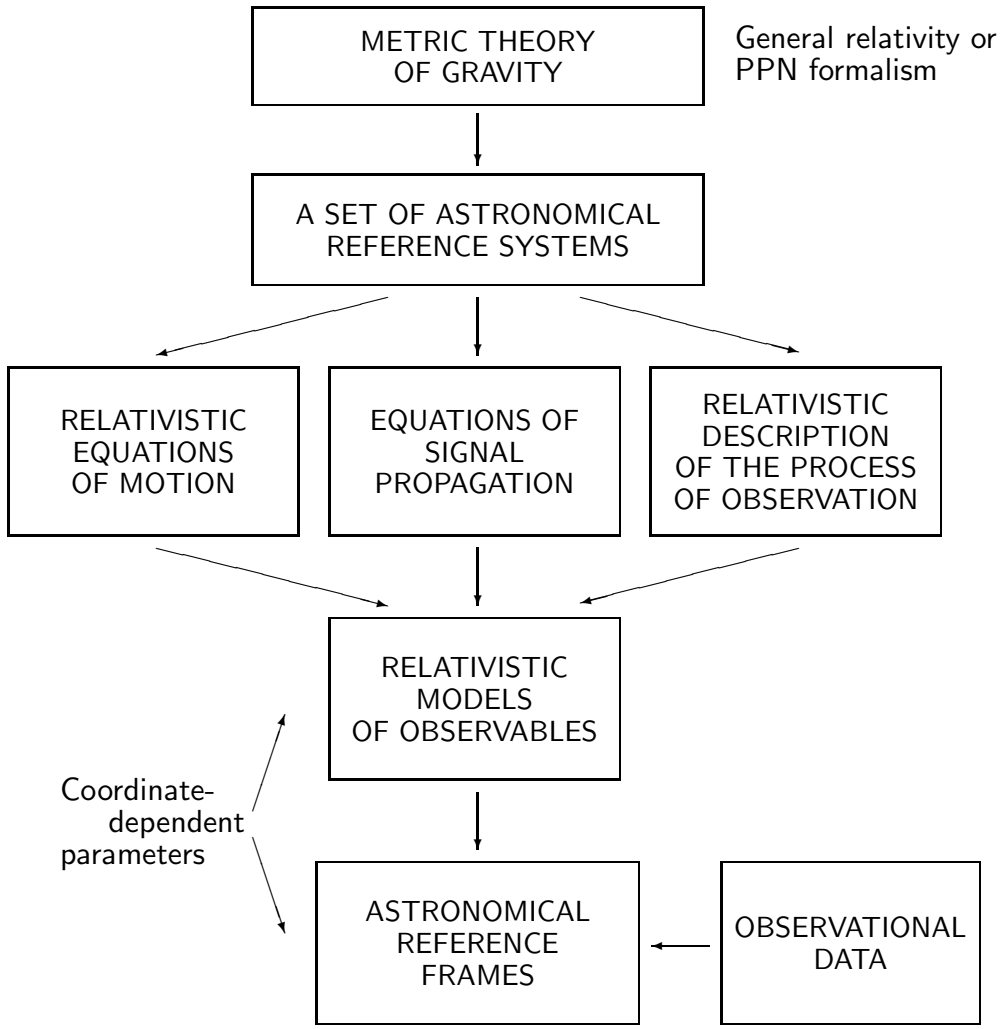

Figure 1.2: General principles of relativistic modeling of astronomical observations (see text for further explanations). Extracted from (Klioner 2003).

between timescales. The construction of the BCRS and its observables is done in the parameterized post-Newtonian formalism as described by McCarthy & Petit (2004).

The relativistic model of the observations contains several parts which are sketched in Fig. 1.2. This includes, the physical description of the observed sources, the rigorous treatment of the signal propagation (photons in this case), and the correct understanding of the observed quantities. All these issues described in the framework defined by the BCRS. This is the context where the work presented in this thesis has been developed.

1.4 The relativistic model for the Gaia observations

Many aspects of the model for very accurate positional measurements have been developed by many authors during the 20th century. This includes the classical tests of light deflection by a spherical symmetric body already described by Einstein itself (Einstein 1915), detailed studies on the description of the Relativistic Reference systems (Misner *et al.* 1973,Chap.6), the description of the Astronomical Reference Frames (Kovalevsky 1971), physical understanding of the coordinate systems and gauge freedom (Will 1980); just to mention some pioneering or reference works in each area.

A detailed model for relativistic astrometric observations including all the required elements (Reference Systems, light propagation, observable quantities) was first given by Klioner & Kopeikin (1992) stimulated by an early project for μas astrometry from space (Reasenberg *et al.* 1988).

The fully relativistic model for the Gaia observations was developed by Klioner (2003) and the precise description of the observer was given in Klioner (2004). These works are fully developed in the parameterized Post-Newtonian approach to the Solar System gravitation. The solution for the light propagation in the Solar System, has also been given in the post-Minkowskian approach by Kopeikin & Schäfer (1999). In the later, the equations for the dynamical fields and for the geodesics are Lorentz invariant. For this reason, their solutions are exact on all the powers of $\boldsymbol{v}/c$. The perturbative approach is only applied to the purely gravitational terms, say those proportional to G. It can be shown that both approaches provide equivalent predictions for the astrometric observables at the expected Gaia accuracy.

1.5 Overview of the work presented in this thesis

Despite the models are very complete in a general sense, they contain many details and a lot effects previously undetectable that require a detailed analysis, study and understanding.

Three topics have been studied in great detail during the realization of this thesis.

1.5.1 Relativistic effects on imaging by a rotating optical system

High accuracy astrometric instruments like Gaia aiming at an accuracy of 1 microarcsecond cannot be considered as point-like observers in the framework of relativistic modeling of observable quantities. Special-relativistic effects on the imaging by a non-point-like arbitrarily moving optical instrument should be discussed. To do that, a special-relativistic reflection law for a mirror of arbitrary shape and motion is derived in the limit of geometrical optics and the relevant effects in light ray propagation within a given instrument with reflecting surfaces (such as propagation delays) will be discussed.

The aberration patterns will be obtained with ray tracing using a full special-relativistic model for two simple rotating optical instruments that slowly rotate with a moderate angular velocity of 60 $''$/s. The idea is to reproduce a Gaia-like optical system to investigate for possible distortions relevant to astrometric measurements at 1 μas level.

Special-relativistic optical modeling of future astrometric instruments is indispensable if a level of a few microarcseconds is a must.

1.5.2 Astrometric modeling of sources in non-linear motion

Space astrometric projects and recent improvements in imaging capabilities require a detailed review of the assumptions of classical astrometric modeling. We will show that Light-Travel Time must be taken into account when modeling the kinematics of astronomical objects in nonlinear motion, even at stellar distances.

A closed expression to include Light-Travel Time in the current astrometric models with nonlinear motion will be worked out and by means of a perturbative approach the expression of the Light-Travel Time signature will be then derived.

Our main aim is to propose a practical form of the astrometric modeling so that it can be applied in astrometric data reduction of sources at stellar distances($d > 1pc$).

We whill show that the Light-Travel Time signature is relevant at μas accuracy (or even at mas) depending on the time span of the astrometric measurements and that information on the radial motion of a source can be obtained through this effect. Some estimates will be provided for known nearby binary systems. The results are not only relevant to the Gaia observations but to any technique that works at very high angular resolution ($< 1\,m$as), such as direct imaging of exoplanets and observations of stars around supermassive blackholes, just to mention a couple of examples.

1.5.3 Light deflection experiments with the planets of the Solar System

Relativistic light deflection effects in high-accuracy astrometric observations close to planets of the solar system will be analyzed using real star catalogs, an appropriate relativistic modeling and the simulation of Gaia-like observations. The gravitational deflection effects under study include deflection due to monopole and quadrupole gravitational fields and due to translational motion of the corresponding body.

We developed a data reduction scheme which combines the speed of the classical Least Squares solution and incorporates the bayesian analysis as a robust way to estimate the magnitude of the effects as well as the confidence levels for the fitted values.

The results will show that important progress will be done in this field with the Gaia data. The monopolar light deflection deflection effect will be measured with a relative error of the order of 10^{-3} for Jupiter alone, which is as accurate as the value obtained by HIPPARCOS from the Sun. The dynamical effects due to the planetary motion will be measured without problems as well, improving by two orders of magnitude the accuracy in the determination of the involved parameters. There is big chance that we will measure the light deflection due to the quadrupolar gravitational field of Jupiter(oblateness), but the final quality will crucially depend on the observability of a very few good events (bright stars observed close to the planet).

1.5.4 Gaia Pocket Simulator and other software

This thesis heavily relied on the development of software. The Gaia community has contributed in the construction of the Gaia Simulator, which contains many detailed models of the universe, the observing device and the data acquisition. Such an effort lets the community obtain raw data which is very close to what is to be expected from the probe. Being very complete, such a system has a need for a high computing power and it would not suit particular investigations.

Since the author has been deeply involved in the development of the Gaia simulator, he has been able to extract and reuse the minimal set of physical models to implement a fully relativistic portable Gaia simulator. This is the essence of the Gaia Pocket Simulator. Moreover, it is designed to directly use existing star catalogs such as 2MASS or GSC2.3.1. Having in mind the development of the thesis, the author has taken care of the final implementation of the models (Anglada–Escudé (2004), Anglada-Escudé *et al.* (2004)) in the official Gaia Simulator that, later on, have been used in the development of the Gaia Pocket Simulator.

A number of data reduction packages have also been developed in Java, using the philosophy of code reutilization. This includes a very general set of interfaces to implement any physical model depending only on a few non-linear parameters, and the algorithms required to perform the fits and extract the scientific information from a generic model. In particular, we developed the code to implement some nonlinear Least Squares algorithms, and the Montecarlo integration of the Likelihood function (Bayesian statistics).

1.6 Generic notation and conventions

Here, we list some notation rules that apply to the whole thesis.

- c is the velocity of light in vacuum.
- Lowercase Latin indices a, i, j, ... take values 1, 2, 3 and refer to spatial components of corresponding quantities.
- Index 0 is used for time components.
- Greek indices α, μ, ν, ... take values 0, 1, 2 and 3 and refer to all space-time components of corresponding quantities.

- The Minkowski metric is denoted by $\eta = \mathrm{diag}(-1, +1, +1, +1)$.
- All Latin indices are lowered and raised by means of the unit matrix $\delta_{ij} = \delta^{ij} = \mathrm{diag}(1, 1, 1)$, and therefore the position of such indices plays no role: $a^i = a_i$.
- The symbol ε_{ijk} is the fully antisymmetric Levi-Civita symbol ($\varepsilon_{123} = +1$).
- Repeated indices imply the Einstein summation rule irrespective of their positions (e.g., $a_i\ b_i = a_1 b_1 + a_2 b_2 + a_3 b_3$).
- The spatial components of a quantity considered as a 3-vector are set in boldface: $\boldsymbol{a} = a^i$.
- The absolute value (Euclidean norm) of a 3-vector $\boldsymbol{a}$ is denoted $|\boldsymbol{a}|$ and is defined by $|\boldsymbol{a}| = \left(a^1\, a^1 + a^2\, a^2 + a^3\, a^3\right)^{1/2}$.
- The scalar product of any two 3-vectors $\boldsymbol{a}$ and $\boldsymbol{b}$ with respect to the Euclidean metric δ_{ij} is denoted by $\boldsymbol{a} \cdot \boldsymbol{b}$ and is defined by $\boldsymbol{a} \cdot \boldsymbol{b} = \delta_{ij} a^i\, b^j = a^i\, b^i$.
- All physical quantities are expressed using the SI units (or MKS) if no particular comment is added in the text.
- Small angles are usually given in fractions of *arcseconds*. The most used are the miliarcsecond ($1\, mas = 10^{-3}\,''$) and the microarcsecond ($1\, \mu as = 10^{-6}\,''$).

Chapter 2

Relativistic effects on imaging by a rotating optical system

2.1 Introduction

High accuracy astrometric instruments like Gaia aiming at an accuracy of 1 microarcsecond cannot be considered as point-like observers in the framework of relativistic modelling of observable quantities. Special-relativistic effects on the imaging by a non-point-like arbitrarily moving optical instrument are discussed. A special-relativistic reflection law for a mirror of arbitrary shape and motion is derived in the limit of geometrical optics. The aberration patterns are computed with ray tracing using a full special-relativistic model for two simple rotating optical instruments. The effect of special-relativistic reflection law on the photocenters of the aberration patterns of an optical system rotating with a moderate angular velocity of 60 $''$/s may be at the level of 1 microarcsecond if the system involves mirrors significantly inclined relative to the optical axis. Special-relativistic optical modelling of future astrometric instruments is indispensable if a level of a few microarcseconds is envisaged.

We investigate possible relativistic effects on the imaging of an optical system with arbitrary motion. In the framework of relativity one usually considers point-like observers. The methods to calculate observed quantities for such observers are well known. It is common to assume that the actual instrumentation of the observer is so

small that one considers the positions and velocities of each part of the instrument to be the same (and that single position and velocity is called the position and velocity of the observer). In reality even for an Earth-based telescope the velocities of different parts of the primary mirror in inertial coordinates (not rotating with the Earth) are slightly different. However, in the past the accuracy of observations was considered to be "too low" and the size of the mirror "too small" for differences to be of practical relevance.

Due to recent technical developments especially for astrometric space missions like Gaia (de Boer *et al.* 2000; Perryman *et al.* 2001; Bienaymé & Turon 2002), JASMINE (Gouda *et al.* 2002) and SIM (Shao 1998) the situation has changed. In the case of Gaia, we deal with a scanning satellite which permanently rotates in space with a period of 6 hours. The size of the primary mirror of Gaia is 1.4 m, comparable with the size of the spacecraft itself. The envisaged best accuracy of Gaia is a few μas (and can be even below that limit in some favorable cases). Therefore, one cannot neglect a priori the difference of velocities of various parts of the instruments. It is our purpose to investigate these effects and estimate their magnitude for Gaia.

The general-relativistic model for Gaia has been formulated by Klioner (2003, 2004). The model uses two principal relativistic reference systems: (1) the Barycentric Celestial Reference System (BCRS) and (2) the Center of Mass Reference System (CoMRS) of the satellite. The former is a global reference system with its origin at the barycenter of the solar system. It has been recommended by the International Astronomical Union for relativistic modelling of high-accuracy astronomical observations (Soffel *et al.* 2003). This reference system is used to model the dynamics of massive bodies, space vehicles (e.g., the Gaia satellite) and light rays within the Solar system. The final Gaia catalogue will contain coordinates of celestial objects in the BCRS. The CoMRS is the local relativistic reference system of the satellite. The theory of such local reference systems was laid down by Ni & Zimmermann (1978) and then elaborated by Klioner & Voinov (1993) and Klioner (2004). The gravitational influence of massive bodies is reduced in the CoMRS as much as possible and, according to the equivalence principle, is represented by tidal potentials. The CoMRS has its origin in the center of mass of the satellite and is kinematically non-rotating with respect to the BCRS. The CoMRS is physically adequate to model phenomena occurring in the immediate neighborhood of the satellite: attitude, the process of observation, etc. According to Klioner (2004) the metric tensor of the

CoMRS differs from the Minkowski metric in three kinds of terms (the gravitational field of the satellite is too small and can be neglected safely): an inertial term due to non-gravitational accelerations of the satellite (for Gaia these accelerations can be relatively large during orbital maneuvers and only about $2 \times 10^{-13}\,\mathrm{m/s^2}$ in between, mainly due to solar pressure); an inertial term due to the slow rotation of the CoMRS relative to the co-moving Fermi-Walker transported locally inertial reference system (with an angular velocity of $\sim 3 \times 10^{-15}\,\mathrm{s^{-1}} = 2\,''$ per century); and tidal gravitational potentials (producing relative accelerations of at most $10^{-12}\,\mathrm{m/s^2}$ at a distance of 2.5 meters from the satellite's center of mass). Simple calculations show that all these terms influence the CoMRS light propagation within a few meters from the satellite's center of mass at a level much lower than the goal accuracy of 1 μas. Therefore, all these terms can be neglected for our purposes and one can consider the CoMRS for a sufficiently small interval of time as an inertial reference system of Special Relativity.

In Section 2.3 we summarize how to calculate the special-relativistic effects in the aberration patterns due to the rotation of the instrument. Section 2.4 is devoted to a description of ray tracing calculations of the relativistic effects in the aberration patterns for two simple optical systems. The details of the derivation of the special-relativistic deflection law are given in the Appendix. There we also introduce a general theoretical scheme we use to treat arbitrarily-shaped and arbitrarily moving mirrors in special relativity.

2.1.1 Notation and conventions

We summarize some particular notation issues relevant to this chapter. Two reference systems (t, x^i) and (T, X^a) will be used. All quantities defined in $x^\mu = (t, x^i)$ are denoted by small Latin characters with space-time and spatial indices taken from second parts of the Greek and Latin alphabet, respectively (μ, ν, ..., i, j, ...). All quantities defined in $X^\alpha = (T, X^a)$ are denoted by capital Latin characters with space-time and spatial indices taken from first parts of the Greek and Latin alphabet, respectively (α, β, ..., a, b, ...).

2.1.2 Coordinate representation of an arbitrary moving mirror

Let us consider an inertial reference system of Special Relativity (t, x^i). We define an arbitrary mirror in arbitrary motion by a bundle of particles moving along worldlines

$$x^\mu_m(t;\xi,\eta) = \left(t, x^i_m(t;\xi,\eta)\right). \tag{2.1}$$

Here ξ and η are two parameters "numbering" the particles. These parameters can be though of as some non-degenerate "coordinate system" on the surface of the mirror which is described by $x^i_m(t;\xi,\eta)$ for any fixed time t. Fixing ξ and η we fix a particle on the surface of the mirror and $x^i_m(t;\xi,\eta)$ is the worldline of that particle in coordinates (t, x^i). Further, we assume that $x^i_m(t;\xi,\eta)$ is differentiable with respect to all its three parameters. This means in particular that the surface of the mirror is assumed to be smooth.

Here we do not pay attention to any physical properties of the mirror as a "physical body" (elasticity, deformations, etc.). We just consider that (2.1) formally defines the position of each point of the mirror at each moment of time. The source of information for $x^i_m(t;\xi,\eta)$ for realistic mirrors and the plausibility of these representation of an arbitrarily shaped and arbitrarily moving mirror is discussed in Section 2.3 above.

Starting from (2.1) for any fixed time t at any fixed point of the mirror characterized by some values of ξ and η we have two three-dimensional vectors tangent to the surface of the mirror at the considered point as

$$l^i = \frac{\partial}{\partial\xi}\, x^i_m(t;\xi,\eta), \tag{2.2}$$

$$m^i = \frac{\partial}{\partial\eta}\, x^i_m(t;\xi,\eta). \tag{2.3}$$

Then a coordinate vector normal to the surface of the mirror at that point can be defined as

$$n^i = \varepsilon_{ijk}\, l^j\, m^k. \tag{2.4}$$

The order of vectors l^i and m^i in (2.4) is arbitrary and corresponds to a choice of the sign in the definition of n^i (if n^i is a normal vector then $-n^i$ is also a normal). Not restricting the generality we assume below that (2.4) defines that n^i which is directed toward the "working surface" of the mirror, that is for any incoming light ray σ^i which hits the mirror at the considered point one has $\boldsymbol{\sigma}\cdot\boldsymbol{n} < 0$. This normal vector n^i has

no physical meaning since it is defined in some arbitrary coordinate system (t, x^i). However, it is straightforward to compute n^i if $x^i_m(t;\xi,\eta)$ is given. Below we show how to relate n^i to a physically meaningful normal vector at some point of the mirror as observed by an observer instantaneously co-moving with the considered point of the surface.

The coordinate velocity of any point of the mirror reads

$$v^i_m = \frac{\partial}{\partial t}\, x^i_m(t,\xi,\eta). \tag{2.5}$$

2.1.3 Transforming the mirror surface from one inertial reference system to another

Let us now define another reference system (T, X^a) moving with constant velocity v^i with respect to (t, x^i). The coordinates (T, X^a) and (t, x^i) are related by a Lorentz transformation of the form

$$\begin{aligned} c\,t &= \Lambda^0_0\, c\,T + \Lambda^0_a\, X^a, && (2.6)\\ x^i &= \Lambda^i_0\, c\,T + \Lambda^i_a\, X^a. && (2.7) \end{aligned}$$

The Λ matrix coefficients are given by

$$\begin{aligned} \Lambda^0_0 &= \gamma, && (2.8)\\ \Lambda^0_a &= k^a\,\gamma, && (2.9)\\ \Lambda^i_0 &= k^i\,\gamma, && (2.10)\\ \Lambda^i_a &= \delta^{ia} + \frac{\gamma^2}{1+\gamma}\, k^i\, k^a, && (2.11)\\ \gamma &= (1 - \boldsymbol{k}\cdot\boldsymbol{k})^{-\frac{1}{2}}\,, && (2.12)\\ \boldsymbol{k} &= \frac{1}{c}\,\boldsymbol{v}. && (2.13) \end{aligned}$$

The inverse transformation reads

$$\begin{aligned} c\,T &= \bar\Lambda^0_0\, c\,t + \bar\Lambda^0_i\, x^i, && (2.14)\\ X^a &= \bar\Lambda^a_0\, c\,t + \bar\Lambda^a_i\, x^i. && (2.15) \end{aligned}$$

where

$$\bar{\Lambda}^0_0 = \gamma, \tag{2.16}$$

$$\bar{\Lambda}^0_i = -k^i\,\gamma, \tag{2.17}$$

$$\bar{\Lambda}^a_0 = -k^a\,\gamma, \tag{2.18}$$

$$\bar{\Lambda}^a_i = \delta^{ia} + \frac{\gamma^2}{1+\gamma} k^i k^a. \tag{2.19}$$

In the reference system (T, X^a) the mirror can be also represented in the same form as in Section 2.1.2

$$X^\alpha_m(T;\xi,\eta) = \left(T, X^a_m(T;\xi,\eta)\right), \tag{2.20}$$

where fixed values for ξ and η should correspond to the same surface particle in both coordinate systems. The vectors tangent and normal to the surface read

$$L^a = \frac{\partial}{\partial\xi} X^a_m(T;\xi,\eta), \tag{2.21}$$

$$M^a = \frac{\partial}{\partial\eta} X^a_m(T;\xi,\eta), \tag{2.22}$$

$$N^a = \varepsilon_{abc}\, L^b\, M^c. \tag{2.23}$$

Here again, N^a is a coordinate normal vector that has no physical meaning. The coordinate velocity of a point of the mirror is given by

$$V^a_m = \frac{\partial}{\partial T} X^a_m(T;\xi,\eta). \tag{2.24}$$

Let us now relate the vectors L^a, M^a, N^a and V^a_m to the corresponding ones in the reference system (t, x^i). We consider the coordinate transformation of the events defined by (2.1) and (2.20)

$$c\,T = \bar{\Lambda}^0_0\, c\,t + \bar{\Lambda}^0_i\, x^i_m(t;\xi,\eta), \tag{2.25}$$

$$X^a_m(T;\xi,\eta) = \bar{\Lambda}^a_0\, c\,t + \bar{\Lambda}^a_i\, x^i_m(t;\xi,\eta). \tag{2.26}$$

The function $X^a_m(T,\xi,\eta)$ is thus defined by (2.25)–(2.26) implicitly since (2.25) should be inverted to give t as a function of T, ξ and η and that t should be substituted into

(2.26) to give the explicit dependence of X^a_m on T, ξ and η. Clearly, that inversion cannot be done explicitly for any $x^i_m(t;\xi,\eta)$. However, the partial derivatives of $X^a_m(T;\xi,\eta)$ representing L^a, M^a and V^a_m can be calculated as derivatives of an implicit function. Some straightforward algebra gives

$$V^a_m = c\,\frac{\bar\Lambda^a_0 + \bar\Lambda^a_i\,k^i_m}{\bar\Lambda^0_0 + \bar\Lambda^0_i\,k^i_m}, \tag{2.27}$$

$$L^a = \bar S^a_i\,l^i \tag{2.28}$$

$$M^a = \bar S^a_i\,m^i \tag{2.29}$$

$$\bar S^a_i = \bar\Lambda^a_i - \bar\Lambda^0_i\frac{\bar\Lambda^a_0 + \bar\Lambda^a_j\,k^j_m}{\bar\Lambda^0_0 + \bar\Lambda^0_j\,k^j_m}, \tag{2.30}$$

or inverting

$$v^i_m = c\,\frac{\Lambda^i_0 + \Lambda^i_a\,K^a_m}{\Lambda^0_0 + \Lambda^0_a\,K^a_m}, \tag{2.31}$$

$$l^i = S^i_a\,L^a, \tag{2.32}$$

$$m^i = S^i_a\,M^a, \tag{2.33}$$

$$S^i_a = \Lambda^i_a - \Lambda^0_a\frac{\Lambda^i_0 + \Lambda^i_b\,K^b_m}{\Lambda^0_0 + \Lambda^0_b\,K^b_m}, \tag{2.34}$$

with $k^i_m = c^{-1}\,v^i_m$ and $K^a_m = c^{-1}\,V^a_m$. Equations (2.27) and (2.31) coincide with the law for velocity addition in Special Relativity.

To test the invertibility of the transformations between tangent vectors, one can check by direct calculation that $S^i_a\bar S^a_j = \delta^i_j$ and $\bar S^a_i S^i_b = \delta^a_b$. Using (2.30) and (2.34) some useful relations can be obtained,

$$\bar S^b_j\,\bar S^c_k\varepsilon_{abc} = \frac{1}{\gamma\,(1-\boldsymbol{k}\cdot\boldsymbol{k}_m)}\;S^i_a\varepsilon_{ijk}, \tag{2.35}$$

$$S^j_b\,S^k_c\varepsilon_{ijk} = \gamma\,(1-\boldsymbol{k}\cdot\boldsymbol{k}_m)\,\bar S^a_i\varepsilon_{abc}. \tag{2.36}$$

To prove (2.35)–(2.36) we used the identity

$$\varepsilon_{ajc}\,\delta^{kb} + \varepsilon_{kac}\,\delta^{jb} + \varepsilon_{jkc}\,\delta^{ab} = \varepsilon_{ajk}\,\delta^{bc}. \tag{2.37}$$

Transformation rules of the coordinate normal vectors

We are ready to derive the transformation rules of the normal vectors $\boldsymbol{n}$ and $\boldsymbol{N}$ since they are required to formulate the reflection law. In order to write N^a in the Mirror Reference System (T, X^a) in terms of a perpendicular vector n^i in an arbitrary reference System (t, x^i) where the mirror is moving we use the transformation rules of the tangent vectors $\boldsymbol{L}$ and $\boldsymbol{M}$ imposing that the velocity $c\,K^a = 0$ (in the comoving frame, the coordinate velocity of the mirror is 0). Then

$$L^a = \bar{P}^a_i l^i \tag{2.38}$$

$$M^a = \bar{P}^a_i m^i \tag{2.39}$$

$$\bar{P}^a_i = \bar{S}^a_i\big|_{K^a=0} = \delta^{ai} + k^a k^i \frac{\gamma^2}{1+\gamma} \tag{2.40}$$

As given in (2.23),the components of the perpendicular vector in the Mirror Reference System are

$$\begin{aligned} N^c &= \varepsilon_{abc} L^a M^b = \varepsilon_{abc} \bar{P}^a_i \bar{P}^b_j l^i m^j \\ &= \left[\varepsilon_{ijc} + 2B_{[ij]c}\right] l^i m^j \end{aligned} \tag{2.41}$$

$$B_{[ij]c} \equiv \frac{1}{2}\left(\varepsilon_{ibc} k^b k^j - \varepsilon_{jbc} k^b k^i\right) \frac{\gamma^2}{1+\gamma}. \tag{2.42}$$

The object B is antisymmetric with respect to i and j indexes. Then, both terms in equation (2.41) are antisymmetric with respect to i and j so, only the antisymmetric part of $l^i m^j$ is required. This is,

$$l^{[i} m^{j]} \equiv \frac{1}{2}\left(l^i m^j - l^j m^i\right). \tag{2.43}$$

This object is proportional to the components of the perpendicular vector $\boldsymbol{n}$ to the surface defined by $\boldsymbol{l}$ and $\boldsymbol{m}$,

$$n^k = \varepsilon_{ijk} l^i m^j = \varepsilon_{ijk} l^{[i} m^{j]}. \tag{2.44}$$

Then, multiplying at both sides of (2.44) by ε^{fgk} we get

$$\begin{aligned} \varepsilon^{fgk} n^k &= \varepsilon^{fgk}\, \varepsilon_{ijk}\, l^{[i} m^{j]} = (\delta_{fi}\delta_{gj} - \delta_{fj}\delta_{gi})\, l^{[i} m^{j]} \\ &= l^{[f} m^{g]} - l^{[g} m^{f]} = 2 l^{[f} m^{g]}. \end{aligned} \tag{2.45}$$

Then, we can substitute $l^{[i} m^{j]}$ in the equation (2.41) by (2.45) obtaining,

$$N^c = \frac{1}{2}\left[\varepsilon_{ijc} + 2B_{[ij]c}\right] \varepsilon^{ijk} n^k. \tag{2.46}$$

We can proceed to the contraction of i and j,

$$\begin{aligned} \varepsilon_{ijc}\varepsilon^{ijk} &= \delta_{jj}\delta_{ck} - \delta_{jk}\delta_{cj} \\ &= 3\delta_{ck} - \delta_{ck} \\ &= 2\delta_{ck}, \end{aligned} \tag{2.47}$$

$$\begin{aligned} \varepsilon_{i'bc} k^b k^j \varepsilon^{ijk} &= (\delta_{bj}\delta_{ck} - \delta_{bk}\delta_{cj})\, k^b k^j \\ &= k^b k^b \delta_{ck} - k^b k^c \delta_{bk} \\ &= k^2 \delta_{ck} - k^k k^c, \end{aligned} \tag{2.48}$$

$$2B_{[ij]c}\varepsilon^{ijk} = 2\left(k^2\delta^{ck} - k^k k^c\right)\frac{\gamma^2}{1+\gamma}. \tag{2.49}$$

Making the substitutions in (2.46),

$$N^c = \frac{1}{2}\left[2\delta^{ck} + 2\left(\frac{\gamma^2-1}{\gamma^2}\delta^{ck} - k^c k^k\right)\frac{\gamma^2}{1+\gamma}\right] n^k \tag{2.50}$$

$$= \gamma\left[\delta^{ck} - \frac{\gamma}{1+\gamma} k^c k^k\right] n^k, \tag{2.51}$$

in vectorial form,

$$\boldsymbol{N} = \gamma\left(\boldsymbol{n} - (\boldsymbol{k}\cdot\boldsymbol{n})\frac{\gamma}{1+\gamma}\,\boldsymbol{k}\right). \tag{2.52}$$

This expression does not depend at all on the particular choice of vectors $\boldsymbol{l}$ and $\boldsymbol{m}$. It is useful to obtain the normalized version of $\boldsymbol{N}$; which is required to compute the

reflection law. Assuming that $\hat{n} = \frac{\boldsymbol{n}}{\|\boldsymbol{n}\|}$ is a unit vector (the normal vector to the surface in the (t, x^i) reference system), the the module of $\boldsymbol{N}$ is

$$\begin{aligned}
\|\boldsymbol{N}\| &= \gamma\left(1 + k^2\frac{\gamma^2}{(1+\gamma)^2}\left(\boldsymbol{k}\cdot\hat{\boldsymbol{n}}\right)^2 - 2\left(\boldsymbol{k}\cdot\hat{\boldsymbol{n}}\right)^2\frac{\gamma}{1+\gamma}\right)^{1/2} \\
&= \gamma\left(1 + \frac{(\gamma-1)(\gamma+1)}{\gamma^2}\frac{\gamma^2}{(1+\gamma)^2}\left(\boldsymbol{k}\cdot\hat{\boldsymbol{n}}\right)^2 - 2\left(\boldsymbol{k}\cdot\hat{\boldsymbol{n}}\right)^2\frac{\gamma}{1+\gamma}\right)^{1/2} \\
&= \gamma\left(1 + \left(\boldsymbol{k}\cdot\hat{\boldsymbol{n}}\right)^2\frac{(\gamma-1)}{(1+\gamma)} - 2\left(\boldsymbol{k}\cdot\hat{\boldsymbol{n}}\right)^2\frac{\gamma}{1+\gamma}\right)^{1\backslash 2} \\
&= \gamma\left(1 - \left(\boldsymbol{k}\cdot\hat{\boldsymbol{n}}\right)^2\right)^{1/2}. \qquad (2.53)
\end{aligned}$$

And finally,

$$\hat{\boldsymbol{N}} \equiv \frac{\boldsymbol{N}}{\|\boldsymbol{N}\|} = \frac{1}{\sqrt{1-(\boldsymbol{k}\cdot\hat{\boldsymbol{n}})^2}}\left(\hat{\boldsymbol{n}} - \boldsymbol{k}\cdot\hat{\boldsymbol{n}}\frac{\gamma}{1+\gamma}\,\boldsymbol{k}\right) \qquad (2.54)$$

$$(2.55)$$

The inverse transformation (to obtain $\boldsymbol{n}$ in terms of $\boldsymbol{N}$) is quite straightforward. One only must use the same development until equation (2.50) and replace the factor $\frac{\gamma^2}{1+\gamma}$ by $\frac{-\gamma}{1+\gamma}$, obtaining

$$\begin{aligned}
n^k &= \frac{1}{2}\left[2\delta^{kc} + 2\left(\frac{\gamma^2-1}{\gamma^2}\delta^{kc} - k^k k^c\right)\frac{-\gamma}{1+\gamma}\right]N^c \\
&= \frac{1}{\gamma}\left[\delta^{kc} + \frac{\gamma^2}{1+\gamma}k^c k^k\right]n^k. \qquad (2.56)
\end{aligned}$$

In vectorial form,

$$\boldsymbol{n} = \frac{1}{\gamma}\left(\boldsymbol{N} + \boldsymbol{k}\cdot\boldsymbol{N}\frac{\gamma^2}{1+\gamma}\boldsymbol{k}\right). \qquad (2.57)$$

Normalizing $\boldsymbol{n}$ and considering that $\boldsymbol{N} = \hat{\boldsymbol{N}}$ is the normal vector to the surface in the (T, X^a) reference system one obtains,

$$\hat{\boldsymbol{n}} \equiv \frac{\boldsymbol{n}}{\|\boldsymbol{n}\|} = \frac{1}{\sqrt{1+\gamma^2(\boldsymbol{k}\cdot\hat{\boldsymbol{N}})^2}}\left(\hat{\boldsymbol{N}} + \boldsymbol{k}\cdot\hat{\boldsymbol{N}}\frac{\gamma^2}{1+\gamma}\boldsymbol{k}\right). \qquad (2.58)$$

2.2 The reflection law

2.2.1 Wave vectors in the two inertial reference systems

In order to consider the light reflection from the mirror we first need to relate the wave vectors of the incoming and outgoing light rays in the two considered coordinate systems. In the reference system (t, x^i) the incoming light ray is characterized by its null wave vector p^μ ($\eta_{\mu\nu}\, p^\mu\, p^\nu = 0$). The unit light ray direction σ^i ($\boldsymbol{\sigma} \cdot \boldsymbol{\sigma} = 1$) in that reference system is related to p^μ as $\sigma^i = p^i/p^0$. In the reference system (T, X^a) the null wave vector of the same light ray is P^α, and the unit light ray direction $\Sigma^a = P^a/P^0$ ($\boldsymbol{\Sigma} \cdot \boldsymbol{\Sigma} = 1$). The frequencies f and F of the light in the corresponding reference systems are linearly proportional to p^0 and P^0, respectively.

The wave vectors p^μ and P^α are related by the Lorentz transformation

$$P^\alpha \;=\; \bar{\Lambda}^\alpha_\mu\, p^\mu, \tag{2.59}$$

which means that the frequencies and unit light ray directions are related as

$$\Sigma^a \;=\; \frac{\overline{\Lambda}^a_0 + \overline{\Lambda}^a_i\, \sigma^i}{\overline{\Lambda}^0_0 + \overline{\Lambda}^0_i\, \sigma^i}, \tag{2.60}$$

$$F \;=\; \left(\overline{\Lambda}^0_0 + \overline{\Lambda}^0_i\, \sigma^i\right)\, f. \tag{2.61}$$

2.2.2 Reflection as seen by an instantaneously co-moving observer

For an observer instantaneously co-moving with the element of the mirror where the light ray is reflected the following simple reflection law is valid (in an inertial reference system of Special Relativity for a mirror at rest)

$$F' \;=\; F, \tag{2.62}$$

$$\boldsymbol{\Sigma}' \;=\; \boldsymbol{\Sigma} - 2\,(\hat{\boldsymbol{N}} \cdot \boldsymbol{\Sigma})\,\hat{\boldsymbol{N}}, \tag{2.63}$$

where $\hat{\boldsymbol{N}}$ is the observable unit normal vector to the surface of the mirror at the point of reflection as discussed in Section 2.1.3 above. The reflection law (2.63) means that the component of $\boldsymbol{\Sigma}$ perpendicular to the surface changes its sign. This automatically guarantees that the angle of incidence is equal to the angle of reflection and that

the incoming ray $\mathbf{\Sigma}$, the reflected ray $\mathbf{\Sigma}'$ and the normal $\hat{\boldsymbol{N}}$ are coplanar. The same equations (2.62) and (2.63) are valid for, respectively, the time and space components of wave vectors before and after reflection.

We consider this reflection law as given, but is well known the method to derive it from Maxwell equations for electromagnetic field for a mirror at rest (Jackson 1975). In the instantaneously co-moving reference system (T, X^a) the coordinate velocity of the reflecting point vanishes but its acceleration may differ from zero. However, the acceleration cannot affect the instantaneous process of reflection considering of the equivalence principle as long as the conditions for geometrical optics are satisfied, i.e., as long as the amplitude, polarization and wave vector of an electromagnetic wave do not change significantly over a distance determined by the wavelength λ. This implies that the acceleration a_m of the mirror should satisfy a constraint of the form $a_m \ll c^2/\lambda$ (see, Mashhoon (2005) for a detailed discussion of accelerated observers in special relativity).

2.2.3 Algebra

We apply the classical Einstein approach to obtain the reflected wave vector in terms of the incoming light ray that consist on applying known physical laws in the reference system where they are simpler (comobile with a surface element), and then apply the required coordinate transformations to obtain the general expression. If $\boldsymbol{\sigma}$ is the tangent unit vector to the incoming light ray, then

$$\sigma^i \to \Sigma^\beta \to \Sigma'^\alpha \to \sigma'^\mu \to \hat{s}^i \tag{2.64}$$

where $\mathbf{\Sigma}$ is the incoming ray in the reference system at rest with the surface element, $\mathbf{\Sigma}'$ is the reflected light ray in the reference system at rest with the surface element, and $\boldsymbol{\sigma}'$ is the reflected light ray on which we are interested. Each step(arrow) can be written explicitly as

$$\Sigma^\beta = \bar{\Lambda}^\beta_\mu \sigma^\mu, \tag{2.65}$$

$$\Sigma'^\alpha = \Sigma^\alpha - 2\hat{N}^\alpha \hat{N}_\beta \Sigma^\beta, \tag{2.66}$$

$$\sigma'^\nu = \Lambda^\nu_\alpha \Sigma'^\alpha. \tag{2.67}$$

that can be combined in a single expression, obtaining

$$\begin{aligned}\sigma'^{\nu} &= \Lambda^{\nu}_{\alpha}\Sigma'^{\alpha} \\ &= \Lambda^{\nu}_{\alpha}\left(\Sigma^{\alpha} - 2\hat{N}^{\alpha}\hat{N}_{\beta}\Sigma^{\beta}\right) \\ &= \Lambda^{\nu}_{\alpha}\Sigma^{\beta}\left(\delta^{\alpha}_{\beta} - 2\hat{N}^{\alpha}\hat{N}_{\beta}\right) \\ &= \Lambda^{\nu}_{\alpha}\bar{\Lambda}^{\beta}_{\mu}\left(\delta^{\alpha}_{\beta} - 2\hat{N}^{\alpha}\hat{N}_{\beta}\right)\sigma^{\mu}. \end{aligned} \tag{2.68}$$

Using the transformations found in Section and some algebra is sufficient to obtain the reflection law from (2.68) in terms of $\boldsymbol{\sigma}$, $\boldsymbol{k}$ and $\hat{\boldsymbol{n}}$.

The first thing one can do is to calculate the contraction of the Lorentz transformation matrices with the δ^{α}_{β} in the equation (2.68). This is,

$$\delta^{\alpha}_{\beta}\Lambda^{\nu}_{\alpha}\bar{\Lambda}^{\beta}_{\mu}\sigma^{\mu} = \Lambda^{\nu}_{\alpha}\bar{\Lambda}^{\alpha}_{\mu}\sigma^{\mu} = \delta^{\nu}_{\mu}\sigma^{\mu} = \sigma^{\nu} \tag{2.69}$$

obtaining for σ'^{ν},

$$\sigma'^{\nu} = \sigma^{\nu} - 2\Lambda^{\nu}_{\alpha}\hat{N}^{\alpha}\bar{\Lambda}^{\beta}_{\mu}\hat{N}_{\beta}\sigma^{\mu} \tag{2.70}$$

The equation (2.23) can be used to write $\hat{\boldsymbol{N}}$ in terms of $\hat{\boldsymbol{n}}$.

$$\hat{N}^{\alpha} = \left(0\ , \hat{N}^{a}\right) = \left(0\ , \frac{1}{F}P^{k}_{a}\hat{n}^{k}\right), \tag{2.71}$$

$$\hat{N}_{\beta} = \eta_{\alpha\beta}\hat{N}^{\alpha} = \delta_{a\beta}\hat{N}^{a} = \left(0\ , \frac{1}{F}P^{k}_{b}\hat{n}^{k}\right)$$

$$F = \sqrt{1 - (\boldsymbol{k}\cdot\hat{\boldsymbol{n}})^{2}}, \tag{2.72}$$

$$P^{k}_{a} = \delta^{ka} - k^{k}k^{a}\frac{\gamma}{1+\gamma}. \tag{2.73}$$

Now, we can calculate separately the temporal part and the spatial part of σ'^{ν}. If we

arrange the terms as

$$\begin{aligned}\sigma'^0 &= \sigma^0 - 2\Lambda^0_\alpha \hat{N}^\alpha \bar{\Lambda}^\beta_\mu \hat{N}_\beta \sigma^\mu \doteq \sigma^0 - 2\Lambda^0_a \hat{N}^a \left(\bar{\Lambda}^0_\mu \hat{N}_0 + \bar{\Lambda}^b_\mu \hat{N}_b\right)\sigma^\mu \\ &= \sigma^0 - 2\Lambda^0_a \hat{N}^a \left(\bar{\Lambda}^b_0 \hat{N}_b \sigma^0 + \bar{\Lambda}^b_j \hat{N}_b \sigma^j\right), \end{aligned} \tag{2.74}$$

$$\sigma'^i = \sigma^i - 2\Lambda^i_a \hat{N}^a \left(\bar{\Lambda}^b_0 \hat{N}_b \sigma^0 + \bar{\Lambda}^b_j \hat{N}_b \sigma^j\right), \tag{2.75}$$

Let us first calculate the $\Lambda^\nu_a \hat{N}^a$ contractions,

$$\Lambda^0_a \hat{N}^a = \Lambda^0_a \frac{1}{F} P^k_a \hat{n}^k = -\boldsymbol{k}\cdot\boldsymbol{n}\frac{1}{F}, \tag{2.76}$$

$$\Lambda^i_a \hat{N}^a = \Lambda^i_a \frac{1}{F} P^k_a \hat{n}^k = \hat{n}^i \frac{1}{F}. \tag{2.77}$$

Those terms in (2.74) with $\bar{\Lambda}^b_\mu \hat{N}_b$ give,

$$\bar{\Lambda}^b_0 \hat{N}_b = \bar{\Lambda}^b_0 \frac{1}{F} P^k_b \hat{n}^k = \boldsymbol{k}\cdot\boldsymbol{n}\frac{1}{F}, \tag{2.78}$$

$$\bar{\Lambda}^b_j \hat{N}_b = \bar{\Lambda}^b_j \frac{1}{F} P^k_b \hat{n}^k = \hat{n}^j \frac{1}{F}. \tag{2.79}$$

An finally substituting into equation (2.74) it is obtained

$$\sigma'^0 = \sigma^0 - 2\boldsymbol{k}\cdot\hat{\boldsymbol{n}}\,\frac{\boldsymbol{\sigma}\cdot\hat{\boldsymbol{n}} - \boldsymbol{k}\cdot\hat{\boldsymbol{n}}\,\sigma^0}{F^2} \tag{2.80}$$

$$\sigma'^i = \sigma^i - 2\hat{n}^i\,\frac{\boldsymbol{\sigma}\cdot\hat{\boldsymbol{n}} - \boldsymbol{k}\cdot\hat{\boldsymbol{n}}\,\sigma^0}{F^2}. \tag{2.81}$$

From this preliminary expression we can already notice that the reflected ray lies on the plane defined by σ^i and $\hat{n}^i$.

Let us note that up to now we have not imposed that σ^α is a null vector. Therefore the reflection law of the equation (2.80) is valid for null or timelike 4-vectors aswell (i.e. the 4-momentum of a massive particle). For the photons (null particles) it is

obtained

$$f' = f\,\frac{1+(\boldsymbol{k}\cdot\hat{\boldsymbol{n}})\,[\,\hat{\boldsymbol{n}}\cdot(\,\boldsymbol{k}-2\,\boldsymbol{\sigma})\,]}{1-(\boldsymbol{k}\cdot\hat{\boldsymbol{n}})^2}, \tag{2.82}$$

$$\boldsymbol{\sigma}' = \frac{\left(1-(\boldsymbol{k}\cdot\hat{\boldsymbol{n}})^2\right)\boldsymbol{\sigma}+2\,(\boldsymbol{k}\cdot\hat{\boldsymbol{n}}-\boldsymbol{\sigma}\cdot\hat{\boldsymbol{n}})\,\hat{\boldsymbol{n}}}{1+(\boldsymbol{k}\cdot\hat{\boldsymbol{n}})^2-2(\boldsymbol{k}\cdot\hat{\boldsymbol{n}})\;(\boldsymbol{\sigma}\cdot\hat{\boldsymbol{n}})}. \tag{2.83}$$

Here, f' and $\boldsymbol{\sigma}'$ are the frequency and the unit direction of the reflected light ray in the reference system (t, x^i). These expressions are valid at each point of the mirror surface in arbitrary motion. Let us remind that $\boldsymbol{k} = \boldsymbol{v}_m/c$, where $\boldsymbol{v}_m$ is the coordinate velocity of the reflecting point of the mirror at the moment of reflection. Velocity $\boldsymbol{v}_m$ can be computed from any mathematical representation of the mirror surface (for example, from (2.5)).

For a timelike 4-vector p'^μ the equivalent expression is obtained as

$$p'^0 = p^0 - 2\boldsymbol{k}\cdot\hat{\boldsymbol{n}}\;\left(\frac{\boldsymbol{p}\cdot\hat{\boldsymbol{n}}-\boldsymbol{k}\cdot\hat{\boldsymbol{n}}\;p^0}{1-(\boldsymbol{k}\cdot\hat{\boldsymbol{n}})^2}\right), \tag{2.84}$$

$$p'^i = p^i - 2\hat{n}^i\;\left(\frac{\boldsymbol{p}\cdot\hat{\boldsymbol{n}}-\boldsymbol{k}\cdot\hat{\boldsymbol{n}}\;p^0}{1-(\boldsymbol{k}\cdot\hat{\boldsymbol{n}})^2}\right), \tag{2.85}$$

where p^μ is wave vector of the particle before the collision. Recalling the relations between wave vectors and frequencies and directions for a photon we see that Eqs. (2.84)–(2.85) are equivalent to (2.82)–(2.83).

Let us note two important properties of (2.82)–(2.83), also applicable to (2.84)–(2.85):

1. In the reference system (t, x^i) the reflected direction $\boldsymbol{\sigma}'$ also lies in the plane defined by the incoming ray $\boldsymbol{\sigma}$ and the normal vector $\hat{\boldsymbol{n}}$.

2. The reflected ray is only affected by the projection of the velocity $\boldsymbol{v}_m$ on the vector $\hat{\boldsymbol{n}}$.

The latter property implies that the relation between $\boldsymbol{\sigma}'$ and $\boldsymbol{\sigma}$ coincides with the usual reflection law (2.63) if the velocity $\boldsymbol{v}_m$ is perpendicular to $\hat{\boldsymbol{n}}$. This case is relevant for liquid (rotating) mirrors and was discussed by Lightman *et al.* (1975,problem 1.19), Ragazzoni & Claudi (1995) and Hickson *et al.* (1995). Our result (no relativistic

effects on reflection law in that case) coincides with that of Lightman *et al.* (1975) and Hickson *et al.* (1995).

Multiplying both sides of (2.83) by $\hat{\boldsymbol{n}}$ and using the following definitions for the angles between vectors (see Fig. 2.1)

$$-\boldsymbol{\sigma}\cdot\hat{\boldsymbol{n}} = \cos\alpha, \tag{2.86}$$

$$\boldsymbol{\sigma}'\cdot\hat{\boldsymbol{n}} = \cos\alpha', \tag{2.87}$$

$$\boldsymbol{k}\cdot\hat{\boldsymbol{n}} = k\cos\left(\varphi-\frac{\pi}{2}\right) = k\,\sin\varphi, \tag{2.88}$$

($k=|\boldsymbol{k}|=|\boldsymbol{v}_m|/c$) one obtains a relation between the angle of incidence α and angle of reflection α'

$$f' = f\,\frac{1+2\,k\,\sin\varphi\,\cos\alpha+k^2\,\sin^2\varphi}{1-k^2\,\sin^2\varphi}, \tag{2.89}$$

$$\cos\alpha' = \frac{2\,k\,\sin\varphi+\left(1+k^2\,\sin^2\varphi\right)\,\cos\alpha}{1+k^2\sin^2\varphi+2\,k\,\sin\varphi\cos\alpha}\ . \tag{2.90}$$

The latter equation can be also re-written into an equation relating $\sin\alpha$ and $\sin\alpha'$:

$$\sin\alpha' = \sin\alpha\,\frac{1-k^2\,\sin^2\varphi}{1+2\,k\,\sin\varphi\,\cos\alpha+k^2\,\sin^2\varphi}. \tag{2.91}$$

Comparing (2.89) and (2.91) one can see that $f\sin\alpha = f'\,\sin\alpha'$.

Angles α, α' and φ are illustrated in Fig. 2.1. The angle α lies between 0 and $\pi/2$ (since we always consider that the incoming light ray comes to the mirror from one particular side of the tangent plane to the mirror's surface at the point of reflection). For the same reason we have $0\le\alpha'\le\pi/2$. Angle φ lies between $-\pi/2$ and $\pi/2$. It is negative if the angle between $\boldsymbol{k}$ and $\hat{\boldsymbol{n}}$ is greater than $\pi/2$ and positive otherwise. Additionaly, our central results have been derived (2.89)–(2.90) directly from Maxwell's equations by a principle of phase matching: the phase of the incoming wave should agree with the phase of the outgoing one (e.g., Jackson (1975), Section 7.3). This generalizes the work of Bolotovskii & Stolyarov (1989) for a flat mirror moving with constant velocity. For an accelerated mirror such a treatment, however, is meaningful only as long as the conditions for geometrical optics are satisfied.

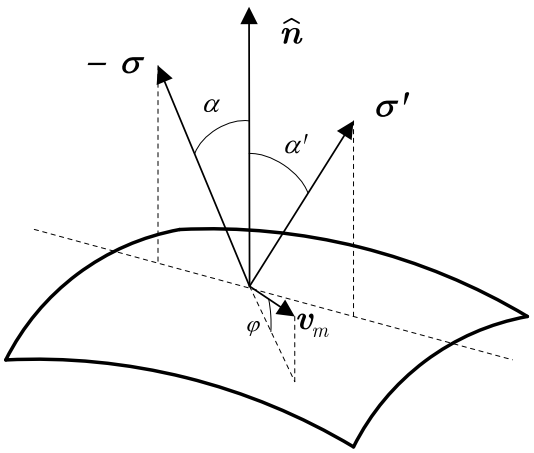

Figure 2.1: Vectors and angles at the point of reflection.

2.2.4 Low velocity limit

It is useful to derive the first-order expansion of (2.82)–(2.90) in powers of v_m/c since in practice the velocity of the mirror will be small compared to the light velocity. One gets

$$f' = f\left(1 - 2\,(\boldsymbol{\sigma}\,\hat{\boldsymbol{n}})\,(\boldsymbol{k}\cdot\hat{\boldsymbol{n}}) + \mathcal{O}(c^{-2})\right), \tag{2.92}$$

$$\begin{aligned}\boldsymbol{\sigma}' &= \boldsymbol{\sigma} - 2\,(\boldsymbol{\sigma}\cdot\hat{\boldsymbol{n}})\,\hat{\boldsymbol{n}} \\ &\quad +2\,(\boldsymbol{k}\cdot\hat{\boldsymbol{n}})\,\left[\left(1 - 2\,(\boldsymbol{\sigma}\cdot\hat{\boldsymbol{n}})^2\right)\,\hat{\boldsymbol{n}} + (\boldsymbol{\sigma}\cdot\hat{\boldsymbol{n}})\,\boldsymbol{\sigma}\right] + \mathcal{O}(c^{-2}),\end{aligned} \tag{2.93}$$

or

$$f' = f\left(1 + 2\,k\,\sin\varphi\,\cos\alpha + \mathcal{O}(c^{-2})\right), \tag{2.94}$$

$$\cos\alpha' = \cos\alpha + 2\,k\,\sin\varphi\,\sin^2\alpha + \mathcal{O}(c^{-2}), \tag{2.95}$$

$$\sin\alpha' = \sin\alpha - k\,\sin\varphi\,\sin 2\alpha + \mathcal{O}(c^{-2}). \tag{2.96}$$

The first two terms in the right-hand side of (2.93) represent just the usual reflection law and the rest contains the largest relativistic effects. Eq. (2.95) shows that

$$\alpha' - \alpha = -2\,k\,\sin\varphi\,\sin\alpha + \mathcal{O}(c^{-2}). \tag{2.97}$$

This expression can be used to estimate the difference $\alpha' - \alpha$ for many realistic situations.

2.3 General scheme of computing relativistic effects due to the rotation of an optical system

Our goal is to discuss and calculate the influence of relativistic effects on the imaging by an optical instrument with some non-inertial motion. We simplify our goal in several directions: (1) we consider here the case of optical instruments consisting of mirrors only (no lenses are considered), (2) we do not consider the effects of wave optics and work in the approximation of geometric optics (see, however, the note at the end of Section 2.5).

For an optical system consisting solely of a number of arbitrarily moving mirrors, the most important relativistic effect is the special-relativistic modification of the reflection law. That modified special-relativistic reflection law will produce a change in aberration patterns as compared to the patterns calculated by using the usual reflection law (here and below by "usual reflection law" we mean that the angles between the normal to the surface of the mirror and the incoming and reflected light ray are equal: $\alpha' = \alpha$ in Fig. 2.1). These perturbed aberration patterns could affect astrometric measurements based on an interpretation of the images obtained in the instrument's focal plane.

2.3.1 Reflection law

First, we formulate the general principles allowing one to calculate the aberration patterns within the framework of Special Relativity. Given a mirror of arbitrary shape in arbitrary motion (see Section 2.1.2 for a formal mathematical description of such an arbitrary mirror and Section 2.3.2 for a discussion of such mirrors from the physical point of view) and a light ray hitting the surface of the mirror at a given point and moment of time, we calculate the parameters of the outgoing (reflected) light ray. The simplified problem of a flat mirror moving with a constant velocity perpendicular to its surface has been considered by Einstein (1905) in the first paper on Special Relativity Theory. In the Appendix the most general case of this problem within Special Relativity is considered in great detail. Slightly modifying the arguments of

Einstein (1905) we first use Lorentz transformations to transform from a laboratory inertial reference system (t, x^i) to an inertial reference system (T, X^a) instantaneously co-moving with the element of the mirror where the reflection of a particular light ray occurs, then apply the known reflection law in that reference system and transform the reflected light ray back into the laboratory reference system. The relation of that scheme to direct calculations involving Maxwell's equations is also discussed in the Appendix. In our calculations we recover a number of known results for various particular cases. An overview of these known results and the corresponding comparison are also given. The main formula used in all the ray tracing calculations of Section 2.4 is the relativistic reflection law given by Eq. (2.83).

2.3.2 Arbitrarily shaped and moving mirrors

A very important point of the whole scheme is that the shapes of the mirrors in laboratory coordinates (t, x^i) and, possibly, the time-dependence of these shapes are assumed to be *given*. We describe the shape of each mirror by a two-parameter family of worldlines of each individual particle of the mirror denoted as $x^i_m(t; \xi, \eta)$. Here ξ and η are two continuous parameters "numbering" the particles that constitute the surface of the mirror. Clearly, for fixed values of ξ and η, function $x^i_m(t; \xi, \eta)$ represents the (t, x^i)-parametrization of the world line of the corresponding particle. For fixed t the same function $x^i_m(t; \xi, \eta)$ represents the instantaneous position and shape of the mirror in the $t = \text{const}$ hyperplane of the coordinates (t, x^i). In this case $(t = \text{const})$ the parameters ξ and η give a non-degenerated two-dimensional coordinate chart on the surface of the mirror. We consider $x^i_m(t; \xi, \eta)$ to be differentiable with respect to ξ and η. This means that the coordinate representation of the surface is a smooth two-dimensional surface for each moment of coordinate time t.

In general there is no inertial reference system where the whole system or any of its mirrors is at rest. In the special cases when such an inertial rest-frame of a mirror does exist, one should consider the shape of the mirror in that rest-frame. In the practical cases considered below such rest-frames do not exist. Moreover, the size of the mirrors is so large that we cannot assume that the velocities of all points of the mirror are approximately constant in any inertial reference system.

We do not consider the question of deformations of the mirrors due to their non-inertial (for example, rotational) motion (i.e., the relation between the intended shapes of the mirrors during their manufacturing and their shapes, e.g., in a rotating satel-

lite, in coordinates (t, x^i)). The behaviour of a mirror as a physical body is a separate question, a rigorous relativistic treatment of which would require at least a special-relativistic theory of elasticity. As long as the angular velocity is constant the deformations and special-relativistic effects on the shape (e.g. Lorentz contraction) are also constant. In this case a rigidly rotating mirror can be considered to be Born-rigid (Pauli 1958,Section 45). We can also argue that the constant deformations are assumed to be properly taken into account during manufacturing so that the rotating mirrors have the assumed forms. One may argue that the mirrors could be made active to retain the prescribed form (which is the case for many larger Earth-bound instruments, but may appear to be a rather bizarre argument in some other cases).

2.3.3 Observable aberration patterns

The last issue is the definition of the observing (imaging) device. In analogy to our representation of the mirrors we first define a coordinate "plane" $x^i_f(t;\zeta,\chi)$ in laboratory coordinates (t, x^i) that coincides with the focal "plane" of the instrument in the Newtonian case. In many cases (e.g. for the case considered in Section 2.4 below) $x^i_f(t;\zeta,\chi)$ can be taken to be a plane in the considered coordinates (that is, for any moment of time there exist $n^i(t)$ independent of ζ and χ such that $\boldsymbol{x}_f \cdot \boldsymbol{n} = 0$). The aberration patterns we calculate below are defined as the set of points at which the light rays from a source hit that coordinate focal plane at some moment $t = t_{\rm obs} = \text{const}$. Generally speaking the aberration patterns cannot be considered as "infinitely small". This means that there is no inertial coordinate system in which the part of the detector (that is, of the focal "plane") registering an aberration pattern can be considered at rest.

If the patterns are "small enough" (which is the typical case for reasonable high-quality optical instruments) one could introduce an inertial reference system (τ, ρ^i) instantaneously co-moving with some central point of the aberration pattern and define the "observable" pattern as a set of points at which the light rays from a source hit that coordinate focal plane at some moment $\tau = \tau_{\rm obs} = \text{const}$ (here one should also take into account the relativistic effects in spatial coordinates and correspondingly treat Lorentz contraction etc.). First, although this approach seems to be more adequate for non-inertial motion it still gives a coordinate-dependent picture because of finite extension of the patterns. Second, we have explicitly checked that this additional Lorentz boost does not influence any of the figures and numerical results given

below.

Note that we are interesting in prediction of the changes in the aberration patterns compared to the prediction made for the "same" optical device without rotation and using Newtonian geometric optics (this latter prediction is typically available from the manufacturers of the instrumentation). From this point of view, our definition of "observed" aberration pattern is adequate. In more realistic case one has to model the process of observation in much more detail (e.g., CCD orientation and position within the instrument, CCD clocking, averaging, TDI mode etc.). Such a detailed modelling is however unnecessary for the purposes of this paper.

Summarizing, our aberration pattern modelling consists of (1) fixing the models of the mirrors $x^i_m(t;\xi,\eta)$ and the focal plane $x^i_f(t;\zeta,\chi)$, and (2) tracing a grid of incoming light rays, which interact with the optical system only at the moments of reflection according to (2.83), until the point of intersection with the focal plane $x^i_f(t;\zeta,\chi)$, and (3) forming the aberration pattern itself and/or calculating its photocenter.

2.4 Relativistic astrometric effects due to rotational motion of the satellite

In order to evaluate the relativistic effects in the aberration patterns of planned scanning astrometric instruments, we consider an extended optical system rotating rigidly with a constant angular velocity relative to the inertial reference system (t, x^i). For a scanning astrometric satellite the real angular velocity is not constant (e.g., because of the required scanning law), but its changes are small and slow, and will be neglected here. Rigid rotation of the optical instrument means that the whole instrument is at rest in a reference system (t, y^i) related to the inertial laboratory reference system (t, x^i) as $y^i = R^i{}_j\, x^j$, $R^i{}_j$ being an orthogonal (rotational) matrix.

To calculate the aberration patterns of several optical systems discussed below we have developed a numerical ray tracing code in Java allowing us to calculate aberration patterns for an arbitrary optical system rigidly rotating in our laboratory coordinates. Each mirror in the system can be individually shaped and oriented in those coordinates. The code allows us to control all intermediate calculations as well as the overall numerical accuracy.

Parameters of the optical systems (size of the mirrors, focal distance, distance of the primary mirror from the rotational axis and angular velocity) considered in Sections 2.4.1 and 2.4.2 below are chosen to qualitatively represent some principal features of planned astrometric missions like Gaia (Perryman *et al.* 2001) or JASMINE (Gouda *et al.* 2002), where a scanning satellite comprising two astrometric telescopes continuously rotates with an angular velocity of $\Omega \sim 60\ ''/\mathrm{s}$.

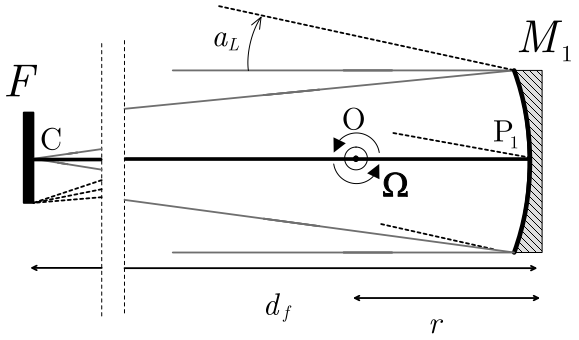

Figure 2.2: A rotating optical system with one mirror.

2.4.1 A one-mirror optical system

The first optical system that we will study consists of one rotating parabolic mirror. A diagram of this optical system is given on Fig. 2.2. The parabolic mirror M_1 is a square mirror of size 1.5 m $\times$ 1.5 m and a focal distance of $d_f = 46.67$ m. The receiver at the focal plane is considered to be 0.814 m $\times$ 0.814 m in size providing a field of view of $\sim 1\,\mathrm{deg} \times 1\,\mathrm{deg}$. This roughly corresponds to the astrometric instruments of Gaia. The rotational axis goes through the origin O of our coordinates perpendicular to the plane of Fig. 2.2. The distance from O to the center of the primary mirror (being the vertex of the parabola) P_1 is $r = 1.5$ m. The distance from P_1 to the center of the focal plane C is obviously the focal distance $d_f = 46.67$ m. The whole optical system is rotating with respect to O with an angular velocity $\Omega = 60\ ''/\mathrm{s}$. The *optical axis* of the system is defined as the path of the light ray which goes perpendicular to the surface of the primary mirror through its center provided that the system does not rotate (represented in Fig. 2.2 by the bold horizontal line going from P_1 to C). Without rotation light rays parallel to the optical axis converge to the single point C in the

focal plane. The direction of an incoming light ray is parameterized with two angles: the *along scan* angle a_L (this angle is changing continuously for a given source because of the rotation; see Fig. 2.2) and the *across scan* angle a_C. The along scan angle is the angle between the instantaneous directions of the optical axis and the incoming light ray projected into the plane containing the optical axis and perpendicular to the vector of angular velocity of the system (i.e., the plane of Fig. 2.2). The across scan angle is the angle between the instantaneous directions of the optical axis and the incoming light ray projected into the plane containing both the optical axis and the vector of angular velocity. The along scan and across scan angles are widely used in the context of scanning astrometric missions like HIPPARCOS (Perryman *et al.* 1997a) and Gaia (Perryman *et al.* 2001).

In order to evaluate the effects due to the rotation of the instrument we calculate aberration patterns for different values of the field angles a_L and a_C as well as the differences of the photocenters for each considered case. To compute aberration patterns a rectangular grid of parallel incoming light rays with direction characterized by some given a_L and a_C is generated. These light rays are then traced through the optical system until they intersect the focal plane. The coordinates of the intersection points produce the corresponding aberration pattern in the focal plane (see, e.g., Figs. 2.3 and Fig.2.5). The photocenter of a pattern is defined as the mean position of all points of that pattern.

We distinguish between two different effects changing the aberration patterns (and their photocenters) of a rotating instrument compared to those of an identical non-rotating instrument. The first effect is the change of orientation of various reflecting surfaces during the time delays needed for a light ray to propagate from the primary mirror to the focal plane. The second effect is the difference between the usual reflection law and the relativistic one.

Clearly, the propagation delays are related only to the finiteness of the light velocity. The delays appear also in the non-rotating case, but can be completely ignored since the orientation of all reflecting surfaces is constant. For a rotating instrument the propagation delays mean, in particular, that the light rays producing an aberration pattern (that is, the light rays intersecting the focal plane at the same moment of time) hit the primary mirror (and, generally speaking, all other mirrors) at different times. The effect of propagation delays can be directly calculated in our ray tracing software by using a specially designed iterative scheme.

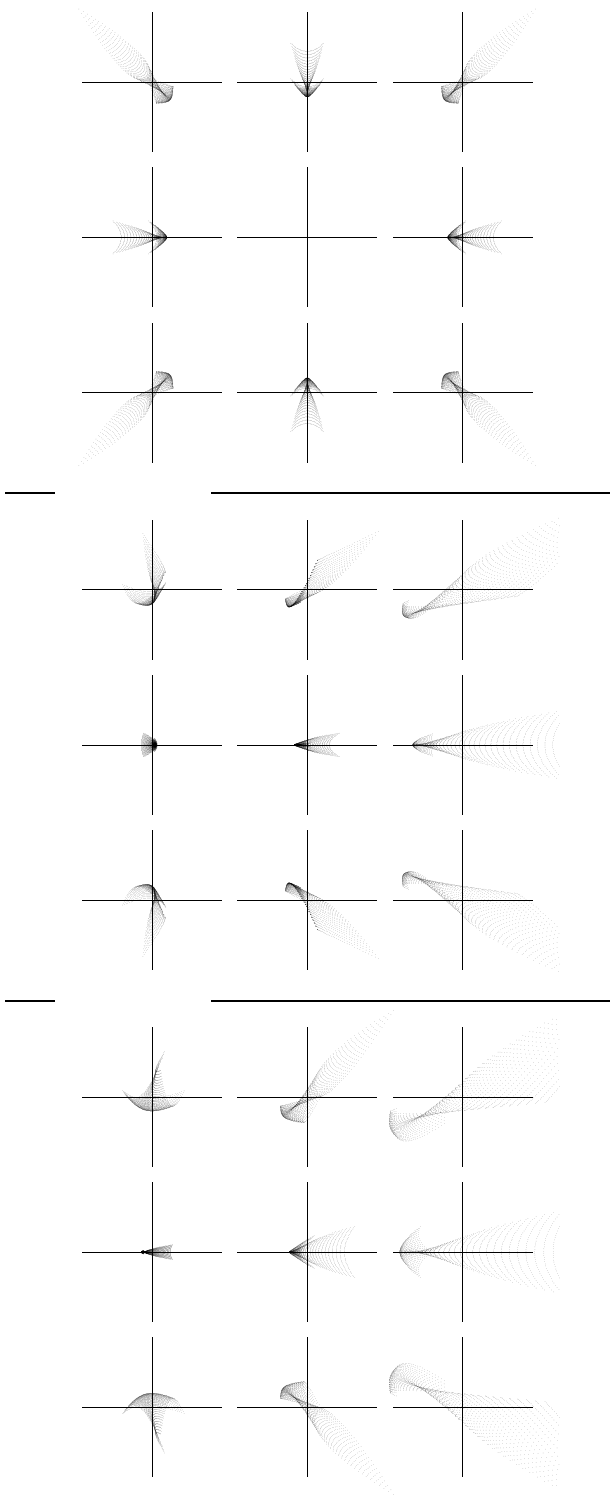

Figure 2.3: Aberration patterns for the one-mirror system: a non-rotating instrument (upper panel), a rotating instrument considering the light propagation delays and using the usual reflection law (middle panel, and a rotating instrument considering both the light propagation delays and the relativistic reflection law (lower panel).

There are several effects related to the propagation delays such as just the constant shift of the aberration patterns due to the change of the orientation of the instrument during the propagation time: an image of a star observed at time $t_{\rm obs}$ is produced by the light rays from the star that hit the primary mirror at time $\sim\ t_{\rm obs} - d_f/c$ when the orientation of the mirror differed by $\sim\ \Omega\, d_f/c$ from the orientation at $t_{\rm obs}$. Similar constant shifts will be caused by intermediate mirrors and by the motion of the focal plane during the propagation delay: during the light propagation the focal plane is moving and the photon hits the focal plane at different positions which correspond to different positions on the sky. This can be computed as $\sim\ \Omega\,(d_f - r)/c$ for the one-mirror system depicted in Fig. 2.2. Note that in the limit when the center of rotation is infinitely far from the instrument (that is, when all parts of the instrument effectively have the same velocity), these constant shifts are fully equivalent to the normal aberration of light. The constant shifts of the aberration patterns, that can be relatively large, lead only to a constant time shift in the orientation parameters of the satellite derived from astrometric observations: the orientation obtained from observations at $t_{\rm obs}$ is actually the orientation the satellite had some small earlier time interval. This has only slight consequences on the measurements for any existing or planned astrometric projects. However, the propagation delays also lead to a deformation of the aberration patterns that depends on the field angles. These aberration pattern deformations together with the deformations due to the relativistic reflection law can be important as illustrated below. The distortions of the shape of the patterns are caused by different velocities of different parts of both mirrors and slightly different incident angles for each mirror.

For the one-mirror case these effects are illustrated in Fig. 2.3. The nine patterns in each of the three panels correspond to nine combinations of the field angles with $a_L = -30', 0', +30'$ (horizontal direction) and $a_C = -30', 0', +30'$ (vertical direction). For the focal length $d_f = 46.67$ m, $30'$ corresponds to about 407 mm in the focal plane coordinates. The size of the axes in focal plane coordinates is 0.5 mm $\times$ 0.5 mm for all patterns. The aberration patterns in the upper panel are calculated for a non-rotating instrument. In the middle panel the aberration patterns are obtained using the usual reflection law, but the effects of the light propagation delays are taken into account. In the lower panel both the light propagation delays and the relativistic reflection law are used. An extremely high angular velocity $\Omega = 5 \times 10^9\ ''/$s is used to exaggerate the distortion and make it clearly visible. The three rightmost patterns in

	$\delta a_L \times 10^{-3}\mu$as			$\delta a_C \times 10^{-3}\mu$as		
$a_C \setminus a_L$	$-30'$	$0'$	$+30'$	$-30'$	$0'$	$+30'$
$-30'$	0.9	-1.2	0.9	1.4	0.0	-1.4
$0'$	0.2	-1.9	0.2	0.0	0.0	0.0
$30'$	0.9	-1.2	0.9	-1.4	0.0	1.4

Table 2.1: The shifts of the aberration patterns for the one-mirror optical system rotating at $\Omega = 60\ ''/\text{s}$ after subtracting the mean value $\delta\overline{a}_L^d + \delta\overline{a}_L^r = 18.3834\ \mu$as.

both the middle and the lower panels are much larger than all other patterns. These six patterns extend to the left from the edge of the Figure by about 3 times the size of the horizontal axis in each pattern. These parts of the patterns are not shown in Fig. 2.3. The axes for each pattern are centered at the corresponding photocenter. Note that these photocenters are significantly shifted between the three panels due to the constant propagation time effects discussed above.

Since for the one-mirror instrument the angle of each light ray with respect to the normal to the mirror at each point of the surface is not greater than $30'$, the effect of the relativistic reflection law on aberration patterns is very small. At point P_1 the velocity vector is perpendicular to the normal to the mirror. Therefore, at this point for any a_L and a_C the relativistic reflection law coincides with the usual one (see Eq. (2.83)). A light ray going through that point will intersect the focal plane at the same point for both the usual and relativistic reflection laws. The light rays of the same grid not going through P_1 have different images when using the usual reflection law and the relativistic one.

For realistic $\Omega = 60\ ''/\text{s}$ the mean shift of the photocenters due to the propagation delays amount to $\delta\overline{a}_L^d = 18.3842\ \mu$as. Note that this number can be reproduced with good accuracy by $\Omega\,(2d_f - r)/c = 18.3807\ \mu$as as discussed above. The field-angle dependent change of the photocenters is at the level of 0.001 μas and is shown in Table 2.1. The change of the photocenters due to the relativistic reflection law is a shift in the along-scan direction $\delta a_L \approx \delta\overline{a}_L^r = -0.0008\ \mu$as and is independent of a_L and a_C at the level of 0.0001 μas.

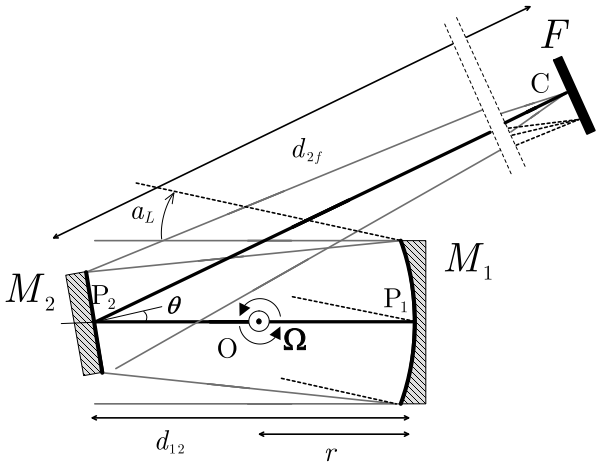

Figure 2.4: Two-mirror optical system.

2.4.2 A two-mirror optical system

Real optical systems usually have more than one mirror. Often the instruments involve mirrors inclined by about 45 deg to the optical axis (i.e., Nasmith focus, beam combiners, beam splitters, etc.). In this case the effects of the relativistic reflection law on the aberration pattern are significantly larger than in the case discussed above. Here we consider an optical system consisting of one parabolic primary mirror and one flat secondary mirror as depicted in Fig. 2.4. A flat secondary mirror M_2 has been added to the optical system depicted in Fig. 2.2. The distance from P_1 to center of the flat mirror P_2 is d_{12}. The whole system is again rigidly rotating with a constant angular velocity Ω in laboratory coordinates. The flat mirror is inclined at an angle θ with respect to the optical axis of the primary mirror. The focal plane position depends on the angle θ. The distance from P_1 to P_2 is $d_{12} = 3$ m, and the distance from P_1 to the rotational axis O is $r = 1.5$ m. The distance from P_2 to the center C of the focal plane is $d_f - d_{12} = d_{2f} = 43.67$ m. The bold line in Fig. 2.4 representing the optical axis goes from P_1 to P_2 and then to the focal plane center C.

We repeat the ray tracing calculations as described in Section 2.4.1 above with this additional flat mirror. We use three different configurations of the flat mirror with inclination angles $\theta = +45$ deg, $\theta = 0$, and $\theta = -45$ deg. Figure 2.5 shows the

aberration patterns obtained with $\theta = 45\,\mathrm{deg}$ (again for a large angular velocity of $\Omega = 5\times10^{7}{}''/\mathrm{s}$, 100 times lower than for Fig. 2.3, was used in order to make the effects visible). The same 9 combinations of a_L and a_C, and the same size and centering of the axes are used for each panel as described above for Fig. 2.3. The upper panel shows the aberration patterns for a non-rotating instrument ($\Omega = 0$). These patterns are identical to those in the left panel of Fig. 2.2. Clearly, the aberration patterns for the rotating instrument, the middle and the lower panel look differently to Fig. 2.3. Numerical values of the shifts of the photocenters δa_L and δa_C for $\Omega = 60\ ''/\mathrm{s}$ are presented in Table 2.2 for inclination angles $\theta = 45\,\mathrm{deg}, 0\,\mathrm{deg}, -45\,\mathrm{deg}$. The mean constant shift $\delta\overline{a}_L^{\,d}$ of the patterns due to the light propagation delays and $\delta\overline{a}_L^{\,r}$ due to the relativistic reflection law are given at the top of each table. The tables show the part of the total shifts dependent on the field angles. The position-dependent effects in $\delta a_L^{\,d}$ and $\delta a_L^{\,r}$ have opposite signs and are 2-3 times larger than the total shift $\delta a_L = \delta a_L^{\,d} + \delta a_L^{\,r}$. On the contrary, the effects in $\delta a_C^{\,d}$ and $\delta a_C^{\,r}$ are of the same sign and are about 2 times less than in the sum $\delta a_C = \delta a_C^{\,d} + \delta a_C^{\,r}$.

As for the one-mirror system, for any value of θ the shifts due to the light propagation delays exceed the level of 1 μas and amount to $\delta\overline{a}_L^{\,d} \sim 2\mu$as. For the two-mirror system $\delta\overline{a}_L^{\,d}$ is significantly lower than for the one-mirror system since the effects of the motion of the primary mirror and the motion of the focal plane largely compensate each other if just one intermediate mirror is present.

For $\theta = 0$ the shifts due to the relativistic deflection law are again very small as was the case for the one-mirror system. The situation with these shifts is different for $\theta = \pm45\,\mathrm{deg}$ where the mean shift $\delta\overline{a}_L^{\,r} \sim 0.3\,\mu$as. For $\theta = \pm45\,\mathrm{deg}$ all the light rays hit the flat surface at an angle of about $\alpha = \pm45\,\mathrm{deg}$ with respect to the normal and the factor $|\sin\alpha|$ appearing in (2.97) is of the order of $1/\sqrt{2} \approx 0.7$. Each light ray of the grid hits the mirror at a slightly different value of α, but the main perturbation due to the relativistic reflection law can be estimated considering the light ray going along the optical axis. Using (2.97) we obtain

$$\delta_2 \quad \simeq \quad 2\,\frac{v}{c}\,\frac{d_{2f}}{d_f}\,\sin^2\theta, \tag{2.98}$$

where d_{2f} is again the distance between P_2 and the focal plane center as shown in Fig. 2.4, and v is the velocity of the point of the mirror lying on the optical axis

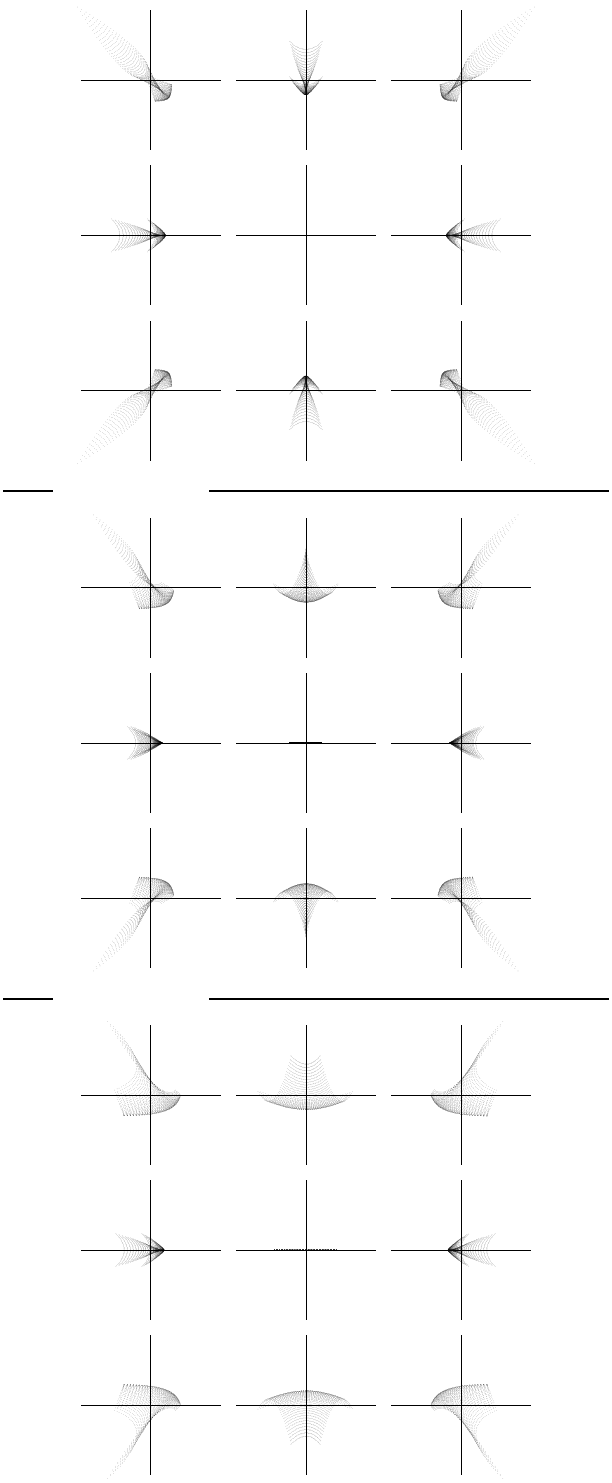

Figure 2.5: Aberration patterns for the two-mirror system with $\theta = 45\,\mathrm{deg}$: non-rotating instrument (upper panel), rotating instrument considering the light propagation delays and using the usual reflection law (middle panel), and rotating instrument considering both the light propagation delays and the relativistic reflection law (lower panel).

$\theta = -45\,\mathrm{deg}: \quad \delta\overline{a}_L^{\,d} = 1.7422\,\mu\mathrm{as}, \quad \delta\overline{a}_L^{\,r} = -0.2776\,\mu\mathrm{as}$

	$\delta a_L \times 10^{-3}\mu$as			$\delta a_C \times 10^{-3}\mu$as		
$a_C \setminus a_L$	$-30'$	$0'$	$+30'$	$-30'$	$0'$	$+30'$
$-30'$	4.6	0.0	−4.5	4.8	4.9	4.9
$0'$	4.5	−0.1	−4.6	0.0	0.0	0.0
$30'$	4.6	0.0	−4.5	−4.8	−4.9	−4.9

$\theta = 0\,\mathrm{deg}: \quad \delta\overline{a}_L^{\,d} = 2.0246\,\mu\mathrm{as}, \quad \delta\overline{a}_L^{\,r} = 0.0006\,\mu\mathrm{as}$

	$\delta a_L \times 10^{-3}\mu$as			$\delta a_C \times 10^{-3}\mu$as		
$a_C \setminus a_L$	$-30'$	$0'$	$+30'$	$-30'$	$0'$	$+30'$
$-30'$	0.0	0.0	0.0	0.0	0.0	0.0
$0'$	0.0	0.0	0.0	0.0	0.0	0.0
$30'$	0.0	0.0	0.0	0.0	0.0	0.0

$\theta = +45\,\mathrm{deg}: \quad \delta\overline{a}_L^{\,d} = 1.7422\,\mu\mathrm{as}, \quad \delta\overline{a}_L^{\,r} = -0.2776\,\mu\mathrm{as}$

	$\delta a_L \times 10^{-3}\mu$as			$\delta a_C \times 10^{-3}\mu$as		
$a_C \setminus a_L$	$-30'$	$0'$	$+30'$	$-30'$	$0'$	$+30'$
$-30'$	−4.5	0.0	4.6	−4.9	−4.9	−4.8
$0'$	−4.6	−0.1	4.5	0.0	0.0	0.0
$30'$	−4.5	0.0	4.6	4.9	4.9	4.8

Table 2.2: The shifts of the aberration patterns for the two-mirror optical system rotating at $\Omega = 60\ ''/\mathrm{s}$ for three values of θ after subtracting the specified mean values $\delta\overline{a}_L^{\,d} + \delta\overline{a}_L^{\,r}$.

($v = \Omega\,(d_{12} - r)$ for the case depicted in Fig. 2.4). One can check that the mean constant shifts $\delta\overline{a}_L^{\,r}$ as shown in Table 2.2 can be recovered from (2.98) almost exactly. If more flat (or almost flat) mirrors are added, the expression can be generalized by

$$|\delta_i| \quad \simeq \quad \left| 2\,\frac{v_i}{c}\,\frac{d_{if}}{d_f}\,\sin\theta_i\,\sin\varphi_i \right|. \tag{2.99}$$

The index i is used to enumerate the surfaces along the light path, $i = 1$ corresponding to the primary mirror. In our case $i = 1$ is the parabolic mirror M_1 and $i = 2$ is the

flat mirror M_2. The angle φ_i is the angle between the velocity and the surface at the intersection of the mirror M_i with the optical axis applying the conventions described on Fig. 2.1. θ_i is the angle between the optical axis and the normal to the surface at the point of intersection. The quantity d_{if} is the distance from the center of the focal plane C to the point where the optical axis crosses the i-th mirror. As defined above d_f is the focal distance of the optical system.

The presence of the factor d_{if}/d_f in (2.98) and (2.99) can be explained by a small perturbation Δ of the propagation direction of a light ray by a mirror located at a distance d_{if} from the focal plane causing a linear shift in the focal plane $d_{if}\,\Delta$ which is efficiently interpreted as an angular shift of $d_{if}/d_f\,\Delta$. In the more general case when the intermediate reflecting surfaces are not flat, Eq. (2.99) is no longer valid, but gives a reasonable idea of the magnitude of the effect provided that all reflecting surfaces are not too different from a flat mirror. The cumulative effect of a series of (almost) flat mirrors will not be a direct addition of all δ_i since the relativistic perturbation may occur at different planes. An analytic expression in vector form can be derived for the combined effect, but since the resulting formula is complicated and still a rough approximation it will not be discussed here. Eq. (2.99) also has been checked for some other optical systems involving more reflecting surfaces of different shapes, sizes and velocities. A good agreement with the numbers from numerical ray tracing was obtained in all cases.

2.5 Concluding remarks

We have considered in detail the main relativistic effect on the imaging by a rotating optical system which is produced by the relativistic modification of the reflection law. We have considered two simple optical systems containing one and two mirrors. Although the size of the primary mirror, the focal length and the angular velocity of rotation of both systems were defined to agree with the corresponding parameters of Gaia, it is not clear how large these effects will be for the real optical scheme of Gaia. We have seen that the effects are small for the one-mirror system and that they may amount of 0.3 μas for the two-mirror system. For a real Gaia optical scheme the effect may be much larger because of the presence of several inclined mirrors. The two examples of a rotating optical system considered above do not allow us to predict the relativity-induced photocenter shifts for a real optical system like Gaia. A detailed

calculation of the photocenter shifts in principle can be done using the ray tracing software developed for this investigation.

The part of the effect that does not depend on the position in the focal plane can be interpreted as a constant change in the orientation of the satellite (as discussed at the end of the previous Section for propagation delay effects). Moreover, if a satellite (like Gaia) has two optically different telescopes, the difference in the main effects for these two telescopes can be interpreted as a change in the angle between the two instruments.

In this paper we confined ourselves to ray tracing in the geometric optics limit. A more strict way to analyze the imaging by a rotating optical system is to apply wave optics and calculate corresponding intensity patterns (PSF or similar characteristics). The intensity patterns would then allow us to predict the observable shifts of the photocenters more reliably than the aberration patterns used in this paper. Preliminary calculation with a simplified model fosters the hope that at optical wavelengths the differences in the photocenter shifts calculated from ray tracing and from wave optics are negligible. However, the effects of propagation delays due to the rotation of the telescope may play a role. This deserves separate investigation.

Chapter 3

Astrometric Light-Travel Time signature of sources in nonlinear motion

3.1 Introduction and notation comments

Advances producing very precise astrometric measurements come essentially from space-borne astrometric missions like SIM(Shao 1998), GAIA(Perryman *et al.* 2001) or JASMINE (Gouda *et al.* 2002), and require a revision of the classic astrometric assumptions at many levels. Some of the concepts that are being reviewed carefully are those involving light signal propagation (Klioner 2003; Le Poncin-Lafitte & Teyssandier 2004) and the description of the astronomical sources and observers (Klioner 2004) in the context of the IAU resolutions (Soffel *et al.* 2003) that aim to define a consistent framework to model astronomical observations.

This effort involves many groups and individuals around the world and one relevant aspect is the appropriate description of stellar motion. This chapter focuses on the impact of Light-Travel Time (LTT) on the observed direction of a source outside the solar system. Such considerations are as old as modern astronomy itself; in the 17^{th} century Ole Römer used it to give the first estimation of the velocity of light.

In solar system dynamics, light travel delays are already widely considered and

applied. Our aim is to show that it is also relevant for distant objects($d > 1\ pc$) and to develop analytic expressions to include the astrometric LTT signature in precise astrometric modeling. We will provide an expression which is algorithmically efficient and fully compatible with the IAU standards (Soffel *et al.* 2003) to the required level of accuracy. A full scheme of a more general astrometric model compatible with the BCRS is given in Klioner (2003). The present work may be seen as a refinement of the formulae given there to generalize stellar motion.

The first two Sections are devoted to establishing the physical framework and defining the relevant quantities. Section 3.3 is devoted to determining the relation between the emission time interval Δt_e and the observation time interval Δt_{obs} to the required accuracy for astrometric purposes.

The baseline astrometric model is stated in Section 3.4.1 where the expression for a point source in linear motion is developed. There we define the concept of *Linear Reference Motion*(LRM) which will be very useful in the later developments. The same development for the source in linear motion was proposed by Klioner & Kopeikin (1992), where the LTT due to the observer's position was already included. Light-Travel Time effects on sources in linear motion and their relation to constant radial velocities is a topic extensively discussed in the literature and directly related to apparent superluminal motion. A good review of this issue is found in Lindegren & Dravins (2003). In Section 3.4.2, the astrometric model is naturally extended to sources in nonlinear motion. A more detailed study of radial nonlinear motion using spectroscopic measurements in the post-Newtonian framework can be found in Kopeikin & Ozernoy (1999). Since the spectroscopic techniques are more sensitive to the local environment of the sources, a more sophisticated model using a larger set of reference systems is required there, and very precise information can be extracted.

Section 3.5 obtains a quantitative description of the astrometric LTT signature for a point source. The LTT signature appears as a second order correction as the *astrometric radial velocity* described in Lindegren & Dravins (2003)).

In Section 3.6, a series of examples show how the LTT signature carries information about the radial geometry of the trajectory of a source. This is of particular interest in binary systems or objects in Keplerian orbits(such as exoplanetary systems), because resolved LTT signatures may lead to the determination of the full set of orbital parameters without spectroscopic measurements, as is commonly required (see Batten 1973,chap. 1).

Section 3.8 provides heuristic relations to evaluate the significance of the LTT effects in the geometrical characterization of any astronomical structure.

The use of LTT effects in epoch observations to determine properties of sources at stellar distances was first proposed by Irwin (1952), whose work is applicable to binary systems with at least one variable component. See Ribas *et al.* (2002) as an example of the use of this technique. Similar and more sophisticated models are used in precise pulsar timing. The timing measurements have been very fruitful in the field of millisecond pulsars in multiple systems. A pulsar works as an ultrastable clock and the time of arrival of the pulses can be measured very precisely in the radio range. A precise theoretical scheme using pulsar timming observations to test general relativity and obtain physical information of a given system is provided in Kopeikin (1995) and Kopeikin (1996). From the observational point of view, some of the most remarkable works are the detection of the first exoplanetary system around PSR1257+12 as reported by Wolszczan & Frail (1992), and the tests of general relativity carried out observing PSR J0437-4715 by van Straten *et al.* (2001).

We summarize some notation issues which only apply to this chapter.

- $\langle \boldsymbol{a} \rangle$ means that the vector must be normalized using its own Euclidean norm $\langle \boldsymbol{a} \rangle = \frac{\boldsymbol{a}}{\|a\|}$.
- A symbol p inside square brackets $[\ldots]$ after a symbol f, means that $f[p]$ is an explicit function of p. This notation is used thoughout this chapter since the arguments of some functions function may appear ambiguous to the reader. In this chapter, round brackets $(\ldots)$ are exclusively used to group algebraic expressions.

3.2 Trajectories, quantities and reference system

Our purpose is to determine the observed direction of a moving object from the position of an observer at rest with respect to the barycenter of the solar system in absence of gravitational fields. To do that, one must describe the motion of a source in terms of the observation instant t_{obs} instead of the emission instant t_e. The relation between an emission time interval Δt_e and its corresponding observation time interval Δt_{obs} will be nonlinear and time dependent due to the nonlinear change

of the distance a light signal must cover. This nonlinear time dependence will add additional apparent nonlinear terms to its motion on the celestial sphere.

We restrict the discussion to a particular inertial frame of special relativity where the space-time metric is assumed to be the *Minkowsky* metric with signature $(-\ +\ +\ +)$. All the quantities and vectors refer to the BCRS spatial coordinates x^i and the time coordinate t describing the events is TCB – see Brumberg & Groten (2001). The BCRS metric is not a *Minkowsky* metric, but since the astrometric LTT signature is already very small, the gravitational light bending and the kinematical aberration can be treated as *a posteriori* effects to the observed direction (see Klioner (2003)). The trajectory of a point source is described as a Linear Reference Motion $\boldsymbol{x}_{LRM}[t]$ plus a nonlinear shift $\boldsymbol{D}[t]$. The spatial part of the trajectory of the *source* in BCRS coordinates is given by

$$\boldsymbol{x_s}[t] = \boldsymbol{x}_{LRM}[t] + \boldsymbol{D}[t] \ , \tag{3.1}$$

$$\boldsymbol{x}_{LRM}[t] = \boldsymbol{x}^0_{LRM} + \boldsymbol{v}^0_{LRM}\left(t - t^0_e\right) \ , \tag{3.2}$$

where $\boldsymbol{x}^0_{LRM}$ are the coordinates of the LRM at some instant t^0_e. This initial instant will be discussed more precisely below. Formally, the constant velocity term $\boldsymbol{v}^0_{LRM}$ could be included in $\boldsymbol{D}[t]$, but it is very useful to keep it apart in order to define properly the *Barycentric astrometric parameters*(see Section 3.4.1) and relate them to the physical quantities in (3.1). As an example, $\boldsymbol{x}^0_{LRM}$ and $\boldsymbol{v}^0_{LRM}$ describe the motion of the center of mass of a binary system and $\boldsymbol{D}$ describes the orbital motion of one of the components.

The value of coordinate time t at the emission event E is denoted by $t_e = t[E]$. The spatial coordinates $\boldsymbol{x_s}$ at the emission event (which coincide with the spatial coordinates of the *source*) are denoted by $\boldsymbol{x_s}[t_e]$. In the same way the value of the coordinate time at the observation event is $t[Obs] = t_{obs}$ and the spatial coordinates of such an event are $\boldsymbol{x}_{obs}[t_{obs}]$. Please note that t_e and t_{obs} are both given in the same time scale, which is TCB.

Since in Minkowsky space-time the light rays follow straight lines, the spatial vector joining an event of emission at t_e and an event of observation at t_{obs} defines the *observed unit direction* as

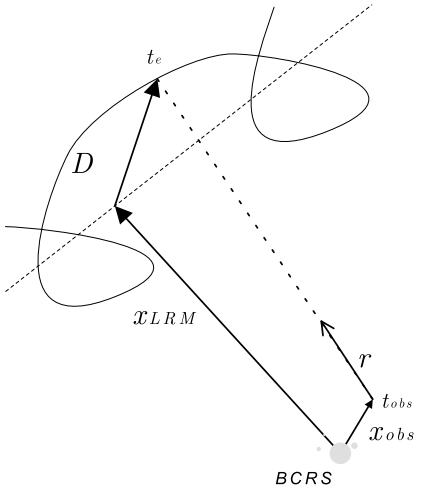

Figure 3.1: Scheme of the vectors involved in the computation of the observed direction at a given event of observation. The vector $\boldsymbol{x}_{LRM}$ is used to define a fiducial Linear Reference Motion, which could be, for example, the trajectory of the center of mass of a binary system. The shift vector $\boldsymbol{D}$ is the nonlinear contribution to the motion. Using again the example of the binary systems, it might be the orbital motion of a component around the center of mass of the system. The little vector $\boldsymbol{r}$ is the observed direction of the incoming light ray at the event of observation.

$$\boldsymbol{r} \quad = \quad \langle \boldsymbol{x_s}\left[t_e\right] - \boldsymbol{x}_{obs}\left[t_{obs}\right] \rangle \, . \tag{3.3}$$

For the later developments, we need to identify the *small time intervals*

$$\mathcal{O}(\epsilon) \sim \frac{\boldsymbol{v}^0_{LRM}\Delta t}{c} \; ; \; \frac{\boldsymbol{D}}{c} \; ; \frac{\boldsymbol{x}_{obs}}{c} \; . \tag{3.4}$$

The vectors in (3.4) have dimensions of time and have typical absolute values going from some minutes to several hours or days (or even years). They are small compared

to the time that a light signal takes to propagate from the emitting source to the observer (typically several years for galactic objects).

From now on, the module $\|\boldsymbol{x}^0_{LRM}\|$ will be written as x^0_{LRM} to simplify the notation. It is also useful to introduce the *small adimensional* quantities

$$\mathcal{O}(1) \sim \frac{\boldsymbol{v}^0_{LRM}\Delta t}{x^0_{LRM}} \; ; \; \frac{\boldsymbol{D}}{x^0_{LRM}} \; ; \frac{\boldsymbol{x}_{obs}}{x^0_{LRM}} \; . \tag{3.5}$$

Relations (3.5) impose that the initial distance between the source and the observer x^0_{LRM} must be much larger than all the other time-dependent displacements $\boldsymbol{v}^0_{LRM}\Delta t$, $\boldsymbol{D}$ and $\boldsymbol{x}_{obs}$. This requirement is usual in the astrometric modeling of objects beyond the solar system. We define the *barycentric reference direction* $\boldsymbol{l_0}$ as the unit vector

$$\boldsymbol{l_0} = \frac{\boldsymbol{x}^0_{LRM}}{x^0_{LRM}} \; , \tag{3.6}$$

which is the direction towards the position of the LRM (i.e. the center of mass of a binary system) given by an observer at the BCRS origin at a given reference instant t^0_{obs}, usually called *barycentric reference epoch*.

With the exception of the initial direction parameterized through two angles, only the parameters producing time dependent changes in the observed direction will produce measurable effects. Despite the frequent appearance of t^0_e throughout the paper, this parameter is not directly measurable. The physical quantities producing time dependent effects are x^0_{LRM}, $\boldsymbol{v}^0_{LRM}$, $\boldsymbol{D}$. They depend only on t^0_e in their *formal* definition implicitly given in (3.1).

3.3 Equation of time delay

In the most general case, the interval of time between the event of observation and the event of emission is related to the *spatial coordinate distance* as

$$
\begin{aligned}
(t_{obs} - t_e) &= \frac{1}{c}\|\boldsymbol{x}_{obs}\,[t_{obs}] - \boldsymbol{x}_{\boldsymbol{s}}\,[t_e]\,\| \\
&+ \Delta_{BCRS}\,[t_e, t_{obs}] + \Delta_{ext}\,[t_e, t_{obs}] \\
&+ \mathcal{O}(2)\ .
\end{aligned}
\tag{3.7}
$$

The Δ terms on the right side can include additional space-time effects due to gravitational contributions due to the BCRS fields (Δ_{BCRS}) and other external fields Δ_{ext} that the photon may feel along its long trajectory. This gravitational contribution is usually known as the Shapiro effect. For a detailed discussion of the Shapiro effect see Kopeikin & Schäfer (1999). We are interested in the relation between the emission interval Δt_e and the observation interval Δt_{obs}. Then, using the relation (3.7) for two different events of emission E^0 and E and their respective observation events Obs^0 and Obs we obtain

$$
\begin{aligned}
\Delta t_{obs} - \Delta t_e &= \frac{\|\boldsymbol{x}_{obs}\,[t_{obs}] - \boldsymbol{x}_{\boldsymbol{s}}\,[t_e]\,\|}{c} \\
&- \frac{\|\boldsymbol{x}_{obs}\,\left[t^0_{obs}\right] - \boldsymbol{x}_{\boldsymbol{s}}\,\left[t^0_e\right]\,\|}{c} \\
&+ \Delta_{BCRS}\,[t_e, t_{obs}] - \Delta_{BCRS}\,\left[t^0_e, t^0_{obs}\right] \\
&+ \Delta_{ext}\,[t_e, t_{obs}] - \Delta_{ext}\,\left[t^0_e, t^0_{obs}\right]\ ,
\end{aligned}
\tag{3.8}
$$

$$
\Delta t_e = t_e - t^0_e\,, \tag{3.9}
$$

$$
\Delta t_{obs} = t_{obs} - t^0_{obs}\,. \tag{3.10}
$$

For most of the stars the absolute value of Δ_{ext} may be very large since the gravitational fields of the galaxies and other mass distributions may contribute; however, in most circumstances, it will not change significantly during the lifetime of a space astrometric mission (even over some hundreds of years). An exception may be objects orbiting large concentrations of mass or gravitational lensing events. In such cases, the model for the observations must be carefully derived not only from the point of view of the LTT. This might be the case for stars moving close to the Milky way's

central black hole (see Ghez *et al.* 1998). An example of such a detailed model is found in Fragile & Mathews (2000). Despite the use of such models to include very sophisticated space-time effects, the astrometric LTT signature due to the nonlinear motion is ignored. The contributions Δ_{BCRS} will heavily depend on the relative position of the observer and the sources of gravitational fields (i.e. Sun, planets). Considering that the physical diameter of such bodies is some orders of magnitude larger that their Schwarschild radius, this Shapiro term adds a very small time shift (a few milliseconds at most). In such an interval of time, the direction of observation will not change more than a few nanoarcseconds which is, by far, an undetectable astrometric quantity with current techniques. From now on we will omit both Δ terms.

The equation of time delay (3.8) depends on the module of the relative position of the observer and the source, and in general, it cannot be used to obtain a closed exact expression of Δt_e in terms of Δt_{obs}. This is due the nonlinear nature of the *module operations* on the right side of (3.8) and the intrinsically nonlinear dependence of $\boldsymbol{x_s}$ with respect to time. A perturbative approach is chosen here to obtain the lowest order contribution that is relevant enough to produce an astrometric shift at μas level of accuracy. With some algebra whose details are given in Appendix B.1, and using the definitions of small quantities provided in (3.4)–(3.5) it is obtained that, at first order

$$\begin{aligned} \Delta t_e = \quad & \alpha_s \quad (\Delta t_{obs} \\ & - \quad \frac{1}{c}\,\boldsymbol{l_0}\cdot\Delta\boldsymbol{D}\left[t_{obs}\right] \\ & + \quad \frac{1}{c}\,\boldsymbol{l_0}\cdot\boldsymbol{\Delta x}_{obs}\left[t_{obs}\right]\Big) + \mathcal{O}(\epsilon^2); \end{aligned} \tag{3.11}$$

In (3.11) some notation shortcuts are applied. These are

$$\alpha_s = \frac{1}{1+\boldsymbol{l_0}\cdot\frac{\boldsymbol{v}^0_{LRM}}{c}}\,, \tag{3.12}$$

$$\boldsymbol{\Delta x}_{obs}\left[t_{obs}\right] = \boldsymbol{x}_{obs}\left[t_{obs}\right] - \boldsymbol{x}_{obs}\left[t^0_{obs}\right], \tag{3.13}$$

$$\Delta\boldsymbol{D}\left[t_{obs}\right] = \boldsymbol{D}\left[t^0_e + \alpha_s\Delta t_{obs}\right] - \boldsymbol{D}\left[t^0_e\right]. \tag{3.14}$$

The factor α_s multiplying the full expression(3.11) is the one responsible for apparent

superluminal velocities.

3.4 Astrometric model for point-like sources

The aim of this section is to provide expressions that complete the astrometric models at μas accuracy incorporating the LTT. Under the assumptions of Section 3.2 and Section 3.3, the observed direction of a point-like source given by an observer at rest at the event of observation is

$$\begin{aligned} \boldsymbol{r}\left[t_{obs}, t_e\right] &= \left\langle \boldsymbol{x}^0_{LRM} + \boldsymbol{v}^0_{LRM}\Delta t_e \right. \\ &+ \left. \boldsymbol{D}\left[t^0_e + \Delta t_e\right] - \boldsymbol{x}_{obs}\left[t_{obs}\right]\right\rangle . \end{aligned} \tag{3.15}$$

The next subsections provide general purpose parametric expressions to be used in the astrometric model for a point-like source outside of the solar system. We applied the formalism of the *local triad* as described in Murray (1983). Section 3.4.2 extends the astrometric model to sources in nonlinear motion including the LTT amplitudes. At this point, the expression of the observed direction (3.15) depends on the emission instant t_e.We will include the LTT in the astrometric model using just the relation between Δt_e and Δt_{obs} given by (3.11) in (3.15).

3.4.1 Linear reference motion

This is the simple case where the source is moving in linear motion (i.e. a single star). Substituting (3.11) in (3.15) and imposing $\boldsymbol{D}\left[t\right] = 0$ for any instant of time t, we obtain

$$\begin{aligned} \boldsymbol{r}_{LRM}\left[t_{obs}\right] &= \left\langle \boldsymbol{l_0}\left(1 + \mu_{r0}\Delta T_{LRM}\right)\right. \\ &+ \left(\mu_{\delta 0}\boldsymbol{p} + \mu^*_{\alpha 0}\boldsymbol{q}\right)\Delta T_{LRM} \\ &+ \left. \boldsymbol{\pi}\left[t_{obs}\right]\right\rangle , \end{aligned} \tag{3.16}$$

$$\begin{aligned}
\boldsymbol{p} &= (-\sin\delta_0\,\cos\alpha_0, && (3.17)\\
&\quad -\sin\delta_0\,\sin\alpha_0,\\
&\quad \cos\delta_0)\,,\\
\boldsymbol{q} &= (\sin\alpha_0, && (3.18)\\
&\quad \cos\alpha_0,\\
&\quad 0)\,,\\
\boldsymbol{l_0} &= (\cos\alpha_0\,\sin\delta_0, && (3.19)\\
&\quad \sin\alpha_0\,\sin\delta_0,\\
&\quad \sin\delta_0)\,,\\
\mu^*_{\alpha 0} &= \mu_{\alpha 0}\,\cos\delta_0 = \frac{\alpha_s \boldsymbol{v}^0_{LRM}\cdot\boldsymbol{q}}{x^0_{LRM}}\,, && (3.20)\\
\mu_{\delta 0} &= \frac{\alpha_s \boldsymbol{v}^0_{LRM}\cdot\boldsymbol{p}}{x^0_{LRM}}\,, && (3.21)\\
\mu_{r0} &= \frac{\alpha_s \boldsymbol{v}^0_{LRM}\cdot\boldsymbol{l_0}}{x^0_{LRM}}\,, && (3.22)\\
\boldsymbol{\pi}\,[t_{obs}] &= \frac{\boldsymbol{x}_{obs}\,[t_{obs}]}{x^0_{LRM}} = \frac{\Pi_0}{AU}\boldsymbol{x}_{obs}\,[t_{obs}]\;, && (3.23)\\
\Delta T_{LRM} &= \Delta t_{obs} + \frac{1}{c}\,\boldsymbol{l_0}\cdot\boldsymbol{\Delta x}_{obs}\,[t_{obs}]\;. && (3.24)
\end{aligned}$$

These definitions extend those given for the HIPPARCOS catalog (see Perryman *et al.* 1997a,vol. 1) and include the Roemer correction due to observer's motion, which was already introduced by Klioner & Kopeikin (1992). The vectors $\boldsymbol{p}$ and $\boldsymbol{q}$ are unit vectors tangent to the celestial sphere at $\boldsymbol{l_0}$ direction, pointing towards the direction of increasing *declination* and *right ascension* respectively. The quantities α_0, δ_0, Π_0, $\mu^*_{\alpha 0}$, $\mu_{\delta 0}$ and μ_{r0}, are the so-called *barycentric astrometric parameters* for a point-like source in rectilinear motion at the barycentric reference epoch t^0_{obs}. The angles α_0 and δ_0 are the right ascension and the declination of the equatorial coordinate system given in radians. The parameter Π_0 is the parallax in radians. The symbol $\mu^*_{\alpha 0}$ is the proper motion in the α_0 direction multiplied by $\cos\delta_0$, which provides the correct angular shift taking into account the distortion of the spherical coordinates towards the poles, and $\mu_{\delta 0}$ is the proper motion in the declination direction; both expressed in $rad\,s^{-1}$. The parameter μ_{r0} is known as *astrometric radial velocity* (see Lindegren & Dravins 2003) given in s^{-1}. *AU* is the Astronomical Unit which is currently defined

as a constant.

3.4.2 Nonlinear motion

The expression that generalizes to point-like sources in nonlinear motion is straightforward. The six astrometric parameters described in Section 3.4.1 are used to define a fiducial LRM while $\boldsymbol{D}$ contains the nonlinear contributions,

$$\begin{aligned} \boldsymbol{r}\left[t_{obs}\right] &= \langle \boldsymbol{l_0}\left(1+\mu_r \Delta T\right) \\ &+ \left(\mu_{\delta 0}\boldsymbol{p}+\mu^*_{\alpha 0}\boldsymbol{q}\right)\Delta T \\ &+ \frac{\boldsymbol{D}\left[t^0_e+\alpha_s \Delta T\right]}{x^0_{LRM}}+\boldsymbol{\pi}\left[t_{obs}\right]\rangle\,, \end{aligned} \tag{3.25}$$

$$\begin{aligned} \Delta T &= \Delta t_{obs} \\ &- \frac{1}{c}\,\boldsymbol{l_0}\cdot\left(\Delta \boldsymbol{D}\left[t_{obs}\right]-\boldsymbol{\Delta x}_{obs}\left[t_{obs}\right]\right)\ . \end{aligned} \tag{3.26}$$

These expressions are sufficient to include LTT in an astrometric data reduction algorithm at μas. In classic astrometry, the LTT terms with $\boldsymbol{D}$ inside ΔT were *safely* neglected since the astrometric measurements were not precise enough. In the next section we will analyze the effect of this LTT term on the observed direction, which is the LTT astrometric signature.

3.5 Analytic estimation of the LTT signature

To estimate the astrometric LTT signature we need to compare (3.25) with the *classical* approach for the observed direction $\boldsymbol{r}_c$. As the *classical* approach we define

$$\begin{aligned} \boldsymbol{r}_c &= \langle \boldsymbol{l_0}\left(1+\mu_r \Delta T_c\right) \\ &+ \left(\mu_{\delta 0}\boldsymbol{p}+\mu^*_{\alpha 0}\boldsymbol{q}\right)\Delta T_c \\ &+ \frac{\boldsymbol{D}\left[t^0_e+\alpha_s \Delta T_c\right]}{x^0_{LRM}}+\boldsymbol{\pi}\left[t_{obs}\right]\rangle\,, \end{aligned} \tag{3.27}$$

$$\Delta T_c = \Delta t_{obs}\,; \tag{3.28}$$

where the difference with respect to (3.25) is essentially in ΔT_c, which *classically*

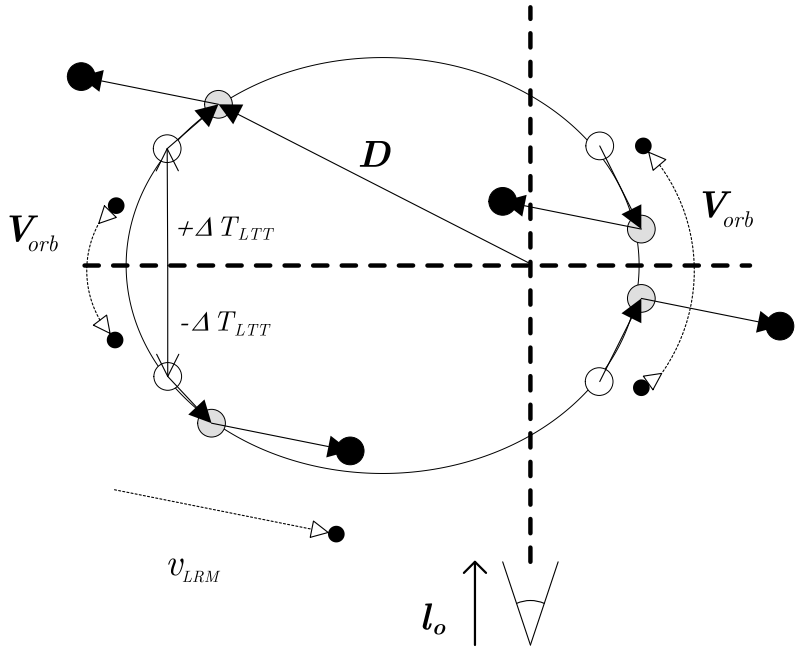

Figure 3.2: Astrometric LTT signature in a binary system. The elliptic orbital motion of a companion is shown in the case where the inclination is 90 deg. The horizontal dashed line is the semi-major axis of the orbit and is perpendicular to the line of sight given by $\boldsymbol{l_0}$. The white circles represent the nonretarded positions of the star at different moments of the orbit. The gray circles are the apparent positions corrected by the Light-Travel Time appliying only the LTT correction due to the instantaneous orbital velocity $\boldsymbol{V}_{orb}$. The black circles are the final apparent position after also considering the motion of the barycenter of the binary system. The proper motion of the system is omitted to simplify the visualization of both the LTT signatures. The pure orbital correction $\boldsymbol{V}_{orb}\Delta T_{LTT}$ changes its orientation continuously depending on the orbital position(gray circles) and it is larger when the object is closer to the center of mass of the system (right side of the figure). On the other hand, the proper motion contribution $\boldsymbol{v}^0_{LRM}\Delta T_{LTT}$ (dark circles) always contributes in the same direction changing only the sign and the amplitude of the perturbation. The projection of the shifts on the plane perpendicular to the line of sight are the astrometrically measurable quantities.

does not include the LTT contribution due to the nonlinear motion of the source with respect to the LRM, and due to the position of the observer with respect to the barycenter of the solar system. Despite the Römer term (dependence in the position of the observer $\boldsymbol{\Delta x}_{obs}\left[t_{obs}\right]$) is already taken into account in the current accurate astrometric models (Klioner & Kopeikin 1992), but we prefer to put in $\boldsymbol{r}$ for consistency.

The comparison of $\boldsymbol{r}$ and $\boldsymbol{r}_c$ is performed by direct subtraction of (3.25) and (3.27) up to $\mathcal{O}(2)$, considering $\mathcal{O}(1) \sim \mathcal{O}(\epsilon)$ all those terms containing expressions proportional to those in (3.4)–(3.5). Then, the astrometric LTT signature $\delta\boldsymbol{r}$ is defined as

$$\delta\boldsymbol{r} \quad = \quad \boldsymbol{r}\left[t_{obs}\right] - \boldsymbol{r}_c\left[t_{obs}\right] \,, \tag{3.29}$$

and, after some algebra

$$\delta\boldsymbol{r} = \boldsymbol{l_0} \times (\boldsymbol{\delta} \times \boldsymbol{l_0}) + \mathcal{O}(3) + \mathcal{O}(1) \times \mathcal{O}(\epsilon^2) \; + \mathcal{O}(2) \times \mathcal{O}(\epsilon^1) \tag{3.30}$$

$$\boldsymbol{\delta} = -\alpha_s \, \frac{\boldsymbol{v}^0_{LRM} + \boldsymbol{V}_{orb}\left[t^0_e + \alpha_s \Delta t_{obs}\right]}{x^0_{LRM}} \Delta T_{LTT} \tag{3.31}$$

$$\Delta T_{LTT} = \frac{\boldsymbol{l_0} \cdot \left(\boldsymbol{\Delta D}\left[t_{obs}\right] - \boldsymbol{\Delta x}_{obs}\left[t_{obs}\right]\right)}{c} \,. \tag{3.32}$$

The presence of the *orbital velocity* vector $\boldsymbol{V}_{orb}$ is justified in Appendix B.1. It is called orbital velocity by direct analogy with the binary system. The LTT shift $\delta\boldsymbol{r}$ is an astrometric detectable quantity since it is in the perpendicular direction to the line of sight $\boldsymbol{l_0}$, as is explicit in (3.30). The LTT shift depends on the radial projection of the *orbital* motion $\boldsymbol{l_0} \cdot \boldsymbol{\Delta D}$. This implies that using accurate astrometric measurements one would, in principle, be able to constrain the radial motion of the source or, on the other hand, if some information of the radial motion of the source is provided (i.e. radial velocities), the fit of the astrometric orbit might be more robust and accurate. In Section 3.6, the relevancy of the astrometric LTT signature will be shown in some well known multiple systems. The *apparent* position of a source is advanced or delayed with respect to the *nonretarded* trajectory. That is why the expression (3.31) is just the *instantaneous proper motion* multiplied by the time interval ΔT_{LTT}, which is also time dependent.

In formula (3.31) two velocities appear instead of the instantaneous total velocity. They are kept separate since the ways they affect the observed direction (their *astrometric signature*) have quite different properties. The *proper motion* term $\boldsymbol{v}^0_{LRM}$ is constant and the time dependence of this part of the astrometric LTT signature will come only from the variations of the ΔT_{LTT} interval. However the *orbital velocity* $\boldsymbol{V}_{orb}$ is intrinsically time dependent, periodic in most cases, and its coupling with the ΔT_{LTT} interval will produce a more *sophisticated* astrometric signature. As shown in Section 3.6, when applied to binary systems, the scaling law of each contribution with respect to the orbital elements is significantly different.

In addition,the term $\boldsymbol{D}\left[t^0_e\right]$ may be included in $\boldsymbol{x}^0_{LRM}$ by imposing $\boldsymbol{D}\left[t^0_e\right] = 0$. However, this assumption may not be useful in practical cases (i.e. when applied to fitting the orbital parameters of a binary system). We will keep the current expression unless we need to implement LTT in the particular modelling of an object.

The LTT signature is one among other astrometric effects becoming relevant at second order astrometric accuracy. These effects include perspective acceleration (or astrometric radial velocity), and all the couplings of the parallax with the proper motion or the non-linear motion. A comprehensive list can be found in Dravins *et al.* (1999). All of them are naturally included in (3.16) and (3.25), since our expressions are directly derived from the kinematical model of the source. Expanding (3.25) up to $\mathcal{O}(2)$ in the small terms (3.5), the vectorial expressions of all such contributions are explicitly obtained. Any astrometric study aiming to obtain information using any second order contribution must properly consider the LTT signature explained in this work.

3.6 Some numerical estimates

Let us naively use the expression (3.31) to obtain some order of magnitude estimates of the LTT signature. The semiamplitudes (denoted by $\overline{\delta \boldsymbol{r}}$) of the astrometric LTT signatures for a component in a binary system in circular orbit can be estimated as

$$\overline{\boldsymbol{\delta r}}_{proper} \sim 15.812 \quad \mu as \quad \frac{a'' \mu_{mas/year}}{\pi_{mas}} \sin i \ , \tag{3.33}$$

$$\overline{\boldsymbol{\delta r}}_{orbital} \sim 99\,353 \quad \mu as \quad \frac{a''^2}{\pi_{mas} P_{year}} \sin i. \tag{3.34}$$

For simplicity, these expressions are obtained imposing $\Delta \boldsymbol{x}_{obs} = 0$. Relations (3.33)–(3.34) are provided using catalog-like parameters where a'' is the projected semi-major axis in $arcseconds$, $\mu_{mas/year}$ is the proper motion module in $mas\, year^{-1}$ and π_{mas} is the parallax in mas. The effect is modulated by the inclination of the orbit.

Kepler's third law can be used to obtain the expressions (3.33) and (3.34) as powers of the orbital period P and the orbital semimajor axis R. It is found that $\overline{\boldsymbol{\delta r}}_{proper}$ scales as R^1 (or $P^{2/3}$), while $\overline{\boldsymbol{\delta r}}_{orbital}$ scales as $R^{1/2}$ (or $P^{1/3}$). This illustrates that for systems with long period orbits the LTT signature due to the coupling with the *proper motion* will be more significant. This is expected since $\boldsymbol{v}^0_{LRM}$ does not depend on the semimajor axis of the orbit(it is only related to the velocity of the center of mass of the system), while $\boldsymbol{V}_{orb}$ becomes smaller at larger orbital distances (i.e. in the solar system, distant planets have lower orbital velocities).

The semiamplitudes obtained using (3.33) and (3.34) for some nearby systems are provided in Table 3.1.

A detailed model to include the astrometric LTT signature in a strict orbital solution of binary systems will be provided in a later work, since some detailed discussion of the definition of the orbital parameters must be provided to keep the astrometric model accuracy at the μas level.

As shown in Table 3.1, long period binaries usually have *larger* LTT signatures coming from the coupling with the *proper motion* term. This is the case of 61 Cyg. In that situation, the LTT signature could be resolved using available long-term lower precision astrometry.

3.6.1 Extened Thiele-Innes elements

The LTT can be introduced in the classical approach by the procedure described in this section. A dynamical model must be assumed. We consider here a binary system in classical keplerian motion. It implicitly assumes Newtonian dynamics and galilean transformations. A more general case is described in the next section.

Let us assume the normal triad $\boldsymbol{pql_0}$ computed using the same definition given in *section 3.4.1.*

Table 3.1: The data in this table were prepared using the *WDS Sixth Catalog of Orbits of Visual Binary Stars* (Hartkopf *et al.* 2004) and the HIPPARCOS catalog (Perryman *et al.* 1997a). The value of some of the orbital parameters shown are average values. The numbers shown here are orientative since the circular model applied is very unrealistic. It can be seen that both contributions, $\delta \boldsymbol{r}_{proper}$ and $\delta \boldsymbol{r}_{orbital}$, may have quite different signification depending on the binary system. In very eccentric systems, like α Cen, the *orbital* term can be considerably larger than the numbers shown here around the perihelion. Another feature that is blurred by the applied approximations is that if the components of the system have different masses, each component might show very different astrometric LTT signatures. The values for AB pic-b are *very* approximated and are based on very recent and sparse data of this candidate to planetary system (Chauvin *et al.* 2005). This values are added here as an example of the applicability of the astrometric LTT signature to general purpose orbital solutions. In this case, the LTT signature would not be very useful to improve the orbital solution due to the very long period and tininess of the signal.

System	*Period*	a''	i	*Parallax*	*Proper motion*	$\Delta\boldsymbol{\sigma}_{proper}$	$\Delta\boldsymbol{\sigma}_{orbital}$
	years	*arcsec*	*deg*	*mas*	*mas/year*	μas	μas
61 Cyg	722.0	14.9	51.85	294	5227	3293	81.7
α Cen	79.9	8.75	79	742	3672	670	415
HD 110314	3.09	0.021	122.9	14	191.9	3.80	0.86
HD 2475	5.65	0.146	64	118	31.01	0.54	2.85
AB pic-b	~ 3000	0.753	??	21.97	47.36	~ 50	~ 1

In the Thiele-Innes approach the offset vector $\boldsymbol{D}$ is obtained as,

$$\begin{aligned} \boldsymbol{D}(t_{obs}, T_{obs}) &= [BX + GY]\,\boldsymbol{p} \\ &+ [AX + FY]\,\boldsymbol{q} \\ &+ [CX + HY]\,\boldsymbol{l_0} \end{aligned} \tag{3.35}$$

$$
\begin{aligned}
A &= a(+\cos w \cos\Omega - \sin w \sin\Omega \cos i) \qquad (3.36)\\
B &= a(+\cos w \sin\Omega + \sin w \cos\Omega \cos i)\\
F &= a(-\sin w \cos\Omega - \cos w \sin\Omega \cos i)\\
G &= a(-\sin w \sin\Omega + \cos w \cos\Omega \cos i)
\end{aligned}
$$

(3.37)

where we have to introduce two additional elements that contain the information of the radial motion

$$
\begin{aligned}
C &= a(+\sin w \sin i)\\
H &= a(+\cos w \sin i)
\end{aligned}
$$

This two elements contain are used to account for the perspective effects and the travel time effects. X and Y are the adimensional elliptic coordinates that contain the time dependency through the *eccentric anomaly* E,

$$X = \cos E - e\,, \qquad (3.38)$$

$$Y = \sqrt{(1-e^2)}\sin E\,. \qquad (3.39)$$

The eccentric anomaly, E, is obtained solving iteratively the Kepler equation

$$\frac{2\pi}{P}\left(\widetilde{t-T}\right) = E - e\sin E\,. \qquad (3.40)$$

To introduce the travel time, the time interval $\widetilde{t-T}$ must be related to the time arguments (t_{obs} and T_{obs}). Let us note that T(Time of passage through the periastron) is also affected by travel time. Up to $\mathcal{O}(2)$ it is sufficient to iterate once using

$$
\begin{aligned}
\widetilde{t-T} &= \alpha_s \left[t_{obs} - T_{obs} - \boldsymbol{l_0}\frac{\boldsymbol{D'}}{c}\right.\\
&+ \left.\boldsymbol{l_0}\left(\boldsymbol{x}_{obs}(t_{obs}) - \boldsymbol{x}_{obs}(T_{obs})\right)\right]\\
&= \alpha_s \left[t_{obs} - T_{obs} - \frac{[CX' + HY']}{c}\right.\\
&+ \left.\boldsymbol{l_0}\left[\boldsymbol{x}_{obs}(t_{obs}) - \boldsymbol{x}_{obs}(T_{obs})\right]\right]
\end{aligned}
$$

where

$$\begin{aligned} X' &= \cos E' - e \\ Y' &= \sqrt{(1-e^2)}\sin E' \end{aligned}$$

and E' is obtained solving Kepler's Equation for t_{obs} and T_{obs},

$$\frac{2\pi}{P}\left(t_{obs} - T_{obs}\right) = E' - e\sin E' \tag{3.41}$$

The T_{obs} is *True Time of passage through the periastron* and may be regarded as an additional parameter to be fitted. Using the *True Time of passage through the periastron* is crucial if one is including Light Travel Time effects in the modeling of the motion of a source since,

- The periastrion will not generally lie on the local tangent plane (i.e. $\boldsymbol{l_0 D}(T) = 0$ not generally holds). Not using the *True* T introduces an spurious amplitude as great as the LTT correction itself
- Classical T depends on the particular position of the observer at the initial epoch t^0_{obs}. Furthermore the predicted future *Times of Passage through the periastron* will fluctuate with respect the nominal value depending on the observer's position at other observation times

With this procedure the astrometry of source in a binary system is described by,

$$\begin{aligned} \boldsymbol{l}_c(t_{obs}) &= \langle \boldsymbol{l_0} + \\ &+ (\mu_p \boldsymbol{p} + \mu_q \boldsymbol{q} + \mu_r \boldsymbol{l_0})\Delta t) \\ &+ \frac{\boldsymbol{D}(t_{obs}, T_{obs})}{x^0_{LRM}} \\ &- \frac{\boldsymbol{x}_{obs}(t_{obs})}{x^0_{LRM}} \Big\rangle \end{aligned} \tag{3.42}$$

$$\begin{aligned} \Delta t &= t_{obs} - t^0_{obs} \\ &- \frac{1}{c}\boldsymbol{l_0}\left[\boldsymbol{D}(t_{obs}, T_{obs}) - \boldsymbol{D}(t^0_{obs}, T_{obs})\right] \\ &+ \frac{1}{c}\boldsymbol{l_0}\left[\boldsymbol{x}_{obs}(t_{obs}) - \boldsymbol{x}_{obs}(t^0_{obs})\right] \end{aligned} \tag{3.43}$$

All the terms different from $\boldsymbol{D}$ are the same as defined in *section 3.4.1.*

The strict definition of the orbital parameters w, Ω, i, P, T and a can be found in any textbook of essential astrometry, i.e. Batten (1973). The conventions used here have been copy/pasted from those used in the HIPPARCOS catalog(see Perryman et al Perryman *et al.* (1997a)).

3.7 Lorentz transformation for relativistic astrometry

It is common that dynamical models for stelar motion are given in some Object Reference System (T, X^a) (i.e. center of mass of a binary or a gas cloud) which is considered inertial. Since our natural coordinate system to describe the observations is the BCRS (t, x^i), let us assume that the Star System is far from the Solar System barycenter (Minkowsky space-time) and that the local gravitational fields are negligible. Then the proper time τ of an observer at the barycenter of the Star System can be used to parameterize the trajectories in the (T, X^a) Reference System (this is equivalent to say that $\tau = T$). For more compact systems or other kind of observable quantities (pulsar timing, frequency shifts), this assumption cannot be applied and the post-Newtonian metric and coordinate transformations should be more adequate.

Assuming that the barycenter of the Star System moves with constant coordinate velocity $\boldsymbol{v}$ in the BCRS, the coordinates (T, X^a) and (t, x^i) are related by a Lorentz transformation of the form

$$c\,t = \Lambda^0_0\, c\,T + \Lambda^0_a\, X^a\,, \tag{3.44}$$

$$x^i = \Lambda^i_0\, c\,T + \Lambda^i_a\, X^a\,. \tag{3.45}$$

The Λ matrix coefficients are given by

$$\Lambda_0^0 = \gamma, \tag{3.46}$$
$$\Lambda_a^0 = k^a \gamma, \tag{3.47}$$
$$\Lambda_0^i = k^i \gamma, \tag{3.48}$$
$$\Lambda_a^i = \delta^{ia} + \frac{\gamma^2}{1+\gamma} k^i k^a, \tag{3.49}$$
$$\gamma = (1 - \boldsymbol{k}\cdot\boldsymbol{k})^{-\frac{1}{2}}, \tag{3.50}$$
$$\boldsymbol{k} = \frac{1}{c}\boldsymbol{v}. \tag{3.51}$$

The inverse transformation reads

$$cT = \overline{\Lambda}_0^0 c\,t + \overline{\Lambda}_i^0 x^i, \tag{3.52}$$
$$X^a = \overline{\Lambda}_0^a c\,t + \overline{\Lambda}_i^a x^i. \tag{3.53}$$

where

$$\overline{\Lambda}_0^0 = \gamma, \tag{3.54}$$
$$\overline{\Lambda}_i^0 = -k^i \gamma, \tag{3.55}$$
$$\overline{\Lambda}_0^a = -k^a \gamma, \tag{3.56}$$
$$\overline{\Lambda}_i^a = \delta^{ia} + \frac{\gamma^2}{1+\gamma} k^i k^a. \tag{3.57}$$

In the SSRS the world line equations for the Star System Barycenter and the target source take the form

$$X_b^\alpha(T_b) = \left(T_b, X_b^i[T_b]\right) = (T_b, X_{b0}^a), \tag{3.58}$$
$$X_e^\alpha(T_e) = \left(T_e, X_e^i[T_e]\right) = (T_e, X_{b0}^a + \mathcal{D}^a[T_e]). \tag{3.59}$$

where $\boldsymbol{X}_{b0}$ is the constant position of the Barycenter of the Star system with respect to some arbitrary coordinate origin. The e symbol is used for events related to the emitting source and b is used for the events related to the Star System Barycenter. T_0 is some reference instant which will be discussed below. Let us assume that the dynamical model which describes the motion of the source in the SSRS is provided

by through $\boldsymbol{\mathcal{D}}$ (i.e. Keplerian motion).

In the BCRS, it is useful to parameterize the stellar motion as a Linear motion term $x_b^i\,[t]$ plus a nonlinear shift, say

$$x_e^i\,[t] = x_b^i\,[t] + D^i\,[t] \tag{3.60}$$
$$x_b^i\,[t] = x_{b0}^i + v^i(t - t_0) \tag{3.61}$$

When transforming the world-line equations from the SSRS to the BCRS, it is obtained

$$x_e^i\,[t_e] = \Lambda_0^i\,c\,T_e + \Lambda_a^i\,\left(X_{b0}^a + \mathcal{D}^a\,[T_e]\right)\,, \tag{3.62}$$
$$x_b^i\,[t_b] = \Lambda_0^i\,c\,T_b + \Lambda_a^i\,X_{b0}^a\,, \tag{3.63}$$

$$c\,t_e = \Lambda_0^0\,c\,T_e + \Lambda_a^0\,\mathcal{D}^a\,[T_e]\,, \tag{3.64}$$
$$c\,t_b = \Lambda_0^0\,c\,T_b + \Lambda_a^0\,X_{b0}^a\,. \tag{3.65}$$

Let us assume that we choose two events (e) and (b) that satisfy

$$T_e - T_b = 0\,, \tag{3.66}$$

which means that they are simultaneous in the Star System Reference System (3.66). Using (3.66) into (3.62) and (3.63) and subtracting them it is obtained

$$x_e^i\,[t_e] - x_b^i\,[t_b] = \Lambda_a^i\,\mathcal{D}^a\,[T_e]\,, \tag{3.67}$$

where X_{b0}^a has disappeared. Note that the time arguments on the left hand-side of (3.67) are not equal (loose of simultaneity), so this expression cannot be used directly to obtain the desired $\boldsymbol{D}(t)$, which should only depend on one t.

However, we can use the subtraction of (3.64)–(3.65)

$$c\,t_e - c\,t_b = +\Lambda_a^0\,\mathcal{D}^a\,[T_e]\,, \tag{3.68}$$

and insert it in the left hand side of (3.67) in such a way that t_b can be removed

obtaining

$$x_e^i\left[t_e\right] - x_b^i\left[t_e\right] + c^{-1}\Lambda_a^0\mathcal{D}^a\left[T_e\right]\, v^i = \Lambda_a^i\,\mathcal{D}^a\left[T_e\right]\,. \tag{3.69}$$

Grouping terms and defining $\boldsymbol{D}$ as

$$D^i = x_e^i\left[t_e\right] - x_b^i\left[t_e\right] \tag{3.70}$$

we find that

$$D^i \;\;=\;\; \left(\Lambda_a^i - c^{-1}\Lambda_a^0 v^i\right)\mathcal{D}^a\left[T_e\right] \tag{3.71}$$

As mentioned before, the time measured by an observer at rest in the Object Reference System is assumed to coincides with the coordinate time T . Then, using (3.44) it can be shown that

$$T_e \;\;=\;\; T_0 + \gamma^{-1}\left(t_e - t_0\right) \tag{3.72}$$

which provides the last required relation to write $\boldsymbol{D}$ as a function of t_e alone. In addition, since the origin of the time coordinate in (T, X^a) is arbitrary, a very convenient choice of the initial instant is $T_0 = t_0 = t_e^0$, where t_e^0 has been discussed on Section 3.2. As a last step, we can substitute in the Λ coefficients ((3.47) and (3.49)) into (3.71) obtaining

$$\boldsymbol{D}\left[t_e\right] \;\;=\;\; \boldsymbol{\mathcal{D}}\left[T_e\right] - \frac{\gamma}{1+\gamma}\left(\boldsymbol{k}\cdot\boldsymbol{\mathcal{D}}\left[T_e\right]\right)\boldsymbol{k} \tag{3.73}$$

$$\boldsymbol{k} \;\;=\;\; \frac{\boldsymbol{v}_{LRM}^0}{c} \tag{3.74}$$

$$T_e \;\;=\;\; t_e^0 + \gamma^{-1}\left(t_e - t_e^0\right) \tag{3.75}$$

where we substituted $\boldsymbol{v}$ by $\boldsymbol{v}_{LRM}^0$, obtaining full compatibility with the astrometric model presented in Section 3.4.2.

Once it is introduced in the astrometric model of Section 3.4.2, one can check that the second term in the right part of (3.73) introduces an astrometric signal

proportional to

$$\frac{D}{x^0_{LRM}}\left(\frac{\boldsymbol{v}^0_{LRM}}{c}\right)^2 \tag{3.76}$$

which is an $\mathcal{O}(3)$ effect, thus negligible even at Gaia accuracy. For example, a visual binary with a separation $\frac{D}{x^0_{LRM}} \sim 1''$ and a spatial velocity with respect to the barycenter of $\boldsymbol{v}^0_{LRM} \sim 200$ km/s, the maximal astrometric effect of the special relativistic term in (3.73) is 0.5 μas. The expression (3.73) essentially contains the effect of the Lorentz contraction and the simultaneity related issues. Therefore we find that using

$$\boldsymbol{D}\left[t_e\right] \;=\; \boldsymbol{\mathcal{D}}\left[t^0_e + \gamma^{-1}\left(t_e - t^0_e\right)\right] , \tag{3.77}$$

is sufficient for practical purposes at the required level of accuracy ($\sim 1\mu$as).

3.8 Conclusions

We have shown that the LTT must be taken into account to obtain accurate models of the observable quantities in precise modern astrometry. Furthermore, since LTT is an object-dependent effect, precise relative astrometric measurements are sufficient to resolve the astrometric LTT signatures. The astrometric LTT signature may be used in highly precise ground-based observations to obtain additional information on a given object. The expressions derived in (3.30)–(3.31) can be applied using $O-C$ techniques with the available astrometric data. LTT must be taken into account in the interpretation of data obtained by the planned space astrometric missions which that will attempt to reach astrometric accuracies of a few μas. As an example, the coupling of the Römer delay with the proper motion and the orbital velocity of a star can mimic the astrometric wobble caused by a planetary mass object with a period of around one year (considering an observer traveling on the vicinity of the earth) if LTT is not properly included in the astrometric model.

It has been found that the LTT signature is boosted by the proper motion of the system. Multiple systems with high proper motions (thick disk, globular clusters, nearby halo objects) might be objects of investigation if properly adapted astrometric models are used.

If the astrometric LTT signature is large, information on the radial geometry of a system can be obtained. In the case of binary systems this information allows us to solve or at least constrain, the full set of orbital elements (and the true masses) without information about radial velocities. Despite that, the amplitudes appearing in Table 3.1 are rather small, even at μas accuracy level). It seems unfeasible to use the astrometric LTT signatures to significantly improve the knowledge of a given system since radial velocity curves are much better measured. The suggestion here is to use the radial velocity measurements as an input to improve the astrometry of a given source using the LTT-corrected orbital description. How to proceed properly in such cases depends on the information available for each object.

When imaging capabilities of exoplanetary systems become available, the fitting of an LTT orbit might lead to constraining the size of the orbit in the line-of-sight direction without the use of spectroscopic measurements, which may be impracticable on such faint objects unless interferometric techniques improve significantly.

The relations (3.33)–(3.34) can be used as a good indicator of whether LTT astrometric effects must be taken into account for more general objects (open clusters, globular clusters, galaxies, fast orbiters around massive black holes) in nonlinear motion. For this purpose we define the *LTT astrometric signal* as

$$\mathcal{L}_{TT} \equiv \frac{V}{c}\frac{L}{d}, \tag{3.78}$$

where V and L are the characteristic *velocity* and *size* of the system, respectively; c is the speed of light in the same units as V; and d is an estimation of the distance to the source given in the same units as L. $\mathcal{L}_{TT}$ is an adimensional quantity that can be directly interpreted as an angle(in radians). If this number is of the order of the astrometric accuracy used to describe an astronomical object outside the solar system, then the LTT should be taken into account in order to obtain a correct interpretation of the data.

For some purposes (such as the construction of an astrometric catalog) it is sometimes useful to make the abstraction that at the reference epoch t^0_{obs} the observer is located at the barycenter of the Solar System. If this is done, the initial direction $\boldsymbol{r}\left[t^0_{obs}\right]$ will not depend on the Römer delay $\boldsymbol{l_0}\cdot\boldsymbol{x}_{obs}\left[t^0_{obs}\right]$ due to the observer position at t^0_{obs} as it does in expressions (3.24) and (3.26) or in the astrometric LTT signature

formula (3.31). Then we can substitute $\boldsymbol{x}_{obs}\left[t_{obs}\right] - \boldsymbol{x}_{obs}\left[t^0_{obs}\right]$ by simply $\boldsymbol{x}_{obs}\left[t_{obs}\right]$ in both equations (3.24) and (3.26) or in (3.31). This consideration is very useful to create an astrometric catalog for a given reference epoch independently of the relative initial position of observer $\boldsymbol{x}_{obs}\left[t^0_{obs}\right]$ and the barycentric reference direction of each source $\boldsymbol{l_0}$.

The application of the LTT has been demonstrated for the case of classical Keplerian orbits. Even for a more sophisticate model, one iteration of the process given in Section3.6.1 is sufficient to account for the LTT to the required accuracy (1μas). We have shown that the coordinate transformation between the Star System reference system and the BCRS do not contribute significantly and that classical predictions of special relativity (Lorentz contraction, loose of simultaneity) cannot be tested with astrometric observations at 1μas accuracy. It is expected (but not demonstrated here) that the local gravitational fields of a given star system are of the same order of the Lorentz effects and that their contribution is not significant to the astrometric modeling. This statement only concerns the coordinate transformations, not the light propagation issues which can certainly produce observable effects (microlensing, shapiro delay, etc.) and are discussed with greater detail by (Kopeikin & Schäfer 1999).

Chapter 4

Light deflection experiments on the Solar System planets

4.1 Introduction

Thank to space astrometry we will able to reach a few microarcsecond accuracy [1] in the position and the motion of the celestial objects (stars and other solar system bodies). When dealing with such precise with so precise measurements, a fully relativistic model for the light propagation and the relativistic reference systems involved have to be used. This, far from being a disadvantadgeous, offers the possibility to fit some parameters in the model, thus testing the fundamental theory of gravitation used (that is General Relativity) and its alternatives with unprecendent accuracy. The standard approach to do that is the parameterized post-Newtonian approximation(ppN)(Will 1980), which provides a version of the solar system metric depending on a number of numerical parameters with a clear phenomenological interpretation (Lorentz invariance properties of the metric, equivalence principle, preferred reference frames, etc.).

Concerning the model for light propagation, it has been shown (Klioner 2003) that the gravitational field of the planets of the Solar system must be taken into account. Therefore, using observations of stars close to the planets some fundamental

[1] one microarcsecond is the thickness of a coin at the surface of the moon or the size of a car at Jupiter as seen from earth.

parameters of the theory can be obtained. At least, three different aspects of the model for light deflection can be phenomenologically studied. They are, the monopolar light deflection that the spherical part of the gravitational field of a planet, the quadrupolar deflection caused by the oblateness of the planet, and the effect of the motion of the gravitating source which forces to consider explicit time-dependecies in the metric and during the integration of the equations of motion for the photons. These three issues have been discussed in great detail by many authors (see for example Klioner & Kopeikin (1992), Will (2003) or Kopeikin (2006a), just to list some of them).

Jupiter is ,without a doubt, the most interesting object, being the most massive body in the Solar System (after the Sun), besides it has a relatively large barycentric velocity, it can be observed very close to its surface and its oblateness is sufficient to cause a significant effect on the light deflection. As for the rest of the planets (with, the exception of Saturn), only the monopolar deflection is relevant even at the Gaia accuracy.

In order to reproduce the Gaia observations with outmost realism, a fully dynamical model has been implemented. It must contain the relevant aspects of the instrument affecting precise astrometric measurements (scanning law, a model for the focal plane, barycentric motion of the probe), and the relevant aspects of the relativistic model for light propagation (precise formulation of the model in the BCRS coordinate system, motion of the sources during the observations, realistic Solar System ephemeris, etc.). In this sense, the Solar System ephemeris play a central role, since such kind of measurements are expected to be quite sensitive to positional errors of the planets. The degree of sensitivity to positional errors is also studied and the requirements for the ephemeris at the time of the Gaia are discussed.

To obtain the maximum scientific outcome, a flexible and robust data reduction scheme has been applied. We present an hybrid approach using nonlinear least squares and the integration of the Bayesian Probability function. The later provides much more information about the significance of the obtained results than the nonlinear least squares.

4.2 Light propagation in the parameterized post-Newtonian approximation

The aim of this section is not to provide a rigorous derivation of the equations of motion for photons (which has been done by many others before), but to give the reader a simple theoretical background in order to interpret the proposed experiments and results in the framework of the parameterized post-Newtonian approximation for the BCRS observable astrometric quantities.

Let us summarize the most important notations which are relevant to this chapter

- β and γ are the parameters of the parametrized post-Newtonian (ppN) formalism which characterize possible deviation of the physical reality from general relativity theory ($\beta = \gamma = 1$ in general relativity);
- the capital italic subscripts $A, B, C, \cdots = 1 \ldots N$ refer to the gravitating bodies of the Solar system;
- the subscript 'o' indicates quantities related to the observer (satellite): e.g. $\boldsymbol{x}_o$ denotes the position of the observer and t_o is the is the instant of observation in the Barycentric Celestial Reference System (BCRS);
- the subscript 'p' denotes quantities related to the light ray (photon): e.g. $\boldsymbol{x}_p(t)$ denotes the BCRS position of the light ray at some moment of time t;
- the subscript 's' denotes quantities related to the source: e.g. $\boldsymbol{x}_s$ denotes the BCRS position of the source;
- the light particles (massless null particles), which are the objects under study, are called *photons*.

The light deflection model used is the one described by Klioner (2003). The relativistic model of the observations contains several parts discussed in the Chapter 1. The effects discussed in this chapter are related to light propagation only.

4.2.1 Relativistic modeling of astrometric observations

Only the signal propagation will be discussed with some detail(Equations in signal propagation in Fig. 1.2) , since it contains all the relevant information for this study.

The described approach is a synthesis of the model developed by S.A. Klioner and his collaborators in a series of papers. In particular, it heavily relies on the results presented in Klioner (2003), Klioner & Peip (2003) and Klioner (2004). The nomenclature and the notations have been taken from there. First, we proceed giving the metric and deriving the equations of motion (Section 4.2.2). Then we sketch the procedure to integrate the equations of motion of a photon when the massive bodies move with constant velocities obtaining the analytical form of the coordinate velocity for the photon(Section 4.2.2). All the features of the light deflection effect are derived in that part. Finally, a few lines describe the formula used to project the coordinate velocity of the photon into the observer reference system obtaining the desired observed direction (Section 4.2.3).

As a general comment, let us note that we work in the limit of geometrical optics, where the light is assumed to propagate as point-like particles (no wave equation, (Misner *et al.* 1973,Chap.22.5)). The mathematical expression for this, is that the geodesic equation is used instead of the General relativistic version of the Maxwell Field equations.

4.2.2 The equations of motion for the photons

Since the standard post-Newtonian approach deals with weak gravitational fields and small velocities for the gravitating bodies (Will 1980), it is standard to write the post-Newtonian metric as the Minkowsky metric $\eta_{\alpha\beta} = diag\,[-+++]$ plus a small perturbing tensor $h_{\alpha\beta}$

$$g_{\alpha\beta} = \eta_{\alpha\beta} + h_{\alpha\beta} \tag{4.1}$$

$$h_{00} = \frac{2}{c^2}\omega\left(t,\boldsymbol{x}\right) + \mathcal{O}(c^{-4})\,, \tag{4.2}$$

$$h_{i0} = -\frac{4}{c^3}\omega^i\left(t,\boldsymbol{x}\right) + \mathcal{O}(c^{-5})\,, \tag{4.3}$$

$$h_{ij} = \frac{2}{c^2}\delta_{ij}\omega\left(t,\boldsymbol{x}\right) + \mathcal{O}(c^{-4})\,. \tag{4.4}$$

where ω and ω^i are the newtonian gravitational potential and the so-called gravito-magnetic field respectively,

$$\omega = \sum_A \frac{GM_A}{r_A} + \frac{1}{2}\sum_A \frac{GI_A^{pq}}{r_A^3}\left(-\delta_{pq} + 3\frac{r_A^p r_A^q}{r_A^3}\right) + \dots , \tag{4.5}$$

$$\omega^i = \sum_A \frac{GM_A}{r_A}\dot{x}_A^i(t) + \dots , \tag{4.6}$$

where $r_A = |\boldsymbol{r}_A|$,

$$\boldsymbol{r}_A(t, \boldsymbol{x}) = \boldsymbol{x} - \boldsymbol{x}_A(t) , \tag{4.7}$$

$\boldsymbol{x}_A$ is the position of body A, and $\dot{\boldsymbol{x}}_A$ is the velocity of body A. The first term on the right–hand side of (4.5) is the spherically symmetric part of the Newtonian gravitational potential (monopole) and the second one is the quadrupolar component of the gravitational field (which depends on the symmetric traceless quadrupolar moment I_A^{ij} of body A, and is explicitly given in Section 4.2.2). In (4.6) the terms due to the body rotation have been omitted since they only produce negligible astrometric effects at μas accuracy (see Klioner (1991)).

This form of the metric coefficients comes from the integration of the Einstein Field equations(not discussed here) and the choice of a suitable coordinate gauge. Here we are working in the so-called *harmonic gauge*, which can be expressed as the following constrain on the metric coefficients

$$h^\beta_{\alpha,\beta} - \frac{1}{2}h^\beta_{\beta,\alpha} = 0. \tag{4.8}$$

The Minkowsky metric $\eta_{\alpha\beta}$ is used to *raise* and *lower* the indices. The explicit dependence of the metric tensor with the position is entirely included in the $h_{\alpha\beta}$ coefficients. In the limit of geometric optics (see Misner *et al.* (1973)), the motion for a photon is described by the null geodesic equation

$$\frac{d^2 x^\alpha}{d\lambda^2} + \Gamma^\alpha_{\mu\nu}\frac{d x^\mu}{d\lambda}\frac{d x^\nu}{d\lambda} = 0 \tag{4.9}$$

which depends on an arbitrary curve parameter λ, also called affine parameter. The Γ symbols are the so-called Cristoffel symbols which are directly obtained from the

metric tensor as

$$\Gamma^{\alpha}_{\mu\nu} = \frac{1}{2} g^{\alpha\beta} \left(g_{\mu\beta,\nu} + g_{\nu\beta,\mu} - g_{\nu\mu,\beta} \right) \tag{4.10}$$

Using the equation for the x^0 (time) component and the null vector condition

$$\frac{dx^{\alpha}}{d\lambda} \frac{dx^{\beta}}{d\lambda} g_{\alpha\beta} = 0 \tag{4.11}$$

the equations of motion can be then written in terms of the coordinate time t instead of the affine parameter λ. To the post-Newtonian order (Will 1980), they read

$$\begin{aligned} \frac{d^2 x^i}{dt^2} &= \frac{1}{2} c^2 h_{00,i} - h_{00,k} \dot{x}^k \dot{x}^i - \left(h_{ik,l} - \frac{1}{2} h_{kl,i} \right) \dot{x}^k \dot{x}^l - \frac{1}{2} h_{00,t} \dot{x}^i \\ &- \left(\frac{1}{c} h_{0k,j} - \frac{1}{2c^2} h_{jk,t} \right) \dot{x}^j \dot{x}^k \dot{x}^i - c \left(h_{0i,k} - h_{0k,i} \right) \dot{x}^k \\ &- h_{ik,t} \dot{x}^k - c h_{0i,t} + \mathcal{O}(c^{-2}) \end{aligned} \tag{4.12}$$

Let us assume that the coordinate trajectory of a photon can be described as a straight line $\boldsymbol{x}_p$ plus a small perturbation due to the gravitational fields

$$\boldsymbol{x}_p = \boldsymbol{x}_0 + c\boldsymbol{\sigma} \left(t - t_0 \right) + \Delta \boldsymbol{x}_p \tag{4.13}$$

where $\boldsymbol{x}_0$ is some position at the t_0 instant. The coordinate velocity is obtained deriving the equation of the trajectory with respect to the coordinate time t

$$c^{-1} \dot{\boldsymbol{x}}_p = \boldsymbol{\sigma} + c^{-1} \Delta \dot{\boldsymbol{x}}_p \,, \tag{4.14}$$

where $c^{-1} \Delta \dot{\boldsymbol{x}}_p$ is the perturbing term to the direction coordinate velocity induced by the gravitational fields.

Substituting (4.13) into (4.12), it is obtained that the equations of motion for the

perturbing term $\Delta\boldsymbol{x}_p$ are

$$\begin{aligned}
\Delta\ddot{\boldsymbol{x}}_p{}^i &= F^i_{pN} + F^i_Q\,, && (4.15)\\
F^i_{pN} &= -\sum_A \frac{GM_A}{r_A^3}\left(R^i_A\right. && (4.16)\\
&+ c^{-2}\left[\dot{\boldsymbol{x}}_p{}^2 r^i_A - 4\left(\boldsymbol{x}_p\cdot\boldsymbol{r}_A\right)\dot{x}^i_p - 4\left(\dot{\boldsymbol{x}}_p\cdot\boldsymbol{v}_A\right)R^i_A\right.\\
&\quad \left.+ 4\left(\dot{\boldsymbol{x}}_p\cdot\boldsymbol{r}_A\right)v^i_A + 3\left(\boldsymbol{v}_A\cdot\boldsymbol{r}_A\right)\dot{x}^i_p\right]\\
&+ c^{-4}\left[4\left(\dot{\boldsymbol{x}}_p\cdot\boldsymbol{r}_A\right)\left(\dot{\boldsymbol{x}}_p\cdot\boldsymbol{v}_A\right)\dot{x}^i_p - \left(\boldsymbol{v}_A\cdot\boldsymbol{R}_A\right)\dot{\boldsymbol{x}}_p^2 x^i_p\right]\Big)\\
&+ \mathcal{O}(c^{-2})\,,\\
F^i_Q &= 6\sum_A \frac{G}{R_A^5} I^{pq}_A r^q_A\left(\delta^{ip} - \frac{2}{c^2}\dot{x}^j_p\dot{x}^p_p + \frac{5}{c^5}\left(\dot{\boldsymbol{x}}_p\cdot\boldsymbol{n}_A\right)\dot{x}^i_p n^p_A - \frac{5}{2}n^i_A n^p_A\right) && (4.17)\\
&+ \mathcal{O}(I_A^3) + \mathcal{O}(c^{-2})\,.\\
n^i_A &= \frac{r^i_A}{r_A}\,, && (4.18)\\
v^i_A &= \frac{\dot{x}^i_A}{c}\,. && (4.19)
\end{aligned}$$

Integration of the equations of motion and light deflection.

Assuming that the gravitational field of the Solar system vanishes at infinity ($h \to 0$), the metric is asymptotically Minkowskian. This provides a natural choice of the first boundary condition which is that the perturbation to the photon coordinate velocity vanishes very far from the sources of the gravitational fields,

$$\lim_{t\to-\infty}\Delta\dot{\boldsymbol{x}}_p(t) = 0\,. \qquad (4.20)$$

Imposing that the post-Newtonian perturbation to the photon trajectory vanishes at the event of observation, the second boundary condition is obtained

$$\Delta\boldsymbol{x}_p(t_o) = 0, \qquad (4.21)$$

and the second order equations of motion in (4.15) can be integrated. We omit the details here for the sake of brevity. A detailed procedure to do that can be found in Klioner (1991). The perturbation to the coordinate velocity can be written in two

parts

$$c^{-1}\Delta\dot{\boldsymbol{x}}_p \quad = \quad c^{-1}\Delta\dot{\boldsymbol{x}}_{pN} + c^{-1}\Delta\dot{\boldsymbol{x}}_Q \tag{4.22}$$

where $c^{-1}\Delta\dot{\boldsymbol{x}}_pN$ contains the monopolar deflection and $c^{-1}\Delta\dot{\boldsymbol{x}}_Q$ the deflection due to the quadrupole.

An analytic expression for the velocity of the photon at any time can be obtained by direct integration (see Klioner (1989)) if the motion of the deflecting bodies are assumed to be rectilinear. In practice, it is enough to suppose that the motion of the bodies is rectilinear during the time interval required by the photon to travel through the solar system.

The advantage of this approach (Klioner 1989) is that it accounts for the motion of the bodies with the required accuracy (linear motion is enough for Solar System applications) without further assumptions. A more sophisticate solution in the post-Minkowskian approach was derived by Kopeikin & Schäfer (1999). It has been proved that both approaches are equivalent at the μas level astrometric of accuracy (Klioner & Peip 2003).

It is useful to define the unit propagation direction $\boldsymbol{\sigma}$ at the past null infinity as

$$\lim_{t\to-\infty}\frac{1}{c}\dot{\boldsymbol{x}}_p(t) \quad = \quad \sigma \tag{4.23}$$

If the object is far enough from the Solar System (say > 1 pc), then $-\boldsymbol{\sigma}$ is equivalent to the instantaneous apparent direction of the source obtained by simple Euclidean considerations. To the corresponding post-Newtonian order, the projection to the BCRS tetrad of the propagation direction can be expressed as the $\boldsymbol{n}$ unit vector given by

$$\boldsymbol{n} \quad = \quad \boldsymbol{\sigma} + \delta\boldsymbol{\sigma}_{pN} + \delta\boldsymbol{\sigma}_Q\,. \tag{4.24}$$

The expressions for $\delta\boldsymbol{\sigma}_{pN}$ and $\delta\boldsymbol{\sigma}_Q$ are given and discussed in the subsequent sections.

Monopolar deflection : PPN γ parameter

The expression for the monopolar part of light deflection reads $\delta\boldsymbol{\sigma}_{pN}$ is

$$\begin{aligned}
\delta\boldsymbol{\sigma}_{pN} &= \boldsymbol{\sigma} \times \frac{1}{c}\Delta\dot{\boldsymbol{x}}\left(t_o\right) \times \boldsymbol{\sigma}\,, && (4.25)\\
\frac{1}{c}\Delta\dot{\boldsymbol{x}}\left(t_o\right) &= -\sum_A \frac{1+\gamma}{2}\frac{2GM_A}{c^2}\left(\hat{\boldsymbol{d}}_A\frac{1}{c}\dot{\mathcal{I}}_A + \boldsymbol{g}_A\frac{1}{c}\dot{\mathcal{J}}_A\right) + \mathcal{O}(c^{-4})\,, && (4.26)\\
\frac{1}{c}\dot{\mathcal{I}}_A &= \frac{|\boldsymbol{g}_A|}{|\boldsymbol{ro}_A|\left(|\boldsymbol{g}_A||\boldsymbol{r}_{oA}| - \boldsymbol{g}_A\cdot\boldsymbol{r}_{oA}\right)}\,, && (4.27)\\
\frac{1}{c}\dot{\mathcal{J}}_A &= \frac{|\boldsymbol{g}_A|}{|\boldsymbol{r}_{oA}|}\,, && (4.28)\\
\hat{\boldsymbol{d}}_A &= \boldsymbol{\sigma} \times \left(\boldsymbol{r}_{oA} \times \boldsymbol{g}_A\right)\,, && (4.29)\\
\boldsymbol{r}_{oA} &= \boldsymbol{x}_o\left(t_o\right) - \boldsymbol{x}_A\left(t_o\right)\,, && (4.30)\\
\boldsymbol{g}_A &= \boldsymbol{\sigma} - c^{-1}\boldsymbol{v}_A\left(t_o\right)\,. && (4.31)
\end{aligned}$$

where $\hat{\boldsymbol{d}}_A$ is the vector distance of closest approach to the A-th gravitating body(up to terms $\mathcal{O}(2)$. This statement is proven in Appendix C.2). The vector $\hat{\boldsymbol{d}}_A$ is similar to the impact parameter vector $\boldsymbol{d}_A = \boldsymbol{\sigma}\times(\boldsymbol{r}_{oA}\times\boldsymbol{\sigma})$, but includes the coordinate velocity vector of the gravitating body $\boldsymbol{v}_A$. The γ parameter is a well-known parameter in the standard parameterized post-Newtonian approximation as described by Will (1980) and general relativity predicts that its value is 1 for all the bodies. The best estimates for γ come from the measured light deflection and related effects by the Sun, as shown in Tab. 4.1. Some first attempts to obtain γ from Jupiter are also given.

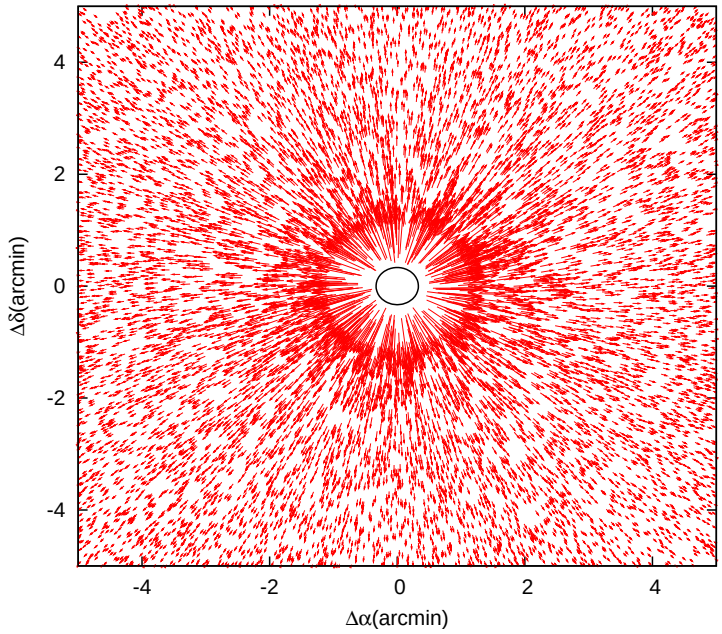

Figure 4.1: Monopolar light deflection applied to a random number of sources around Jupiter. The central circle indicates the instantaneous position of Jupiter (at the retarded instant). The shifts have been exaggerated.

Year	Method	Value	Uncertainity	Publication
1918	Light deflection, Optical	$\simeq 1.0$	0.30	Eddington (1919)
1918–1960	Light deflection, Optical	$\simeq 1.0$	0.10	Various authors
1960–1980	Light deflection, Radio and VLBI	1.00	$\simeq 0.05$	Various authors
1995	Light deflection, VLBI	0.9996	0.0017	Lebach *et al.* (1995)
1997	Light deflection, Optical(HIPPARCOS)	0.997	0.003	Froeschle *et al.* (1997)
2004	Global VLBI solution, Radio	0.99992	0.00023	Shapiro *et al.* (2004)
2003	Shapiro time delay, Doppler tracking	1.000021	0.000023	Bertotti *et al.* (2003)
1991	Shapiro time delay, VLBI on Jupiter	$\simeq 1.0$	0.3–0.4	Treuhaft & Lowe (1991)
2006	Light deflection, HST optical	$\simeq 1.0$	0.12	Whipple *et al.* (1996)

Table 4.1: Review of of direct measurements of the γ parameter through light propagation effects

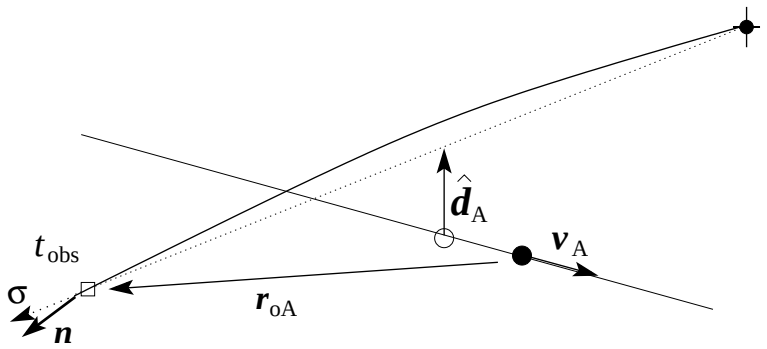

Figure 4.2: Scheme of the vectors involved in light deflection formula (4.25). The dark circle on the right is the position of the massive body at the instant of observation t_{obs} , while the white one is the position of the body at the instant of closest approach. The vector $\boldsymbol{\sigma}$ is tangent to the unperturbed trajectory of the photon (dashed line). The vector tangent to the trajectory of the photon(solid curve from the star to the observer) at the instant of observation is $\boldsymbol{n}$. The position of the observer at the instant of observation is illustrated with a white box. The vector $\hat{\boldsymbol{d}}$ is the minimal distance between the trajectory of the photon and the massive body.

The dependence of the light deflection effect with the mass obtained dynamically (say GM_A product) from the integration of the Solar System ephemeris (asteroids, satellites, planets and the Sun) is a fundamental prediction of the theory. An observed significative discrepancy would seriously compromise the consistency of General Relativity at a very deep level (strong equivalence principle, Einstein field equations or geometric interpretation of the gravitational field). This fully justifies the effort to obtain γ for each planet independently.

The first published work that explicitly measures the Jupiter monopolar deflection was presented by Treuhaft & Lowe (1991), who statistically confirmed the presence of the light deflection effect, but did not really give an estimate of γ. From their results one can infer an accuracy of $30\% - -40\%$ in the determination of γ. A similar experiment with a very bright star transiting close to Jupiter was performed by the Astrometry group of the Hubble Space Telescope, Whipple *et al.* (1996). Using the discussion given on the report, one can infer that they checked the value of $\gamma = 1$ with an error of 12%. Despite that the observations performed by Fomalont & Kopeikin (2003) seem sensitive enough to provide an estimation of γ, they chose to assume its nominal value from the Sun estimations ($\gamma = 1$). This issue is discussed again in

Section 4.2.2.

Just to mention other indirect measurements of γ, the current VLBI full sky solution contains a global $\gamma = 1$, obtaining the ICRF orientation at the level of a few tens of μas (McCarthy & Petit 2004). The Solar System ephemeris are also sensitive to a combination of γ and the post-Newtonian parameter β but it is not a light deflection experiment and their constrains have been only analyzed in the global context (just a global γ as it comes from the metric) where the Sun (Pitjeva 2005) is the main contributor.

Planet motion: the dynamical α_r parameter

The standard post-Newtonian theory for light deflection predicts that the observed deflection pattern depends explicitly on the state of motion of the deflecting body. Acceleration terms come only from the gravitational interaction with the Sun during the propagation of the photon through the Solar System and produce negligible effects ($< 0.5\mu$as). Assuming linear motion the deflection formula (4.25) explicitly depends on the instantaneous velocity of the body at the instant of observation. A numerical coefficient multiplying the velocity can be inserted in (4.31) as

$$\hat{\boldsymbol{g}}_A \quad = \quad \boldsymbol{\sigma} - \alpha_r c^{-1} \boldsymbol{v}_A\,(t_o) \tag{4.32}$$

where α_r equals 1 if the integration of the photon trajectory under the assumptions of general relativity is correct.

The compactness of the solution given in (4.25) hides that the motion of the massive bodies enters in the equations of motion for the photon in two ways. One is through the h_{0i} components of the metric (the so-called gravitomagnetic field), which explicitly depends on the instantaneous velocity of the bodies $\boldsymbol{v}_A$(see (4.6)). The other one is through the explicit dependence of the gravitational *potentials* onthe motion of the bodies(h_{00} and h_{ij} components). In (4.2)–(4.4) all the relative position vectors $\boldsymbol{r}_A$ depend on time through the Newtonian potential in (4.5). This experiment (and Gaia observations in general) are only sensitive to the explicit dependence on time in the position of the bodies since the gravitomagnetic contribution is too small (see Appendix C.3). Therefore we call α_r the *dynamical* parameter.

It has been claimed by Nordtvedt (1991), that gravitomagnetism (effect of the h_{0i} components in the motion of the bodies) was already confirmed by the LAGEOS and

Lunar Laser Ranging experiments. This claim has been recently criticized by Kopeikin (2007), arguing confusion of real torques with spurious coordinate effects. Gravity probe B, tries to obtain a direct measurement of the gravitomagnetism through the analysis of the precession of gyroscopes in free fall. Their results are expected to be released during 2007.

Concerning this explicit dynamical dependence of light deflection, only the measurements performed by Fomalont & Kopeikin (2003) on Jupiter have confirmed the prediction of General Relativity since α_r was explicitly obtained from their data with an accuracy of 20%. Despite their parameterizations is slightly different from the one used here, it is possible to show that they are equivalent (Klioner & Peip 2003). They used the most precise astrometric VLBI technique which consist in measuring the differential gravitational time delay between VLBI stations.

Cassini radio link experiment (Bertotti *et al.* 2003) was also sensitive to α_r for the Sun, but it was not directly fitted during their data reduction (see Kopeikin (2006b) for a detailed discussion of the issue). The experiment consisted in measuring the gravitational frequency shift of radio signals as Cassini transited behind the Sun in his route to Saturn.

An alternative way to introduce the dynamical effects has been recently spread by S.Kopeikin since it emerges naturally in the post-Minkowskian approach to General Relativity. In this approach, the positions of the deflecting bodies are considered at some retarded instant t_A^r with respect to the instant of observations t_{obs}

$$t_A^r = t_{obs} - \alpha_r \frac{1}{c} \left| \boldsymbol{x}_{obs}(t_{obs}) - \boldsymbol{x}_A(t_A^r) \right| . \tag{4.33}$$

which must be solved iteratively (one Newtonian iteration is sufficient, see Klioner & Peip (2003)). Then, the formula to be used for $\delta\sigma_{pN}$ is the same as (4.25) with

$\boldsymbol{v}_A = 0$ for all the bodies and their positions evaluated at t_A^r,

$$\delta\boldsymbol{\sigma}_{pN} = \boldsymbol{\sigma} \times \left(\frac{1}{c} \Delta\dot{\boldsymbol{x}} \left(t_o, t_A \right) \times \boldsymbol{\sigma} \right) , \tag{4.34}$$

$$\frac{1}{c} \Delta\dot{\boldsymbol{x}} \left(t_o, t_A \right) = - \sum_A \frac{2GM_A}{c^2} \left(\boldsymbol{d}_{rA} \frac{1}{c} \dot{\mathcal{I}}_A + \boldsymbol{\sigma} \frac{1}{c} \dot{\mathcal{J}}_A \right) + \mathcal{O}(c^{-4}) , \tag{4.35}$$

$$\frac{1}{c} \dot{\mathcal{I}}_A = \frac{1}{|\boldsymbol{r}_{oA}^r| \left(|\boldsymbol{r}_{oA}^r| - \boldsymbol{\sigma}_A \cdot \boldsymbol{r}_{oA}^r \right)} , \tag{4.36}$$

$$\frac{1}{c} \dot{\mathcal{J}}_A = \frac{1}{|\boldsymbol{r}_{oA}^r|} , \tag{4.37}$$

$$\boldsymbol{d}_A^r = \boldsymbol{\sigma} \times \left(\boldsymbol{r}_{oA}^r \times \boldsymbol{\sigma} \right) , \tag{4.38}$$

$$\boldsymbol{r}_{oA}^r = \boldsymbol{x}_o \left(t_o \right) - \boldsymbol{x}_A \left(t_A^r \right) , \tag{4.39}$$

By expanding (4.25) in powers of $\frac{v}{c}$, it can be shown that the leading terms of both equations coincide down to $1\mu as$ accuracy for any situation in the Solar System context.

The formal equivalence of both approaches (dynamical and retarded) has derived in an intensive discussion on the interpretation of the light deflection experiment carried out by Fomalont & Kopeikin (2003), where the authors claimed that the obtained value of α_r is a direct measurement of the speed of propagation of the gravitational field. In their approach the use of the retarded position is directly related to the retarded gravitational potentials that appear when solving the Einstein equations in the post-Minkowskian approach.

We prefer to interpret the α_r parameter in the dynamical sense and in our code, we use the standard formula (4.25) as it comes from the direct integration of the trajectories for the photons.

Since the accelerations in the Solar System are small, it is easy to realize that a value of α_r different from 1 is equivalent to a positional shift of the gravitating body along its trajectory in the retardation approach. That is, we should be evaluating the position of the body at a wrong instant of time along its trajectory. This is also true (but not so evident) in the fully dynamical picture (see equations (4.25)–(4.31)).

A positional error in the center of mass of a gravitating body can be also interpreted as a spurious mass dipolar moment of the gravitational field (Kopeikin 2006a).By definition, the center of mass is chosen by imposing that the mass dipolar moment of the gravitating body must be zero. The reason is that only *positive*

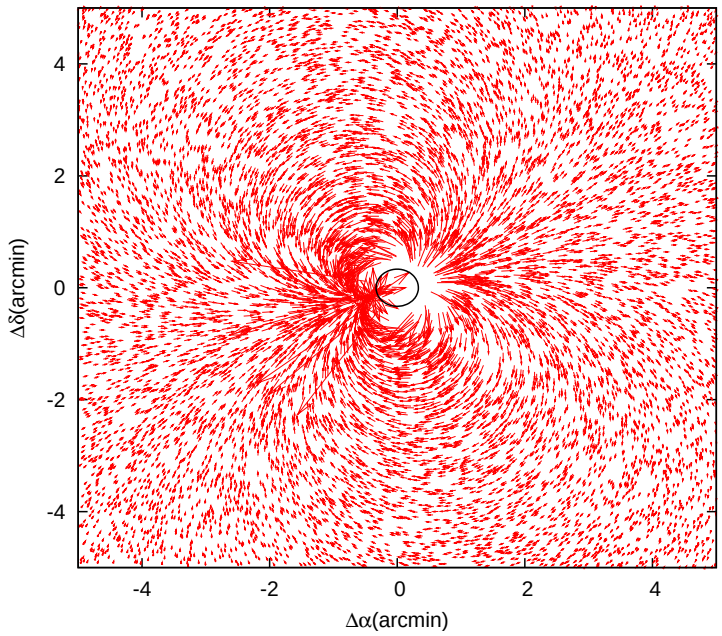

Figure 4.3: Visual representation of the effect of a dynamical parameter different than 1 applied to a random number of sources around Jupiter. A dipolar structure is clearly seen in the deflection pattern. The *shift* vectors have been exaggerated to make the image more visual.

gravitational charges(masses) can exist in the standard paradigm. It can be clearly seen in Fig. 4.3 that the deflection pattern reflects this *dipole* nature of the dynamical/positional effects. Then, if such dipole becomes apparent in the Gaia data, two explanations will naturally emerge. One is that, the value of α_r is not equal to one, thus general relativity does not give the correct prediction(whatever the reason is), or the accuracy of the ephemeris for Jupiter is not as good as they are supposed to be.

In review, positional errors along the instantaneous velocity of the gravitating body given by the ephemeris are virtually undistinguishable from discrepancies in α_r. By chance, the required accuracy ($\sim$ 100 km, this is shown in 4.4.4) coincides with the current accuracy of the ephemeris. Any dipole-like effect, if present, must be examined very carefully.

Quadrupolar deflection : ϵ parameter

The deflection of the quadrupolar part of the gravitational field emerges naturally from the equations of light propagation in the first post-Newtonian approximation. As it happens for the trajectories of massive bodies, it is expected that the mass multipoles do have an influence on the trajectories of massless particles. Since it has a strong dependence on the impact parameter, it has not been yet measured on any solar system body, but it is assumed to be very relevant on the gravitational macrolenses in clusters of galaxies. In that cases, the quadrupolar deflection is assumed to be that given by GR and it is used to infer the properties and density profiles of the lenses (Kopeikin 2006a). So far, only the quadrupolar deflection from Jupiter is expected to be measured with a reasonable signal to noise ratio. The nominal mass quadrupole of the planets is estimated dynamically from the ephemeris integration and the observed rotation axis.

A numerical value multiplying the quadrupolar deflection term can be added in (4.24) as $\epsilon\delta\boldsymbol{\sigma}_Q$. The expression for the quadrupole deflection is rather complicate. We use the prescription given by (Klioner & Blankenburg 2003) which is based on

the the work of Klioner (2003).

$$\begin{aligned}
\delta\boldsymbol{\sigma}_Q &= \frac{1}{2c^2}\left(1+\gamma\right)G\sum_A \qquad (4.40)\\
&\left(\alpha'_A\frac{1}{c}\dot{\mathcal{U}}_A\left(t_o\right)+\beta'_A\frac{1}{c}\dot{\mathcal{E}}_A\left(t_o\right)+\gamma'_A\frac{1}{c}\dot{\mathcal{F}}_A\left(t_o\right)+\delta'_A\frac{1}{c}\dot{\mathcal{V}}_A\left(t_o\right)\right),\\
\alpha'_A &= 2\boldsymbol{f}_A-2\left(\boldsymbol{f}_A\cdot\boldsymbol{\sigma}\right)-\left(\boldsymbol{g}_A\cdot\boldsymbol{\sigma}+4\boldsymbol{f}_A\cdot\boldsymbol{h}_A\right)\boldsymbol{h}_A\,, \qquad (4.41)\\
\beta'_A &= 2\left(\boldsymbol{f}_A\cdot\boldsymbol{\sigma}\right)\boldsymbol{h}_A\,, \qquad (4.42)\\
\gamma'_A &= -\left(\boldsymbol{g}_A\cdot\boldsymbol{\sigma}-\boldsymbol{f}_A\cdot\boldsymbol{h}_A\right)\boldsymbol{h}_A \qquad (4.43)\\
\delta'_A &= 2\boldsymbol{g}_A-2\left(\boldsymbol{g}_A\cdot\boldsymbol{\sigma}\right)\boldsymbol{\sigma}-4\left(\boldsymbol{f}_A\cdot\boldsymbol{\sigma}\right)\boldsymbol{h}_A\,, \qquad (4.44)\\
\frac{1}{c}\dot{\mathcal{U}}_A\left(t_o\right) &= d_A\frac{2r_oA-\boldsymbol{\sigma}\cdot\boldsymbol{r}_{oA}}{r_{oA}^3\left(r_{oA}-\boldsymbol{\sigma}\cdot\boldsymbol{r}_{oA}\right)^2}\,, \qquad (4.45)\\
\frac{1}{c}\dot{\mathcal{E}}_A\left(t_o\right) &= a\frac{r_{oA}^2-3\left(\boldsymbol{\sigma}\cdot\boldsymbol{r}_{oA}\right)^2}{r_{oA}^5}\,, \qquad (4.46)\\
\frac{1}{c}\dot{\mathcal{F}}_A\left(t_o\right) &= -3d_A\frac{\boldsymbol{\sigma}\cdot r_{oA}}{r_{oA}^5}\,, \qquad (4.47)\\
\frac{1}{c}\dot{\mathcal{V}}_A\left(t_o\right) &= -\frac{1}{r_{oA}^3}\,, \qquad (4.48)
\end{aligned}$$

where the following notation shortcuts have been applied

$$\begin{aligned}
\boldsymbol{r_{oA}} &= \boldsymbol{x}_o\left(t_o\right)-\boldsymbol{x}_{oA}\left(t_o\right)\,, \qquad (4.49)\\
r_{oA} &= \left|r_{oA}\right| \qquad (4.50)\\
\boldsymbol{d}_A &= \boldsymbol{\sigma}\times\left(\boldsymbol{r}_{oA}\times\boldsymbol{\sigma}\right)\,, \qquad (4.51)\\
d_A &= \left|\boldsymbol{d}_A\right|\,, \qquad (4.52)\\
\boldsymbol{h}_A &= \frac{\boldsymbol{d}_A}{d_A}\,, \qquad (4.53)\\
f_A^i &= I_{ij}^A h_A^j\,, \qquad (4.54)\\
g_A^i &= I_{ij}^A\sigma^j\,, \qquad (4.55)
\end{aligned}$$

The matrix I_A^{ij} is symmetric and traceless and has, therefore, five independent components which can be calculated from the second zonal harmonic coefficient $J_{2\,A}$ (in the case of the giant planets other second order coefficients are negligible), the mass M_A and the equatorial radius L_A of the planet, and the equatorial coordinates

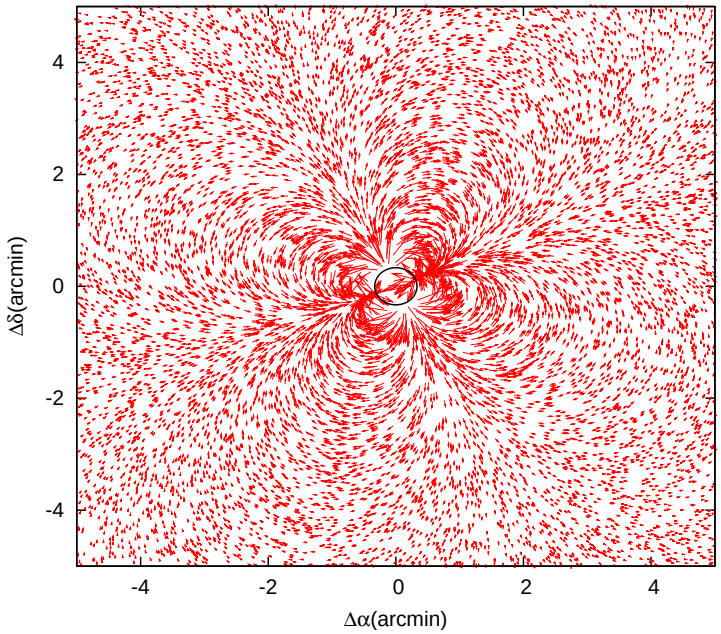

Figure 4.4: Quadrupolar light deflection applied to a random number of sources around Jupiter. The quadrupolar structure of the deflection pattern is very obvious in the figure. The length of the *shift* vectors has been exaggerated to make the image more visual.

$(\alpha^A_{\rm pole}, \delta^A_{\rm pole})$ of the north pole of its figure axis (Klioner 2003) :

$$I^A_{ij} = M_A\, L_A^2\, J_{2\,A} \begin{pmatrix} A & B & C \\ B & D & E \\ C & E & -A-D \end{pmatrix}, \tag{4.56}$$

$$A = \frac{1}{3} - \cos^2\alpha^A_{\rm pole}\, \cos^2\delta^A_{\rm pole}, \tag{4.57}$$

$$B = -\frac{1}{2}\sin 2\alpha^A_{\rm pole}\, \cos^2\delta^A_{\rm pole}, \tag{4.58}$$

$$C = -\frac{1}{2}\cos\alpha^A_{\rm pole}\, \sin 2\delta^A_{\rm pole}, \tag{4.59}$$

$$D = \frac{1}{3} - \sin^2\alpha^A_{\rm pole}\, \cos^2\delta^A_{\rm pole}, \tag{4.60}$$

$$E = -\frac{1}{2}\sin\alpha^A_{\rm pole}\, \sin 2\delta^A_{\rm pole}. \tag{4.61}$$

Deviations from the predicted value should indicate wrong assumptions on the hydrodynamical models for the planets (i.e. the presence of a fast rotating core) or a failure on the prediction of the light deflection effect by the standard theory of light propagation, thus compromising the dark matter estimations on galaxy clusters inferred from the light deflection contribution (Kopeikin 2006a).

The values of the angular coordinates used of the poles are given in Tab. 4.2.2, which has been obtained from Seidelmann *et al.* (2005). It is available in electronic form through `http://astrogeology.usgs.gov/Projects/WGCCRE/`.

Ephemeris uncertainties: δ_l,δ_m shifts

The light deflection effect observed for a given planet clearly depends on the actual position of its center of mass ($\boldsymbol{x}_A$). Given some coordinates (say BCRS coordinates), the trajectory of the center of mass of a body are the events where the mass dipole of the body vanishes for any t. Then, an error on the expected position of a body provided by the ephemeris of the solar system can be observed as a spurious dipolar gravitational field. This analogy is used by some authors (Kopeikin 2006a) to describe the associated light deflection pattern as a dipolar deflection effect. We prefer to avoid such an interpretation since it is a purely coordinate effect which obfuscates the real issue, the positional accuracy of the ephemeris required for testing the light deflection

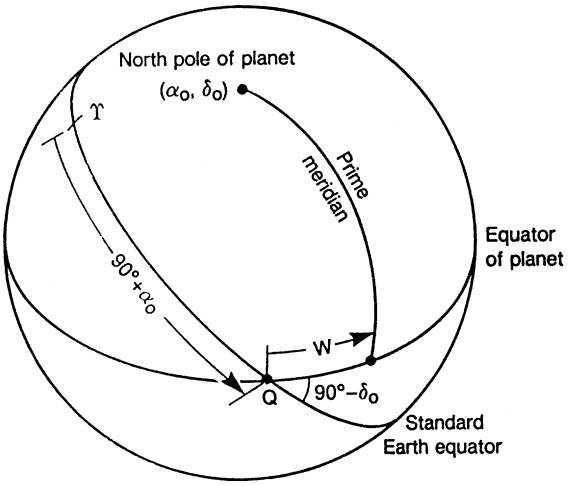

Figure 4.5: Reference system used to define orientation of the planet.

Table 4.2: Recommended values for the direction of the north pole of rotation of the Sun and planets (2000)

α_0, δ_0 are standard equatorial coordinates with equinox J2000 at epoch J2000. Approximate coordinates of the north pole of the invariable plane are $\alpha_0 = 273.^\circ85$, $\delta_0 = 66.^\circ99$.

T = interval in Julian centuries (of 36525 days) from the standard epoch.

The standard epoch is 2000 January 1.5, i.e., JD 2451545.0 TCB.

Sun	$\alpha_0 = 286.^\circ13$	$\delta_0 = 63.^\circ87$
Mercury	$\alpha_0 = 281.01 - 0.033T$	$\delta_0 = 61.45 - 0.005T$
Venus	$\alpha_0 = 272.76$	$\delta_0 = 67.16$
Earth	$\alpha_0 = 0.00 - 0.641T$	$\delta_0 = 90.00 - 0.557T$
Mars	$\alpha_0 = 317.68143 - 0.1061T$	$\delta_0 = 52.88650 - 0.0609T$
Jupiter	$\alpha_0 = 268.05 - 0.009T$	$\delta_0 = 64.49 + 0.003T$
Saturn	$\alpha_0 = 40.589 - 0.036T$	$\delta_0 = 83.537 - 0.004T$
Uranus	$\alpha_0 = 257.311$	$\delta_0 = -15.175$
Neptune	$\alpha_0 = 299.36$	$\delta_0 = 43.46$
Pluto	$\alpha_0 = 313.02$	$\delta_0 = 9.09$

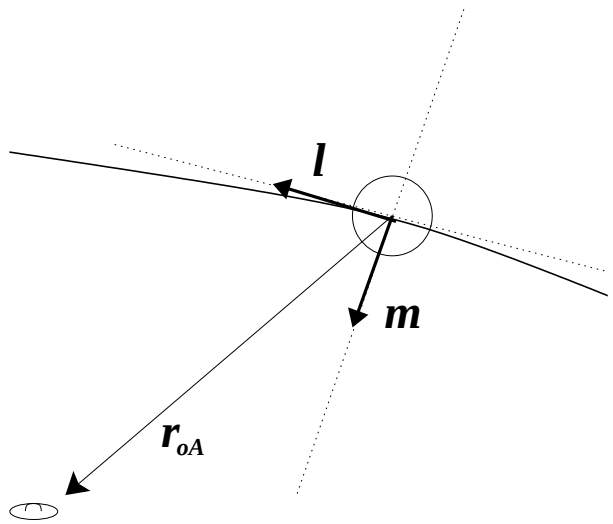

Figure 4.6: Ortonormal unit vectors used to correct the position given by the ephemeris.

effect.

We introduce a parameterized two dimensional shift to the body nominal position as

$$\boldsymbol{x}_A = \boldsymbol{x}_A^{eph} + \delta_l \boldsymbol{l}_A + \delta_m \boldsymbol{m}_A \tag{4.62}$$

where $\boldsymbol{x}_A^{eph}$ is the position of the solar system body A provided by the ephemeris (i.e. Standish (2004), Fienga *et al.* (2006), or Pitjeva (2005)). The two unit vectors $\boldsymbol{l}_A$ and $\boldsymbol{m}_A$ are constructed on the instantaneous position of the body at the instant of observation as

$$\boldsymbol{l}_A = \left\langle \boldsymbol{v}_A^{eph} \right\rangle \tag{4.63}$$

$$\boldsymbol{m}_A = \langle \boldsymbol{r}_{OA} \times \boldsymbol{l}_A \rangle \tag{4.64}$$

where $\boldsymbol{l}_A$ is a unit vector in the instantaneous direction of motion, $\boldsymbol{m}_A$ is perpendicular to the instantaneous velocity and to the apparent direction the planet. This parametrization is chosen to introduce all the correlation of the positional errors with the dynamical parameter α_r in δ_l.

The ephemerides shifts cannot be obtained as full mission parameters since they depend on the uncertainty of the ephemeris as a function of time. If the ephemeris shifts can be obtained with the required accuracy, each transit will provide a positional measure of the planet. The quality of the equivalent measurement of the planet position clearly depends on how many bright stars are observed close to the planet during each transit.

4.2.3 Observed unit direction and aberration

Just for the sake of completeness, let us briefly describe the formula used to compute the direction measured by an inertial observer at the satellite position (Center of Mass Reference system, see Klioner (2004)). In general, the observed unit direction is given by the projection of the tangent null vector to the local tetrad of an arbitrary observer. The observer's local tetrad can be determined from its trajectory and the BCRS metric up to a spatial rotation which must be fixed by convention. One standard convention is to impose that the spatial axis of the satellite reference system are chosen to be oriented as the BCRS (kinematically non-rotating tetrad). In such a way, some non-inertial forces are introduced. They can be completely neglected (as the tidal gravitational fields) as long as the observer is small (a few meters) and the data acquisition process is not too long (a few minutes). A detailed discussion on this issue can be found in Klioner (2004).

We adopt the approach given in Klioner (2003). The observed unit direction by a given inertial observer whose spatial axis are assumed to be kinematically non-rotating can be computed as

$$\boldsymbol{s} = \left(\boldsymbol{n} + \left\{ \frac{\Gamma}{c} + [\,\Gamma - 1\,]\, \frac{\boldsymbol{v}\cdot\boldsymbol{n}}{|\boldsymbol{v}|^2} \right\} \boldsymbol{v} \right) \frac{1}{\Gamma\,(1+\boldsymbol{v}\cdot\boldsymbol{n}/c)}, \tag{4.65}$$

$$\Gamma = \frac{1}{\sqrt{1-|\boldsymbol{v}|^2/c^2}}, \tag{4.66}$$

$$\boldsymbol{v} = \dot{\boldsymbol{x}}_o \left(1 + \frac{1}{c^2}\,(1+\gamma)\,\omega(\boldsymbol{x}_o) \right) + \mathcal{O}(c^{-4}). \tag{4.67}$$

where $\boldsymbol{v}$ is the BCRS coordinate velocity of the observer at the instant of observation. This expression is the general relativistic version of the light aberration described by special relativity (setting $\omega = 0$ the special relativistic formula is recovered).

4.3 Local tests. Overview of the experiment

This study is focussed on the determination of the parameters in the relativistic model for light propagation using Gaia observations close to the planets of the Solar System. In order to make it realistic, a number of relevant features inherent to the Gaia observations must be taken into account. They are; an schematic model of the Gaia focal plane, an astrometric error model, realistic Solar System ephemeris and the nominal Gaia orbit, a realistic scanning law, and a fully relativistic model for the light propagation in the Solar System (as described in the previous sections). To perform this experiment several conceptual simplifications with respect to the actual Gaia design have been applied. The relevant features of the adopted approach are detailed in the next subsection.

4.3.1 Relevant aspects of the Gaia mission and Simulated data

Two astrometric focal planes

The instrument consists on two independent fields of view pointing towards two different directions. Each field of view consists on a patch of the sky of $0.7\,\mathrm{deg} \times 0.7\,\mathrm{deg}$ parameterized using two angular coordinates a_L and a_C. The across scan a_C is the angle between a star and the instantaneous plane of rotation. The along scan angle a_L is the angle between the source and the center of the field of view projected in the scanning direction. The angle a_L is much better measured than a_C and contains most of the relevant astrometric information.

Simulation process and astrometric error model

Each FoV contains nine CCD columns[2](see Fig. 4.7). The along scan angles of the nine CCD columns are assumed to be known and constant. As the satellite slowly rotates, the stars slowly cross the CCD columns in the a_L direction. The instant at which a star crosses the nominal position of a CCD column [3] is the simulated quantity that is used in the data reduction as the input.

The full simulation process to produce the instants of CCD transits is described below step by step

[2]They are also organized in 9 CCD rows but this is irrelevant for our discussion here
[3]position of the last pixel in a CCD column

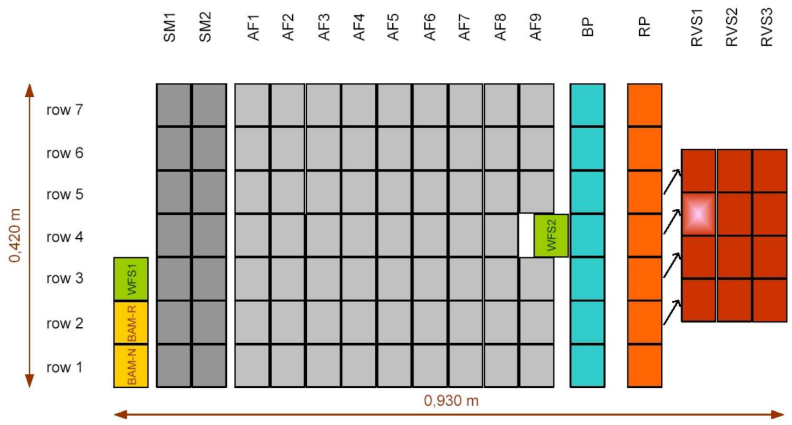

Figure 4.7: The Gaia focal plane. The viewing directions of both telescopes are superimposed on this common focal plane which features 7 CCD rows, 17 CCD strips, and 106 large-format CCDs, each with 4500 TDI lines, 1966 pixel columns, and pixels of size 10μm along scan $\times$30μm across scan (59 mas $\times$ 177 mas). Star images cross the focal plane from left to right. The astrometric CCDs are those depicted in light gray. Figure courtesy of EADS Astrium.

- The approximate position of a planet is computed in the CoMRS each $\Delta = 30$ minutes as $t_p^n = t_p^{n+1} + \Delta$ with $t_p^0 = JD2012$.
- If it the planet is observed close enough to the central position of one of the FoV, we have a planetary transit. A catalog input stream of all the sources around the planet is initialized. The source in the catalog are stored in 1 deg $\times$1 deg files. Typically, 9 catalog files are processed at each planetary transit.
- The information of one star is retrieved from the catalog.
- The along scan angle of the CCD column a_L^{CCD} is retrieved from the instrument model.
- Here starts the core iteration process to determine the instant of transit. The seed value for the instant of transit is t_p^n.
- The astrometric model of an object, the light propagation model, and the ephemeris information of the observer (position and velocity) are used to obtain the observed direction of a source in the CoMRS.

- The scanning law(and a simple instrument model) is used to build the rotation matrix (attitude matrix) required to transform the observed direction to its current FoV coordinates. The difference between the along scan angle of the source and the current CCD column is obtained as $\delta^{(i)} = a_L^i - a_L^{CCD}$. If the across scan angle is larger than the size of the focal plane, the iterative process is interrupted and the star is discarded since it falls outside the focal plane.

- If $|\delta| > 0.5\mu$as, the current instant of time is corrected by $t^{(i+1)} = t(i) - \delta\Omega$, where $\Omega = 60'' s^{-1}$ is the scanning rate. This process is repeated until convergence is reached or the maximum number of iterations is overpassed.

- The astrometric error model is used to add the noise to the measurements as a function of the star photometric information in the catalogs.

- This process is repeated for each CCD column

- A telemetry segment is generated containing the catalog information (astrometry and photometry) the Field of view and the nine instants of transit. The telemetry segment is stored in the telemetry file generated for this planetary transit.

- The process is repeated until there are no more stars in the catalog input stream. The telemetry file is closed. This closes the cycle of a single transit simulation.

- The full process is repeated until the end of mission instant is reached by t^p.

This simulation cycle is sketched in the block diagram in Fig. 4.8.

The error model applied is very simple and (in our simplified version) only depends on the V magnitude. Using a random number generator, Gaussian noise is added to each instant of CCD transit. The standard deviation of the noise generator is given by

$$\sigma_t = \frac{A_{15}}{\Omega} \times 10^{0.2(V-15)} \,. \tag{4.68}$$

where V is the visual magnitude of the star, $A_{15} = 300\mu as$ is the accuracy per CCD transit reached for a star of magnitude 15 and $\Omega = 60'' \, s^{-1}$ is the scanning rate. For stars brighter than $V = 12$ the accuracy does no longer depend on the limiting magnitude and it is fixed to $90\mu as$. Stars brighter than $V < 8$ are not considered since they are too bright and it is not clear if good quality astrometry can be obtained.

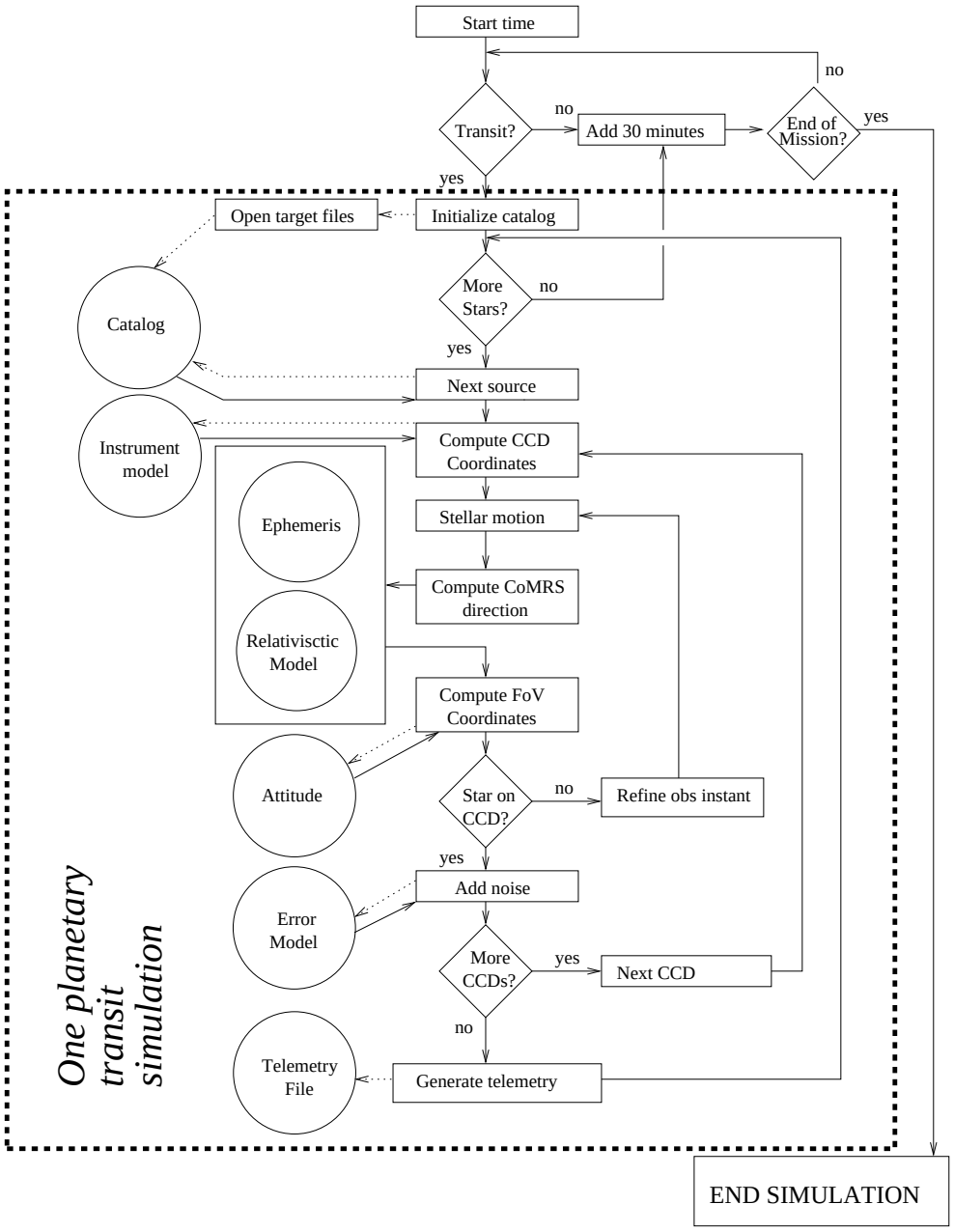

Figure 4.8: Block diagram of the simulation cycle. The dashed lines indicate that a *query* and some information is sent to some independent piece of code (circles). The circles contain pieces of code or libraries which job depends on the particular models used for the simulations. In Fortran, each circle should be a library with some subroutines, in Java one *interface* should be defined with at least one implementing class for each circle. The details on the software implementing this block diagram are given in Appendix A.

The result of a full mission simulation one telemetry file per planetary transit. Typically 120 telemetry transit files are obtained. It is an ASCII file, and each line contains the information of a stellar transit. A telemetry file looks like

```
    RA        DE        B       V    FoV       t1       ...      t9
226.50150 -17.6458   16.78   15.78   -1   2956.265197 ...   2956.265626
226.50166 -17.9079   17.15   15.90   -1   2956.265271 ...   2956.265701
...
```

where RA is the Right Ascension in degrees, DE is the declination in degrees, B and V are Johnson magnitudes and $t1 \ldots t9$ are the instants of transit for each CCD. `FoV` is a flag to identify which FoV is used ($+1$ or -1). Each row represents one star.

Gaia scanning law

The Gaia scanning law has been carefully designed to assure full sky coverage each 6 months with a reasonable sampling rate. At the end of mission it is guaranteed that each part of the sky will observed between 50 and 250 times, being 80 the average number of observations per object (this not applies to solar system objects because they continously change their position). Figure 4.9 shows an example of the sky coverage rate at the end of the 5 years mission assuming that the nominal scan law is preserved along the mission.

The satellite slowly rotates on the plane perpendicular to the instantaneous rotation axis $\boldsymbol{z}$ completing a revolution each 6 hours. The $\boldsymbol{z}$ axis precesses very slowly (roughly one precession cycle each 2 months) on a cone of 45 deg around the instantaneous direction of the Sun. The angle that regulates the 6 hours revolution period is called "revolving phase" and the angle on the cone around the sun is called "precession phase".

Given the initial instant, the nominal scanning law has two free parameters, the *initial revolving phase* and the *initial precession phase*, which determine the whole sequence of observations.

Since the precession rate is very small, the initial revolving phase η_0 is not very relevant for the number of times a star is going to be observed, but it is important in our experiment because the relatively fast motion of the planets. Jupiter takes 3 hours to move a distance equal to its radius. A star that provides a very strong measurement

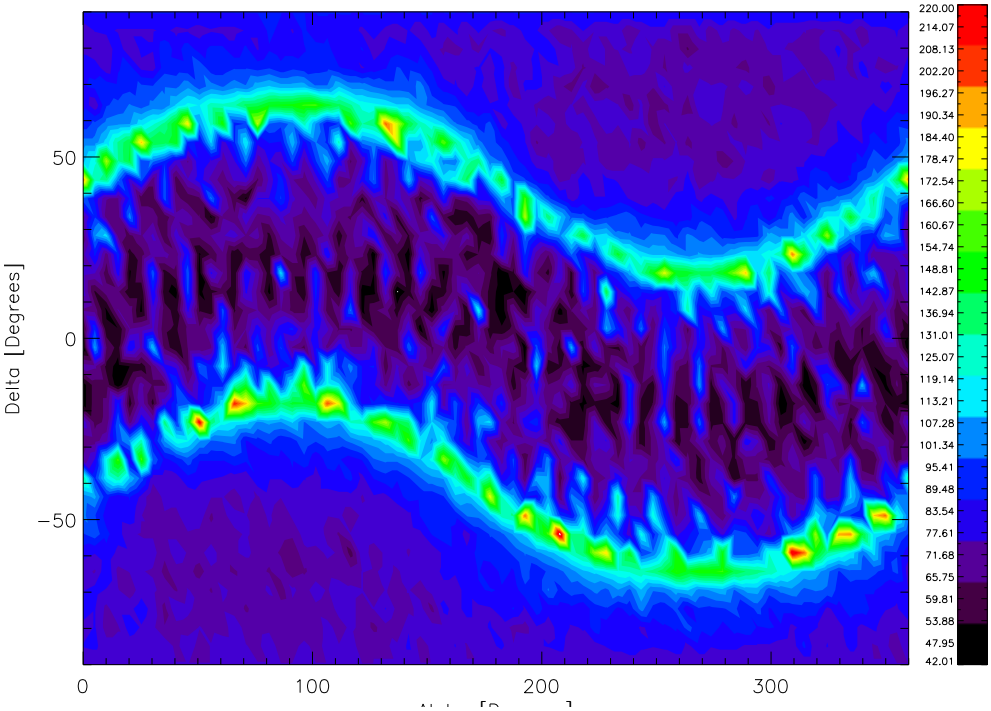

Figure 4.9: Diagram of the sky coverage. The color indicates the number of times a given direction is observed after a 5 years mission. The horizontal axis corresponds to the right ascencion angle (in degrees) and the vertical axis is declination (in degrees).

of the quadrupole, can be observed with almost null quadrupolar deflection a couple of hours later.

A careful combination of both, can greatly improve the local deflection experiment, specially for the Jupiter quadrupolar deflection. Section 4.3.2 is devoted to this issue.

The sky Catalog

The Catalog used is GSC2.3.1[4] which contains around a billion objects Spagna *et al.* (2006). Despite it is not highly reliable at the faintest magnitudes ($V > 19$), it is statistically comparable to the expected Gaia catalog. The GSC2.3.1 catalog provides the photometry of the stars in three photograhpic bands F_{pg},J_{pg} and N_{pg}; and B and V Johnson colors for for brighter objects. In order to obtain the B and V magnitudes for the faint sources ($12 < V < 20$), at least two relations are required. One them is provided by the GSC 1.1 catalog realization (Russell *et al.* 1990), which relates the photographic F_{pg} with B and V as

$$J_{pg} = V + \alpha\,(B - V) \tag{4.69}$$

where $\alpha = +0.72$. The additional relation has been obtained from the statistical properties of the bright stars. Assuming that the $(F_{pg}-J_{pg})$ color index is proportional to $(B - V)$ it is obtained that

$$(F_{ng} - J_{ng}) = \kappa\,(B - V) \tag{4.70}$$

where κ is obtained from a linear fitting using the bight stars of the catalog and is equal to $\simeq 0.8$. On very faint stars, only one magnitude is known(J_{pg} or F_{pg}). In this case, the average $(F_{pg} - J_{pg})$ color index obtained again from the bright objects is used to obtain approximated B and V colors.

The stars are considered static and their position is assumed without uncertainties. The uncertainties emerging from potentially poor astrometric characterization of the sources are assumed to be contained in the error model given in (4.68).

[4]as available through the web site `http://galex.stsci.edu/GSC2/GSC2WebForm.aspx`

4.3.2 Preliminar considerations. Optimizing the initial parameters of the scanning law

The scientific outcome of the Gaia mission concerning the tests on the Giant planets critically depends on favorable conditions at the moment of observation of the planet. This is a critical issue for the measure of the Jupiter Quadrupolar deflection and the gravitomagnetic effect, since both contributions show a strong dependence on the angular separation of the star with the planet (ψ^{-3} and ψ^{-2} respectively). For the quadrupole, it is expected to achieve most of the accuracy from a few good observational events; this is, bright stars observed close to the planetary limb. Only stars observed beyond 1.1 times the radii of the planet are considered since it is a hard limit to the Gaia observational capabilities close to bright extended sources.

A typical process of simulation/reduction has a typical duration of three or four days (running on a single Pentium4-like machine). In order to test a large number of different initial conditions, instead of preforming the full simulation-reduction process, we define the Signal-to-Noise Ratio of a parameter P as

$$SNR_P = \sqrt{\sum_i SNR_P^{(i)\,2}}, \tag{4.71}$$

$$P = \gamma, \epsilon, \alpha_r, \dots, \tag{4.72}$$

where $SNR_P^{(i)}$ is the Signal-to-Noise Ration of the i-th observation alone(full focal plane transit of a star). For a single observation, the SNR is the contribution of each effect (monopole, quadrupole, dynamical) projected in the instantaneous scanning direction divided by the error of the measurement. Therefore, the SNR contribution of the i-th observation is

$$SNR_P^{(i)} = \frac{\boldsymbol{u} \cdot \boldsymbol{s}^{(i)},_P}{\sigma_{(i)}}, \tag{4.73}$$

$$\boldsymbol{s}^{(i)},_P = \frac{\partial \boldsymbol{s}^{(i)}}{\partial P}, \tag{4.74}$$

where $\boldsymbol{u}$ is the instantaneous scanning direction, $\boldsymbol{s}^{(i)}$ is the observed direction in the Satellite Reference System, $\partial \boldsymbol{s}^{(i)}/\partial P$ is the partial derivative of the observed direction $\boldsymbol{s}$ with respect to the parameter K and $\sigma_{(i)}$ is the formal error of the i-th measure (obtained from the error model, see (4.68)). The inverse of SNR should coincide with

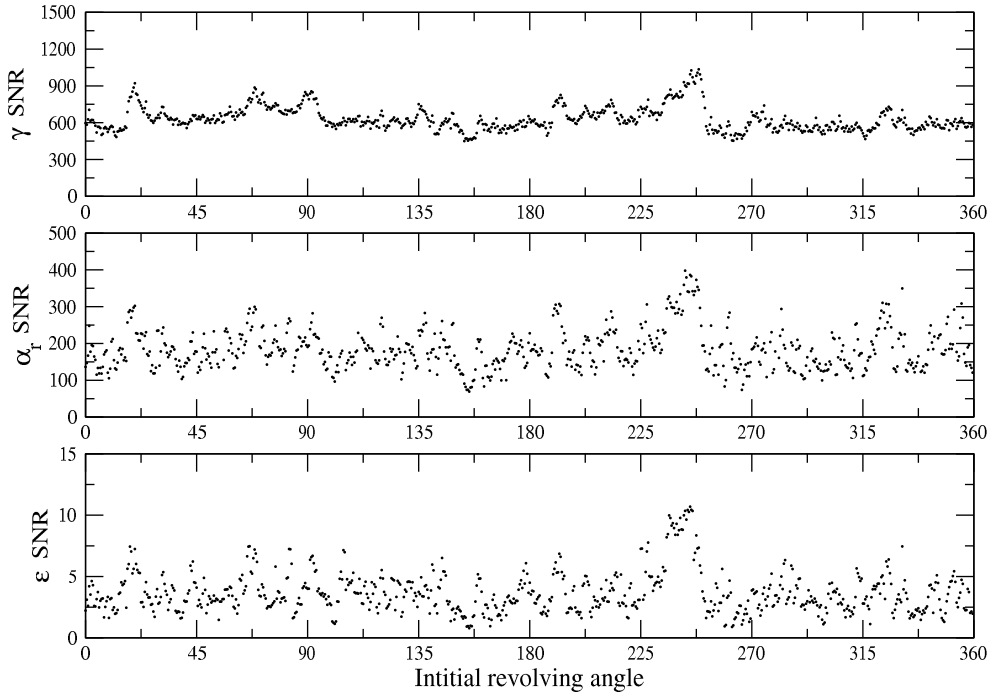

Figure 4.10: Full mission SNR obtained for the parameters of Jupiter as a function of the initial revolving angle. The initial revolving angle is sampled at each 0.5 deg from 0 deg to 360 deg.

the relative error σ_P/P. Explicity, it is expected that

$$\frac{\sigma_P}{\langle P\rangle} \quad = \quad \frac{1}{SNR_P}\,. \tag{4.75}$$

A full SNR of γ, the dynamical coefficient and the quadrupolar deflection can be numerically obtained in a couple of minutes if a limited version of the catalog up to $V < 16$ is used. This permits to test many different configurations

As an example, we show the SNR obtained for the three parameters in the model for different choices of the initial precession phase(see Fig. 4.10–4.13). JD2012 is used as the start of mission used and initial revolving phase is fixed to 0. The results for the retardation parameter and the J_2 coefficient are shown in Fig. 4.10. It is clear that a careful choice of the initial precession phase ξ_0 can improve the expected accuracy

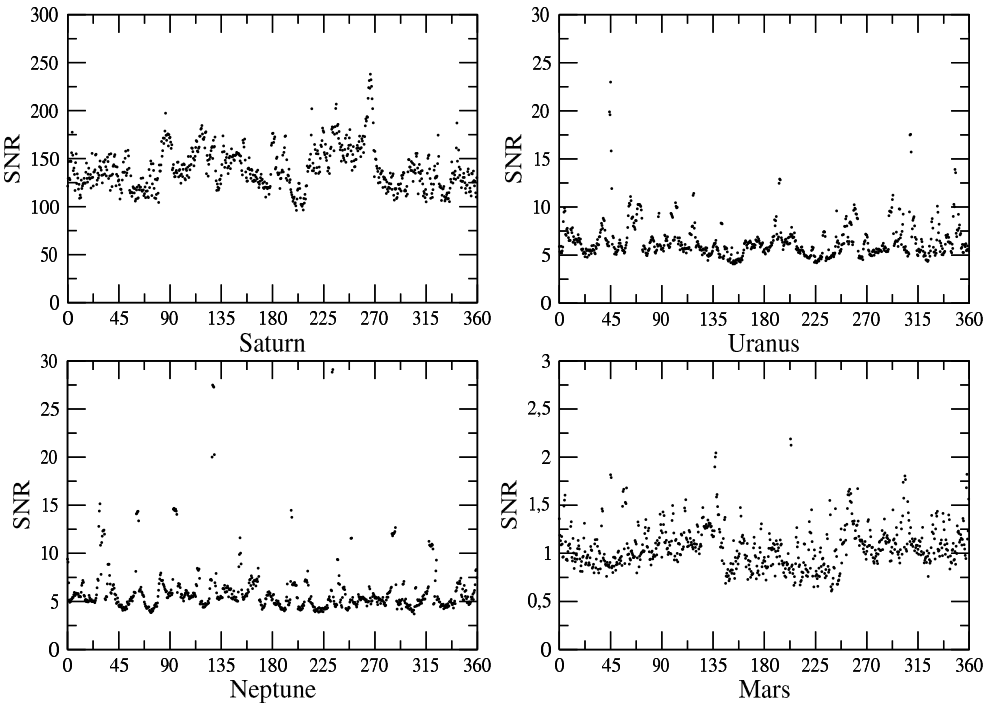

Figure 4.11: Full mission SNR for the γ parameter for the other relevant planets.

of such parameters (specially for the quadrupolar deflection, that has a peak when $\xi_0 = 245\,\mathrm{deg.}$).

Similar analysis can be carried out on Saturn and the other planets. In the case of Saturn, the SNR for the monopolar deflection predicts that it will be measured with reasonable accuracy ($\sigma_\gamma \sim 5\,10^{-3}$). Concerning the quadrupole, even in the best situation one can only expect a $SNR_{J_2} \sim 3$ in very favorable circumstances. For the dynamical parameter, a good choice of the initial phases can produce a complementary measurement to the one obtained from Jupiter alone. It would be a lucky coincidence that the optimal ξ_0 for Saturn coincides with the one for Jupiter.

The numbers shown in this section are only estimations, and are given only to illustrate the different quality of the results that can be obtained under different potential scenarios.

In the analysis discussed in the following sections, we generate simulated data

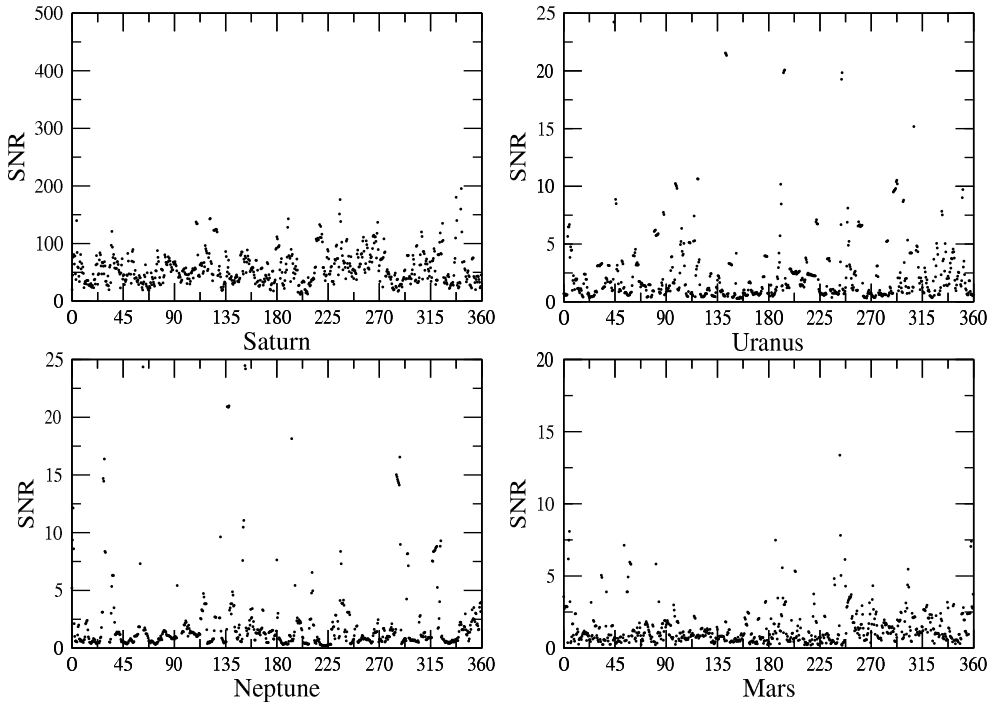

Figure 4.12: SNR for the α_r parameter for the other relevant planets.

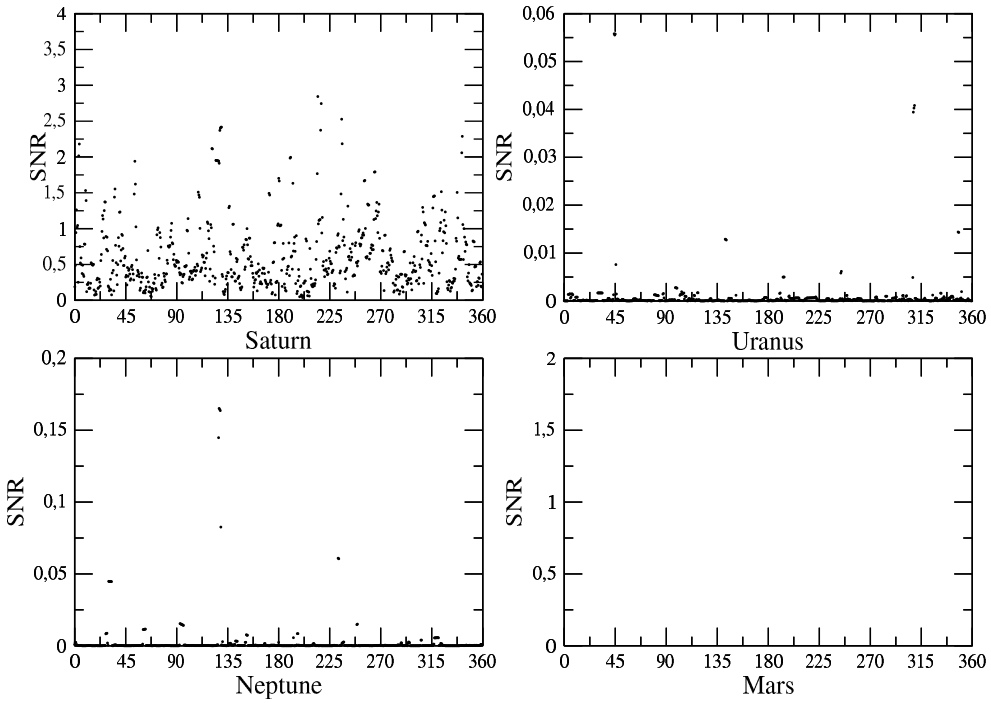

Figure 4.13: SNR for the ϵ parameter for the other relevant planets.

under two of such potential scenarios. The first data set is generated for an average quality ξ_0 selection (say $\xi_0 = 0\,\mathrm{deg}$). Let us call it *Standard SNR* and this provides the expected accuracy under normal mission operation circumstances. Let us note that unfortunate combinations of the initial conditions can lead to even poor results (see Fig. 4.10). The second data set is generated choosing ξ_0 which provides the best SNR expectation for the measure of the quadrupole deflection J_2 ($\xi_0 = 246\,\mathrm{deg}$, see Fig. 4.10). In both datasets, the start of mission instant is assumed to and be JD2012 and the initial revolving phase is set to 0.

4.3.3 Data analysis

Given a simulated dataset, we can limit the number of objects used in the reduction by restricting the maximal angular distance ψ_{max} at which the stars are considered from the planet and by using objects than brighter than a limiting magnitude V_l.

The adopted data reduction procedure is performed in two blocks. First an iterative Least-square solution is used to get an approximation to the best solution. Afterwards, the Montecarlo integration of the Bayesian Probability Distribution Function (PDF) is applied to obtain the expected values, the correlations and the the standard deviations of the parameters.

Nonlinear Least square

This step of the data reduction consists into obtaining the set of parameters contained in the model that minimize the sum of quadratic differences between the expected and the actually measured focal plane positions.

$$\Xi^2 = \sum_i \frac{\left(F^{obs}(t_i) - F^{teo}(t_i;\gamma,\alpha_r,\epsilon_A,\ldots)\right)^2}{\sigma_i^2} \tag{4.76}$$

where $F_(i)^{obs}$ is the focal plane position of a CCD column in the along scan direction and $F_(i)^{teo}$ is the along scan angle of the star image predicted by the model.

Since the model for $F_(i)^{obs}$ is not linear with the parameters, we used an iterative procedure to get the best fit values. The mathematical details of the procedure can be found in any basic textbook on statistics (i.e. Press *et al.* (1992)). Given a set of values for the parameters $\boldsymbol{\lambda_0}$(seed values), a first order Taylor expansion of the

function is obtained around $\boldsymbol{\lambda}_0$.

$$F_{(i)} \simeq F_{(i)}(\boldsymbol{\lambda}_{(0)}) + \left.\frac{\partial F_{(i)}}{\partial \lambda^k}\right|_{\boldsymbol{\lambda}_0} \delta\lambda^k \tag{4.77}$$

The partial derivatives are obtained numerically. If N_S is the number of full transits and for each transit we have 9 *instant of CCD transits*, we have $N_S \times 9$ linear condition equations of the form

$$\frac{F^{obs}_{(i)} - F^{teo}_{(i)}}{\sigma_i^2} = \frac{1}{\sigma_i^2} \sum_k \left.\frac{\partial F_{(i)}}{\partial \lambda^k}\right|_{\boldsymbol{\lambda}_i} \delta\lambda^k \tag{4.78}$$

where $\boldsymbol{\lambda}_i$ is the i-th refinement of the parameters. The three unknowns are the corrections $\delta\lambda_k$ to be applied to each relativistic parameter in order to get closer to the Least Square solution. With the updated parameters, the partial derivatives and the residuals $F^{obs}_{(i)} - F^{teo}_{(i)}$ are recomputed and a new set of condition equation is solved until convergence is reached. Since the problem is well behaved, the solution is reached in two or three iterations.

Since we are dealing with a large number of observations (a few millions), the normal equations (see Press *et al.* (1992)) are built directly adding the observations one by one instead of building first the condition equations. This saves a lot of memory and processing time. Such a standard least-square solution is the most economical way to proceed but it is only reliable under well defined conditions (Gaussian noise, no biases in the data, no local minimas, etc.). The covariance matrix containing the correlations between the parameters is also obtained. They are used in the next step of the data reduction (Montecarlo intergation of the Bayesian probability function) to set the limits of integration (only parameter values at 5 σ of the least square solution are used).

Bayesian analysis

After the least-square solution is found, a bayesian analysis is used to obtain the probability density function of the parameters given the data. Since it is a quite intensive computer task it is not used to perform the initial fit of the parameters (least squares approach works quite faster) but it is a robust way to estimate and evaluate the quality of the obtained values.

The details of the *Bayesian* procedure are described in the Appendix C.1. The Probability Distribution Function for the parameters given the data is sampled around the least-squeare solution, and Montecarlo integration is used to compute the central moments of the PDF and obtain the expected values, variances and correlations of the parameters. This is the final product of our data reduction scheme.

Data reduction block diagram

The block diagram describing the data reduction process is given in Fig. 4.14. The process can be described as follows

- Initialize all the required modules (ephemeris, satellite model, etc.)
- Put all the telemetry files inside one single file (full mission telemetry file).
- Open the full mission telemetry file and check which stars satisfy the reduction conditions. This is if they are bright enough $V < V_l$ and if they are observed close enough to Jupiter $\Psi < \Psi_{max}$).
- A list with the good sources is generated (the list of good sources is uploaded in memory if they are not too much to speed-up computations).
- Begin the non-Linear Least square loop
- A telemetry segment of a good star is readed.
- For each CCD transit instant, the predicted field angle and the partial derivatives with respect the parameters are computed.
- The information of each single CCD transit is accumulated in the normal equations (the condition equations would require a lot of memory). Each equation is weighted depending on the mangitude of the star. The weight is computed from the expected noise amplitude obtained from the error model as a function of the star brightness in the V band.
- When all the CCD transits of all the stars are processed, the normal equations are solved and the relativistic parameters updated.
- The non-Linear Least Square loop is done at least 3 times to be sure that the system has converged.

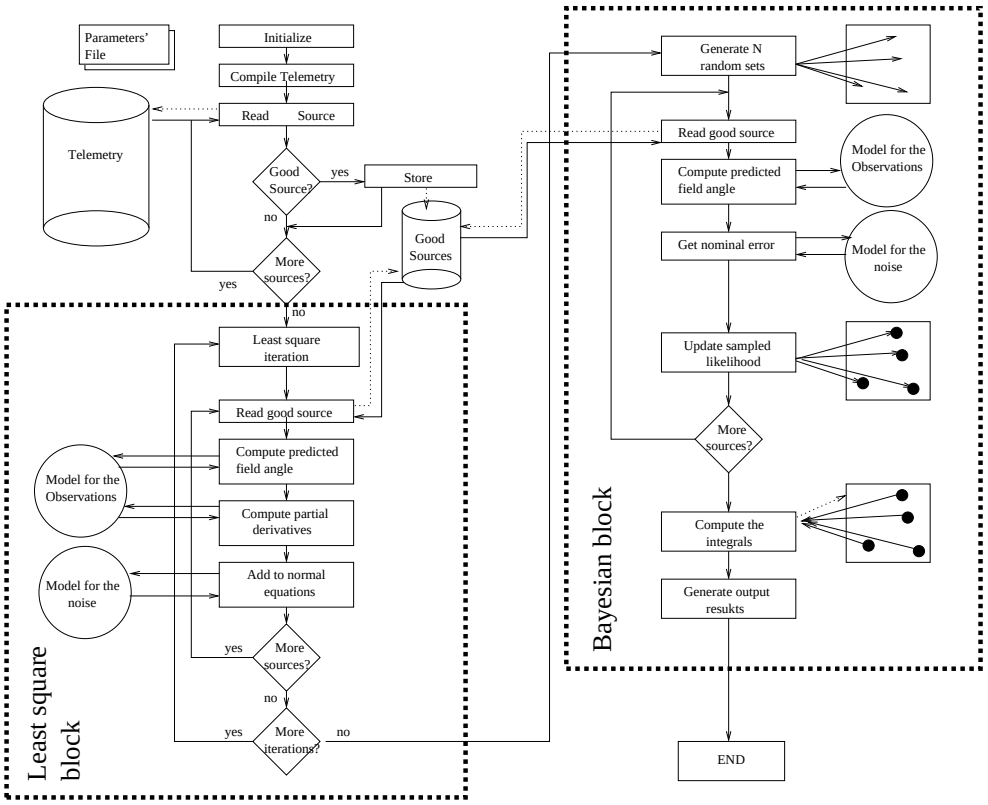

Figure 4.14: Block diagram of the simulation cycle. The dashed lines indicate that a *query* and some information is sent to some independent piece of code (circles). The circles contain pieces of code or libraries which job depends on the particular models used for the simulations. In Fortran, each circle should be a library with some subroutines, in Java one *interface* should be defined with at least one implementing class for each circle. The details on the software implementing this block diagram are given in Appendix A.

The results of this first block are the best fit values for the parameters, and the covariance matrix. Then the bayesian part begins using this information

- A collection of N different combinations of parameters is generated. The generation is restricted up to ± 5 standard deviations from the Non-linear Least Squares solution.
- A telemetry segment of a good star is readed. For each CCD transit time, the likelihood function is computed (see Appendix C.1)at each point of the collection. In such a way, the likelihood function is updated as new observations are readed and processed.
- The normalization and the numerical integrals of the likelihood function are computed and the expected values, the confidence intervals, the correlations and the higher moments of the bayesian probability distribution function are obtained.

The least square solution is relatively faster than the Bayesian procedure. For the whole set of observations (using all the stars within $30'$ up to $V \sim 20$), it takes around four days of computing time in a single PC (PentiumIV–3GHz, 1Gb RAM, under Linux/OS).

4.4 Obtained results. Jupiter

4.4.1 Monopolar deflection

As it is shown in Table 4.3, the measure of the Jupiter deflection alone is potentially capable to provide an independent measure of γ better than the one obtained by the full HIPPARCOS mission for the Sun (see Tab. 4.1. The final accuracy will depend on the final instrument performance and the initial conditions for the scanning law, but not very critically.

Since, for small angles, the monopolar deflection falls as ψ^{-1}, stars relatively far from the apparent direction of the planet still contribute significantly to the measure. This is clearly seen in Fig. 4.15–4.16, where different maximum angular distances are used. Despite the improvement is not very spectacular it is clear that, at least, sources up to $10'$ should be considered in the fit of γ. The dependence with the limiting

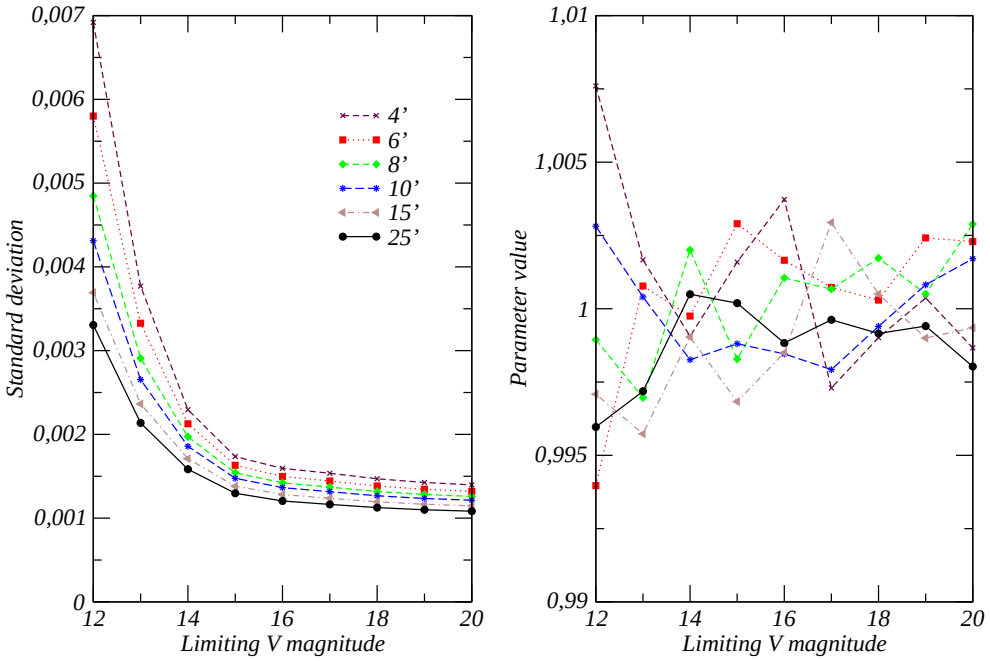

Figure 4.15: (Left)Standard deviation on the accuracy of the γ determination as a function of the maximum angular distance permited and the limiting magnitude. Slight improvement is achieved enlarging the area around the planet. A much stronger dependence on the limiting mangitude is evident. (Right) Corresponding least square values for the γ parameter

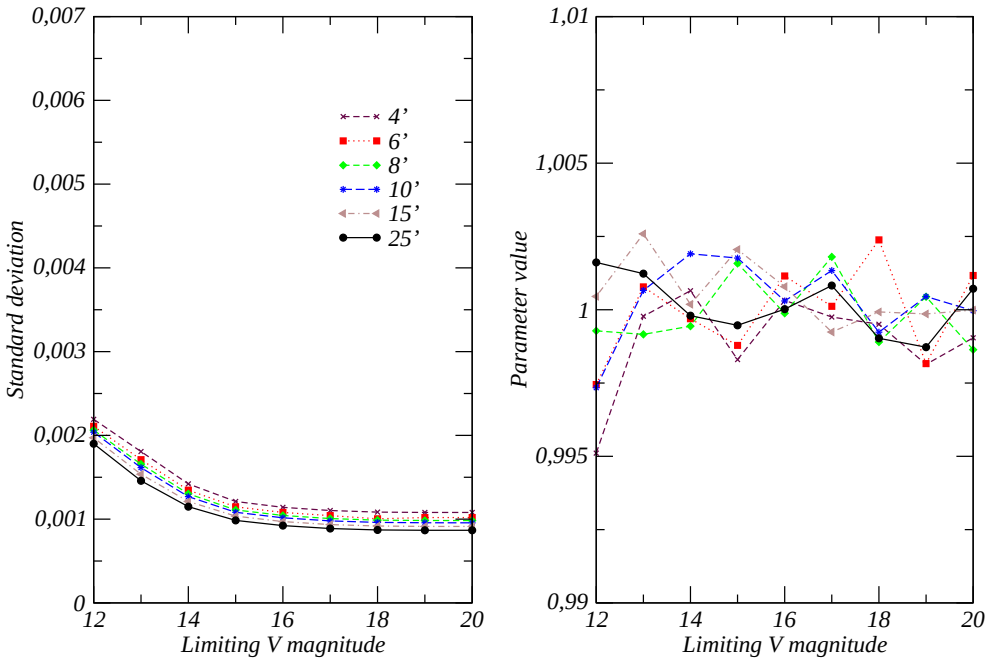

Figure 4.16: Same as Fig.4.15 but using an an optimized choice of the initial coinditions. The optimization is based on the SNR of J_2 but is clearly seen in the figure that the value of γ is also significantly improved.

magnitude is much more obvious in Fig. 4.15. Despite the faintest stars provide inaccurate measures, the number of them grows exponentially with the magnitude. From the catalog statistics $N_V \sim 10^{0.45\,V_l}$ and the error model in (4.68), it can be obtained that the astrometric SNR of any parameter scales as

$$SNR \sim 10^{0.025\,V_l}\,. \tag{4.79}$$

Since the index in the exponent is positive, increasing the limiting magnitude always helps to the solution in a statistical sense. Very faint objects may be strongly affected by systematics, thus using stars up to $V \sim 17$ seems to be a good compromise. This discussion is also for other relativistic parameters for all the other planets as well.

Since the correlation of γ with the other two parameters is not very large in a full mission reduction (never larger than a 30%), all of them can be fitted simultaneously. The situation is slightly more delicated for single transit experiments, which is discussed in Section 4.4.4.

Compared to previous estimations of γ ((Treuhaft & Lowe 1991) and Whipple *et al.* (1996)) from the Jupiter deflection alone, we conclude that the Gaia measure of the Jovian monopolar deflection is a very competitive experiment, quite independently from the initial scanning law parameters.

4.4.2 Quadrupolar deflection

The final accuracy at which J_2 can be measured strongly depends on many observational factors. The strong SNR dependence on the scanning law initial conditions has been shown in Fig. 4.10. Since the quadrupolar effect strongly depends on the angular separation of the source and Jupiter, it should be clearly stated which is the minum distance from the Jupiter limb at which measurements can be performed. Since this is not clear at the present stage, we consider the best case, which assumes that all the source can be observed at 0.1 planet radii from its surface.

Contrary to the situation discussed by Kopeikin (2006a) where only a few number of objects is available, J_2 is not highly correlated in a global sense with the other parameters relevant to the deflection process. Despite the quadrupolar deflection has tangent components to the relative position of the star and the center of mass of Jupiter, the orientation and the structure of such shifts are quite different from the dynamical correction(i.e. the rotation axis of Jupiter is sensibly tilted with respect

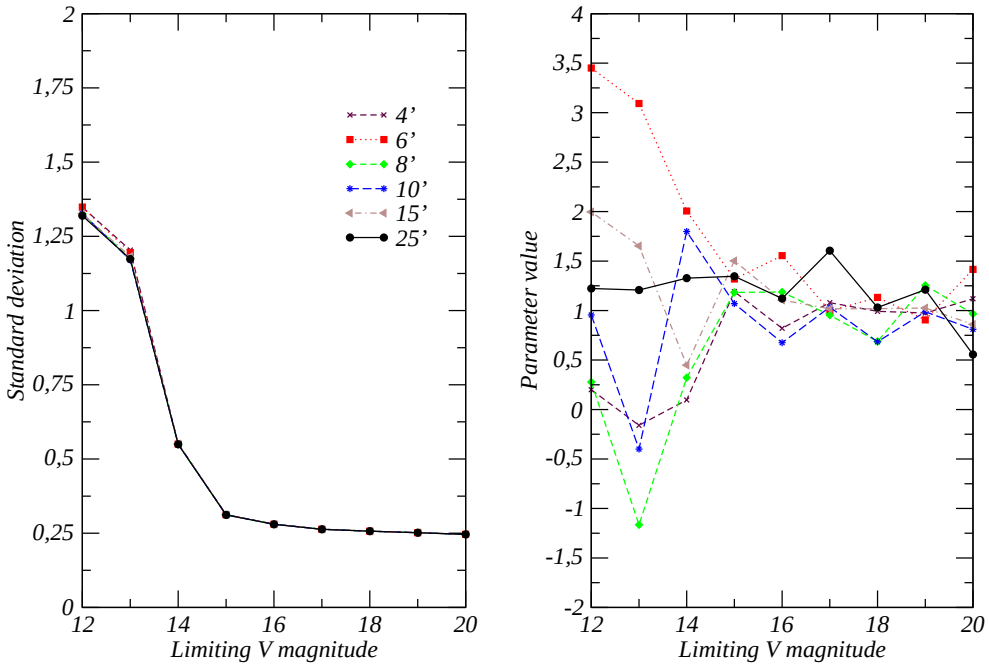

Figure 4.17: (Left)Standard deviation on the accuracy of the ϵ parameter determination as a function of the maximum angular distance permited and the limiting magnitude. A strong dependence on the limiting mangitude is clearly seen. (Right) Corresponding least square values for the ϵ parameter. Despite the formal dispersion does not improve with the increase of the angular separation, the values with $25'$ (black circles on the right pane show better stability around the nominal value ($\epsilon = 1$), even at lower magnitudes.

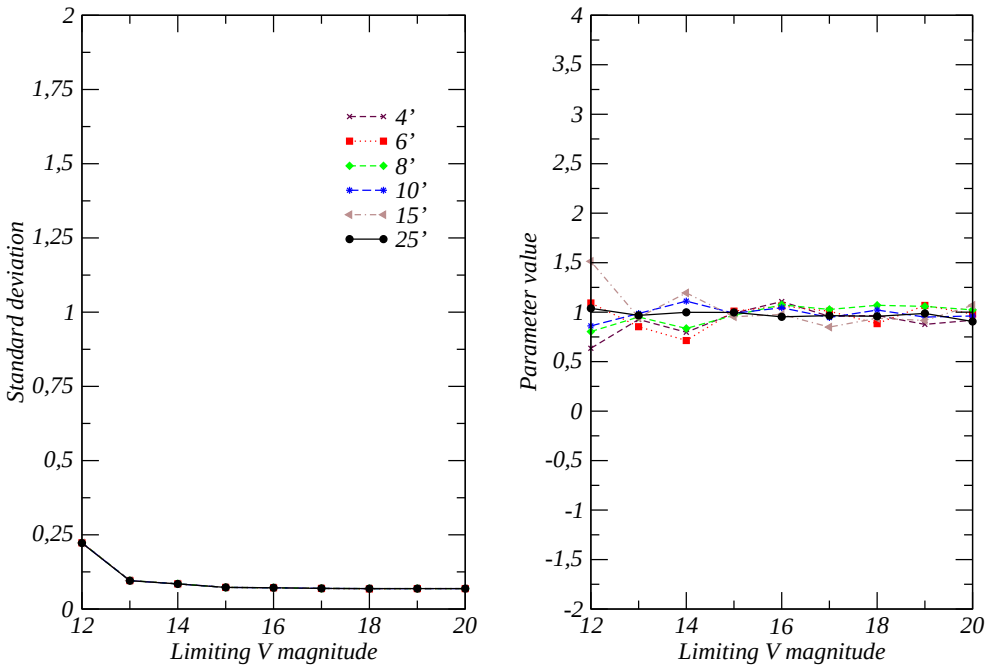

Figure 4.18: Same as Fig.4.17 but using an an optimized choice of the initial coinditions. The optimization is based on the SNR of J_2.It is clearly seen that in this case, the bright stars already contribute a lot to the accuracy of J_2 even if they are a few. As the number of stars grows with the limiting magnitude a weak improvement is visible. Again, to increase the maximal angular distance does not contribute to the solution.

to the ecliptic pole). The degree of correlation depends, of course, on the number of observed sources and their geometrical distribution around the planet.

The accuracy obtained from the data reduction experiments, agree with the SNR a priori expectations (see Fig. 4.10). Examining the transit events occured by a good choice of the intitial scanning conditions, one can realize that most of the accuracy of the $SNR \sim 10$ solutions come from 1 or two favorable transits. The analysis of one of such events is detailed in 4.4.4.

Up to the date, there is no direct measurement of the quadrupolar light deflection from Jupiter. As for the Solar System ephemeris, there exists some constrains in the value of J_2 coming from the integration of the orbits of the Solar System bodies(Essentially asteroids in the main asteroid belts) and the Jovian moons.

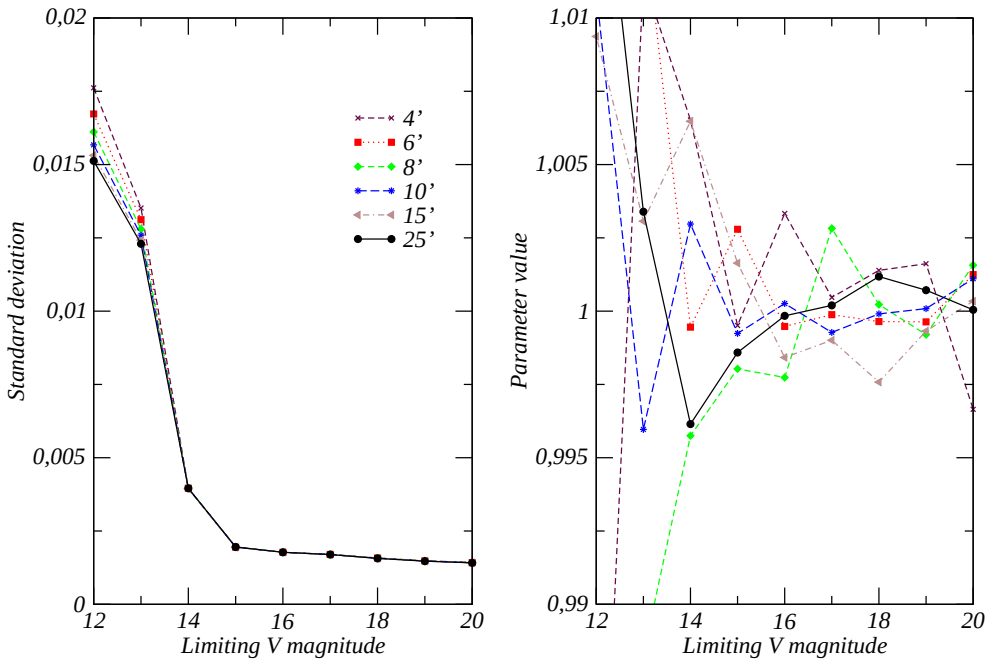

Figure 4.19: (Left)Standard deviation on the accuracy of the α_r parameter determination as a function of the maximum angular distance permited and the limiting magnitude. A strong dependence on the limiting mangitude is evident and no improvement is obtained using larger angular distances. (Right) Corresponding least square values for the α_r parameter.

4.4.3 Dynamical coefficient

Up to the date, the effect on the deflection of the motion of a gravitating body has only been measured explicitly by Fomalont & Kopeikin (2003). Independently of the controversy generated by their interpretation, the experiment confirmed the prediction of General Relativity with an accuracy of 20%.

If one expands the expression for the light deflection effect by a moving body up to $G\frac{v}{c}$ order, it is obtained that the main contributions arise from the explicit motion of Jupiter which amplitude is proportional to $\sim G\frac{v}{c}\psi^{-2}$. This produces a very strong signal for sources observed close to the Jupiter limb. The expansion contains other terms proportional to $G\frac{v}{c}\psi^{-1}$, which are too small to produce observable effects. Among this smaller terms, there is the explicit dependence of light deflection with

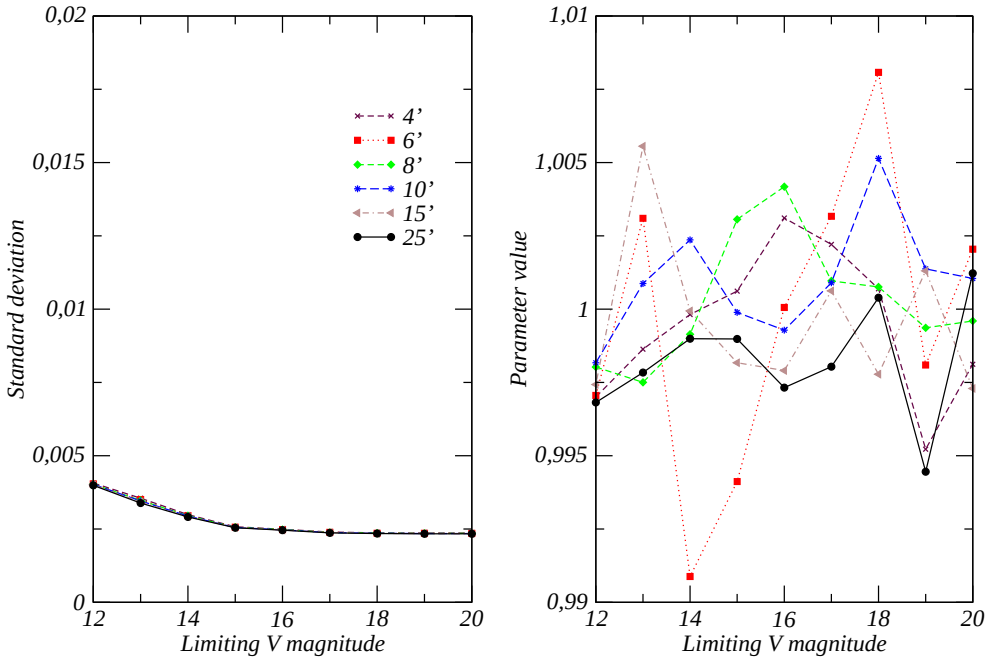

Figure 4.20: Same as Fig.4.19 but using an optimized choice of the initial coinditions. The optimization is based on the SNR of J_2.As for the quadrupole the bright stars contribute very much and no significant improve is observed when using large maximal angles. Despite the formal dispersion decreases when increasing the limiting mangitude, the obtained value becomes more unstable that the results obtained from the the non-optimized situation. This is caused by a few bright V=14 sources with a high SNR in a transit where the correlation between this parameter and the J_2 is high.

the so-called gravitomagnetic part of the metric, say h_{0i}, which produce a maximal deflection of $1.6\mu as$ at the limb of Jupiter (see Appendix C.3). Therefore, the Gaia observations are not suitable to measure gravitomagnetic effects on light deflection by the planets of the Solar system.

We find that the dynamical coefficient can be fitted up to a few parts in 10^{-3} without difficulties, which will improve by two orders of magnitude the measure given by Fomalont & Kopeikin (2003). This parameter is heavily correlated with positional errors of the ephemeris in the instantaneous direction of motion of the body. Due to that, it is not possible to fit simultaneously the dynamical coefficient and ephemeris

Body	ψ	V_l	N	$\langle\gamma\rangle \pm \sigma$	$\langle\alpha_r\rangle \pm \sigma$	$\langle\epsilon\rangle \pm \sigma$
Standard	$4'$	16	1690	1.003 ± 0.0016	1.000 ± 0.0034	0.82 ± 0.28
	$25'$	20	337621	0.9980 ± 0.0011	1.0001 ± 0.0028	0.55 ± 0.24
J_2 optimized	$4'$	16	7565	1.0003 ± 0.001	1.0031 ± 0.002	1.11 ± 0.07
	$25'$	20	288574	1.0007 ± 0.0008	1.001 ± 0.002	0.91 ± 0.06
J_2 Best single transit	$4'$	16	76	1.0001	0.0012	1.0012
	$25'$	20	5386	1.0007 ± 0.009	1.001 ± 0.011	0.91 ± 0.12

Table 4.3: Expected values and standard deviations obtained from the Montecarlo integration of the bayesian Probability Distribution Function for a few illustrative cases. Let us remark that the best single transit(last row) for optimized initial conditions gives better estimates of J_2 than the full mission case with non optimal initial conditions(first row)

positional corrections in the direction of motion of the body. This is discussed in great detail in Section 4.4.4.

	γ	α_r	ϵ
γ	1.000	0.170	-0.000
α_r	–	1.000	0.186
ϵ	–	–	1.000

Table 4.4: Correlation matrix obtained from the solution with optimized initial conditions using $25'$ as the maximal angular distance permited and a limiting magnitude of 20. No relevant correlations are observed for the full mission solution between the three parameters. This is not the case for a single transit analysis (see Section 4.4.4).

4.4.4 Single transit analysis and ephemeris shifts of Jupiter

Let us now check the sensitivity of the light deflection effect to positional errors coming from some solar system ephemeris. This is done by fitting the free parameters in (4.62) in addition to the relativistic parameters. It is expected that for one single planetary transit, the parameters and the positional errors will be highly correlated. Let us analyze what happens with the best single transit for Jupiter (with higher SNR for J_2) that is obtained from the optimized initial conditions ($\xi_0 = 246\,\mathrm{deg}$).

We can start by assuming that the values of the relativistic parameters are known. In this case, the expected values of the shifts are 0 since the ephemeris used in the data reduction process are the same used in the data simulation. The obtained results

are shown in Table 4.5).

Body	Angular apperture	Limiting magnitude	Number of stars	$\langle\delta_l\rangle \pm \sigma$ (km)	$\langle\delta_m\rangle \pm \sigma$ (km)
Jupiter	$4'$	16	76	85 ± 130	-65 ± 340
	$25'$	20	5386	26 ± 130	330 ± 340

Table 4.5: Correction to the ephemeris position of Jupiter obtained through fitting the light deflection effect in favorable observing circumstances. Note that the solution using only $4'$ and stars up to $V = 16$ (76 objects) provides the same accuracy as the one with $25'$ and stars up to $V = 20$(5386 objects). This is because the sensitivity of light deflection to positional errors is proportional to the square of the inverse angle between the star and the planet, say ψ^{-2}.

In addition we study the relation between the ephemeris shifts and the relativistic parameters by computing the correlation matrix between all five parameters (γ, α_r, ϵ δ_l and δ_m). The correlation matrix in Table 4.6 is obtained evaluating (but not solving) the normal equations of the linearized Least square problem with the nominal values of all the parameters (Press *et al.* 1992).

When the correlation between two parameters is close to 1, only one parameter (say P_1) can be safely obtained (or a combination of both). The other parameter(say P_2) must be known a priori. An error in the assumed value of P_1 at 1–σ level, directly perturbs the fitted value of P_2 at 1–σ level as well. Table 4.6 shows that only the γ parameter can be simultaneously fitted with the ephemeris shifts for a single transit. Both α_r and ϵ are very correlated with the ephemeris shifts.

The high correlation between ϵ, α_r and δ_l occurs because most of the signal *signal* comes from one star per transit (see Fig. 4.21). This has some consequences. Using the discussion about the high correlated parameters, the accuracy from the ephemeris must be at the level of the accuracy obtained if only the shifts were fitted (see Tab. 4.5). In the case under analysis, this implies that the positional accuracy provided by the ephemeris must be better than 100 km, otherwise the value obtained for the relativistic parameters is not reliable. Since a few transits contribute to the value of ϵ and α_r, this is a full mission requirement.

In principle, the ephemeris shifts could be fitted from the observations by solving together with the relativistic parameters. This is, however, worthless because the maximal accuracy that can be achieved for each single transit is not competitive with simpler ground based techniques and the current version of the Solar System

	γ	α_r	ϵ	δ_l	δ_m
γ	1.000	0.220	0.102	0.204	−0.561
α_r	–	1.000	**0.958**	**0.999**	0.374
ϵ	–	–	1.000	**0.959**	0.570
δ_l	–	–	–	1.000	0.385
δ_m	–	–	–	–	1.000

Table 4.6: Correlation matrix obtained when trying to fit simultaneously the relativistic parameters and the ephemeris shifts for a single transit analysis. Since a discrepant value of the α_r is equivalent to a positional shift along the trajectory of the planet δ_l, they are almost 100% correlated. The quadrupolar coefficient is also highly correlated with the positional errors since most of the signal comes form one single star, and there is no way to distinguish between a positional error or a stronger quadrupolar effect. This is not the case of γ where many stars contribute to its value.

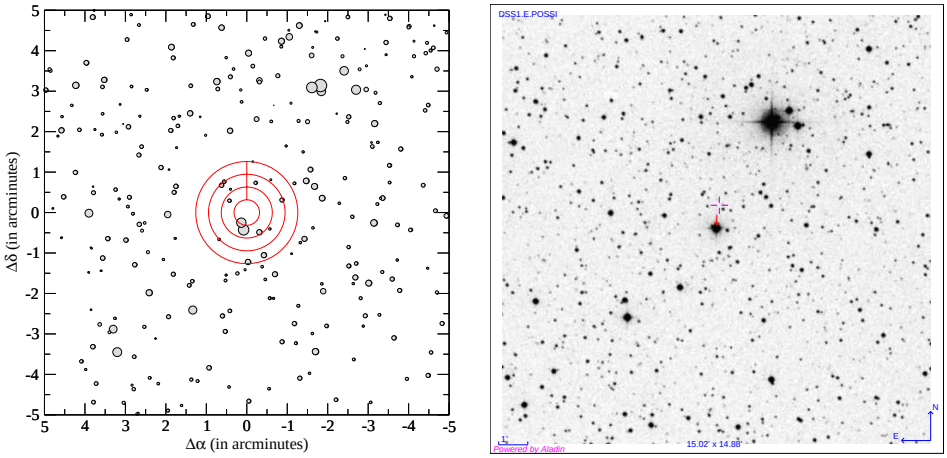

Figure 4.21: Snapshots of the field under study at the instant of observation. On the left pane, the plot is obtained from the catalog information. The size of the disks indicate the brightness of the stars. The central red circle is the apparent size of Jupiter and the largest red circle indicates the area within 4 Jupiter radii. The right pane is the same field as can be retrieved from the Aladdin Applet `http://aladin.u-strasbg.fr/java/nph-aladin.pl` (Bonnarel *et al.* 2000). One can identify all the bright sources on both images by paying attention to the image scales.

ephemeris. This is shown in Appendix C.4.

This is not strictly true for a few number of transits which coincide with those that are significant for the estimation of ϵ and α_r. As it is shown in Table 4.6, the high correlation does not permit to estimate the parameters and the positional corrections independently. The conclusion is that the accuracy of the ephemeris must be guaranteed at the level of 100 km in order to permit significative results for the quadrupole and the α_r parameter.

4.5 Other planets

The light deflection can be observed and some parameters can be measured with a different degree of success in the other planets of the Solar System observed by Gaia (this excludes Mercury and Venus).

In the case of Saturn, the monopolar deflection will be observed and measured with good accuracy. This is not the case for the quadrupolar deflection, since the expected signal-to-noise ratio will never exceed 3 (see Fig. 4.13). Even in such favorable circumstances, the rings and the dusty environment of Saturn will severely disturb the measurements. For the retardation coefficient, the expected sensitivity is considerable and the Saturn observations could be combined with those from Jupiter to fit the retardation parameter in a global sense.

For Uranus and Neptune, the monopolar deflection will be detected with a good degree of confidence but they will not produce such competitive measurements as in the case of Jupiter and Saturn. The quadrupole of this planets will be definitely much below the detection level(see Fig. 4.13). For the retardation coefficient, the situation is slightly better, and some estimation of its value can be achieved from these planets alone.

The monopolar deflection of Mars is at the limb of being detectable. A SNR larger than 2 for Mars γ is not expected in any case. A determination of the quadrupole and the retardation are completely excluded.

4.6 Observing the jovian satellites. Overview

Jupiter is permanently surrounded by its satellites, being some of them very bright objects in terms of the Gaia standards. Since many of them will be observed during

Body	N. of Observations	$\langle\gamma\rangle \pm \sigma$	$\langle\alpha_r\rangle \pm \sigma$	$\langle\epsilon\rangle \pm \sigma$
Saturn	4 654 612	1.003 $\pm$0.004	0.991 $\pm$0.005	1.52 $\pm$0.40
Uranus	625 234	1.02 ± 0.04	0.97 ± 0.04	–
Neptune	521 241	0.95 ± 0.06	1.01 ± 0.04	–
Mars	3 519 346	1.0 ± 0.5	1.2 ± 0.2	–

Table 4.7: Best case Standard deviations in the relevant parameters obtained for the other planets observed by Gaia.

each transit, we have checked the potential outcome of their observations in terms of the relativistic parameters of the light deflection. Despite the philosophy of the experiment is quite the same (observed shift with respect the non perturbed direction), the astrometric observations of the Jovian Satellites differ in many aspects from the stellar observations and are rather complex.

- They are always observed at a few radii from the planet. Observing them does not critically depend on the choice of the initial conditions of the scanning law. Therefore, their observations will be anyway available.
- The larger ones (Galilean satellites) are not point-like sources as seen by Gaia. Most likely, they will not be processed by the on-board detection system because of their size.
- All of them move significantly during a Gaia transit causing a distorted PSF.
- Their orbits contain many uncertainties, being the position of the center of mass of Jupiter one of them. Positional uncertainties of 100 meters correspond to 30μas at the distance of Jupiter.
- They show time dependent motion of the photocenter motion due to their rotation and irregular shapes. Their photocenter is related to the position of their center of mass in a complicate way.

Their intrinsic proximity to Jupiter is the only advantage of the previous list. All the other comments in the previous list are serious troubles. However, a simple experiment to determine the potential SNR contribution to the relativistic parameters can be easily performed. This is the purpose of this section.

Satellite	Diameter (km)	Angular size(mas)	V (mag)	Semi-major axis(a/R_j)	Period (days)	i (deg)
Io	3643	1000	5.0	6.2	1.77	0.04
Europa	3122	860	5.3	9.5	3.55	0.47
Ganymede	5262	1450	4.6	15.3	7.16	0.17
Callisto	4821	1330	5.7	26.9	16.69	0.19
Metis	12	12	17.5	1.83	0.30	0.019
Adrastea	16	4.4	18.7	1.84	0.30	0.054
Amalthea	168	43	14.1	2.59	0.50	0.380
Thebe	98	27	16.0	3.17	0.68	1.080

Table 4.8: Physical data and orbital parameters of relevance obtained from `http://ssd.jpl.nasa.gov`. Only the satellites that can be observed close enough to Jupiter are listed. All the quantities are average values.

4.6.1 Orbits and data

In what follows, the moons are considered as point like sources with a time dependent position. The orbits of the moons with respect to Jupiter are assumed to be known with sufficient accuracy (say $\sigma < 300$ meters which is probably very unrealistic). The orbits are computed using the orbital elements obtained from `http://ssd.jpl.nasa.gov`. The useful list of moons and their relevant features for this study (apparent diameter, brightness, orbital radius, inclination, etc.) are given in Table4.8.

4.6.2 Light deflection and Signal to Noise Ratio

Despite Jupiter has around 60 natural satellites, only a few of them lie on the line of sight between Gaia and Jupiter. It is found that only, the Inner group and the Galilean moons, can potentially provide significant measurements of the light deflection effect. This is depicted in Fig. 4.22 and Fig. 4.23.

Since no observations from the Galilean satellites will be obtained by Gaia (their angular size is too large for the on-board detection system), only the members of the inner group have chances to provide some significant results. The SNR along its orbit is illustrated in Fig. 4.23. In this sense, the larger moon Amalthea is the more promising one, since it can produce many observations with a moderately high SNR and the accumulated observations during the mission can potentially provide a

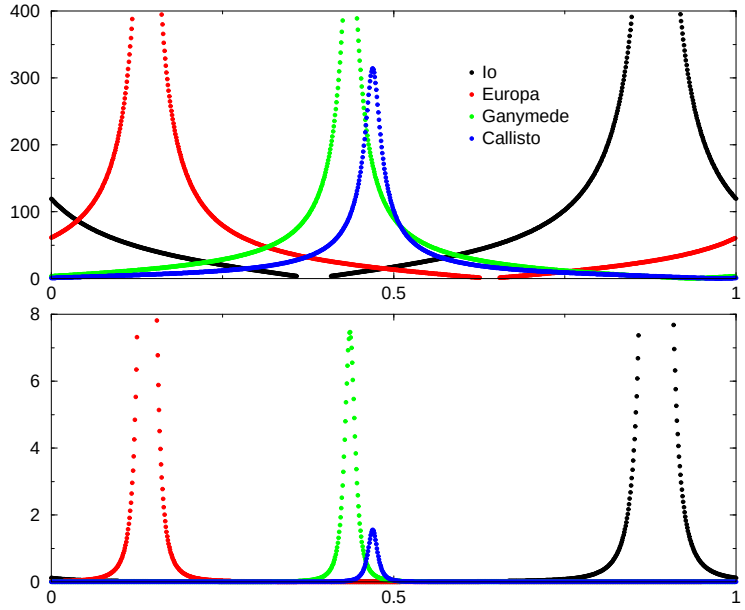

Figure 4.22: Signal to noise Ratio of the monopolar (top) and quadrupolar (bottom) light deflection along the orbit of the Galilean satellites as seen from the earth. Since the orbital periods of the moons are much smaller than the Gaia mission, they will be observed in random positions along their orbits. The points missing correspond to instants where the satellite is in directly in front or behind the Jupiter disk.

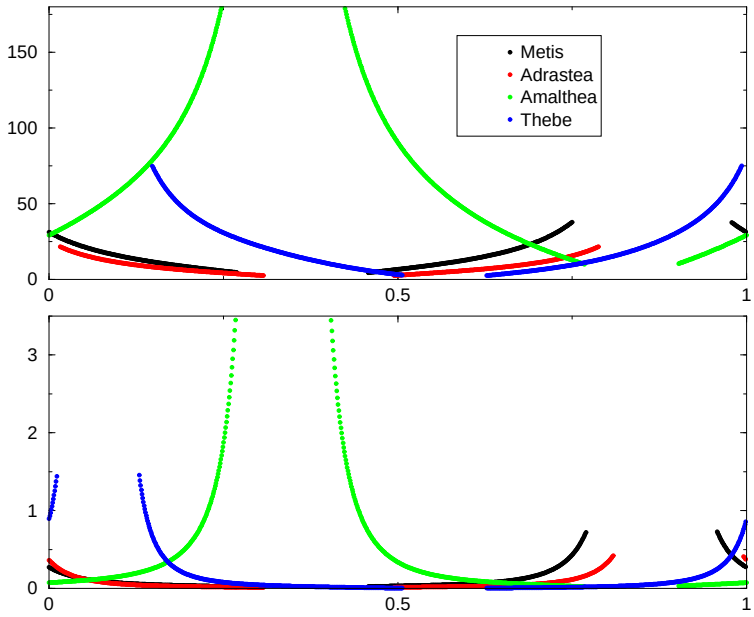

Figure 4.23: Signal to noise Ratio of the monopolar (top) and quadrupolar (bottom) light deflection along the orbit of the inner satellites as seen from the earth. Since the orbital periods of the moons are much smaller than the Gaia mission, they will be observed in random positions along their orbits.

reasonable good value for J_2, which can potentially overpass the value obtained from the stars only. This assessment is just a guess since the observation of good events is very random.

4.6.3 Full mission prospects

In order to assess the maximal accuracy reachable from the moons, we ran a number of full mission simulations with different scanning law initial conditions and different start of mission instants. The results are very sensitive to the initial conditions because the moons move very fast, and the final outcome is highly unpredictable.

However, we can obtain a guess of the expected SNR for the different parameters under study (γ and ϵ) by trying many different initial conditions (Montecarlo tests). The results are shown in table 4.9.

We have excluded the analysis of the dynamical parameter since it is intrinsically

Parameter	Maximal SNR	Average SNR per single transit	Accumulated SNR after 80 transits	Final accuracy
γ	180	143	1280	0.0008
ϵ	3.5	1.25	11.2	0.09

Table 4.9: Maximal and typical signal to noise ration using the observations of the inner satellites for a single planetary transit. These values have been obtained by simulating and averaging the results obtained by a large number of Jupiter transits. The potential final accuracy in each parameter is shown in the last column.

correlated with positional uncertainties of Jupiter in addition to the uncertainties in the moons orbits, which can perturb too much the interpretation of the obtained results. Despite Table 4.9 give very promising numbers, we suspect that this experiment will not lead to significant results due to the required accuracy in predicting the position of the moons.

4.7 Conclusion

Gaia is (potentially) a highly competitive experiment observing light deflection from planets. Without any doubt, it will provide the measurement of γ and the dynamical parameter α_r (at least for Jupiter) with an unprecedent accuracy, even compared to VLBI observations, which are limited to a very few number of radio sources that can be observed close enough to the planet. It is clear that a careful choice of the initial conditions of the scanning can boost significantly the scientific outcome of such experiments.

Our data reduction approach (nLS+bayes) seems appropriate to process the data. In such an approach, the relativistic parameters of the planets will be obtained at full accuracy at the end of the mission. Even though, their values can be updated on each public data release of Gaia.

However, the situation of the measure of the quadrupole is quite uncertain. It has been shown that specific initial conditions for the scanning law can greatly improve the chances of obtaining a good measure of the quadrupolar light deflection by Jupiter. Some technical issues not discussed here, such as the stray light or the dusty environment of Jupiter can severely compromise the chances to obtain a reasonable

measure of the quadrupole. This issue is under investigation, but will not be settled down until the industrial development of the probe is more advanced. The most serious issue is the minimal angular distance at which an astrometric measure can be obtained with reasonable accuracy. We assumed the best case limit, which is that stars as close as 0.1 Jupiter radii from its surface.

The Jovian moons could potentially provide interesting and even, very competitive measurements of the relativistic parameters (specially γ and J_2). The observations of the moons will be there anyway, and if most of the complications can be handled (fast motion, extended sources, very close to Jupiter), they will be used to improve the values of the relativistic parameters. For technical reasons, it seems now clear that the Galilean satellites will not be even catched by the on-board detection algorithm. Therefore, the best hope lies upon the largest inner satellites Amalthea and Thebe. Once the issue about the proximity at which an object can be observed from Jupiter and the centroiding of extended sources become clear, further work is planned in this sense if some chances of obtaining good observations still remain.

Chapter 5

Conclusions

Since each chapter contains its own section of conclusions, we will not further discuss them at this point. Only general comments will be given in this section. In this thesis we tried to understand the relativistic modeling of the observations by working in specific parts of the model from the relativistic description of the observer (Chapter 2), accurate description of star kinematics (Chapter 3), and extraction of relativistic information from the Gaia data (Chapter 4). This work may not be exhaustive, but it solved, or at least clarified, several gray points which were identified as critical for the successful exploitation of the Gaia mission.

In addition, most of the work of these last years has been deployed inside the Gaia Software tools, that are being developed for the real data reduction pipeline by many people across the ESA member states. A proof of this is the Gaia Pocket Simulator (Appendix A), that is a compilation of the software tools developed by the author to be used in the real data simulation and data reduction software being used currently.

Concerning the relativistic modeling of optical devices in rotation, the relevant (special) relativistic effects have been identified and quantified. It has been shown that the images can be affected from relativistic effects at the μas level (image shifts and small distortions) but they can easily be handled or absorbed by the current Gaia data calibration procedure.

It has been shown that detailed kinematic description is required to describe the motion of the stars including the light travel time effects. This adds some complexity to the models but permits us to obtain additional information from the astromet-

ric measurements. We also found that the coordinate transformations between the object reference systems to the BCRS are not relevant to the interpretation of the observations and that the classical kinematical models can be safely applied.

Finally we have analyzed the potentiality of the light deflection experiments using astrometric observations of stars (or moons) around the planets of the Solar System. It has been shown that in the case of Jupiter, very good and accurate tests of the standard light deflection model can be done by adjusting some free parameters in the post-Newtonian approach to General relativity. Most likely, the light deflection from the quadrupolar gravitational field of Jupiter will be detected, and even measured with a good degree of accuracy if certain fine tuning of the scanning law is allowed. The light deflection will be measured in all the other planets visible by Gaia, except for Mars which is too small to produce significant deflection. The data reduction approach (least squares + integration of the likelihood function) has been proven sufficient and adequate.

As mentioned, not all effects studied in this thesis will finally be useful for the Gaia mission, but we only know this after a careful study of each one. There are still many *small* pieces of the puzzle which may be put together. This work will continue until the launch of Gaia in the context of REMAT (RElativistic Models And Tests), group inside the Gaia Data reduction consortium responsible for the relativistic aspects of the Gaia observations). A comprehensive list of remaining tasks can be found in the list below[1].

- Global tests
  - Light deflection experiments (**)
  - Local Positional Invariance
  - Local Lorentz Invariance
  - Random microlensing noise (*)
  - Primordial Gravitational Waves
  - Acceleration of the Solar System (*)
- Local tests
  - Monopolar light deflection (**+)

[1] extracted from `http://www.ari.uni-heidelberg.de/gaia/CU3talks/Splinter1/klioner1.pdf`

  - Quadrupolar light deflection (**+)
  - Gravitational sources in motion (**+)
  - Perihelion precession (**)
  - Non-Schwarzschild effects
  - Strong Equivalence principle with Trojans, (*)
  - J_2 of the Sun (**)
  - Variation of the gravitational constant (**)

- Relativistic objects
  - Relativistic binaries(*+)
  - Microlensing events
  - QSO macrolensing (*)
  - Super-massive blackholes

One star indicates that some work has been done or there is already somebody taking care of it. Two stars indicates that a lot of work has been done and the topic is in an advanced state. Further preparatory work is expected to be done by the community until the mission launch and beyond. The plus sign flags the task were the author has contributed.

We hope that the work presented in this thesis will be added to the growing number of examples that show the excellence and uniqueness of the Gaia mission, flagship of the European expertise, not only in astrometry, but also on astrophysics and space sciences.

Appendix A

Gaia Pocket Simulator

A.1 Introduction and the Java language

In this work, we have reused a considerable amount of the code that was previously developed for other parts of the Gaia mission. Our software is fully coded in Java, and heavily relies on object oriented programming techniques and a few number of *design patterns* which have shown to be very useful. The Gaia Pocket simulator is, essentially, a set of interfaces, implementing classes and factories providing the tools to generate Gaia-like observations for testing purposes.

The Java language provides a natural tool to implement code reutilization and encapsulation; the *interface*. An interface is a class (piece of code that is usually in a separate file) that establishes how a set of algorithms will appear to the rest of the world, quite independently of their particular implementation.

In the block diagram of 4.8, the core of the simulation processing is depicted. The circles represent the independent pieces of code that will be represented by java interfaces. In such a way, once the simulation core is prepared, one can freely move from one algorithm implementation to another with minimal effort(even during runtime). Each circle is clearly related to a very particular task.

The full mission simulations are conducted by a class (driver or main class) that initializes a set of factories (pieces of code that provide implementations of interfaces under request) and implements the block diagram described in Fig. 4.8. The factories contain *static* methods that can be recalled at any level of the software project, and

provide universal access to the models chosen by the user during initialization.

In the following section, only the most used interfaces and methods are discussed in terms of their tasks. More detailed information can be found in the code documentation and the technical notes that describe the algorithms.

A.1.1 Design patterns

Design patterns are rules of *good* programming which have been extensively used by many years by the code developers in any software language.

We used some of them. Design patterns will be described as required in the explanation of the code below. The ones more extensively used are

- Singleton, see A.2.1
- Wrapper, see A.2.1
- Interface, see A.1.2
- Object factory, see A.2.1
- Abstract object factory, see A.2.3

In general, the programming languages do not contain specific instructions to apply the design patterns, and their particular implementation changes from one language to another. Object Oriented languages (as Java or C++) are better suited to design patterns since they have been specifically created to solve complex software engineering problems. By contrast, design patterns are much more difficult to handle in procedural languages such as old versions of Fortran (or ANSI C) and require a deep understanding of the languages and the compilers to be used.

A.1.2 Some Java programming concepts

A number of basic Java language programming concepts are required to understand the following sections. Java is an Object Oriented language which permits the utilization of advanced software engineering concepts as the design patterns listed above.

It should be noted that this is not an introduction to the Java language or semantics. Therefore, it is assumed that the reader is familiar with concepts of standard programming.

Java classes and instances

The Java code is created in standard ASCII files. Usually each file contains the definition of a class, which is the most elementary building block of a Java program. A class is a model of an Object. Therefore, a class contains methods and attributes that describe the object and define how it interacts with the world. A method is the analog of a subroutine and the attributes (some numbers or other Objects) contain information of the object. Thinking in a real world example, an attribute is the color of a car, and a method would be the action to turn on the engine. A runtime realization of a class is called an *instance*. Many instances of the same class can exist simultaneously.

Let us think naively of a simple example. The code of a Java class representing a parrot is

```
public class Parrot{
    public String race;
    public double age;
    private boolean isAlive;

    public Parrot(String newrace, double newage) {
        race = newrace;
        age = newage;
        isAlive = true;
    }

    public void say(String message) {
        if(isAlive) System.out.println( message.replaceAll("a","e") );
    }

    public void describeYourself() {
        say("I'm a " + race + ". I'm " + age + " years old.");
    }

    public double getYourAgeInDays() {
        double ageindays = age*365.25;
```

```
        return ageindays;
    }


    public void killParrot() {
        say("aaaargh!");
        isAlive = false;
    }
}
```

Let us explain what actually does each piece of code

- `public class Parrot{` is the declaration of the name of the object defined by this class. The word 'public' means that this class can be used by any piece of code and that we can forget it by now.
- `public double age;` The Parrot has an age, this is, the number of years from the instant he emerged from the egg. It is stored as a `double` precision number which is one of the numeric Java basic types. The others are `short, int, long and float`. The short, int and long types are integer numbers of 16, 32, 64 bits respectively. The `float` and `double` types represent floating point numbers with 32 and 64 bits respectively.
- `public String race;` Our `Parrot` class, as the real ones, is of one race. We define it as a "String", the Java standard way to deal with texts. `String` is not a basic type like `double`, but it is a Java standard class (distributed with the compiler by Sun). Thanks to that, the String object contains many methods to manipulate it's content in a very straightforward way (see the `replaceAll` method below).
- `private boolean isAlive;`. The `boolean` type can only take two values : `true` or `false`. This attribute will be used to check if the parrot is able to speak or not. It is declared as `private` since the external user does not need to know this information to perform normal "Parrot" operations. The permissions are discussed in the next section.
- `public Parrot(String newrace, double newage) {...}` This is the constructor. This "method" will be used to create an instance of a Parrot; say, a

living copy in memory of our Parrot object. To create a Parrot, the race and the age must be provided as arguments of the constructor. It will automatically set the Parrot to life by setting the variable `isAlive` to `true`.

- `public double getYourAgeInDays()` This method will make some operations with the `age` attribute of the Parrot and return the result in days. The answer will be given as a `double`. This is why the keyword `double` is in the method definition.

- `public void say(String message) {...}` . This is a method that will make the parrot repeat the `message` if he is still alive, this is, if the `boolean isAlive` is true. The `System.out.println(...)` is just the way to say to Java that a message must be given to the standard output (i.e. display). Since our parrot is not very clever, it will confuse all the "a" by "e". To do that, we take advantage of the method `replaceAll` of the `String` object. You will see the results in a few moments. The `void` tag indicates that this method does not return any information to the code that is calling it.

- `public void describeYourself() {...}` Calling this method, the Parrot will describe himself using directly its own `race` and `age` attributes and calling its own method `say`. This is a standard example of a method which provides some processed information in terms of the current values of some attributes.

- `public void killParrot() {...}` This method will set the `boolean isAlive` to `false`, thus the parrot will not be able to `say` anything else.

Then our Parrot is ready to be used. Let us create another class, called Main, which will do some stuff with Parrots.

```
public class Main {
    public static void main(String args[]) {
        // Creating an instance of a Parrot
        Parrot myParrot = new Parrot("African grey", "Grey",100.0);

        // Creating an instance of another Parrot
        Parrot anotherParrot = new Parrot(
            "Blue Eyed Cackatoo", "white",100.0);
```

```
        // Let us speak a little bit with the African grey
        myParrot.say("Hello world!");
        myParrot.describeYourself();
        myParrot.killParrot();
        myParrot.say("That's all folks!");     // despite of the effort,
                                               // it is too late for him

        // The other parrot says a few words about his partner
        double ageOfTheFirstParrot = myFirstParrot.getYourAgeInDays();
        mySecondParrot.say("The first parrot lived "
            + ageOfTheFirstParrot + ".");
    }
}
```

The first line declares that a class called Main is defined here. The `public static void main` is just the standard way to tell to the Java Virtual Machine that this method is the one that must be executed when the class is executed through the command line. The rest of the code is self commented. Let us show the output

```
> Hello world!
> I'm e Africen grey. I'm 100.0 yeers old.
> eeeergh!
> The first perrot lived 36525.0 deys.
```

Java permissions

In the previous examples, we have used the `public` keyword extensively in the method and variable declaration. Since most of the Parrot methods were public, we were able to call them without problems. By contrast, the `isAlive` flag was declared `private`. A `private` attribute or method can only be used or modified from the same class; say, only methods inside Parrot can modify the value of `isAlive`(the constructor and the `killParrot()` method). If one tries

```
        myParrot.killParrot();
        myParrot.isAlive = true
```

in the `Main` example, the program will not even compile. This programming technique permits to create complex software structures which are hidden to the user and protected against misusage. It is a recommended practice to declare all the attributes in a class as private and add the methods to modify or retrieve them, if required.

Static methods

The `static` keyword was used by the `Main` class in the main method. This keyword can be used in any method or attribute. In an attribute, it means that all the instances of this class will share the same value of the attribute. In a method, it means that it can be accessed without creating an instance of the class. The static attributes and methods are also called *class attributes and methods*.

The static methods and attributes mimic global variables in other computing languages and its a good coding practice to avoid using them except in very particular applications, such as parameter container classes (i.e. Gaia Parameter database) or Object factories (discussed below).

Heritage and wrappers

A typical feature of the Object Oriented programming languages is *heritage*. A class can inherit the methods and attributes of another one by *extending* it, adding more functionality to the mother class, usually called super-class. The best way to see it is with an example. Let us create another class called `CleverParrot`, that does not make mistakes repeating messages and includes a method to revive it

```
public class CleverParrot extends Parrot {
    public void say(String message) {
        if(isAlive) System.out.println(message);
    }

    public void reviveParrot() {
        if(!isAlive) say("I have returned!");
        isAlive = true;
    }
}
```

Apart from improving the `say` method, we have added a new functionality which permits to revive the `CleverParrot` and let him speak again. Let us remark that in addition to the newly defined methods, the `CleverParrot` contains also all the methods and variables of the mother class.

Let us put this in practice with another class with a `main` method.

```
public class MainClever {
    public static void main(String args[]) {
        // Creating an instance of another a CleverParrot
        CleverParrot myCleverParrot =
            new CleverParrot("Blue Eyed Cackatoo", "white",100.0);

        // Let us speak a little bit with the African grey
        myCleverParrot.say("Hello world!");
        myCleverParrot.describeYourself();  //
        myCleverParrot.killParrot();
        myCleverParrot.say("That's all folks!");
        // now it is dead, it will not work!

        // now we revive it
        myCleverParrot.reviveParrot();
        myCleverParrot.say("Hello world again!");
    }
}
```

Notice that `describeYourself` nor `killParrot` were not in the definition of `CleverParrot`, but thanks to *inheritance* we can use this methods as with the `Parrot` case. Each class can only inherit methods and attributes from one class, it can only have a superclass.

To gather the functionalities of several classes into a single one, there is a design pattern (programming strategy) called *Wrapper*. A wrapper class includes several classes as private attributes and provides access to them by explicit recoding of the desired methods. Let us show it with an example. Let us create a Bunch of Parrots as

```
public class BunchOfParrots {
```

```
    private Parrot oldparrot;
    private CleverParrot youngParrot;
    private CleverParrot unpoliteParrot;

    public void say(String message) {
        oldParrot.say(message);
        unpoliteParrot.say("Stupid!");
        youngParrot.say("Spell it correctly! " + message);
    }
}
```

This silly example shows how a wrapper works. It is often more desirable to use wrappers than to extend classes, since it has a lower impact on the structure of a software project. The wrapper combined with the Java *interface*, provides a very powerful tool for software developing that preserves encapsulation, code recycling and functionality.

The Java interfaces

A Java interface is the abstract concept of how an object must behave. It is coded as a class, but only the methods and attributes are declared, without specifying what they actually do. Let us define an interface called TalkingEntity,

```
public interface TalkingEntity {
    public void say(String message);
}
```

Since all the previously defined classes contain a `say` method (`Parrot`,`CleverParrot`, `BunchOfParrots`) all of them are candidate implementation of the `TalkingEntity` interface. This must be specified in the code by modifying their first line,

```
public class Parrot implements TalkingEntity {...}
public class CleverParrot extends Parrot implements TalkingEntity{...}
public class BunchOfParrots implements TalkingEntity {...}
```

Doing this, we can define methods that will blindly accept any object implementing a desired interface without specifying if this is a `Parrot`, a `BunchOfParrots` or whatever. Let us write an example

```
public class InterfaceExample {
    public static void main(String args[]) {
        // Creating an instance of Parrot
       Parrot myParrot =
           new Parrot("Blue Eyed Cackatoo", "white",100.0);

       // Creating an instance of CleverParrot
       CleverParrot myCleverParrot =
           new CleverParrot("Blue Eyed Cackatoo", "white",100.0);

       // Creating an instance of a bunch of parrots
       BunchOfParrots myBunch = new BunchOfParrots();

       Example.saySomething(myParrot);
       Example.saySomething(myCleverParrot);
       Example.saySomething(myBunch);
    }

    public static void saySomething(TalkingEntity talker) {
        talker.say("Something!");
    }
}
```

Notice that the `saySomething` method will work quite independently of what the `talker` object is actually. We have used the `static` quality of the method `saySomething` to call it without creating an instance of `InterfaceExample`. The interfaces are a very powerful tool to decouple different parts of a software project, and permit the usage of advanced design patterns. Interfaces are widely used in the Gaia Pocket Simulator.

A.2 The simulator code

Let us now review the most important pieces used to simulate Gaia-like observations. They are discussed in terms of their interaction (interfaces) and the details of what algorithms are actually doing can be found elsewhere.

A.2.1 Attitude

The attitude interface contains only one public method. It transforms a unit direction in the Center of Mass Reference System (Klioner 2004) given in a 3-dimensional `double` array (a unit vector), to the rotated coordinates each focal plane applying a spatial rotation computed through the scanning law. Despite there are many documents describing and optimizing the details of the attitude implementation, from the user level all the details are hidden to him behind a simple interface

```
public interface Attitude {
  /**...*/
  public double[] getDirection(double att_ep0, double tobs,
                               double[] svec);
}
```

There are three implementations of the Attitude interface. They are

```
attitude.EulerAttitudeMatrix
attitude.LennartAttitude
attitude.NoneAttitude
```

The first is the most used one. It builds the rotation matrix directly from the Euler Angles from the scanning law (`attitude.MignardScanLaw.java`) and it's optimum for simulation purposes. The scanning law cannot be directly accessed by the user, and in this sense, the implementations of the `Attitude` interface *wrap* it together with the algebraic algorithms to manipulate matrices, vectors or quaternions. This is an example of the *wrapper* design pattern.

The implementations of the attitude interface contain several buffered attributes in order to avoid unnecessary calculations of the rotation matrix in repetitive calls. The second one (`attitude.LennartAttitude`) builds the rotation matrix through the quaternion formalism producing exactly the same results as `attitude.EulerAttitudeMatrix`. This was the first one implemented since it was directly extracted from the Fortran subroutines for GDAAS2-Source updating, provided by Lennart Lindegren. The third one is a dummy attitude which applies no rotation to the given direction (rotation matrix is the identity) and it is used for test purposes only.

All the constructors of the implementing classes of the Attitude interface have private access. In addition, only one instance of the attitude interface can be uploaded in memory. This strong encapsulation prevents overloading the memory with many copies of the same thing. The only way to obtain the current instance of the Attitude implementation is through an Object factory(see below) designed with this purpose. The strategy of only permitting a single instance of an object to be uploaded in memory is known as the *Singleton* design pattern.

Attitude Factory

In order to provide access to all the code levels to the attitude interface implementations, an *Object Factory* design pattern is used. An object factory is a class with public and (most likely) static methods that generate Instances of classes (usually, each factory produces instances from only one interface), that can be recalled for other pieces of code. The `AttitudeFactory` class has as public methods

```
public static void setDefaultAttitude(int attID);
public static Attitude getAttitude(int attID){...}
public static Attitude getAttitude() {...}
```

Several `int` static flags are available to choose between implementations (see code documentation).

At any moment, any part of the code can retrieve an instance of the default attitude implementation through `getAttitude()`, and even change the default returned implementation through `setDefaultAttitude(int attID)`.

A.2.2 Solar System Ephemeris

The Solar System ephemeris and the Gaia orbit are implemented under the `SolarSystemEphemeris` interface. The public methods are

```
public interface SolarSystemEphemeris {
    public double[] getR(double tcb, int obID);
    public double[] getV(double tcb, int obID);
}
```

that provide the position and the velocity of the planets and the Gaia probe as a function of the BCRS time coordinate TCB. A number of `static int` flags are available to specify the object of interest. The details of the parameters and the implementation can be found in the code documentation and the reference documents Mignard (2003a) and Mignard (2003b).

Three implementations of this interfaces are used,

```
gaia.gaiaephemeris.GaiaEphemeris.java
gaia.gaiaephemeris.RealEphemeris.java
gaia.gaiaephemeris.GaiaNoisyEphemeris.java
```

The first one provides the nominal orbits for the planets and Gaia. The second one is based on the nominal orbits but it is able to introduce positional and velocity shifts. The third one introduces periodic sinusoidal variations to the position of the planets to emulate periodic positional errors.

Another implementation of `SolarSystemEphemeris` is `DE405Ephemeris.java`, which provides access to the popular JPL ephemeris. This implementation has not been used, since it does not contain the Gaia probe orbit (for obvious reasons), and the combination of the standard Gaia ephemeris with DE405 could lead to some fundamental inconsistencies (Klioner 2006).

The ephemeris are also accessible to all the code levels through an `EphemerisFactory`.

A.2.3 Catalog access

An abstract catalog provides access to lists of sources of any kind (not only stars, see `ObservableSource` in Sec. A.2.6) This is

```
public interface AbstractCatalog {
    public ObservableSource getSource(int ID);
    public int getNumberOfSources();
}
```

The implementations of `AbstractCatalog` interface are responsible for reading the catalog files (whatever the format used) and for parsing them to `ObservableSource` objects. We used three implementations of `AbstractCatalog`,

```
cataloginterfaces.CatalogReader.java
```

```
cataloginterfaces.EmptyCatalog.java
universe.jupiter.JovianSystemCatalog.java
```

where the first one is devoted to read from our intermediate catalog format (we previously parsed GSC2.3.1 and 2MASS a compressed format, with the minimum amount of information required from the sources). The second one is a catalog without sources (which is sometimes required). The third one contains the moons of Jupiter as `ObservableSource`s. This is a good example of the advantages of using interfaces.

In some sense, the implementations of `AbstractCatalog` are `ObjectFactories` of `ObservableSources`. When an interface is used to define factories, it is usually said that an *Abstract object factory* design pattern is used.

A.2.4 Error model

The error model is implemented via the `AstrometricErrorBudget` interface

```
public interface AstrometricErrorBudget {
    public double getAL_Noise(
        ObservableSource source,double ep0, double tobs);

    public double getAC_Noise(
        ObservableSource source,double ep0, double tobs);
}
```

that provides the standard deviation of the astrometric measure from a source at a certain moment. The details can be found in the code documentation. The `AstrometricErrorBudget` has three implementations,

```
errorbudget.FlatAstrometricErrorBudget
errorbudget.NullAstrometricErrorBudget
errorbudget.Gaia2AstrometricErrorBudget
```

The `NullAstrometricErrorBudget` is used to produce noiseless data. The `FlatAstrometricErrorBudget` assumes that the error is the same for all the objects (for testing purposes) and `Gaia2AstrometricErrorBudget` is used to add noise to the observations according to the *Gaia2* design version (see Section 4.3.1). There is also a factory

```
public class AstrometricErrorBudgetFactory {
    ...
    public static void setDefaultErrorBudget(int errID){...}
    public static AstrometricErrorBudget getErrorBudget(int errID){...}
    public static AstrometricErrorBudget getErrorBudget() {...}
}
```

which provides universal access to the error model used and is widely used through our code (similar to the attitude factory in Section A.2.1).

A.2.5 Instrument model

The schematic model of the instrument and the methods to generate the transit times for the telemetry segments are performed by the implementations of the `GaiaAstrometricInstrument` interface. This permits to implement the changing specifications of the Gaia model used as the design evolves. Typically, the classes implementing this interface make extensive use of the Gaia Parameter Database (de Buijne 2006), which is included in the code directly from the file distributed on the web page.

```
public interface GaiaAstrometricInstrument {

    public double[] CCD_readOutAngle(int FoV, int row, int col);

    public int checkFoV(double[] f,
                        double AL_TOLERANCE,
                        double AC_TOLERANCE);

    public double[] getObservationTimes(ObservableSource source,
                                        double att_ep0,
                                        double catalog_ep0,
                                        double tobs);

    public double[] getAcrossArray(ObservableSource source,
                                        double att_ep0,
                                        double catalog_ep0,
```

```
                                        double tobs);

    public double getAC_SIZE();
    public double getAL_SIZE();
    public double getBASIC_ANGLE();
    public double getSCANNING_RATE();

    public double[] getCloseTransitTimes(ObservableSource source,
                                         double att_ep0,
                                         double catalog_ep0,
                                         double tobs);

    public double getSingleTransitTime(ObservableSource source,
                                         double att_ep0,
                                         double catalog_ep0,
                                         double tobs);
}
```

This interface has an Object Factory called `GaiaAstrometricInstrumentFactory`. This factory is able to provide `GaiaAstrometricInstrument` implementations in agreement with Gaia1 and Gaia2 designs. They are

```
gaia.instrument.AstrometricInstrumentGAIA2.java
gaia.instrument.AstrometricInstrumentGAIA_old.java
```

where the main difference between these two versions are the number and geometric distribution of the CCDs and the focal length of the telescope(size of the fields of view).

A.2.6 Observable source

A very important part of the code relies on the `ObservableSource` interface. All the astrometric related issues (kinematics, light deflection, etc.) are internally managed by the classes implementing this interface, greatly simplifying the task of the instrument model implementation (see previous Section). The interface reads,

```
public interface ObservableSource {
```

```
    public int getSourceID();
    public double[] getInitialDirection();
    public double[] getCoMRS(double ep0, double tobs);
    public double[] getInitialPosition();
    public double[] getInitialVelocity();
    public double getVmag(double ep0, double tobs);
    public double getBmag(double ep0, double tobs);
    public double[] astrometricCatalogEntry();
    public double[] physicalCatalogEntry();
}
```

This interface contains a lot of methods. To simplify the task of the developer an *Adapter* design pattern is used in this case. (`universe.Star` object is an adapter). An adapter is a class (usually abstract) which implements all the methods of an interface in the most generic and simple way. The developer can still reimplement the methods by himself if required by extending the adapter (*heritage* is a feature of the Jave language). The class `universe.Star.java` is an example of such an adapter. The most used implementations of `ObservableSource` are

```
universe.Star
universe.DummySource.java
universe.FrozenStar.java
universe.jupiter.Satellite.java
...
```

which we will not detail here for brevity's sake. The observable sources are generated by implementations of the `AbstractCatalog` interface. Let us note that, from the interface point of view, a star and a Satellite from Jupiter are perfectly equivalent.

A.2.7 Relativistic Model

The relativistic and astrometric model is implemented via the `AstrometricModel` interface

```
public interface AstrometricModel {
    public double[] getDirection(ObservableSource source,
```

```
                                    double ep0,
                                    double tobs);
    public double[] getDirection(double[] qso_dir,
                                    double ep0,
                                    double tobs);
}
```

Several implementing classes have been developed which are essentially updates of the original one (relativisticmodel.lennart.GaiaAstrometricModel) including new feaures as different γ_A for each body, the dynamical parameter α_r (in the retardation and the dynamical picture), the quadrupolar part of the light deflection, etc. Some of the are listed bellow

`relativisticmodel.lennart.GaiaAstrometricModel`
`relativisticmodel.lennart.EnhancedAstrometricModel`

where `EnhancedAstrometricModel` essentially wraps `GaiaAstrometricModel` and includes the methods to get/set the relativistic parameters. These classes are managed by the implementations of the `ObservableSource` interface, and are perfectly hidden to the client algorithms (instrument model, attitude, etc.), since such algorithms do not require the details of the relativistic model. In this sense, `ObservableSource` implementations are *wrappers* of the `AstrometricModel`.

A.3 Data reduction code

A data reduction framework have been developed with the philosophy of having a small set of generic classes with the minimal methods required to apply classical and advanced data reduction techniques. It is very flexible and could even be used to solve more general problems that the one discussed in this thesis.

There are two data reduction packages. The `fitting.function` essentially contains the interface to plug any physical model into the algorithms of the `fitting.algorithms`.

A.3.1 The `fitting.function` package

It contains a very simple interface

```
public interface FittingFunction {
    public void setParameters(double[] parvals);
    public double[] getParameters();
    public double getValue(double[] x);
    public double[] getPartial(double[] x);
}
```

and an, even simpler, adapter

```
public abstract class FittingFunctionAdapter implements FittingFunction{
    public abstract double getValue(double[] x, double[] par);
    ...
}
```

where the ... represent all the implemented methods of the `FittingFunction` interface. To implement any physical model, the developer only has to define what must be given by the `getValue` method, given some input data (i.e. the instant of observation and the astrometric parameters of a star) and some values of the parameters to be fitted in the model (the `double[] par` array, the values of the relativistic parameters). Defining this method alone, the FittingFuntionAdapter class is able to do all the operation required by the `FittingFunction` interface. As an example, the partial derivatives are computed internally by calling the `getValue` with slightly perturbed values of the parameters. The `FittingFunctionAdapter` also contains other useful methods,

```
public void setDeltaValues(double[] in_delta)
public double getPartial(double[] x, double[] par,int parNumber)
```

Let us note that if the user wants to implement the analytical computation of the partial derivatives of some of the parameters, he only has to implement again the

```
public double[] getPartial(double[] x);
```

method when extending the `FittingFunctionAdapter`. This approach enabled us to test different models and parameterizations, with a minimal code redesign.

A.3.2 The fitting.algorithms package

There are a few algorithms implemented that have been used for this work. They are contained in this package. The classes containing the algorithms are

`fitting.algorithms.IterativeMultilinearRegression.java`
`fitting.algorithms.LeastSquaresSolution.java`
`fitting.algorithms.bayes.BayesianInference.java`
`fitting.algorithms.bayes.MontecarloIntegration.java`

The details of how they work can be found in the documentation of the code. Let us add a few words of the main features of each algorithm.

- `LeastSquaresSolution`. This class implements the classical non-linear Least Squares algorithm described in Press *et al.* (1992). The observations are gathered and all the condition equations are stored in memory. The normal equations are build by algebraic manipulation of the condition equations and solved by standard methods. It is fast and easy to use but requires a lot of memory if the data set is large.

- `IterativeMultilinearRegression`. The same as `LeastSquaresSolution` but it does not store the condition equation and the normal equations are built directly. It saves a lot of memory. It is not as fast as `LeastSquaresSolution` since the observations must be reinserted at each iteration of the non-linear fit, but it is very suitable for large sets of data.

- `BayesianInference`. It samples the Bayesian PDF in a rectangular grid on the parameter space, and the integrals of the PDF are computed on the grid permitting the usage of very optimal integration routines. Nevertheless the number of grid elements grows very fast with the number of parameters. This is $\sim s^N$, where s is the number of grid points for each parameter and N is the number of parameters. If we have 5 parameters in the model and we want to have 10 values per parameter, the number of grid points is 10^5.

- `MontecarloIntegration`. This class performs the integration of the PDF in a random collection of parameter values. It enables to reduce the number of required points. This class is the one used to produce the results presented in this work.

A.3.3 Data reduction core classes

The data reduction code consists on a class extending the `FittingFunctionAdapter` and a driver class which prepares the data and applies the desired algorithms described

above.

The implementation of the `FittingFunctionAdapter` is called `PlanetaryFunction.java`. It is a quite complex extension of the adapter which permits to specify which parameters are fitted, and the target planet under study. It computes numerically the partial derivatives of all the parameters except for the quadrupole, which is obtained in a semi-analytical way (since the effect is not large, it is very sensitive to floating point errors).

The driver class is the `bin.PlanetParameterFit.java`, whose methods permit to specify the telemetry file to be processed, the limiting magnitude of the used stars, the maximal angular separation from the planet, the algorithm used, etc. Again, the details of the implementation and all its methods can be found in the code documentation. It can be executed on a shell supporting a java virtual machine. In this case, the data reduction parameters must be provided in a formatted ascii file. A sample parameters file is distributed with the code.

A.4 A data simulation example

```
public class SimulatorExample {

     public static void main(String args[]) {
         CatalogBuffer catalogBuffer;
         AbstractCatalog catalog;
         PlanetTelemetryGenerator telemetryGenerator;
         int counter;
         String telemetryName;
         double catalogBuffer
         double previousInstantOfTime;
         double t;

      // The simulator will look for the first planetary transit from
      // this date
         previousInstantOfTime = 0.0;  //  in days from JD2010
```

```
// Defines the time step applied to check if there is a planet
// close to the Field of view
   time_interval = 0.01; // in days

// This class manages the interaction of the instrument with
// the sources, the catalogs and does most of the work
   telemetryGenerator = new PlanetTelemetryGenerator();

// This parameter determines how many catalog files will be
// processed. Each catalog file contains 1x1 deg. A large
// tolerance will slow down the process since many more
// sources will be processed unnecessarily.
   bufferTolerance = 1.0*Math.PI/180.0;

// Initialize the catalog buffer. A catalog buffer generates
// AbstractCatalog objects from the catalog files.
   catalogBuffer = new CatalogBuffer();


// Setting up the factories

   // Choosing the version of the instrument
   GaiaAstrometricInstrumentFactory.setDefaultInstrument(
       GaiaAstrometricInstrumentFactory.GAIA2);

   // Choosing the error model
   AstrometricErrorBudgetFactory.setDefaultErrorBudget(
      AstrometricErrorBudgetFactory.GAIA2);

   // Choosing the attitude representation
   AttitudeFactory.setDefaultAttitude(AttitudeFactory.EULER);


// Compute the precise transit instant
```

```
    t = telemetryGenerator.getNextPlanetTransitTime(
            previousInstantOfTime,
            EphemerisMonitor.JUPITER, //Planet observed.
            0.5*Math.PI/180,          // Maximum angular
                                      // of the planet from
                                      // the center of the FOV
            time_interval);           // In days. Time interval
                                      // used to seek for
                                      // planetary transits.
    telemetryGenerator.initTelemetryFile("demo.TM");

// The catalog buffer prepares the access to
// the stars around the position of the planet
    catalogBuffer.generateBufferAround(
        body,t,catalogBufferTolerance);

// Get the first catalog
    catalog = catalogBuffer.retrieveNextCatalog();

// Loop over the catalog files
    while(cat!=null) {

      // simulate for this planetary transit.
      telemetryGenerator.generate(
          Ephemeris.JUPITER,
          cat,
          t-2*time_interval,   // Initial simulation instant.
          t+2*time_interval,   // Final simulation instant.
          ep0);                // Catalog reference epoch,
                               // in days from 2010).

      // retrieve the next catalog. If not more catalogs
      // are available a "null" value is returned
      cat = cat_buff.retrieveNextCatalog();
```

```
          }
          telemetryGenerator.closeTelemetryFile();

     }// End of the "main" method
} // End of the class
```

Appendix B

Additional material to : Astrometric Light-Travel Time signature of sources in nonlinear motion

B.1 First order derivation of Equation of time delay

The first term on the right side of the equation (3.8), to first order as defined in (3.4)–(3.5), reads

$$\begin{aligned} \frac{|\boldsymbol{x}_{obs}\,[t_{obs}] - \boldsymbol{x_e}\,[t_e]|}{c} &\simeq \frac{1}{c}\; x^0_{LRM} \\ &+ \boldsymbol{l_0} \cdot \frac{\boldsymbol{v}^0_{LRM}\Delta t_e}{c} \;+\; \boldsymbol{l_0} \cdot \frac{\boldsymbol{D}\,[t_e]}{c} \\ &- \boldsymbol{l_0} \cdot \frac{\boldsymbol{x}_{obs}\,[t_{obs}]}{c} \;+\; \mathcal{O}(2); \end{aligned} \tag{B.1}$$

The second term of the right hand of (3.8) is straightforward using t^0_e instead of t_e in the last expression (B.1). After some algebra the emision time interval Δt_e can

be written as

$$\begin{aligned}\Delta t_e &= \frac{1}{1+\boldsymbol{l_0}\cdot\frac{\boldsymbol{v}^0_{LRM}}{c}}\Big(\,\Delta t_{obs} \\ &- \boldsymbol{l_0}\cdot\frac{\boldsymbol{D}\left[t_e\right]-\boldsymbol{D}\left[t^0_e\right]}{c} \\ &+ \boldsymbol{l_0}\cdot\frac{\boldsymbol{x}_{obs}\left[t_{obs}\right]-\boldsymbol{x}_{obs}\left[t^0_{obs}\right]}{c}\Big) \\ &+ \mathcal{O}(2);\end{aligned} \tag{B.2}$$

The term multiplying the full expression is responsible for apparent superluminal velocities. For this reason we call this term superluminal factor

$$\alpha_s = \frac{1}{1+\boldsymbol{l_0}\cdot\frac{\boldsymbol{v}^0_{LRM}}{c}}; \tag{B.3}$$

In spite of the suppression of the second order terms there is still a dependency on t_e on the right hand of equation(B.2) in $\boldsymbol{D}$. This equation is enough to solve Δt_e iteratively. But our purpose is to obtain a closed form accurate to $\mathcal{O}(1)$. To solve this we consider

$$\begin{aligned}\boldsymbol{D}\left[t_e\right]-\boldsymbol{D}\left[t^0_e\right] &= \boldsymbol{D}\left[t^0_e+\alpha_s\Delta t_{obs}+\delta t\right] \\ &- \boldsymbol{D}\left[t^0_e\right],\end{aligned} \tag{B.4}$$

$$\begin{aligned}\delta t = &- \alpha_s\,\boldsymbol{l_0}\cdot\frac{\boldsymbol{D}\left[t_e\right]-\boldsymbol{D}\left[t^0_e\right]}{c} \\ &+ \alpha_s\,\boldsymbol{l_0}\cdot\frac{\boldsymbol{x}_{obs}\left[t_{obs}\right]-\boldsymbol{x}^0_{obs}\left[t^0_{obs}\right]}{c} \sim \mathcal{O}(1);\end{aligned} \tag{B.5}$$

Taking this into account, we can write to first order in δt

$$\begin{aligned}\frac{\boldsymbol{D}\left[t_e\right]-\boldsymbol{D}\left[t_e^0\right]}{c} = \\ \frac{\boldsymbol{D}\left[t_e^0+\alpha_s\Delta t_{obs}\right]-\boldsymbol{D}\left[t_e^0\right]}{c} \\ +\frac{\boldsymbol{V}_{orb}\left[t_e^0+\alpha_s\Delta t_{obs}\right]}{c}\,\delta t+\mathcal{O}(2)\end{aligned} \tag{B.6}$$

In (B.6) the term $\frac{\boldsymbol{V}_{orb}}{c}\delta t$ is of $\mathcal{O}(2)$ and will be neglected in (B.2). The development (B.6) is also used to justify the appearance of $\boldsymbol{V}_{orb}$ in equation (3.31). These are all the ingredients needed to obtain the relation of Δt_e in terms of Δt_{obs} to first order

$$\begin{aligned}\Delta t_e &= \alpha_s\,(\Delta t_{obs} \\ &- \boldsymbol{l_0}\cdot\frac{\boldsymbol{D}\left[t_e^0+\alpha_s\Delta t_{obs}\right]-\boldsymbol{D}\left[t_e^0\right]}{c} \\ &+ \boldsymbol{l_0}\cdot\frac{\boldsymbol{x}_{obs}\left[t_{obs}\right])-\boldsymbol{x}_{obs}\left[t_{obs}^0\right]}{c}\Bigg) \\ &+ \mathcal{O}(2)\end{aligned} \tag{B.7}$$

which is the same as equation (3.11) with the suitable notation shortcuts explained in (3.12)–(3.14).

Appendix C

Additional material : Light deflection experiments on the the Solar System planets

C.1 Building the *a posteriori* Probability Density Function

In a simulation/reduction process, all the features of the data are perfectly controlled and a set of different data sets can be used to compute confidence levels and expected values of the parameters. But real data contain uncontrolled features like outliers, non-gaussian behavior of the errors, unmodeled biases, etc. In order to obtain the full statistical characterization of the parameters, we proceed by using a Bayesian approach.

Our purpose is to obtain the expected values and the standard deviations of the parameters using the *a posteriori* Probability Density Function (PDF) of the parameters and compare them with those provided by the least square solution.

Consider a set of statistically independent observations $X_i \in \hat{X}$ and a continuous

set of plausible models describing the observations specified by the values of some parameters

$$\boldsymbol{\theta}^s \quad = \quad [\theta_1^s, \theta_2^s, \ldots \theta_N^s] \tag{C.1}$$

where N is the number of free parameters and s is used to enumerate the possible elections of the parameter values. The probability that a given election of $\boldsymbol{\theta}^s$ satisfies the data $\hat{X}$ is provided by the *Bayes Theorem* as

$$P(\boldsymbol{\theta}^s|\,\hat{X}) = \frac{P(\hat{X}|\,\boldsymbol{\theta}^s)P\left(\boldsymbol{\theta}^s\right)}{\sum_{s'} P\left(\hat{X}|\,\boldsymbol{\theta}^{s'}\right) P\left(\boldsymbol{\theta}^{s'}\right)} \tag{C.2}$$

On the right hand side $P(\boldsymbol{\theta}^K)$ reflects our previous knowledge of the problem (state-of-art, previous experiments, faith,etc.) and is called the *a priori probability* of $\boldsymbol{\theta}^K$ being true. The term $P(\hat{X}|\boldsymbol{\theta}^K)$ is the probability that the new data fits the model assuming the $\boldsymbol{\theta}^K$ is true. Note that it is not equal to $P(\boldsymbol{\theta}^K|\,\hat{X})$ which is the probability that the model satisfies the data, given that the data is true. Roughly speaking, the new observations $\hat{X}$ update our knowledge of trueness of $\boldsymbol{\theta}^K$. In the denominator we have the sum over all the possible values of the parameters $\boldsymbol{\theta}^K$ weighted again by their *a priori* probabilism $P(\boldsymbol{\theta}^K)$. This denominator is not really important and can be determined by usual normalization methods (analytically or numerically depending on the particular problem). If no *a priori* knowledge of $\boldsymbol{\theta}$ is available, $P(\hat{\theta})$ is assumed to be a uniform distribution. The left side of (C.2), $P(\boldsymbol{\theta}^K|\,\hat{X})$, is the Probability Density Function we are looking for.

The $P(\hat{X}|\boldsymbol{\theta}^K)$ can be obtained from the data as follows. Assuming statistical independence of the elements in $\hat{X}$, the probability of observing all the $\hat{X}$ independently is the product of the probabilities of each individual X_i to happen,

$$P(\hat{X}|\hat{\theta}) \simeq L(\hat{X};\hat{\theta}) = \prod P(X_i|\hat{\theta}) \tag{C.3}$$

where $P(X_i|\theta)$ is the probability that each individual observation X_i fits the model for a given set of $\boldsymbol{\theta}^K$. L is the so-called Likelihood function and is proportional to $P(\hat{X}|\hat{\theta})$ except for an arbitrary normalization factor which, again, is unimportant until we need to normalize the PDF.

Assuming that the instrument provides the error of each measurement, and using

the error model (a Gaussian one in our case but it is not necessary), we have

$$L(\hat{X};\boldsymbol{\theta}^K) = \prod_i \frac{1}{\sqrt{2\pi}\sigma_i} \exp\left[\frac{\left(X_i - X_{teo}(\boldsymbol{\theta}^K)\right)^2}{\sigma_i^2}\right] \tag{C.4}$$

Let us remark that different noise models can be used (Poisson, Log-Normal distribution, etc.) and that the free parameters of the noise models could also be inserted in the $\hat{\theta}$ set. For computational reasons, it is simpler to work with the logarithm of L (the product is then a sum) and recover at the end the PDF at the same time as the normalization is obtained.

In our procedure, the model to be tested enters in X_{teo} which is computed using a given $\hat{\theta}^K$. Let us note that there is an infinite number of K combinations of parameter values. Instead of obtaining a grid sampling the PDF, we can directly obtain the moments of the distribution using Montecarlo integration. In such a way we can obtain the expected values and the standard deviations of the parameters as

$$Z = \int_V L(\hat{\theta};\hat{X})\, P(\hat{\theta}) d\Omega \tag{C.5}$$

$$\langle\theta_k\rangle = \frac{1}{Z}\int_V \theta_k^2\, L(\hat{\theta}|\hat{X})\, P(\hat{\theta}) d\Omega \tag{C.6}$$

$$\sigma_{\theta_k} = \sqrt{\langle\theta_k^2\rangle - \langle\theta_k\rangle^2} \tag{C.7}$$

where Z is the normalization factor. Note that an homogeneous grid of N parameters using n different values for each parameter contains n^N points. This is, if we fit 4 parameters using 10 values for each one, we need to compute 10 000 points!. If the likelihood function is smooth enough, the accuracy of the Montecarlo integration scale is $\frac{1}{\sqrt{N}}$, independently of the number of parameters.

In our approach we generate randomly 1000 parameter sets uniformly distributed around the Least-square solution in the interval $\theta_K \pm 5\sigma_K$.

C.2 Instant of closest approach and impact parameter

Let us write the trajectory of a photon and a massive body as two particles moving with constant velocities(straight lines) as

$$\begin{aligned} \boldsymbol{x}_p(t) &= \boldsymbol{x}_{p0} + c\boldsymbol{\sigma}(t - t_0)\,, & \text{(C.8)} \\ \boldsymbol{x}_A(t) &= \boldsymbol{x}_{A0} + c\boldsymbol{\mu_A}(t - t_0)\,, & \text{(C.9)} \\ \boldsymbol{\mu} &= \frac{\boldsymbol{v}_A}{c} & \text{(C.10)} \end{aligned}$$

where $\boldsymbol{x_{p0}}$ is some arbitrary position of the photon along its trajectory and $\boldsymbol{x_{A0}}$ is some arbitrary position of the massive body along its trajectory. Then we can freely choose t_0 as the instant of observation. Then the instant of closest approach is obtained minimizing the distance vector $\boldsymbol{x_{p0}}$ is the position of the photon/observer at that instant and $\boldsymbol{x_{A0}}$ is the position of the massive body. The instant of closest approach is obtained through the minimization of the module of the separation vector $\boldsymbol{r}_A(t)$ as

$$\begin{aligned} \frac{d}{dt}|\boldsymbol{r}|_A &= 0 & \text{(C.11)} \\ \boldsymbol{r}_A(t) &= \boldsymbol{x_p}(t) - \boldsymbol{x_A}(t) & \text{(C.12)} \end{aligned}$$

where (C.12) can be written as

$$\begin{aligned} \boldsymbol{r}_A(t) &= \boldsymbol{r}_{A0} + c\boldsymbol{g}(t - t_0)\,, & \text{(C.13)} \\ \boldsymbol{r}_{A0} &= \boldsymbol{x}_{p0} - \boldsymbol{x}_{A0}\,, & \text{(C.14)} \\ \boldsymbol{g} &= \boldsymbol{\sigma} - \boldsymbol{\mu_A}\,. & \text{(C.15)} \end{aligned}$$

Then, the minimum distance condition in (C.11) provides the instant of closest approach as

$$t_{ca} = t_0 - \frac{\boldsymbol{r}_{A0}\cdot\boldsymbol{g}}{c\,g^2}\,, \qquad \text{(C.16)}$$

Subtracting (C.8) and (C.9) and using (C.16) it is obtained that

$$\boldsymbol{r}\left(t_{ca}\right) = \boldsymbol{r}_{A0} - \frac{1}{g^2}\boldsymbol{g}\left(\boldsymbol{r}_{A0}\cdot\boldsymbol{g}\right), \tag{C.17}$$

that can be writen as

$$\boldsymbol{r}\left(t_{ca}\right) = \frac{\boldsymbol{g}\times\boldsymbol{r}_{A0}\times\boldsymbol{g}}{g^2} \tag{C.18}$$

We can perform a taylor expansion keeping only the terms proportional to $\boldsymbol{\mu} = \boldsymbol{v}/c$ obtaining that $\boldsymbol{r}\left(t_{ca}\right)$ is equivalent to

$$\boldsymbol{r}\left(t_{ca}\right) = \boldsymbol{\sigma}\times\left(\boldsymbol{r}_{A0}\times\boldsymbol{g}\right) + \mathcal{O}(c^{-2}) = \hat{\boldsymbol{d}}_A\,, \tag{C.19}$$

which is the vector in equation (4.29).

C.3 Gravitomagnetic light deflection

In order to evaluate the amount of deflection caused directly by the non-diagonal term h_{0i} in the metric, let us rewrite the equations of motion for the photon using only the spherical symmetric part of the gravitational field and putting a numerical coefficient α multiplying h_{0i}. To simplify the notation, let us assume that only one body is causing the light deflection and that it moves in rectilinear motion, say

$$\boldsymbol{x}\left(t\right) = \boldsymbol{x}_0 + \boldsymbol{v}t\,. \tag{C.20}$$

Let us assume that the unperturbed trajectory of the photon is given by

$$\boldsymbol{x}_N\left(t\right) = \boldsymbol{x}_{0N} + c\boldsymbol{\sigma}t\,, \tag{C.21}$$

where $\boldsymbol{x}_N$ is the newtonian unperturbed trajectory of the photon and $\boldsymbol{k}$ is its unperturbed propagation direction. After some algebra it is found that the equations of motion can be rewritten as

$$\delta\ddot{\boldsymbol{x}}_p = \delta\ddot{\boldsymbol{x}}_p|_{\alpha=1} + 4\left(\alpha-1\right)GM\,\frac{\left(\boldsymbol{v}\cdot\boldsymbol{\sigma}\right)}{c}\,\frac{\boldsymbol{\sigma}\times\left(\boldsymbol{r}\times\boldsymbol{\sigma}\right)}{r^3} + \mathcal{O}(G^1\frac{v^2}{c^2}) \tag{C.22}$$

$$\boldsymbol{r} = \boldsymbol{x}_p\left(t\right) - \boldsymbol{x}\left(t\right) \tag{C.23}$$

where $\delta\ddot{\boldsymbol{x}}_p|_{\alpha=1}$ are the same equations of motion as in (4.15). Let us note that if $\alpha = 1$ the second term vanishes and the standard solution is recovered. Therefore, one can easily integrate (C.22) (the required integral can be found in Klioner & Kopeikin (1992)) and find that the gravitomagnetic contribution to the light deflection at the post-Newtonian order is

$$\frac{1}{c}\delta\dot{\boldsymbol{x}}_{pG} = 4\alpha\frac{GM}{c^2}\frac{\boldsymbol{\sigma}\times(\boldsymbol{r}\times\boldsymbol{\sigma})}{r\,(r-\boldsymbol{\sigma}\cdot\boldsymbol{r})}\;\frac{\boldsymbol{v}\cdot\sigma}{c} + \mathcal{O}(G^1\frac{v^2}{c^2}) \tag{C.24}$$

which is simply the classical Schwarschild deflection times a term proportional to v/c which is of the order of $\simeq 10^{-4}$ for any solar system body. We can write (C.24) in terms of the aspect angle ψ (apparent angle between the planet and the direction of the source). It reads

$$\delta_G = 2\delta_{Sch}\frac{\boldsymbol{v}\cdot\sigma}{c}\,, \tag{C.25}$$

$$\delta_{Sch} = \frac{2GM}{c^2}\frac{1}{r}c\tan\frac{\psi}{2}\,. \tag{C.26}$$

As an example, for Jupiter it means $2\cdot 16000$ mas $\cdot 0.5\cdot 10^{-4} = 1.6\mu$as the maximal effect. The Sun is more massive, but it moves slower, thus obtaining a maximal amplitude of $1.75''\times 0.5\cdot 10^{-7} = 0.16\mu$as, which is even smaller than for Jupiter. The effect is maximal when the velocity and the direction of the source are parallel. The gravitomagnetic deflection caused by the planet rotation gives similar numbers. A detailed treatment of this case can be found in (Klioner & Kopeikin 1992).

C.4 Ephemeris positional measurements

Table C.1: Ephemeris correction to the position of Jupiter obtained from observation of the light deflection effect during a simulated full Gaia mission. Only transits giving an astrometric accuracy(last column is in arcseconds) better than the instantaneous size of the planet are given.

Julian date	Year	Used stars	$\delta_l \pm \sigma$ km	$\delta_m \pm \sigma$ km	σ''
2456117.5661	2012.5	109	35267.2 ± 23721	135698.7 ± 41486.4	6.87
2456271.9115	2012.9	153	-4583.9 ± 13397.5	13193.7 ± 23331	3.52
2456271.9805	2012.9	156	-4607.1 ± 3653.9	-10414.4 ± 0	0.48
2456284.4080	2013.0	139	48372.3 ± 32880.2	82122.4 ± 40040.5	6.87
2456284.4770	2013.0	137	-14870.1 ± 25815.2	-26661.8 ± 47701.1	7.21
2456325.6688	2013.1	100	-2965.5 ± 8818.3	9576.4 ± 7065.2	1.59
2456473.2722	2013.5	84	16284.1 ± 11364.5	20740.4 ± 8787.4	2.12
2456473.3411	2013.5	148	-3479.7 ± 14760.2	-9932.1 ± 30330.9	4.98
2456681.1259	2014.1	293	44115.7 ± 11405.9	-97012.6 ± 45583.8	6.38
2456714.5827	2014.2	261	2847.9 ± 5726.6	20825.2 ± 24122	3.56
2456714.6516	2014.2	325	5809.7 ± 8199	-19455.2 ± 20615.5	3.18
2456738.3180	2014.2	295	-6687.3 ± 25545.5	-37527.2 ± 37095.2	6.70
2456738.3869	2014.2	294	-9793.7 ± 25912.4	22799.1 ± 36642.8	6.68
2456831.8702	2014.5	262	-73885.6 ± 29698.4	-54745.9 ± 34194.7	6.81
2456849.5427	2014.5	238	5189.3 ± 13484.6	44262 ± 36331.5	5.68
2456849.6117	2014.5	236	-2074.2 ± 12819.4	59303.6 ± 39743.6	6.12
2456887.5590	2014.6	237	4162.1 ± 12204.1	-14978.4 ± 20943.6	3.34
2457061.7040	2015.1	248	63920.2 ± 46243	6319.8 ± 9904.5	6.36
2457095.3453	2015.2	471	10544.2 ± 8212.1	19866.3 ± 12705.2	2.16
2457095.4142	2015.2	361	-7739.6 ± 7573.8	-2936.6 ± 12180	2.05
2457242.7653	2015.6	446	-10229.7 ± 9398.2	23841.7 ± 12969.3	2.27
2457242.8342	2015.6	300	-5652.5 ± 6614.3	-674.6 ± 13988.3	2.20
2457278.2175	2015.7	447	638.3 ± 4854.8	-3963.9 ± 4136.9	0.85
2457278.2867	2015.7	433	2861.8 ± 4024.4	-7013.4 ± 11188	1.59

Julian date	Year	Used stars	$\delta_l \pm \sigma$ km	$\delta_m \pm \sigma$ km	σ''
2457300.4557	2015.8	293	-6858.8 ± 18933.2	-8080.5 ± 20245.2	3.60
2457400.6842	2016.0	627	-27957.6 ± 24300.2	-13093.8 ± 11246.6	3.42
2457400.7532	2016.0	759	7333.2 ± 14585.5	12012.4 ± 32011.2	4.51
2457400.9342	2016.0	950	12917.7 ± 10426.6	12267 ± 9770.3	1.83
2457401.0032	2016.0	951	5267.1 ± 3193.8	-7768.7 ± 6307.1	0.91
2457401.1842	2016.0	963	9335.6 ± 10330.1	153.1 ± 15232.8	2.36
2457401.2532	2016.0	963	37265.6 ± 28031.1	-30291.8 ± 22199.4	4.58
2457401.4341	2016.0	989	-6731.9 ± 16980.7	2587.3 ± 11762.6	2.64
2457401.5031	2016.0	987	899.5 ± 15394.7	3493.2 ± 13710.3	2.64
2457401.6835	2016.0	991	46197.2 ± 34101.9	22232.9 ± 14063.6	4.72
2457401.7526	2016.0	992	-35179.4 ± 16069.6	10357.8 ± 22141	3.51
2457401.9335	2016.0	898	-29264.3 ± 19014.3	28391.7 ± 11166.5	2.82
2457402.0026	2016.0	854	7280 ± 4556.9	6908.9 ± 5962.5	0.96
2457402.1835	2016.0	752	-5206.9 ± 8479	13305.2 ± 13123.2	2.00
2457402.2525	2016.0	708	1930.7 ± 9613.6	-9242.1 ± 11191.4	1.89
2457402.4335	2016.0	622	14750.1 ± 13920.3	17814.9 ± 17862.8	2.90
2457402.5025	2016.0	593	7624.5 ± 6364.4	30358 ± 24463.2	3.25
2457402.6835	2016.0	541	4747.8 ± 5283.1	1769.8 ± 7967.7	1.23
2457402.7525	2016.0	536	-744.6 ± 14264.8	992.6 ± 10918.6	2.30
2457402.9335	2016.0	517	-8027.3 ± 8915.9	-2049.2 ± 6019	1.38
2457403.0025	2016.0	532	-1554.5 ± 16164.2	15369.2 ± 13705.9	2.72
2457403.1835	2016.0	591	-4620.7 ± 25134.5	882.8 ± 34577.2	5.49
2457403.2525	2016.0	629	29348.2 ± 24829.6	28865.3 ± 30720.4	5.07
2457403.4343	2016.0	716	-3234.2 ± 10832.1	-10102.2 ± 16096.1	2.49

Julian date	Year	Used stars	$\delta_l \pm \sigma$ km	$\delta_m \pm \sigma$ km	σ''
2457403.5034	2016.0	771	-19285.5 ± 8084.6	223.4 ± 5320.6	1.24
2457403.6843	2016.0	891	498.3 ± 2578.2	3908.9 ± 6220.6	0.87
2457403.7533	2016.0	934	3646.5 ± 16344.9	2563.5 ± 20252.1	3.34
2457403.9343	2016.0	995	-16920.7 ± 15454.3	-23883.5 ± 24502.4	3.72
2457404.0032	2016.0	1000	55870.1 ± 21041.4	35791.1 ± 18569.1	3.60
2457404.1843	2016.0	978	3040.2 ± 26448.3	20495 ± 14696.2	3.88
2457404.2532	2016.0	984	11683.1 ± 22210.9	-28282 ± 31046.4	4.91
2457404.4341	2016.0	981	8321 ± 8573.3	11943.5 ± 14267.1	2.14
2457404.5031	2016.0	984	-2411.4 ± 0	-4471.2 ± 0	0.00
2457404.6841	2016.0	975	6942.8 ± 10494.9	25983 ± 12624.2	2.11
2457404.7531	2016.0	911	-2690.9 ± 17470.4	-5557.5 ± 13527.7	2.84
2457404.9341	2016.0	548	9870.8 ± 14678.2	14951.5 ± 24186.2	3.64
2457450.6896	2016.2	1722	25943.9 ± 9394.3	-31403.7 ± 14671.9	2.39
2457492.0588	2016.3	1800	-2651.9 ± 6548.4	6189.6 ± 8350.9	1.56
2457492.1278	2016.3	1794	2790 ± 7865.2	737.1 ± 5512	1.41
2457492.3087	2016.3	852	12461.7 ± 15260.4	8630.9 ± 10435.5	2.71
2457503.1270	2016.3	743	3149.1 ± 5373.9	-6956 ± 7317.1	1.35
2457503.3079	2016.3	1574	-1062.5 ± 3280.8	-339.5 ± 4311.9	0.81
2457503.3769	2016.3	1570	-3793.9 ± 4061.8	-3690 ± 3549	0.80
2457503.5578	2016.3	975	-2720.2 ± 4178.1	460 ± 7275.8	1.25
2457598.8610	2016.6	653	-3673.8 ± 7057.2	-1958 ± 4697.3	1.24
2457625.2685	2016.6	373	-13671.3 ± 12030.7	-3044.2 ± 12642.8	2.44
2457625.3372	2016.6	645	6777.1 ± 14104.8	-17091.1 ± 10675	2.47
2457657.2340	2016.7	883	-4431.6 ± 20001.2	1714.6 ± 7989.3	2.86

Julian date	Year	Used stars	$\delta_l \pm \sigma$ km	$\delta_m \pm \sigma$ km	σ''
2457657.3029	2016.7	686	-8335 ± 6884.3	385.8 ± 5961	1.21
2457806.1468	2017.1	9618	-1464.6 ± 2996.6	448 ± 1774	0.46
2457806.2156	2017.1	7957	2301.5 ± 2354.9	-539 ± 1463.6	0.37
2457837.6102	2017.2	11129	-495.2 ± 1455.1	-1059.9 ± 2404.5	0.39
2457837.6790	2017.2	11114	497.7 ± 2200	1076 ± 2483.6	0.46
2457864.1583	2017.3	9437	-690.8 ± 1525.7	660.9 ± 1399.6	0.30
2457864.3390	2017.3	5367	556.7 ± 6371.3	1528.5 ± 13138	2.13
2457959.5721	2017.6	4809	-193.7 ± 2618.7	2376.2 ± 3171.3	0.61
2457959.6411	2017.6	4914	-2691.1 ± 2225.3	5939.2 ± 2303.7	0.48
2457959.8221	2017.6	4888	776.3 ± 1612.3	361 ± 3051.9	0.51
2457959.8911	2017.6	3645	-87.2 ± 2554.6	-600.6 ± 2096.5	0.49
2457970.5693	2017.6	2882	-3887.3 ± 15768.4	199.7 ± 5097.5	2.43
2457970.6382	2017.6	2887	6271 ± 6442.1	-3347.7 ± 5025	1.20
2457970.8192	2017.6	1966	2702.7 ± 2623.8	-8191.2 ± 7809.3	1.21
2458012.3287	2017.7	1966	-3230.2 ± 4774.4	-4820.2 ± 6226.4	1.08
2458055.9451	2017.8	7999	5740.7 ± 2885.2	1467.9 ± 2679.5	0.51
2458056.0141	2017.8	8022	-3328.8 ± 3928.2	1041.9 ± 4634.8	0.78
2458056.1950	2017.8	8040	-1100.9 ± 2079.8	1975 ± 2189	0.39
2458056.2640	2017.8	6501	1878.3 ± 2825.5	1951 ± 2751.8	0.51
2458064.5144	2017.8	5076	3229.8 ± 1555.8	1820.7 ± 1641.4	0.29
2458064.6954	2017.8	8409	951.4 ± 4248.1	2965.4 ± 3938.4	0.74
2458064.7644	2017.9	8410	810.5 ± 3432.7	3126.1 ± 3668.7	0.64
2458064.9454	2017.9	8381	3738.6 ± 3586.2	-4134.4 ± 1670.5	0.50
2458065.0144	2017.9	6965	-302.8 ± 2106.5	-234.6 ± 1824.8	0.36

Table C.2: Ephemeris correction obtained from observations of Saturn using the light deflection effect during a simulated full Gaia mission. The last column is the positional error translated to astrometric displacement.

Julian date	Year	Used stars	$\delta_l \pm \sigma$ km	$\delta_m \pm \sigma$ km	σ''
2456117.5661	2012.5	109	35267.2 ± 23721	135698.7 ± 41486.4	6.87
2456271.9115	2012.9	153	-4583.9 ± 13397.5	13193.7 ± 23331	3.52
2456271.9805	2012.9	156	-4607.1 ± 3653.9	-10414.4 ± 0	0.48
2456284.4080	2013.0	139	48372.3 ± 32880.2	82122.4 ± 40040.5	6.87
2456284.4770	2013.0	137	-14870.1 ± 25815.2	-26661.8 ± 47701.1	7.21
2456325.6688	2013.1	100	-2965.5 ± 8818.3	9576.4 ± 7065.2	1.59
2456473.2722	2013.5	84	16284.1 ± 11364.5	20740.4 ± 8787.4	2.12
2456473.3411	2013.5	148	-3479.7 ± 14760.2	-9932.1 ± 30330.9	4.98
2456681.1259	2014.1	293	44115.7 ± 11405.9	-97012.6 ± 45583.8	6.38
2456714.5827	2014.2	261	2847.9 ± 5726.6	20825.2 ± 24122	3.56
2456714.6516	2014.2	325	5809.7 ± 8199	-19455.2 ± 20615.5	3.18
2456738.3180	2014.2	295	-6687.3 ± 25545.5	-37527.2 ± 37095.2	6.70
2456738.3869	2014.2	294	-9793.7 ± 25912.4	22799.1 ± 36642.8	6.68
2456831.8702	2014.5	262	-73885.6 ± 29698.4	-54745.9 ± 34194.7	6.81
2456849.5427	2014.5	238	5189.3 ± 13484.6	44262 ± 36331.5	5.68
2456849.6117	2014.5	236	-2074.2 ± 12819.4	59303.6 ± 39743.6	6.12
2456887.5590	2014.6	237	4162.1 ± 12204.1	-14978.4 ± 20943.6	3.34
2457061.7040	2015.1	248	63920.2 ± 46243	6319.8 ± 9904.5	6.36
2457095.3453	2015.2	471	10544.2 ± 8212.1	19866.3 ± 12705.2	2.16
2457095.4142	2015.2	361	-7739.6 ± 7573.8	-2936.6 ± 12180	2.05
2457242.7653	2015.6	446	-10229.7 ± 9398.2	23841.7 ± 12969.3	2.27
2457242.8342	2015.6	300	-5652.5 ± 6614.3	-674.6 ± 13988.3	2.20
2457278.2175	2015.7	447	638.3 ± 4854.8	-3963.9 ± 4136.9	0.85
2457278.2867	2015.7	433	2861.8 ± 4024.4	-7013.4 ± 11188	1.59

Julian date	Year	Used stars	$\delta_l \pm \sigma$ km	$\delta_m \pm \sigma$ km	σ''
2457300.4557	2015.8	293	-6858.8 ± 18933.2	-8080.5 ± 20245.2	3.60
2457400.6842	2016.0	627	-27957.6 ± 24300.2	-13093.8 ± 11246.6	3.42
2457400.7532	2016.0	759	7333.2 ± 14585.5	12012.4 ± 32011.2	4.51
2457400.9342	2016.0	950	12917.7 ± 10426.6	12267 ± 9770.3	1.83
2457401.0032	2016.0	951	5267.1 ± 3193.8	-7768.7 ± 6307.1	0.91
2457401.1842	2016.0	963	9335.6 ± 10330.1	153.1 ± 15232.8	2.36
2457401.2532	2016.0	963	37265.6 ± 28031.1	-30291.8 ± 22199.4	4.58
2457401.4341	2016.0	989	-6731.9 ± 16980.7	2587.3 ± 11762.6	2.64
2457401.5031	2016.0	987	899.5 ± 15394.7	3493.2 ± 13710.3	2.64
2457401.6835	2016.0	991	46197.2 ± 34101.9	22232.9 ± 14063.6	4.72
2457401.7526	2016.0	992	-35179.4 ± 16069.6	10357.8 ± 22141	3.51
2457401.9335	2016.0	898	-29264.3 ± 19014.3	28391.7 ± 11166.5	2.82
2457402.0026	2016.0	854	7280 ± 4556.9	6908.9 ± 5962.5	0.96
2457402.1835	2016.0	752	-5206.9 ± 8479	13305.2 ± 13123.2	2.00
2457402.2525	2016.0	708	1930.7 ± 9613.6	-9242.1 ± 11191.4	1.89
2457402.4335	2016.0	622	14750.1 ± 13920.3	17814.9 ± 17862.8	2.90
2457402.5025	2016.0	593	7624.5 ± 6364.4	30358 ± 24463.2	3.25
2457402.6835	2016.0	541	4747.8 ± 5283.1	1769.8 ± 7967.7	1.23
2457402.7525	2016.0	536	-744.6 ± 14264.8	992.6 ± 10918.6	2.30
2457402.9335	2016.0	517	-8027.3 ± 8915.9	-2049.2 ± 6019	1.38
2457403.0025	2016.0	532	-1554.5 ± 16164.2	15369.2 ± 13705.9	2.72
2457403.1835	2016.0	591	-4620.7 ± 25134.5	882.8 ± 34577.2	5.49
2457403.2525	2016.0	629	29348.2 ± 24829.6	28865.3 ± 30720.4	5.07
2457403.4343	2016.0	716	-3234.2 ± 10832.1	-10102.2 ± 16096.1	2.49

Julian date	Year	Used stars	$\delta_l \pm \sigma$ km	$\delta_m \pm \sigma$ km	σ''
2457403.5034	2016.0	771	-19285.5 ± 8084.6	223.4 ± 5320.6	1.24
2457403.6843	2016.0	891	498.3 ± 2578.2	3908.9 ± 6220.6	0.87
2457403.7533	2016.0	934	3646.5 ± 16344.9	2563.5 ± 20252.1	3.34
2457403.9343	2016.0	995	-16920.7 ± 15454.3	-23883.5 ± 24502.4	3.72
2457404.0032	2016.0	1000	55870.1 ± 21041.4	35791.1 ± 18569.1	3.60
2457404.1843	2016.0	978	3040.2 ± 26448.3	20495 ± 14696.2	3.88
2457404.2532	2016.0	984	11683.1 ± 22210.9	-28282 ± 31046.4	4.91
2457404.4341	2016.0	981	8321 ± 8573.3	11943.5 ± 14267.1	2.14
2457404.5031	2016.0	984	-2411.4 ± 0	-4471.2 ± 0	0.00
2457404.6841	2016.0	975	6942.8 ± 10494.9	25983 ± 12624.2	2.11
2457404.7531	2016.0	911	-2690.9 ± 17470.4	-5557.5 ± 13527.7	2.84
2457404.9341	2016.0	548	9870.8 ± 14678.2	14951.5 ± 24186.2	3.64
2457450.6896	2016.2	1722	25943.9 ± 9394.3	-31403.7 ± 14671.9	2.39
2457492.0588	2016.3	1800	-2651.9 ± 6548.4	6189.6 ± 8350.9	1.56
2457492.1278	2016.3	1794	2790 ± 7865.2	737.1 ± 5512	1.41
2457492.3087	2016.3	852	12461.7 ± 15260.4	8630.9 ± 10435.5	2.71
2457503.1270	2016.3	743	3149.1 ± 5373.9	-6956 ± 7317.1	1.35
2457503.3079	2016.3	1574	-1062.5 ± 3280.8	-339.5 ± 4311.9	0.81
2457503.3769	2016.3	1570	-3793.9 ± 4061.8	-3690 ± 3549	0.80
2457503.5578	2016.3	975	-2720.2 ± 4178.1	460 ± 7275.8	1.25
2457598.8610	2016.6	653	-3673.8 ± 7057.2	-1958 ± 4697.3	1.24
2457625.2685	2016.6	373	-13671.3 ± 12030.7	-3044.2 ± 12642.8	2.44
2457625.3372	2016.6	645	6777.1 ± 14104.8	-17091.1 ± 10675	2.47
2457657.2340	2016.7	883	-4431.6 ± 20001.2	1714.6 ± 7989.3	2.86

Julian date	Year	Used stars	$\delta_l \pm \sigma$ km	$\delta_m \pm \sigma$ km	σ''
2457657.3029	2016.7	686	-8335 ± 6884.3	385.8 ± 5961	1.21
2457806.1468	2017.1	9618	-1464.6 ± 2996.6	448 ± 1774	0.46
2457806.2156	2017.1	7957	2301.5 ± 2354.9	-539 ± 1463.6	0.37
2457837.6102	2017.2	11129	-495.2 ± 1455.1	-1059.9 ± 2404.5	0.39
2457837.6790	2017.2	11114	497.7 ± 2200	1076 ± 2483.6	0.46
2457864.1583	2017.3	9437	-690.8 ± 1525.7	660.9 ± 1399.6	0.30
2457864.3390	2017.3	5367	556.7 ± 6371.3	1528.5 ± 13138	2.13
2457959.5721	2017.6	4809	-193.7 ± 2618.7	2376.2 ± 3171.3	0.61
2457959.6411	2017.6	4914	-2691.1 ± 2225.3	5939.2 ± 2303.7	0.48
2457959.8221	2017.6	4888	776.3 ± 1612.3	361 ± 3051.9	0.51
2457959.8911	2017.6	3645	-87.2 ± 2554.6	-600.6 ± 2096.5	0.49
2457970.5693	2017.6	2882	-3887.3 ± 15768.4	199.7 ± 5097.5	2.43
2457970.6382	2017.6	2887	6271 ± 6442.1	-3347.7 ± 5025	1.20
2457970.8192	2017.6	1966	2702.7 ± 2623.8	-8191.2 ± 7809.3	1.21
2458012.3287	2017.7	1966	-3230.2 ± 4774.4	-4820.2 ± 6226.4	1.08
2458055.9451	2017.8	7999	5740.7 ± 2885.2	1467.9 ± 2679.5	0.51
2458056.0141	2017.8	8022	-3328.8 ± 3928.2	1041.9 ± 4634.8	0.78
2458056.1950	2017.8	8040	-1100.9 ± 2079.8	1975 ± 2189	0.39
2458056.2640	2017.8	6501	1878.3 ± 2825.5	1951 ± 2751.8	0.51
2458064.5144	2017.8	5076	3229.8 ± 1555.8	1820.7 ± 1641.4	0.29
2458064.6954	2017.8	8409	951.4 ± 4248.1	2965.4 ± 3938.4	0.74
2458064.7644	2017.9	8410	810.5 ± 3432.7	3126.1 ± 3668.7	0.64
2458064.9454	2017.9	8381	3738.6 ± 3586.2	-4134.4 ± 1670.5	0.50
2458065.0144	2017.9	6965	-302.8 ± 2106.5	-234.6 ± 1824.8	0.36

Bibliography

Altamirano, P., Babusiaux, C., Luri, X. & Masana, E. (2005) Gaia Simulator Reference document. "Gaia Technical Note p. 26.

Anglada–Escudé, G. (2004) Astrometria al microsegon d'arc. Aplicació a la Missió GAIA. Universitat de Barcelona.

Anglada-Escudé, G., Torra, J., Luri, X., Jordi, C. & Figueras, F. (2004) Implementation of fundamental algorithms. "Gaia Technical Note p. 31.

Batten, A. H. (1973) Binary and Multiple Systems of Stars, vol. textbook. Pergamon Press Ltd, Chicago.

Bertotti, B., Iess, L. & Tortora, P. (2003) A test of general relativity using radio links with the Cassini spacecraft. Nature425:374–376.

Bienaymé, O. & Turon, C. (2002) GAIA: A European Space Project, vol. textbook. Les Ulis: EDP Sciences.

Bolotovskii, B. M. & Stolyarov, S. N. (1989) Reflection of light on a moving mirror and related problems. Uspekhi Fizicheskikh Nauk(in russian) 159(1):155–180.

Bonnarel, F., Fernique, P., Bienaymé, O., Egret, D., Genova, F., Louys, M., Ochsenbein, F., Wenger, M. & Bartlett, J. G. (2000) The ALADIN interactive sky atlas. A reference tool for identification of astronomical sources. A&AS143:33–40.

Brumberg, V. A. & Groten, E. (2001) IAU resolutions on reference systems and time scales in practice. A&A367:1070–1077.

Busonero, D. (2006) Modelling and simulation of theAstroGaia3LSFs. "Gaia Technical Note p. 10.

Chauvin, G., Lagrange, A.-M., Zuckerman, B., Dumas, C., Mouillet, D., Song, I., Beuzit, J.-L., Lowrance, P. & Bessell, M. S. (2005) A companion to AB Pic at the planet/brown dwarf boundary. A&A438:L29–L32.

Cutri, R. M., Skrutskie, M. F., van Dyk, S., Beichman, C. A., Carpenter, J. M., Chester, T., Cambresy, L., Evans, T., Fowler, J., Gizis, J., Howard, E., Huchra, J., Jarrett, T., Kopan, E. L., Kirkpatrick, J. D., Light, R. M., Marsh, K. A., McCallon, H., Schneider, S., Stiening, R., Sykes, M., Weinberg, M., Wheaton, W. A., Wheelock, S. & Zacarias, N. (2003) 2MASS All Sky Catalog of point sources. The IRSA 2MASS All-Sky Point Source Catalog, NASA/IPAC Infrared Science Archive. http://irsa.ipac.caltech.edu/applications/Gator/.

de Boer, K. S., Gilmore, G., E., H., Lattanzi, M. G., Lindegren, L., Luri, X., Mignard, F., de Zeeuw, P. T., Pace, O., Perryman, M. A. C., Hechler, M., Volonte, C. & Favata, F. (2000) GAIA: Composition, Formation and Evolution of the Galaxy, Concept and Technology Study Report. ESA-SCI.

de Buijne, J. (2006) Gaia Parameter Database – contents maintenance. "Gaia Technical Note p. 29.

de Felice, F., Vecchiato, A., Crosta, M. T., Bucciarelli, B. & Lattanzi, M. G. (2006) A General Relativistic Model of Light Propagation in the Gravitational Field of the Solar System: The Dynamical Case. ApJ653:1552–1565.

Dravins, D., Lindegren, L. & Madsen, S. (1999) Astrometric radial velocities. I. Non-spectroscopic methods for measuring stellar radial velocity. A&A348:1040–1051.

Eddington, S. A. (1919) Report on the relativity theory of gravitation. Unknown .

Einstein, A. (1905) Elektrodynamik bewegter Körper. (German)[Electrodynamics of moving bodies]. Ann. Physik 17:891–921.

Einstein, A. (1915) Zur allgemeinen Relativitätstheorie. Sitzungsberichte der Königlich Preußischen Akademie der Wissenschaften (Berlin), Seite 778-786. pp. 778–786.

Fey, A. L., Ma, C., Arias, E. F., Charlot, P., Feissel-Vernier, M., Gontier, A.-M., Jacobs, C. S., Li, J. & MacMillan, D. S. (2004) The Second Extension of the International Celestial Reference Frame: ICRF-EXT.1. AJ127:3587–3608.

Fienga, A., Manche, H., Laskar, J. & Gastineau, M. (2006) INPOP06: a new planetary ephemeris. Nomenclature, Precession and New Models in Fundamental Astronomy, 26th meeting of the IAU, Joint Discussion 16, 22-23 August 2006, Prague, Czech Republic, JD16, #15 16.

Fomalont, E. B. & Kopeikin, S. M. (2003) The Measurement of the Light Deflection from Jupiter: Experimental Results. ApJ598:704–711.

Fragile, P. C. & Mathews, G. J. (2000) Reconstruction of Stellar Orbits Close to Sagittarius A*: Possibilities for Testing General Relativity. ApJ542:328–333.

Fricke, W., Schwan, H., Corbin, T., Bastian, U., Bien, R., Cole, C., Jackson, R., Jaehrling, R., Jahreiss, H., Lederle, T. & Roeser, S. (1994) Fifth Fundamental Catalogue (FK5) - Extension (Fricke+ 1991). VizieR Online Data Catalog 1175:0+.

Fridlund, C. V. M. (2000) Darwin - The Infrared Space Interferometry Mission. ESA Bulletin 103:20–25.

Froeschle, M., Mignard, F. & Arenou, F. (1997) Determination of the PPN Parameter gamma with the HIPPARCOS Data. In: ESA SP-402: Hipparcos - Venice '97. pp. 49–52.

Gambis, D. (1999) First extension of the ICRF, ICRF-Ext.1. IERS Annual report pp. 87–114.

Ghez, A. M., Klein, B. L., Morris, M. & Becklin, E. E. (1998) High Proper-Motion Stars in the Vicinity of Sagittarius A*: Evidence for a Supermassive Black Hole at the Center of Our Galaxy. ApJ509:678–686.

Gouda, N., Tsujimoto, T., Kobayashi, Y., Nakajima, T., Yasuda, N. & Matsuhara, H. (2002) Japanese Astrometry Satellite Mission for Infrared Exploration. Ap&SS280:89–94.

Graue, R., Kampf, D., Röser, S., Bastian, U. & Seifert, W. (2003) DIVA optical telescope. In: Blades, J. C. & Siegmund, O. H. W. (eds.), Future EUV/UV and Visible Space Astrophysics Missions and Instrumentation. Edited by J. Chris Blades, Oswald H. W. Siegmund. Proceedings of the SPIE, Volume 4854, pp. 9-20 (2003). vol. 4854 of *Presented at the Society of Photo-Optical Instrumentation Engineers (SPIE) Conference*, pp. 9–20.

Guirado, J. C., Ros, E., Jones, D. L., Lestrade, J.-F., Marcaide, J. M., Pérez-Torres, M. A. & Preston, R. A. (2001) Space-VLBI phase-reference mapping and astrometry. A&A371:766–770.

Hartkopf, W. I., Mason, B. D. & Worley, C. E. (2004) Sixth catalog of orbits of visual binary stars. U.S. Naval Observatory web page 12 July 2004 Realease.

Hemenway, P. D., Duncombe, R. L., Bozyan, E. P., Lalich, A. M., Argue, A. N., Franz, O. G., McArthur, B., Nelan, E., Taylor, D., White, G., Benedict, G. F., Crifo, F., Fredrick, L. W., Jefferys, W. H., Johnston, K., Kovalevsky, J., Kristian, J., Perryman, M. A. C., Preston, R., Shelus, P. J., Turon, C. & van Altena, W. (1997) The Program to Link the HIPPARCOS Reference Frame to an Extragalactic Reference System Using the Fine Guidance Sensors of the Hubble Space Telescope. AJ114:2796+.

Hickson, P., Bhatia, R. & Iovino, A. (1995) No relativistic aberration of liquid mirrors. A&A303:L37.

Hirabayashi, H., Murata, Y., Edwards, P. G., Asaki, Y., Mochizuki, N., Inoue, M., Umemoto, T., Kameno, S., Gurvits, L. I. & Lobanov, A. P. (2007) Design of the Near-term Next Generation Space-VLBI Mission VSOP-2, Exploring the Cosmic Frontier, ESO Astrophysics Symposia European Southern Observatory, Volume . ISBN 978-3-540-39755-7. Springer, 2007, p. 37, pp. 37+.

Hobbs, D., Lammers, U., Bastian, U. & O'Mullane, W. (2007) AGIS software test plan. "Gaia Technical Note p. 24.

Horner, S. D., Germain, M. E., Greene, T. P., Johnston, K. J., Monet, D. G., Murison, M. A., Phillips, J. D., Reasenberg, R. D., Seidelmann, P. K. & Urban, S. E. (1998) FAME - The Full-sky Astrometric Mapping Explorer. In: Bulletin of the American Astronomical Society. vol. 30 of *Bulletin of the American Astronomical Society*, pp. 1269+.

Hummel, C. A., Hutter, D. J. & Elias, II, N. M. (1999) Double star and wide angle astrometry with NPOI. In: Bulletin of the American Astronomical Society. vol. 31 of *Bulletin of the American Astronomical Society*, pp. 955+.

Irwin, J. B. (1952) The Determination of a Light-Time Orbit. ApJ116:211+.

Jackson, J. D. (1975) Classical Electrodynamics. John Wiley and Sons.

Johnston, K. J., Dorland, B. N., Gaume, R. A., Hajian, A. R., Harris, H. C., Hennessy, G. S., Monet, D. G., Munn, J. A., Olling, R. P., Pier, J. R., Zacharias, N., Coste, K., Pravdo, S., Danner, R., Grillmair, C., Stauffer, J. R., Seidelmann, P. K. & Seager, S. (2004) The Origins Billion Star Survey. In: Bulletin of the American Astronomical Society. vol. 205 of *Bulletin of the American Astronomical Society*, pp. 511+.

Klioner, S. A. (1989) Light deflection by the moving bodies. Institute of Applied Astronomy, preprint in Russian 6.

Klioner, S. A. (1991) Influence of the Quadrupole Field and Rotation of Objects on Light Propagation. Soviet Astronomy 35:523+.

Klioner, S. A. (2003) A Practical Relativistic Model for Microarcsecond Astrometry in Space. AJ125:1580–1597.

Klioner, S. A. (2004) Physically adequate proper reference system of a test observer and relativistic description of the GAIA attitude. Phys. Rev. D69(12):124001+.

Klioner, S. A. (2006) TDB or TCB: does it make a difference? Nomenclature, Precession and New Models in Fundamental Astronomy, 26th meeting of the IAU, Joint Discussion 16, 22-23 August 2006, Prague, Czech Republic, JD16, #20 16.

Klioner, S. A. & Blankenburg, R. (2003) Technical report on the implementation of the GAIA relativistic model. GAIA Technical note p. 17.

Klioner, S. A. & Kopeikin, S. M. (1992) Microarcsecond astrometry in space - Relativistic effects and reduction of observations. AJ104:897–914.

Klioner, S. A. & Peip, M. (2003) Numerical simulations of the light propagation in the gravitational field of moving bodies. A&A410:1063–1074.

Klioner, S. A. & Voinov, A. V. (1993) Relativistic theory of astronomical reference systems in closed form. Phys. Rev. D48:1451–1461.

Kopeikin, S. M. (1995) On possible implications of orbital parallaxes of wide orbit binary pulsars and their measurability. ApJ439:L5.

Kopeikin, S. M. (1996) Proper Motion of Binary Pulsars as a Source of Secular Variations of Orbital Parameters. ApJ467:L93.

Kopeikin, S. M. (2006a) Gravitational bending of light by planetary multipoles and its measurement with microarcsecond astronomical interferometers. astro-ph/0611358 p. "14".

Kopeikin, S. M. (2006b) The orbital motion of Sun and a new test of general relativity using radio links with the Cassini spacecraft. gr-qc/0604060 p. "10".

Kopeikin, S. M. (2007) Comment on "The gravitomagnetic influence on gyroscopes and on the lunar orbit". ArXiv General Relativity and Quantum Cosmology e-prints .

Kopeikin, S. M. & Ozernoy, L. M. (1999) Post-Newtonian Theory for Precision Doppler Measurements of Binary Star Orbits. ApJ523:771–785.

Kopeikin, S. M. & Schäfer, G. (1999) Lorentz covariant theory of light propagation in gravitational fields of arbitrary-moving bodies. Phys. Rev. D60(12):124002+.

Kovalevsky, J. (1971) The 1964 IAU System and the Geodetic Reference System 1967. Celestial Mechanics 4:279+.

Le Poncin-Lafitte, C. & Teyssandier, P. (2004) Influence of the multipole moments of a giant planet on the propagation of light. In: SF2A-2004: Semaine de l'Astrophysique Francaise. pp. 55+.

Lebach, D., Corey, B., Shapiro, I., Ratner, M., Webber, J., Rogers, A., Davis, J. & Herring, T. (1995) Measurement of the solar gravitational deflection of radio waves using very-long-baseline interferometry. Phys. Rev. Lett. 75:1439–1442.

Levy, G. S., Linfield, R. P., Edwards, C. D., Ulvestad, J. S., Jordan, Jr., J. F., Dinardo, S. J., Christensen, C. S., Preston, R. A., Skjerve, L. J., Stavert, L. R., Burke, B. F., Whitney, A. R., Cappallo, R. J., Rogers, A. E. E., Blaney, K. B., Maher, M. J., Ottenhoff, C. H., Jauncey, D. L., Peters, W. L., Reynolds, J., Nishimura, T., Hayashi, T., Takano, T., Yamada, T., Hirabayashi, H., Morimoto, M., Inoue, M., Shiomi, T., Kawaguchi, N., Kunimori, H., Tokumaru, M. & Takahashi, F. (1989) VLBI using a telescope in Earth orbit. I - The observations. ApJ336:1098–1104.

Lightman, A. P., Press, W. H., Richard, H. P. & Teukolsky, S. A. (1975) Problem book in Relativity and Gravitation. Princeton University Press.

Lindegren, L. & Dravins, D. (2003) The fundamental definition of "radial velocity". A&A401:1185–1201.

Linfield, R. P., Levy, G. S., Ulvestad, J. S., Edwards, C. D., Dinardo, S. J., Stavert, L. R., Ottenhoff, C. H., Whitney, A. R., Cappallo, R. J., Rogers, A. E. E., Hirabayashi, H., Morimoto, M., Inoue, M., Jauncey, D. L. & Nishimura, T. (1989) VLBI using a telescope in Earth orbit. II - Brightness temperatures exceeding the inverse Compton limit. ApJ336:1105–1112.

Ma, C., Arias, E. F., Eubanks, T. M., Fey, A. L., Gontier, A.-M., Jacobs, C. S., Sovers, O. J., Archinal, B. A. & Charlot, P. (1998) The International Celestial Reference Frame as Realized by Very Long Baseline Interferometry. AJ116:516–546.

Makarov, V. V. & Kaplan, G. H. (2005) Statistical Constraints for Astrometric Binaries with Nonlinear Motion. AJ129:2420–2427.

Masana, E., Anglada-Escudé, G., Luri, X., López-Martí, B., Llimona, P., Figueras, F., Jordi, C. & Torra, J. (2004) Astrometric Binary Stars: data generation and derivation of field angles. "Gaia Technical Note p. 21.

Mashhoon, B. (2005) Nonlocality of Accelerated Systems. International Journal of Modern Physics D 14:171–179.

McCarthy, D. D. & Petit, G. (2004) IERS Conventions (2003). IERS Conventions (2003). Dennis D. McCarthy and Gérard Petit (eds.), International Earth Rotation and Reference Systems Service (IERS). IERS Technical Note, No. 32, Frankfurt am Main, Germany: Verlag des Bundesamtes für Kartographie und Geodäsie, ISBN 3-89888-884-3, 2004, 127 pp. online version at: http://www.iers.org/iers/publications/tn/tn32/.

Mignard, F. (2003a) Prototype of the ephemeris of the Earth for GAIA. "Gaia Technical Note p. 20.

Mignard, F. (2003b) Prototype of the ephemeris of the GAIA spacecraft. "Gaia Technical Note p. 7.

Misner, C. W., Thorne, K. S. & Wheeler, J. A. (1973) Gravitation. San Francisco: W.H. Freeman and Co., 1973.

Monet, D. G., Levine, S. E., Canzian, B., Ables, H. D., Bird, A. R., Dahn, C. C., Guetter, H. H., Harris, H. C., Henden, A. A., Leggett, S. K., Levison, H. F., Luginbuhl, C. B., Martini, J., Monet, A. K. B., Munn, J. A., Pier, J. R., Rhodes, A. R., Riepe, B., Sell, S., Stone, R. C., Vrba, F. J., Walker, R. L., Westerhout, G., Brucato, R. J., Reid, I. N., Schoening, W., Hartley, M., Read, M. A. & Tritton, S. B. (2003) The USNO-B Catalog. AJ125:984–993.

Murray, C. A. (1983) Vectorial astrometry. Bristol: Adam Hilger, 1983.

Ni, W. & Zimmermann, M. (1978) Intertial and gravitational effects in proper reference frame of an accelerated, rotating observer. Phys. Rev. D17:1473–1476.

Nordtvedt, K. (1991) Lunar laser ranging reexamined: The non-null relativistic contribution. Phys. Rev. D43:3131–3135.

Pauli, W. (1958) Theory of Relativity. Pergamon Press.

Perryman, M. A. C. & ESA (1997) The HIPPARCOS and TYCHO catalogues. Astrometric and photometric star catalogues derived from the ESA HIPPARCOS Space Astrometry Mission. ESA Publications Division, 1997.

Perryman, M. A. C., Lindegren, L., Kovalevsky, J., Hoeg, E., Bastian, U., Bernacca, P. L., Crézé, M., Donati, F., Grenon, M., van Leeuwen, F., van der Marel, H., Mignard, F., Murray, C. A., Le Poole, R. S., Schrijver, H., Turon, C., Arenou, F., Froeschlé, M. & Petersen, C. S. (1997a) The HIPPARCOS Catalogue. A&A323:L49–L52.

Perryman, M. A. C., Lindegren, L., Kovalevsky, J., Hoeg, E., Bastian, U., Bernacca, P. L., Crézé, M., Donati, F., Grenon, M., van Leeuwen, F., van der Marel, H., Mignard, F., Murray, C. A., Le Poole, R. S., Schrijver, H., Turon, C., Arenou, F., Froeschlé, M. & Petersen, C. S. (1997b) The HIPPARCOS Catalogue. A&A323:L49–L52.

Perryman, M. A. C., de Boer, K. S., Gilmore, G., Høg, E., Lattanzi, M. G., Lindegren, L., Luri, X., Mignard, F., Pace, O. & de Zeeuw, P. T. (2001) GAIA: Composition, formation and evolution of the Galaxy. A&A369:339–363.

Pitjeva, E. V. (2005) High-Precision Ephemerides of Planets–EPM and Determination of Some Astronomical Constants. Solar System Research 39:176–186.

Portell, J., Figueras, F., Fabricius, C., Lpez-Martí, B., Luri, X., Jordi, C. & Torra, J. (2006) Final revision of the GDAAS2 Large-Scale Test (LST). "Gaia Technical Note p. 72.

Press, W. H., Teukolsky, S. A., Vetterling, W. T. & Flannery, B. P. (1992) Numerical recipes in FORTRAN. The art of scientific computing. Cambridge: University Press, —c1992, 2nd ed.

Ragazzoni, R. & Claudi, R. U. (1995) An unusual aberration of very large liquid mirror telescopes. A&A297:L53.

Reasenberg, R. D., Babcock, R. W., Chandler, J. F., Gorenstein, M. V., Huchra, J. P., Pearlman, M. R., Shapiro, I. I., Taylor, R. S., Bender, P., Buffington, A., Carney, B., Hughes, J. A., Johnston, K. J., Jones, B. F. & Matson, L. E. (1988) Microarcsecond optical astrometry - an instrument and its astrophysical applications. AJ96:1731–1745.

Ribas, I., Arenou, F. & Guinan, E. F. (2002) Astrometric and Light-Travel Time Orbits to Detect Low-Mass Companions: A Case Study of the Eclipsing System R Canis Majoris. AJ123:2033–2041.

Russell, J. L., Lasker, B. M., McLean, B. J., Sturch, C. R. & Jenkner, H. (1990) The Guide Star Catalog. II - Photometric and astrometric models and solutions. AJ99:2059–2081.

Seidelmann, P. K. (1982) 1980 IAU theory of nutation - The final report of the IAU Working Group on Nutation. Celestial Mechanics 27:79–106.

Seidelmann, P. K., Archinal, B. A., A'Hearn, M. F., Cruikshank, D. P., Hilton, J. L., Keller, H. U., Ost, J., Simon, J. L., Stooke, P., Tholen, D. J. & Thomas, P. C. (2005) Report of the IAU/IAG Working Group on Cartographic Coordinates and Rotational Elements: 2003. Celestial Mechanics and Dynamical Astronomy 91:203–215.

Serraller, I., Fabricius, C., Portell, J., Figueras, F., Torra, J. & Jordi, C. (2007) IDT implementation. "Gaia Technical Note p. 45.

Shao, M. (1998) SIM: the space interferometry mission. In: Proc. SPIE Vol. 3350, p. 536-540, Astronomical Interferometry, Robert D. Reasenberg; Ed. pp. 536–540.

Shapiro, S., Davis, J., Lebach, D. & Gregory, J. (2004) Measurement of the solar gravitational deflection of radio waves using geodetic very-long-baseline interferometry data, 1979–1999. Phys. Rev. Lett. 92:121101.

Soffel, M., Klioner, S. A., Petit, G., Wolf, P., Kopeikin, S. M., Bretagnon, P., Brumberg, V. A., Capitaine, N., Damour, T., Fukushima, T., Guinot, B., Huang, T.-Y., Lindegren, L., Ma, C., Nordtvedt, K., Ries, J. C., Seidelmann, P. K., Vokrouhlický, D., Will, C. M. & Xu, C. (2003) The IAU 2000 Resolutions for Astrometry, Celestial Mechanics, and Metrology in the Relativistic Framework: Explanatory Supplement. AJ126:2687–2706.

Spagna, A., Lattanzi, M. G., McLean, B., Bucciarelli, B., Drimmel, R., Greene, G., Loomis, C., Morbidelli, R., Pannunzio, R., Smart, R. & Volpicelli, A. (2006) The Guide Star Catalog II: Properties of the GSC 2.3 Release. Exploiting Large Surveys for Galactic Astronomy, 26th meeting of the IAU, Joint Discussion 13, 22-23 August 2006, Prague, Czech Republic, JD13, #49 13.

Standish, E. M. (2004) An approximation to the errors in the planetary ephemerides of the Astronomical Almanac. A&A417:1165–1171.

Stone, R. C. (1998) New Observations Testing the Adopted HIPPARCOS Link to the International Celestial Reference Frame. ApJ506:L93–L96.

Treuhaft, R. N. & Lowe, S. T. (1991) A measurement of planetary relativistic deflection. AJ102:1879–1888.

van Straten, W., Bailes, M., Britton, M., Kulkarni, S. R., Anderson, S. B., Manchester, R. N. & Sarkissian, J. (2001) A test of general relativity from the three-dimensional orbital geometry of a binary pulsar. Nature412:158–160.

Whipple, A. L., Jefferys, W. H., Benedict, G. F., Hemenway, P. D., McArthur, B., McCartney, J., Nelan, E., Shelus, P. J., Story, D., Duncombe, R., van Altena, W. F., Franz, O. G., Wasserman, L. H. & Fredrick, L. W. (1996) Observation of the Gravitational Deflection of Light by Jupiter. In: Bulletin of the American Astronomical Society. vol. 28 of *Bulletin of the American Astronomical Society*, pp. 1187+.

Will, C. M. (1980) Theory and experiment in gravitational physics,rev. ed. University Press, Cambridge.

Will, C. M. (2003) Propagation Speed of Gravity and the Relativistic Time Delay. ApJ590:683–690.

Wolszczan, A. & Frail, D. A. (1992) A planetary system around the millisecond pulsar PSR1257 + 12. Nature355:145–147.

Zacharias, N., Monet, D. G., Levine, S. E., Urban, S. E., Gaume, R. & Wycoff, G. L. (2004a) The Naval Observatory Merged Astrometric Dataset (NOMAD). In: Bulletin of the American Astronomical Society. vol. 36 of *Bulletin of the American Astronomical Society*, pp. 1418+.

Zacharias, N., Urban, S. E., Zacharias, M. I., Wycoff, G. L., Hall, D. M., Monet, D. G. & Rafferty, T. J. (2004b) The Second US Naval Observatory CCD Astrograph Catalog (UCAC2). AJ127:3043–3059.

Epíleg

M'acomiado amb unes paraules que a molts us semblaran extranyes per que, de ben segur, seran familiars a la part de l'audiència que ja ha passat per aquest trangul. No deixar-ne testimoni seria trair a la realitat, i no vull deixar a l'atzar de la memoria taidora una part important de la lliçó que he après.

Encara que sembli un tòpic he acabat molt fart de tot plegat. No conservo molts bons records dels darrers mesos, en els que he dedicat una bona part del temps a la redacció d'aquesta tesi. Hi han hagut moments llargs, massa llargs, de desesperació i ostracisme, on la muntanya semblava massa alta, la pendent massa forta i el camí estava totalment desdibuixat. I he seguit endevant, no tant per l'ilusió oblidada dels meus primers dies com a doctorant, sinó per l'inèrcia d'una promesa: que des del capdamnunt estant, hom pot girar-se i satisfet afirmar que el camí recorregut ha valgut la pena.

He arribat al capdamunt però era de nit. No puc explicar-vos les maravelles del viatge perquè ara mateix estic massa cansat per mirar enrera. Només em queden forces per estirar-me i contemplar el cel cobert d'estels, la guia, la musa. Ara resta esperar que amb el pas dels dies, la boira d'aixequi i el sol m'inspiri per rempendre de nou el camí amb la força i la serenitat perdudes.

Comença una nova etapa. O més ben dit, n'acaba una altra. Permeteu-me doncs, aixecar el cap i mirar endevant amb optimisme i preguem perquè les ferides obertes pel cinisme no tardin a cicatritzar.